# The Binding of the Micronutrient Transition Metals to the Alkylation Products of Chemical Warfare Agent, Sulfur Mustard, and Thiols, Potentially Giving New Understanding to Physiological Effects of Exposure and Increased Toxicity

A dissertation submitted in partial fulfillment
of the requirements for the degree of
Doctor of Philosophy in Chemistry

by

Colin O'Donnell
James Madison University
Bachelor of Science in Chemistry, 2015

December 2022
University of Arkansas

This dissertation is approved for recommendation to the Graduate Council.

Wesley Stites, Ph.D.
Dissertation Director

Stefan Kilyanek, Ph.D.
Committee Member

Francis Millett, Ph.D.
Committee Member

Josh Sakon, Ph.D.
Committee Member

**Abstract**

Model compounds, 3,6,9-trithaiundecane-1,11-dicarboxylic acid (TTDPA), 2,5,8-trithianonane-1,9-dicarboxylic acid (TTDAA), and 1,11-diamide-3,6,9-trithiaundecane (TTDAce), closely related to the adducts formed by cysteine alkylation of the chemical weapon, sulfur mustard, were synthesized. It is shown that TTDPA forms complexes with key metal micronutrients: copper, nickel, cobalt, manganese, and zinc. Though the strength of binding to TTDPA varies, the complexes in many cases precipitate from solution. All metals produced a visible precipitate upon interaction with TTDPA under the conditions tested, however only $Cu^{2+}$, $Mn^{2+}$, and $Zn^{2+}$ produced enough to be measured. The mass of formed precipitate seemed to peak at an equimolar ratio of TTDPA to metal even when the concentration of the metal was in a 5-fold excess. However, in the case of $Mn^{2+}$ the reaction occurred so slowly that very little precipitate was recovered in the equimolar ratio, but a large amount was observed days later. Crystal structure data shows that the tridentate thioether portion of TTDPA is sufficient to form a complex with a $Cu^{2+}$ ion and a chloride, meaning that the alkylation adducts formed by cysteine or larger cysteine containing peptides or proteins contain all the functionality needed to bind to copper. Surprisingly, there were two distinct crystals formed from interactions of TTDPA with $CuCl_2$. In both forms, the three sulfurs of the adduct model bind to a single $Cu^{2+}$ with a coordination number of four. The remaining site in the tetrahedral complex is a chloride, but with key differences in how this chloride interacts in the two forms. The first form was a clear crystal with a dimeric structure and two TTDPA:$Cu^{2+}$ complexes bridged by a single chloride ion (μCl-bis-(Cu-L)). The second form was a green crystal and was a monomeric structure without bridged $Cu^{2+}$ ions (L-CuCl) in the key interaction between the three sulfurs of the adduct model. However, the carboxylate groups at the ends of the ligand in the green crystal coordinate to an additional $Cu^{2+}$ ion, forming an octahedral complex with two TTDPA ligands, one water

molecule and another $Cu^{2+}$ ion. Even with the addition of the copper bound carboxylate, the copper – tridentate ligand interaction was enough to give sufficient binding and stability. Although these two structures existed in all ratios of ligand to metal, in the captured precipitate the μCl-bis-(Cu-L) was always the dominate product. The ready formation of these complexes leads us to hypothesize that localized depletion of such metals could ensue due to complex formation with the thiol alkylation products of sulfur mustard. These metal micronutrients play pivotal roles in burn wound healing and cellular protection from oxidative stress. The effective reduction of $Cu^{2+}$, $Mn^{2+}$, and $Zn^{2+}$ concentration could, for example, limit function of superoxide dismutase enzymes leading to an increase in oxidative stress on the cell. Copper is itself toxic and pulling it out of enzymes and the carefully regulated copper transport and storage system to form complexes which might catalyze the formation of reactive oxygen species is another potential concern. Thus, the findings proposed in this research suggest a new hypothesis explaining the increased toxicity of sulfur mustard relative to similar monofunctional alkylating agents and the unexplained symptoms of mustard exposure.

**Acknowledgements**

First, I would like to thank my mom and dad for the continued support of these many years; and all of family and friends who supported me throughout this long and arduous journey. I know I would not have been able to complete this journey without you. Secondly, I would like to thank Dr. Stites for all of his guidance and words of encouragement to keep going through this process to finish my degree. I would also like to thank anyone not specifically mentioned for the support over the years in figuring out problems or new solutions to attempt over the course of my research. Lastly, I would like to dedicate this to my family members who could not be here to see me complete my doctoral degree but always believed in me and encouraged me to keep going.

**Table of Contents**

## Lists of Figures

## List of Schemes

## List of Tables

## List of Graphs

## Chapter 1

## Introduction

During World War I, Germany unleashed sulfur mustard, also commonly known as mustard gas, on enemy troops for the first time in human history. Although sulfur mustard has been used multiple times since then, it is usually associated with World War I and the Iran-Iraq War of the 1980s. This does not mean that sulfur mustard is no longer a threat to mankind. Accidental exposure is still a danger as stockpiles of sulfur mustard and unexploded munitions remain all over the world; and since it is easily produced from common chemicals there is still a real threat of terrorist organizations synthesizing and using the weapon. In fact, there have been reports as recently as 2015 of the Islamic State in Iraq and Syria (ISIS) making and using sulfur mustard on its enemies (1).

Sulfur mustard was not initially developed with the intent of being a chemical weapon. First synthesized in 1822 by César-Mansuète Despretz there was not mention of irritant properties, just simply that it was a vicious odorless liquid (2). It was not until 1860 that the first mention of sulfur mustard's irritant properties was published in literature. Albert Niemann noted that the smallest drop on the skin would cause the delayed formation of a blister that was very difficult to heal (3). The modern synthetic route for sulfur mustard production was published in 1912 by Hans T. Clark, which used thiodiglycol and warm hydrochloric acid; two chemicals that are cheap and readily available. While working with purified sulfur mustard Clark dropped a flask which caused the sulfur mustard to splash all over him, this results in months of hospitalization as he was covered in excruciating burns and blisters (4).

The first large scale use of sulfur mustard was in 1917 during the battle of Ypres in Belgium during World War I. Germany was the first to use this terrible new weapon, but it soon was

utilized by both sides. At the height of the war the United States was producing 30 tons per day (5). Over the course of World War I, sulfur mustard earned the name “The King” or “The King of Chemical Weapons” due to widespread usage, unique chemical properties, and ability to strike fear into the enemies. Among those unique chemical properties, sulfur mustard vapors are about 5.5x heavier than air, hover just above the ground, and sink into trenches. For a molecule that is quite reactive, mustard is surprisingly long lived. Liquid mustard persists in the environment from days to weeks depending on the climate, causing problems for one’s enemies long after the initial attack. Another key element was that gas protection at the time did little to stop exposure to sulfur mustard. The rudimentary gas masks of the era might stop inhalation of the vapor or droplets but did nothing to prevent skin exposure. By the end of World War I alone sulfur mustard alone accounted for a total of 2.6% of all British soldier casualties (5,6).

Following World War I sulfur mustard was sporadically used. The most recent major usage of the weapon was during the 1980s in the Iran-Iraq war. During this conflict it is believed some 100,000 soldiers were exposed and tens of thousands of those soldiers are still alive today (7) and continue to deal with the long-term consequences of exposure. The usage of sulfur mustard disappeared for a couple decades until the mid-2010s when ISIS started synthesizing and deploying crude version of sulfur mustard in their roadside bombs. There have been at least 3 confirmed uses of sulfur mustard by ISIS from 2012-2015 (1).

Although sulfur mustard was discovered 200 years ago and first widely used 100 years ago, its exact mechanism of action is still not totally understood. Symptoms of sulfur mustard exposure are wide ranging and some can vary from person-to-person, but the most common are: irritation of the lungs and airway, blister formation, skin necrosis, blindness, vomiting, fatigue, and slow healing wounds. There are three commonly accepted hypotheses to explain the effects of sulfur

mustard on the body and although they explain the majority of the major symptoms, they leave many symptoms unanswered for. The first hypothesis is the alkylation of DNA or proteins resulting in three unique products: DNA-DNA (or RNA), DNA-protein, or protein-protein adduct formation. These products create a highly toxic cellular environment and overtax the DNA repair pathways ultimately results in cellular death (8). The second hypothesis revolves around alkylation and depletion of the specific antioxidant glutathione. Glutathione is the body's most abundant low molecular weight antioxidant and is responsible for keeping oxidative damage in the cell to a minimum (9). Sulfur mustard will cross-link glutathione molecules, removing them from the equation, and allowing oxidative stress within the cell to run rampant. When this happens, free radicals cause damage to proteins, DNA, and lipid structures; this damage will eventually reach a critical point resulting in cellular death (10). Inflammation is one of the body's initial and key responses to damage and is the center point of the third hypothesis. The inflammatory response caused by sulfur mustard is a more general response and triggers cytokine storms leading to mass inflammation of exposed areas. When this response does not fix the problem caused by exposure the immune system then signals for cellular apoptosis. It is this inflammatory response that is usually held responsible for the blistering, skin shedding, and mass necrosis caused by sulfur mustard exposure (11). These three hypotheses explain many of the symptoms of exposure, however a few they do not explain as well include: temporary blindness, vomiting, slow wound healing, short-term memory loss and fatigue.

Sulfur mustard led to the research of other types of alkylating agents: nitrogen mustard, oxygen mustard, half-mustard, sesquimustard, and O-mustard. Some of these sulfur mustard derivatives such as sesquimustard are up to five times more potent and blistering than normal mustard;

whereas others like nitrogen mustard, oxygen mustard, and half-mustard as significantly less toxic and have actually been studied as chemotherapy drugs (17,18).

The lack of explanation for these less studied symptoms was a reason for the research conducted for this dissertation. As laid out in this dissertation, studies conducted by our lab have shown that analogs of the reaction products of sulfur mustard expected to form in the body have strong affinities for biologically important metals such as manganese, copper, zinc, cobalt, and nickel. In fact, when these analogs are mixed with cations of these metals at physiological pH, they form complexes and immediately precipitate out of solution. This supports a new hypothesis that exposure to sulfur mustard can deplete the body of these key micronutrient metals, causing some of these unexplained symptoms.

These metallic micronutrients are also known to be important for burn wound healing as well as cognitive function. The unexplained sulfur mustard symptoms of temporary cognitive issues, temporary blindness, vomiting, dermatitis, slow wound healing, and fatigue fit in to the realm of known symptoms caused by the deficiency of these metals. Zinc is the most abundant of these five, with approximately ~2300mg in the body and common deficiency symptoms include: delayed wound healing, recurrent infection, and increased oxidative stress (12,13). Copper is found in the amount of ~70mg in the body and plays key roles in antioxidant functionality. Common deficiency symptoms are increased oxidative stress, delayed wound healing, and defects in skin elasticity (12,14). Manganese is a key metal for the protection of mitochondria from oxidative stress and is found in ~16-40mg. Deficiency leads to dermatitis and cognitive issues. (19,20). Little is known about the function of nickel but there is ~15mg in the body. Deficiency does cause problems with iron absorption and can cause an increase in inflammation (12,15). Our bodies contain the least amount of cobalt with only 1-2mg, most of which is bound

in the form of Vitamin B12. Cobalt deficiency can manifest itself in poor vision, fatigue, and short-term memory loss (12,16).

The results of laboratory experimentation presented here show complex formation between sulfur mustard product analogs and metals. It is possible that sulfur mustard exposure could cause drops in the available metal micronutrient concentration leading at the very least to a significant perturbation in the metabolism of these metals and perhaps to an effective deficiency, particularly locally. The metal micronutrient deficiency symptoms match with under- or unexplained sulfur mustard exposure symptoms. Some of these metals are also rather toxic when drawn out of their regular metabolic pathways. Thus, it seems plausible that sulfur mustard products may bind to free metals in the body and contribute to these symptoms. This hypothesis is novel. If proven correct, this would help fill in the gaps of understanding about sulfur mustard exposure and it would potentially also lead to improved treatments for those exposed.

## 1.1 Reference


1. Patocka, J. Syria conflict and chemical weapons: what is the reality. *Mil Med Sci Lett* **2016**, *85* (1), 39-43.

2. Duchovic, R. J.; Vilensky, J. A. Mustard gas: its pre-World War I history. *Journal of chemical education* **2007**, *84* (6), 944.

3. Guthrie, F. XIII. —On some derivatives from the olefines. *Quarterly Journal of the Chemical Society of London* **1860**, *12* (1), 109-126.

4. Meyer, V. Ueber thiodiglykolverbindungen. *Berichte der deutschen chemischen Gesellschaft* **1886**, *19* (2), 3259-3266.

5. Fitzgerald, G. J. Chemical warfare and medical response during World War I. *American journal of public health* **2008**, *98* (4), 611-625.

6. Wattana, M.; Bey, T. Mustard gas or sulfur mustard: an old chemical agent as a new terrorist threat. *Prehospital and disaster medicine* **2009**, *24* (1), 19-29.

7. Roshan, R.; Rahnama, P.; Ghazanfari, Z.; Montazeri, A.; Soroush, M. R.; Naghizadeh, M. M.; Melyani, M.; Tavoli, A.; Ghazanfari, T. Long-term effects of sulfur mustard on civilians' mental health 20 years after exposure (The Sardasht-Iran Cohort Study). *Health and quality of life outcomes* **2013**, *11* (1), 1-7.

8. Anderson, D.; Benton, B.; Wang, Z.-Q.; Smith, W.; Ray, R.; Rosenthal, D. S.; Simbulan-Rosenthal, C. M.; Liu, W. F.; Velena, A.; Smulson, M. E. PARP determines the mode of cell death in skin fibroblasts, but not keratinocytes, exposed to sulfur mustard. *Journal of investigative dermatology* **2001**, *117* (6), 1566-1573.

9. Meister, A.; Anderson, M. E. Glutathione. *Annual review of biochemistry* **1983**, *52* (1), 711-760.

10. Batal, M.; Rebelo-Moreira, S.; Hamon, N.; Bayle, P.-A.; Mouret, S.; Cléry-Barraud, C.; Boudry, I.; Douki, T. A guanine-ethylthioethyl-glutathione adduct as a major DNA lesion in the skin and in organs of mice exposed to sulfur mustard. *Toxicology letters* **2015**, *233* (1), 1-7.

11. Keyser, B. M.; Andres, D. K.; Holmes, W. W.; Paradiso, D.; Appell, A.; Letukas, V. A.; Benton, B.; Clark, O. E.; Gao, X.; Ray, P. Mustard gas inhalation injury: therapeutic strategy. *International journal of toxicology* **2014**, *33* (4), 271-281.

12. Emsley, J. *Nature's building blocks: an AZ guide to the elements*; Oxford University Press, 2011.

13. Livingstone, C. Zinc: physiology, deficiency, and parenteral nutrition. *Nutrition in Clinical Practice* **2015**, *30* (3), 371-382.

14. Altarelli, M.; Ben-Hamouda, N.; Schneider, A.; Berger, M. M. Copper deficiency: causes, manifestations, and treatment. *Nutrition in Clinical Practice* **2019**, *34* (4), 504-513.

15. Kumar, S.; Trivedi, A. A review on role of nickel in the biological system. *Int. J. Curr. Microbiol. Appl. Sci* **2016**, *5* (2), 719-727.

16. Langan, R. C.; Goodbred, A. J. Vitamin B12 deficiency: recognition and management. *American family physician* **2017**, *96* (6), 384-389.

17. Blum, M.-M.; Richter, A.; Siegert, M.; Thiermann, H.; John, H. Adduct of the blistering warfare agent sesquimustard with human serum albumin and its mass spectrometric identification for biomedical verification of exposure. *Analytical and bioanalytical chemistry* **2020**, *412* (28), 7723-7737.

18. Wang, Q.-Q.; Begum, R. A.; Day, V. W.; Bowman-James, K. Sulfur, oxygen, and nitrogen mustards: stability and reactivity. *Organic & biomolecular chemistry* **2012**, *10* (44), 8786-8793.

19. Zoroddu, M. A.; Aaseth, J.; Crisponi, G.; Medici, S.; Peana, M.; Nurchi, V. M. The essential metals for humans: a brief overview. *Journal of inorganic biochemistry* **2019**, *195*, 120-129.

20. Smith, M. R.; Fernandes, J.; Go, Y.-M.; Jones, D. P. Redox dynamics of manganese as a mitochondrial life-death switch. *Biochemical and biophysical research communications* **2017**, *482* (3), 388-398.

# CHAPTER 2

## History of Sulfur Mustard – A Review

### 2.1 Introduction

A chemical warfare agent can be defined as a chemical used to cause intentional death or harm through its toxic properties (1). Modern chemical warfare agents are divided into 5 different classifications: blister agents (vesicants), choking agents (pulmonary agents), blood agents (cyanogenic agents), nerve agents, and riot-control agents (1,2). Blistering agents affect the airways as well as the eyes, skin, and almost all mucus membranes. These agents are the most common and exposure results in burns, cell death, and irreversible damage to the lung tissue; examples include phosgene oxime, lewisite, and, most prominently, the subject of this dissertation, sulfur mustard.

The first large scale use of modern chemical weapons occurred during World War I during the German invasion of Belgium in 1915 (2). At the time the main chemical weapon used was chlorine gas ($Cl_2$), which upon entering the body reacts with water in the lungs to for hydrochloric acid (HCl) and hypochlorous acid (HOCl) which imposed significant oxidative stress and caused major lung damage (3). Following the use of chlorine, both sides began using phosgene (carbonyl chloride, $COCl_2$) which like its chlorine counterpart would react in airways (4). As protections against chemical weapons such as gas masks became readily available, soldiers were easily shielded against phosgene and chlorine gas. Thus, a shift in research began and new chemical weapons were utilized that could penetrate even the most advanced protection apparatus. Come 1917, the German army unleased a weapon that later become known as “The King of Chemical Weapons” or “The King of Battle Gases”, the weapon sulfur mustard. Sulfur mustard or mustard gas (Figure 2.1) are the common names for the chemical 1-chloro-2[(2-chloroethyl) sulfanyl] ethane (CAS Number 505-60-2); other frequently used names include:

Bis(2-chloroethyl) sulfide, HD, dichlorodiethyl sulfide, and 1,1'-thiobis[2-chlororethane]. Unlike previously used weapons such as chlorine or phosgene gases, it was a vesicant which causes blisters upon exposure.

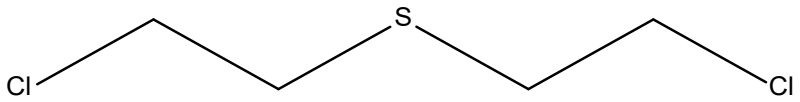


*Figure 2.1. Chemical structure of Sulfur Mustard.*

Before being used as a chemical weapon by Germany in 1917, the first published account of sulfur mustard was in 1822 by Belgium born chemist César-Mansuète Despretz (5). Despretz's discovery was that the combination of sulfur dichloride and ethylene yield a viscous and odorous liquid; however, his publication did not include any mention of irritant properties. It was over 30 years before sulfur mustard appeared in literature again, this time by French chemist Alfred Richie who repeated Despretz's work, without citing him. Richie's publication did not include any synthetic pathways or properties of the reaction's product. All the publication stated was that mustard was a yellow liquid that boiled around 185-200°C (5). The first mention of sulfur mustard's irritant properties appeared in literature in 1860, when German chemist Albert Niemann followed the reactions of Despretz and noted that if the smallest drop were to contact the skin, a blister would appear sometimes hours later and was difficult to heal. Also in 1860, Frederick Guthrie, a British chemist, published a paper titled *On some Derivatives from the Olefines*, in which he produced sulfur mustard by bubbling ethylene gas through a flask containing sulfur dichloride (6). Guthrie noted the product had a pungent mustard smell and a taste like that of horseradish. It is this odor that is responsible for the name of mustard, not any actual association with the plant or condiment. It was also noted the vapors would attack the

skin on the fingers and around the eyes destroying the epidermis, while the liquid would cause skin blisters anywhere there was contact (6).

In 1886 German chemist Victor Meyer published the paper *Ueber Thiodiglykolverbindungen* (About Thiodiglycol Reactions) in which he proposed a novel synthetic route for the formation of sulfur mustard. Meyer's synthesis involved reacting 2-chloroethanol with potassium sulfide, then treating the mixture with phosphorus trichloride and thiodiglycol (5,7). In his publication, Meyer noted the result was an oily product that caused delayed wounds and that these wounds were exceptionally difficult to heal (7). Hans T. Clarke published the last novel sulfur mustard synthesis route in 1912, in his paper titled *CLXX—4-Alkyl-1:4-thiazans*. In Clarke's paper he adapted Meyer's route by replacing the second step, Clarke noted that the thiodiglycol could be added to warm hydrochloric acid instead of using phosphorus trichloride (8). While working with a flask of purified sulfur mustard, Clarke accidently dropped it, resulting in him being covered in excruciating burns that required months of hospitalization to heal. It is believed that this incident was the inspiration of the Germans to use sulfur mustard as a chemical weapon (5). Clarke's synthesis method, later known as the Meyer-Clarke method (Scheme 2.1) became the predominant synthesis route as the required starting materials, thiodiglycol and hydrochloric acid, were cheap and readily available.

The synthetic route was also simple and straight forward; just add thiodiglycol to warm hydrochloric acid. Although sulfur mustard was first used by Germany, both sides of the war,

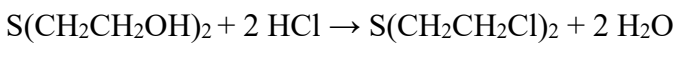

$$S(CH_2CH_2OH)_2 + 2\ HCl \rightarrow S(CH_2CH_2Cl)_2 + 2\ H_2O$$

Scheme 2.1. Balanced equation for Meyer-Clarke synthesis.

including the United States, used it on their enemies. Sulfur mustard became “The King” for a plethora of reasons, notably: it was cheap and simple to produce, it could persist for days or weeks on dry ground and, the vapor being heavier than air, it would hug the ground and fill trenches. During the height of production, the United States alone was producing 30 tons of sulfur mustard per day (4). Sulfur mustard had a delayed onset of symptoms, soldiers would be uncomfortable at first and then blisters would develop. Although not quick to evaporate, if exposed to the vapor for long enough eye damage would occur (Figure 2.2). It was widely reported that exposure to gases during the war caused major psychological damage to soldiers known simply as “gas fright”.

*FIGURE 2.2 Top left: Chlorine being released from gas canisters over the western front; Top right: British soldiers blinded by sulfur mustard during the Battle of Estaires in 1918 (4). Bottom row, skin reaction to liquid sulfur mustard exposure; far left is day 1, middle is day 2, far right is day 7 following exposure (20).*

Chemical gas attacks were so effective during World War I that over 30% of all soldiers were exposed to them at some point during the war. For the British 80% of chemical casualties could be attributed to sulfur mustard alone (approximately 154,000 solders). In fact, over the course of the entire war, sulfur mustard accounted for 2.6% of total casualties inflicted on the British (4,9). Following World War I, sulfur mustard was used throughout conflicts around the world: Italy in Ethiopia in the 1930s, Japan in China in the 1930-1940s, Egypt in Yemen in the 1960s, and the Iran-Iraq war in the 1980s (9). During the Iran-Iraq war it is believed that over 100,000 soldiers were exposed, and as of 2013 45,000 of those soldiers were still alive and dealing with the lifelong consequences of exposure (10).

One of the main reasons sulfur mustard was so effective was its chemical properties (Table 2.1). In particular: its vapor density, persistency, latency, and toxicity. The inhalation toxicity of sulfur mustard is given by the degree of atmospheric exposure, given in units of milligrams per minute of exposure per cubic meter ($mg \bullet min/m^3$) and includes vapors and aerosol droplets. Exposure levels are often broken down into four categories related to the degree of injury: threshold, injured (nondisabling), incapacitation, and lethal (10,11). The toxicity of given dosage varies by exposure route (Table 2.2) but for a respiratory tract exposure the threshold dosage was 12-70 $mg \bullet min/m^3$, injured was <100 $mg \bullet min/m^3$, incapacitated ~250 $mg \bullet min/m^3$, and lethal 1500 $mg \bullet min/m^3$ (11,12). The average atmospheric concentration of sulfur mustard during a World War I attack was 20 $mg/m^3$ with a maximum of 33 $mg/m^3$, meaning that to sustain a lethal dosage an unprotected soldier would have to be exposed for only approximately 50-75 minutes (12). Gas mask prevent lung exposure, but even the most effective gas mask could not prevent skin exposure and the development of blisters.

*TABLE 2.1 Physical and Chemical Properties of Sulfur Mustard.*

| Chemical and Physical Properties of Sulfur Mustard | |
|---|---|
| Chemical Formula | $C_4H_8Cl_2S$ |
| Molar Mass | 159.07 g • $mol^{-1}$ |
| Appearance | Colorless oil, smell of garlic and/or horseradish |
| Density | 1.27 g/mL |
| Boiling Point | 217°C (423°F, 490K) |
| Vapor Density compared to Air | 5.5 |
| Solubility in Water | 7.6 mg/L |

*TABLE 2.2 Vapor Exposure Limits of Sulfur Mustard, Looking at Various Exposure Routes and Their Biological Endpoints.*

| Route of Exposure | Threshold | Injured | Incapacitated | Death or Permanent Injury |
|---|---|---|---|---|
| Vapor – Eyes ($mg•min/m^3$) | 12 | 50-100 | 200 | >800 |
| Vapor – Respiratory Tract ($mg•min/m^3$) | 12-70 | <100 | 200 ($ICt_{50}$) | 1,000-1,500 ($LCt_{50}$) |
| Vapor – Skin ($mg•min/m^3$) | 5 | 100-300 | 1,000 (low humidity) 2,000 (high humidity) | 10,000 ($LCt_{50}$) |
| Liquid – Skin | 32 mg/man | N/A | 3,000-7,000 mg/man | 64 mg/kg (lethal dose) |

**Where $ICt_{50}$ is Incapacitation Concentration and Time, where 50% of persons are incapacitated, and $LCt_{50}$ is the Lethal Concentration and Time where persons die 50% of the time. Table adapted from (11,12).*

Since chemical weapons were often referred to as 'gases' in World War I, even today this agent is often called mustard gas. However, mustard is an oily liquid with a fairly low vapor pressure of 0.065 to 0.336 torr over 20 to 40°C (13). But even at those relatively low vapor pressure levels, it is toxic enough to cause harm (14,15). The vapor density of sulfur mustard is about 5.5x greater than air, allowing it to sink, usually hovering about 6-12 inches above ground level; these

vapors would also persist anywhere from a day in warmer climates to several weeks in colder weather (4,9). Sulfur mustard hydrolyzes readily in water, with a half-life of just a few minutes, but it is only sparingly soluble in water. This means that surfaces contaminated with the agent remain dangerous for days to weeks (16-18).

Although the latency of symptom onset varied by exposure level, it, on average, takes hours for symptoms to start appearing. The average exposure timeline is as follows: earliest skin irritation ~ 1 hour, raised and irritated skin ~8-12 hours, blister formation ~16-48 hours, maximum blister formation and skin necrosis ~45-72 hours, complete skin loss ~6-9 days, and finally complete healing in ~22-29 days (11). One of the major advantages of this from the perspective of the attacker was although it did not kill a high percentage of those exposed, it removed many soldiers from the battlefield and bogged down hospital systems, reducing the capacity to treat other patients since the recovery period was so long.

The first major agreement and banning of the usage of chemical weapons came from the Geneva Protocol of 1925. The protocol stated “the use in war of asphyxiating, poisonous or other gases, and all analogous liquids, materials, or devices, has been justly condemned... this prohibition shall be universally accepted as part of International Law” (19). Although attempts to prohibit their employment were successful at first, chemical weapons were still used, including by countries who had signed the Protocol. A major flaw in the Geneva Protocol of 1925 was that while it prohibited the use of such gases, it did not prohibit the invention, possession, stockpiling, or production of such weapons. It was not until 1980, when negotiations of the Chemical Weapons Convention (CWC) began, was there to be a more comprehensive treaty in place around chemical weapons. In 1993, the Convention on the Prohibition of the Development, Production, Stockpiling, and Use of Chemical Weapons and on their Destruction, was opened by

the CWC for countries to sign. Eventually 193 countries, including the United States, Britain, and Germany, signed the treaty and it took full effect in April of 1997 (1). Along with the outright ban on usage and development of new weapons, the convention also established a timeline for countries to follow on the destruction of stockpiles of these weapons. The United States military constructed specific facilities to properly and safely destroy these weapons; one such facility, the Pine Bluff Chemical Agent Disposal Facility, was located in Arkansas.

**2.2 Reference**


1. United Nations. Convention on the prohibition of the development, production, stockpiling and use of chemical weapons and on their destruction. *Organization for the Prohibition of Chemical Weapons* **2005**.

2. Ganesan, K.; Raza, S.; Vijayaraghavan, R. Chemical warfare agents. *Journal of pharmacy and bioallied sciences* **2010**, *2* (3), 166.

3. White, C. W.; Martin, J. G. Chlorine gas inhalation: human clinical evidence of toxicity and experience in animal models. *Proceedings of the American Thoracic Society* **2010**, *7* (4), 257-263.

4. Fitzgerald, G. J. Chemical warfare and medical response during World War I. *American journal of public health* **2008**, *98* (4), 611-625.

5. Duchovic, R. J.; Vilensky, J. A. Mustard gas: its pre-World War I history. *Journal of chemical education* **2007**, *84* (6), 944.

6. Guthrie, F. XIII.—On some derivatives from the olefines. *Quarterly Journal of the Chemical Society of London* **1860**, *12* (1), 109-126.

7. Meyer, V. Ueber thiodiglykolverbindungen. *Berichte der deutschen chemischen Gesellschaft* **1886**, *19* (2), 3259-3266.

8. Clarke, H. T. CLXX.—4-Alkyl-1: 4-thiazans. *Journal of the Chemical Society, Transactions* **1912**, *101*, 1583-1590.

9. Wattana, M.; Bey, T. Mustard gas or sulfur mustard: an old chemical agent as a new terrorist threat. *Prehospital and disaster medicine* **2009**, *24* (1), 19-29.

10. Roshan, R.; Rahnama, P.; Ghazanfari, Z.; Montazeri, A.; Soroush, M. R.; Naghizadeh, M. M.; Melyani, M.; Tavoli, A.; Ghazanfari, T. Long-term effects of sulfur mustard on civilians' mental health 20 years after exposure (The Sardasht-Iran Cohort Study). *Health and quality of life outcomes* **2013**, *11* (1), 1-7.

11. Smith, W. J.; Dunn, M. A. Medical defense against blistering chemical warfare agents. *Archives of dermatology* **1991**, *127* (8), 1207-1213.

12. Rall, D. P.; Pechura, C. M. Veterans at risk: The health effects of mustard gas and lewisite. **1993**.

13. Bent, H.; Francel, R. The Vapor Pressure of "Mustard Gas"(β, β'-Dichloroethylsulfide), Diphenyl Ether and their Mixtures. *Journal of the American Chemical Society* **1948**, *70* (2), 634-637.

14. Malaviya, R.; Abramova, E. V.; Rancourt, R. C.; Sunil, V. R.; Napierala, M.; Weinstock, D.; Croutch, C. R.; Roseman, J.; Tuttle, R.; Peters, E. Progressive lung injury, inflammation, and fibrosis in rats following inhalation of sulfur mustard. *Toxicological Sciences* **2020**, *178* (2), 358-374.

15. McNutt, P. M.; Kelly, K. E.; Altvater, A. C.; Nelson, M. R.; Lyman, M. E.; O'Brien, S.; Conroy, M. T.; Ondeck, C. A.; Bodt, S. M.; Wolfe, S. E. Dose-dependent emergence of acute and recurrent corneal lesions in sulfur mustard-exposed rabbit eyes. *Toxicology Letters* **2021**, *341*, 33-42.

16. Mizrahi, D. M.; Goldvaser, M.; Columbus, I. Long-term evaluation of the fate of sulfur mustard on dry and humid soils, asphalt, and concrete. *Environmental science & technology* **2011**, *45* (8), 3466-3472.

17. Jung, H.; Kah, D.; Lim, K. C.; Lee, J. Y. Fate of sulfur mustard on soil: Evaporation, degradation, and vapor emission. *Environmental Pollution* **2017**, *220*, 478-486.

18. Jung, H.; Choi, S. Behavior of sulfur mustard in sand, concrete, and asphalt matrices: Evaporation, degradation, and decontamination. *Journal of Environmental Science and Health, Part A* **2017**, *52* (12), 1121-1125.

19. United Nations. Protocol For the Prohibition of The Use in War of Asphyxiating, Poisonous or Other Gases, And of Bacteriological Methods of Warfare, 1925 (Geneva Protocol Of 1925). *OPCW: The Legal Texts* **2015**, 737-737.

20. Le, H.; Knudsen, S. Exposure to a First World War blistering agent. *Emergency medicine journal* **2006**, *23* (4), 296-299.

## CHAPTER 3

## Physiological Response following Sulfur Mustard Exposure – A Current Understanding

### 3.1 Introduction

The exact mechanism of action of sulfur mustard is still yet undetermined; however, there are a few accepted hypotheses for the physiological damage caused by exposure. It would first be prudent to understand what happens to the sulfur mustard molecule upon entering the body. Upon the inhalation or skin absorption of a molecule of sulfur mustard it is rapidly converted into a highly reactive episulfonium ion, ethylene episulfonium (Figure 3.1), with this species being the active alkylating agent. Each molecule of sulfur mustard is able to form the episulfonium ion twice and thus alkylate twice.

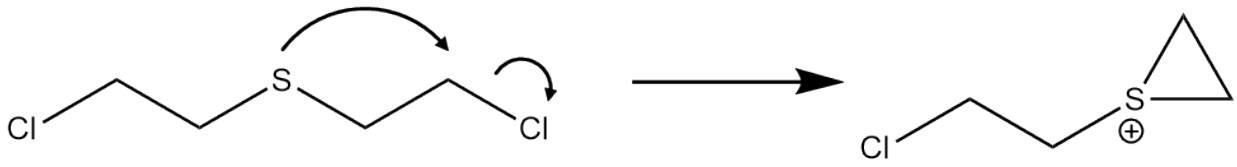


*FIGURE 3.1 Formation of the alkylating agent episulfonium, following the absorption of sulfur mustard by the body. Following the first attack, the reaction will occur a second time, resulting in another sulfonium ion formation.*

The main target of alkylation from sulfur mustard are nucleotides (specifically purine bases) and thiol moieties found in polypeptides, such as glutathione. The alkylation of DNA or protein results in a cross-linking product, that falls into 3 different categories: DNA-DNA (or RNA), DNA-Peptide, or Peptide-Peptide (Figure 3.2).

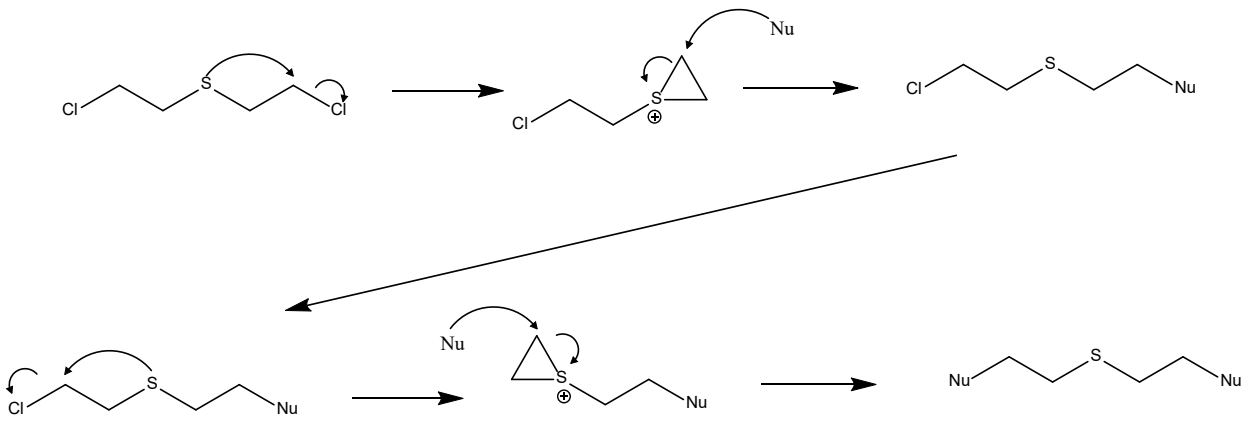


*FIGURE 3.2 Generic mechanism for the formation of adducts of DNA or protein following the alkylation and crosslinking by sulfur mustard. The difference is in protein a thiol (-SH) group is the nucleophile instead of the nitrogen in DNA.*

Past research has showed that the ability of sulfur mustard to form difunctional products is directly related to its toxicity levels, meaning that monofunctional analogs are significantly less toxic to the cell than their difunctional counterparts (1,28). Proteins and peptides alkylated by sulfur mustard react preferentially at free thiols. Dimer formation can occur (2). To better understand the metabolic fate of sulfur mustard a study conducted at the George Washington School of Medicine injected rats, mice, and two terminal cancer patients with dosages of radiolabeled sulfur mustard and monitored their blood, urine and feces (3). It was found that 80-90% of the radioactivity left the blood of humans within minutes, and the 10-20% that remained persisted for multiple days; leading to the conclusion that the sulfur mustard bound permanently to some blood molecules, most likely proteins (3). In the rat and mice studies they determined that 78% and 81% of radioactivity, respectively, left the animals within the first 24 hours, and 87% and 86% left within the first 48 hours, respectively (3). Radioactively labeled sulfur mustard ($^{14}C$) was used to measure the amount of sulfur mustard in rat organs following an IV-injection, it was determined that highest dosages were in the kidney, liver, and lung (34). This

$^{14}C$ study also found that maximum sulfur mustard concentration was found within 2-3 hours of exposure; and radioactivity slowly decreased after 24 hours with almost all radiation was gone within 96 hours (34). When following radioactive sulfur mustard ($^{14}C$) in rats via inhalation, it was found the highest concentrations were in the lungs, liver, and blood within the first 8 hours, but highest in the kidneys after 168 hours (35). It also recorded that measurable levels of radiation were detected in the urine as early as 8 hours, with the majority happening in the first 48 hours; the sulfur mustard had a clearance half-life of about 12.6 hours (35). The most revealing conclusion of the study was approximately 61% of sulfur mustard that enters the body reacts to form mono- or difunctional crosslinked products, the rest is simply metabolized into a form of thiodiglycol and excreted through the urine; and comparatively little appears to react with non-cysteinyl nucelophiles, such as nucleotides or other amino acid side chains (Figure 3.3) (3).

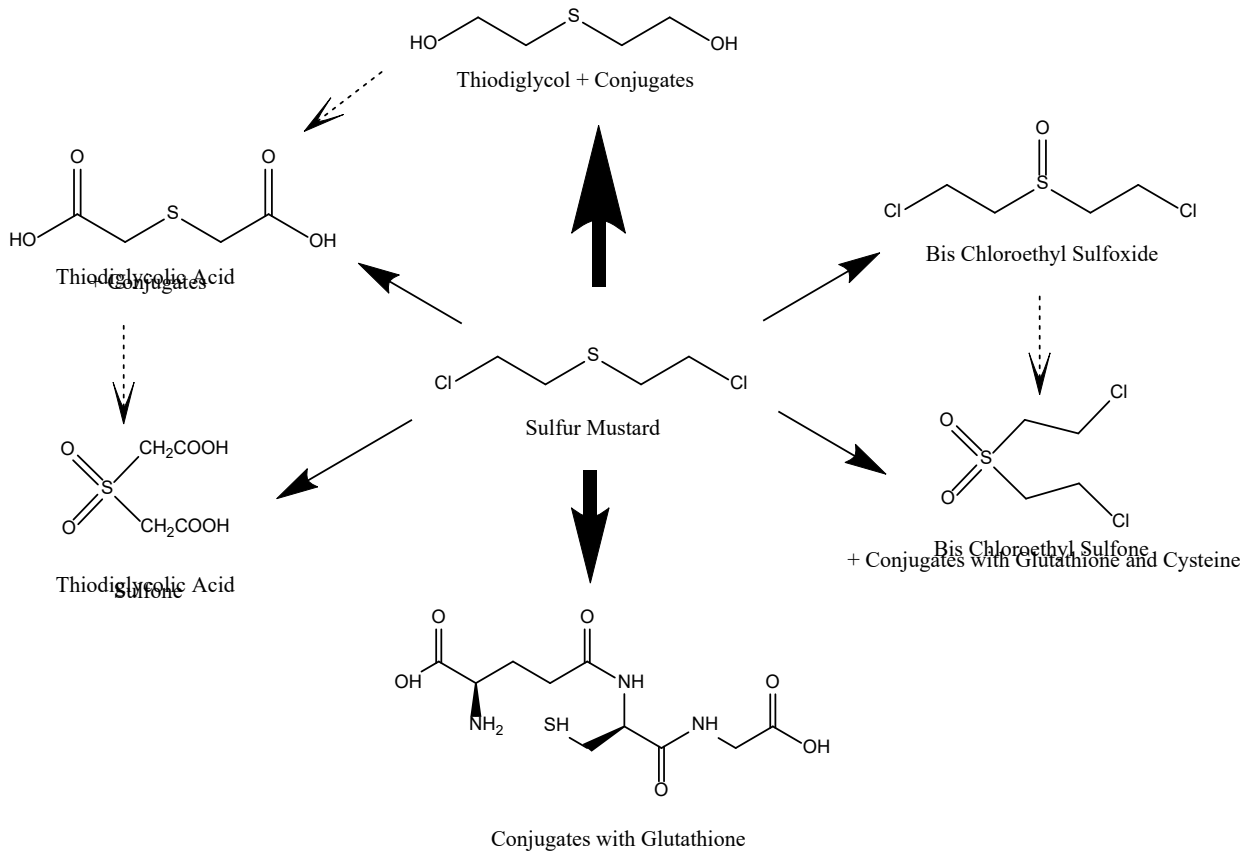


*FIGURE 3.3 Metabolic fate of sulfur mustard following the absorption and reaction within the cells. After (29).*

There are three commonly cited hypotheses to explain damage caused by sulfur mustard exposure. The first hypothesis is that sulfur mustard causes a hyper-activation of the poly (ADP-ribose) polymerase-1 (PARP-1), also known as $NAD^+$ ADP-ribosyltransferase 1, DNA repair pathway, after alkylation of DNA bases. It is proposed that when PARP-1 is hyper-activated it causes a depletion of nicotinamide adenine dinucleotide ($NAD^+$) which leads to cellular apoptosis (4,5). The second hypothesis is that exposure to sulfur mustard causes a depletion in glutathione, the cell's most common and powerful antioxidant, leading to oxidative stress on the cells. It is proposed that this unchecked oxidative stress eventually causes irreversible damage leading to cellular apoptosis (5,6). The third hypothesis is sulfur mustard causes a mass

inflammatory response, that results in cell shedding, cellular death, and chronic inflammation. This runaway response results in the build-up of tumor necrosis factor alpha (TNF-α) and Interleukin proteins (IL) that eventually signals for mass cellular apoptosis (7,8).

The crosslinking of DNA by sulfur mustard results primarily from the alkylation of the N7 positions of guanine and the N3 positions of adenine. These alkylations result in the formation of N7-hydroxyethylthioethyl-guanine (N7-HETE-Gua) and N3-hydroxyethylthioethyl-adenine (N3-HETE-Ade) respectively, but can also result in bi-adduct formation, usually a bi-guanine adduct bis(N7-guanine-ethyl) sulfide (5,9). Quantitative analysis revealed that the DNA adducts form in approximately the following distributions: ~10-42% guanine crosslinks, 1-10% adenine monoadducts, and 60-80% guanine monoadducts (9). It is known that the difunctional adducts are much more toxic than the monoadduct counterparts (33). Although the majority of alkylation products of DNA are monoadducts, they are only named as such because only part of the molecule is alkylated to DNA; the other portion of the molecule can be alkylated to a protein or a peptide.

This crosslinking of DNA leads to the hyper-activation of DNA repair pathways; in particular PARP-1 for DNA double stranded breaks (DSBs) and the base excision repair (BER) pathway for DNA single stranded breaks (SSBs) (4,10). However, since sulfur mustard usually causes DNA DSBs, the focus will be on the PARP-1 pathway. PARP-1 is a 116-kDa protein belonging to a family of 18 proteins; composed of a C-terminal catalytic domain, N-terminal DNA-binding domain, a central auto-modification domain, and nuclear localization sequence (11). PARP-1 is activated by genotoxic stress and binds itself to damaged DNA, specifically DSBs, and signals for DNA repair proteins. It functions by synthesizing poly (ADP)ribose (PAR) via $NAD^+$ for the use of the repair proteins, When PARP-1 is hyper-activated, it can lead to a rapid depletion of

cellular $NAD^+$ levels (11,12). The depletion of $NAD^+$ is occurs because PARP-1 utilizes the $NAD^+$ to synthesize the ADP ribose and also to transfer the PAR moieties to proteins; without an abundance of $NAD^+$ this process would not be possible (10). DNA repair is already an energy intensive and time-consuming process, when there is mass damage to DNA the cell sometimes needs longer to repair the DNA. In these instances, PARP-1 can activate key proteins such as p53, which is a tumor protein and when activated hold the cell in the G1 growth phase; thus, allowing PARP-1 more time to fix DNA damage (4). Once PARP-1 has completed the repair of DNA it signals for caspase-3, catalyzed by ATP, which cleaves PARP-1 from DNA allowing to cell to continue to the S phase of replication (12,13). During the hyper-activation of PARP-1 there is a dramatic decrease in $NAD^+$ in the cell, as well as a dramatic decrease in ATP. When $NAD^+$ is depleted PARP-1 can no longer bind to and recruit DNA repair proteins; and as ATP is depleted caspase-3 can no longer clear PARP-1 from DNA so it remains and uses more $NAD^+$ producing PAR 12,13). When PARP-1 fails, due to the depletion of $NAD^+$ and ATP, it will signal for the cell to enter apoptosis; thus, destroying the cell as to prevent damage during cellular reproduction (4-5,9-13).

The second major hypothesis also revolves around alkylation of peptides; however, the specific focus is on the antioxidant glutathione and the increase of cellular oxidative damage. Glutathione (γ-L-Glutamyl-L-cysteinylglycine) is the most readily abundant low molecular weight cellular antioxidant (Figure 3.4) (14,15). Glutathione exists in two forms: the reduced form, GSH, and the oxidized form, GSSG. The GSH-GGSG couple is the major redox couple in mammalian cells, and this ratio can be used to measure the redox metabolism of cells. (15,16,36). The ratio of GSH-GSSG is very important as the GSH form is what scavenges for free radicals. Glutathione exists in millimolar concertation with a total cellular concentration of 2-17mM, and

exists about 90% in the reduced form (GSH); while in the cytosol glutathione exists ~99.97% in the reduced form (30). The concentration of protein thiols (cysteine) is also vitally important, along with many other proteins it is a key component glutathione and of superoxide dismutase (SOD), which protects the DNA and lipids from oxidation (31). These protein thiols are much more abundant than glutathione, existing at 10-50mM and represent ~70% of the total amount of reduced thiols in the cell (30).

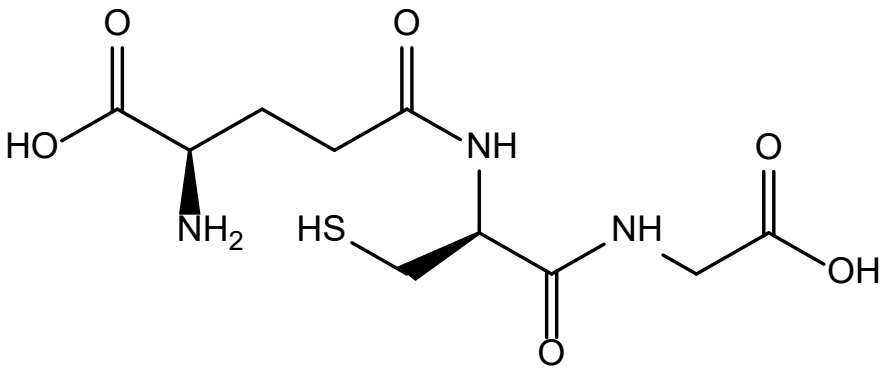


*Figure 3.4 Structure of Glutathione.*

When exposed to sulfur mustard the increase in oxidative stress and reduction of glutathione (GSH) are bonded together through two channels. The first being sulfur mustard can directly form an adduct with GSH thereby removing it from circulation; the second being normal oxidative stress in the cell, such as lipid peroxidation. These normal levels of oxidative stress begin to get out of control because GSH is not available to regulate the levels of stress, to which more antioxidants stores are depleted at a faster rate than they can be regenerated to keep up with the demand in cellular repair. (6,7). The depletion leads to an increase in reactive oxygen species which will eventually damage DNA, proteins, and lipids causing toxic side effects in the cell. One constant in sulfur mustard exposure investigations is the oxidation and modifications of proteins and lipids and a decrease in cellular antioxidant enzyme activity and expression (17).

Multiple independent studies on the exposure of sulfur mustard on rats and mice have found drastically decreased levels of glutathione in the muscles, kidney, lung, and liver cells (7,17). One such study looked at the levels of glutathione S-transferase (GST) activity in the liver and lung; they found a significant decrease activity and production which enhances the cells reactive oxygen species and oxidative damage (18). Glutathione S-transferase is also significant as it can act as a regulator molecule that ultimately results in the cell entering apoptosis. As glutathione is depleted and the GST activity is decreased there is a decrease in regulation of apoptosis factors. One factor in particular, caspase 3, has been shown to have an increased activity in affected cells, this increased activity triggers the cell to enter apoptosis (7).

The first two hypothesis contain major similarities and differences with each other but differ in which molecules are being affected (DNA or proteins). However, they are actually more connected, one key toxic product of sulfur mustard exposure has been shown to be bi-adducts of glutathione and DNA (Figure 3.5). An effective detection system was developed to specifically look for these DNA-GSH adducts and experiments were then carried out on rodents.

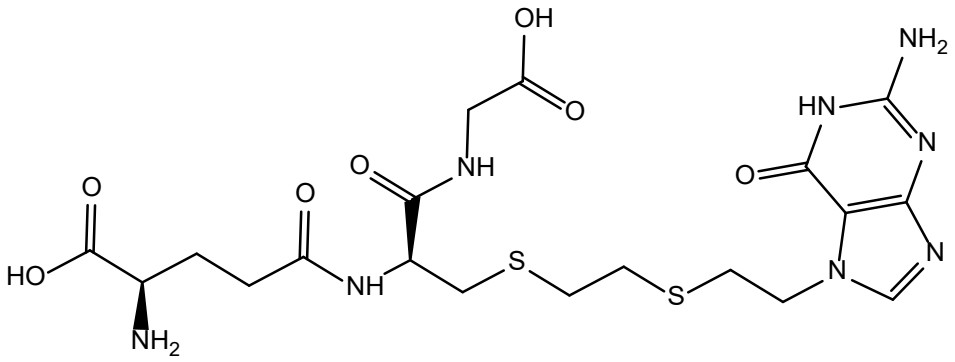


*FIGURE 3.5 Glutathione – DNA (GSH-DNA) adduct, one of the most toxic products of sulfur mustard exposure.*

The product of significance was the S-[2-(N7-guanyl)-ethylthioethyl]-glutathione (N7Gua-ETE-GSH) adduct, which is glutathione cross-linked to the N7 position of guanine in DNA (6,19). The N7Gua-ETE-GSH is the only major DNA-protein adduct that was found when looking at both rodent and human samples (19). One study sought to determine how much of this adduct was formed and what the concentrations were like in various organs. Rodent skin was exposed to sulfur mustard and monitored from 2 hours to 3 weeks. The results showed the formation of the N7Gua-ETE-GSH adduct in a concertation of 91±15 adducts per $10^6$ normal bases just 2 hours after exposure (6). It was determined the half-life of N7Gua-ETE-GSH was only 2.5 days, and no longer detectable in various organs after 2 weeks. The ranking of adduct formation in various organs was found to be as follows, brain > lungs > kidneys > spleen, with the brain being the highest and the spleen the lowest. This N7Gua-ETE-GSH adduct was determined to be a key marker of the mutagenetic activity and toxicity of sulfur mustard (6).

The final widely accepted hypothesis used to explain the physiological effects of sulfur mustard exposure revolves around inflammation. Inflammation is the one of the body's first responses to injury and is often a very generic and non-descript response. In sulfur mustard exposure victims' inflammation of the exposure sight is usually one of the first physical symptoms; red irritated and raised skin accompanied by large fluid filled blisters will usually occur in the first 24-48 hours following exposure. After the initial symptoms victims of exposure often deal with chronic inflammation, especially in the lungs, mass necrosis, and shedding of the epithelial cells. This inflammatory response of mass necrosis and epithelial cell shedding usually occur during a high dosage of skin exposure to sulfur mustard, usually in liquid form, as opposed to inhalation exposure. Since most lethal sulfur mustard exposure happens via gas and aerosol exposure, most research and studies have focused on inflammation of the lungs and airways. The results of this

research found 3 major proteins, or families of proteins, to be key culprits: surfactant protein-D (SP-D), tumor necrosis factor-alpha (TNF-α), and the interleukin (IL) family specifically IL-1, IL-6, IL-8, IL-12 (8,20-22). When cells are first exposed to sulfur mustard a sudden and rapid increase of TNF-α and IL proteins occur. These are destructive pro-inflammatory cytokines that result in cellular apoptosis and have been linked directly to massive cellular shedding (20). One study looking at the lungs of rodents found that following exposure there was a massive upregulation of TNF-α, whereas in the baseline samples there was no TNF-α found in lung cells (21). The increase in TNF-α triggers apoptosis, which results in the release of ATP and crystallized uric acid (5). Normally this is not an issue and easily controlled; however, when a large number of cells are dying at once the mass release of these two compounds signals for the production of the IL proteins. The IL family of proteins are inflammatory recruitment cytokines, that recruit more inflammation to the area, and can trigger cellular apoptosis ultimately resulting in more cellular death. Normally this vicious cycle of inflammation in the lungs is controlled by SP-D, which negatively regulates lung inflammation; however, through some undiscovered mechanism sulfur mustard significantly decreases SP-D expression (21). The decrease is SP-D expression has also been linked to an increase in cellular susceptibility to reactive oxygen specials and oxidative damage (21).

Of the accepted hypotheses for the physiological response to sulfur mustard exposure, the first two hypotheses, alkylation of DNA and depletion of glutathione, are easily connected, while the third hypothesis, revolving around inflammation, is a more generic response and appears harder to piece together with alkylation, but actually fits perfectly. Both crosslinking based hypothesis result in cellular apoptosis, cellular apoptosis results in an inflammation response. The reduction in glutathione results in an increase in reactive oxygen species, this increase also triggers an

inflammation response. These three hypotheses are so interconnected that it seems they can trigger and amplify each other (Figure 3.6). Although these three hypotheses do a comprehensive job at explaining many symptoms of sulfur mustard exposure, there are still many common symptoms that do not fit directly into these hypotheses.

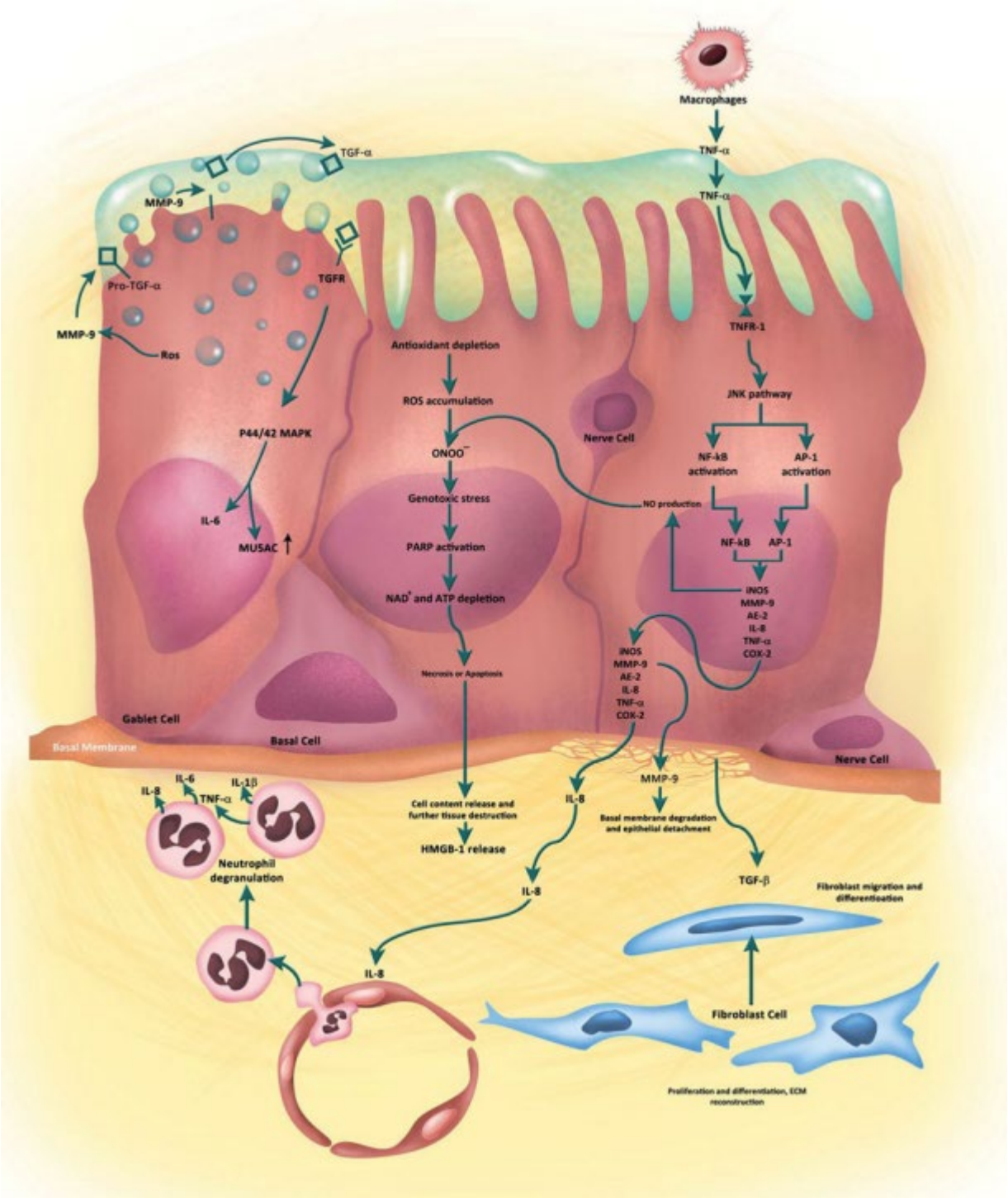


*FIGURE 3.6 Pictural representation of the connection of all three major accepted hypotheses; The cross-linking of DNA-DNA, protein-protein, and inflammation. Representation demonstrates how each hypothesis can trigger the other and/or amplify the damages caused by the other. Figure from (5).*

The overall effects of sulfur mustard exposure include a long list of various symptoms that take hours or even days to develop. The exact mechanism of action to support these symptoms is not fully understood either. Most common symptoms of exposure include: lung irritation, blister formation, skin irritation and necrosis, temporary blindness, short-term memory loss, slow healing wounds, fatigue and weakness, nausea, vomiting, diarrhea, anemia, and many more (23-27). As previously stated, the typical timeline for exposure symptoms to appear are as follows: earliest skin irritation ~ 1 hour, raised and irritated skin ~8-12 hours, blister formation ~16-48 hours, maximum blister formation and skin necrosis ~45-72 hours, complete skin loss ~6-9 days, and finally complete healing in ~22-29 days (23). The most debilitating symptoms of sulfur mustard exposure are those that take hours or days to heal, such as blisters, skin irritation, and lung problems are explained by the commonly accepted hypotheses of sulfur mustard exposure. Following blister formation and healing, one such symptom of skin liquid exposure is the hyper- or hypopigmentation of the skin. It is believed that hyperpigmentation is caused by the reduced of intracellular glutathione levels, and that hypopigmentation is caused by the destruction of melanocytes (melanin producing cells); some studies have shown that these melanocytes are the most susceptible cell type of sulfur mustard exposure (37,38).

Although major known symptoms of mustard gas can be explained by the hypotheses above, there are many more common symptoms that do not have an explanation or are not fully explained. For example, it is known why the blisters form on skin after exposure; however, it remains unexplained why these blisters take longer to heal and why they are more painful than normal (32). Impaired cognition is also a commonly reported symptom of mustard gas exposure that is not understood, but there is dose dependent relation between memory issues and sulfur mustard exposure (24). Other unexplained symptoms include blindness lasting multiple days,

diarrhea, nausea, vomiting, increased infections, fatigue, and weakness (23-27). It could be possible that some of these symptoms are the result of decreased key metallic micronutrients required for normal functionality, through the chelation of these metals by these sulfur mustard exposure products.

### 3.2 References


1. Roberts, J.; Pascoe, J.; Plant, J.; Sturrock, J.; Crathorn, A. Quantitative aspects of the repair of alkylated DNA in cultured mammalian cells: I. The effect on HeLa and Chinese hamster cell survival of alkylation of cellular macromolecules. *Chemico-Biological Interactions* **1971**, *3* (1), 29-47.

2. Byrne, M. P.; Broomfield, C. A.; Stites, W. E. Mustard gas crosslinking of proteins through preferential alkylation of cysteines. *Journal of protein chemistry* **1996**, *15* (2), 131-136.

3. Davison, C.; Rozman, R. S.; Smith, P. K. Metabolism of bis-β-chloroethyl sulfide (sulfur mustard gas). *Biochemical pharmacology* **1961**, *7* (1), 65-74.

4. Anderson, D.; Benton, B.; Wang, Z.-Q.; Smith, W.; Ray, R.; Rosenthal, D. S.; Simbulan-Rosenthal, C. M.; Liu, W. F.; Velena, A.; Smulson, M. E. PARP determines the mode of cell death in skin fibroblasts, but not keratinocytes, exposed to sulfur mustard. *Journal of investigative dermatology* **2001**, *117* (6), 1566-1573.

5. Nourani, M. R.; Mahmoodzadeh Hosseini, H.; Azimzadeh Jamalkandi, S.; Imani Fooladi, A. A. Cellular and molecular mechanisms of acute exposure to sulfur mustard: a systematic review. *Journal of Receptors and Signal Transduction* **2017**, *37* (2), 200-216.

6. Batal, M.; Rebelo-Moreira, S.; Hamon, N.; Bayle, P.-A.; Mouret, S.; Cléry-Barraud, C.; Boudry, I.; Douki, T. A guanine-ethylthioethyl-glutathione adduct as a major DNA lesion in the skin and in organs of mice exposed to sulfur mustard. *Toxicology letters* **2015**, *233* (1), 1-7.

7. Pohanka, M.; Stetina, R.; Svobodova, H.; Ruttkay-Nedecky, B.; Jilkova, M.; Sochor, J.; Sobotka, J.; Adam, V.; Kizek, R. Sulfur mustard causes oxidative stress and depletion of antioxidants in muscles, livers, and kidneys of Wistar rats. *Drug and chemical toxicology* **2013**, *36* (3), 270-276.

8. Ahmad, S.; Ahmad, A. Emerging targets for treating sulfur mustard–induced injuries. *Annals of the New York Academy of Sciences* **2016**, *1374* (1), 123-131.

9. Mangerich, A.; Debiak, M.; Birtel, M.; Ponath, V.; Balszuweit, F.; Lex, K.; Martello, R.; Burckhardt-Boer, W.; Strobelt, R.; Siegert, M. Sulfur and nitrogen mustards induce characteristic poly (ADP-ribosyl) ation responses in HaCaT keratinocytes with distinctive cellular consequences. *Toxicology letters* **2016**, *244*, 56-71.

10. Jowsey, P. A.; Williams, F. M.; Blain, P. G. DNA damage responses in cells exposed to sulphur mustard. *Toxicology letters* **2012**, *209* (1), 1-10.

11. Sethi, G. S.; Dharwal, V.; Naura, A. S. Poly (ADP-ribose) polymerase-1 in lung inflammatory disorders: a review. *Frontiers in immunology* **2017**, *8*, 1172.

12. Hinshaw, D. B.; Lodhi, I. J.; Hurley, L. L.; Atkins, K. B.; Dabrowska, M. I. Activation of Poly [ADP-Ribose] Polymerase in Endothelial Cells and Keratinocytes: Role in anin VitroModel of sulfur mustard-Mediated Vesication. *Toxicology and applied pharmacology* **1999**, *156* (1), 17-29.

13. Tahmasbpour, E.; Reza Emami, S.; Ghanei, M.; Panahi, Y. Role of oxidative stress in sulfur mustard-induced pulmonary injury and antioxidant protection. *Inhalation toxicology* **2015**, *27* (13), 659-672.

14. Meister, A.; Anderson, M. E. Glutathione. *Annual review of biochemistry* **1983**, *52* (1), 711-760.

15. Wu, G.; Fang, Y.-Z.; Yang, S.; Lupton, J. R.; Turner, N. D. Glutathione metabolism and its implications for health. *The Journal of nutrition* **2004**, *134* (3), 489-492.

16. Halprin, K. M.; Ohkawara, A. The measurement of glutathione in human epidermis using glutathione reductase. *J. Invest. Dermatol* **1967**, *48* (2), 149.

17. Kaboudanian Ardestani, S.; Taravati, A.; Kianmehr, Z.; Hajizadeh Dastjerdi, A.; Pourfarzam, S.; Soroush, M. R.; Naghizadeh, M. M.; Ghazanfari, T. Altered levels of GST activity, Vit C, TPX and Cu in individuals with long-term sulfur mustard-induced lung complications. *Inhalation Toxicology* **2018**, *30* (13-14), 483-491.

18. Varmazyar, M.; Kianmehr, Z.; Faghihzadeh, S.; Ghazanfari, T.; Ardestani, S. K. Time course study of oxidative stress in sulfur mustard analog 2-chloroethyl ethyl sulfide-induced toxicity. *International immunopharmacology* **2019**, *73*, 81-93.

19. Koga, N.; Inskeep, P. B.; Harris, T. M.; Guengerich, F. P. S-[2-(N7-guanyl) ethyl] glutathione, the major DNA adduct formed from 1, 2-dibromoethane. *Biochemistry* **1986**, *25* (8), 2192-2198.

20. Keyser, B. M.; Andres, D. K.; Holmes, W. W.; Paradiso, D.; Appell, A.; Letukas, V. A.; Benton, B.; Clark, O. E.; Gao, X.; Ray, P. Mustard gas inhalation injury: therapeutic strategy. *International journal of toxicology* **2014**, *33* (4), 271-281.

21. Malaviya, R.; Sunil, V. R.; Cervelli, J.; Anderson, D. R.; Holmes, W. W.; Conti, M. L.; Gordon, R. E.; Laskin, J. D.; Laskin, D. L. Inflammatory effects of inhaled sulfur mustard in rat lung. *Toxicology and applied pharmacology* **2010**, *248* (2), 89-99.

22. Ghanei, M.; Poursaleh, Z.; Harandi, A. A.; Emadi, S. E.; Emadi, S. N. Acute and chronic effects of sulfur mustard on the skin: a comprehensive review. *Cutaneous and ocular toxicology* **2010**, *29* (4), 269-277.

23. Smith, W. J.; Dunn, M. A. Medical defense against blistering chemical warfare agents. *Archives of dermatology* **1991**, *127* (8), 1207-1213.

24. Pinkston, J. B. *Neuropsychological effects of acute mustard gas exposure*; Louisiana State University and Agricultural & Mechanical College, 2001.

25. Thomsen, A. B.; Eriksen, J.; Smidt-Nielsen, K. Chronic neuropathic symptoms after exposure to mustard gas: a long-term investigation. *Journal of the American Academy of Dermatology* **1998**, *39* (2), 187-190.

26. Rafati-Rahimzadeh, M.; Rafati-Rahimzadeh, M.; Kazemi, S.; Moghadamnia, A. A. Therapeutic options to treat mustard gas poisoning–Review. *Caspian Journal of Internal Medicine* **2019**, *10* (3), 241.

27. Le, H.; Knudsen, S. Exposure to a First World War blistering agent. *Emergency medicine journal* **2006**, *23* (4), 296-299.

28. Gros-Désormeaux, F.; Caffin, F.; Igert, A.; Guatto, N.; Piérard, C. Is CEES a good analog of sulfur mustard? Macroscopic aspect, histology, and molecular biology comparisons between sulfur mustard and CEES-induced skin lesions. *Toxicology Letters* **2022**, *361*, 21-28.

29. Rall, D. P.; Pechura, C. M. Veterans at risk: The health effects of mustard gas and lewisite. **1993**.

30. Turell, L.; Radi, R.; Alvarez, B. The thiol pool in human plasma: the central contribution of albumin to redox processes. *Free Radical Biology and Medicine* **2013**, *65*, 244-253.

31. Ulrich, K.; Jakob, U. The role of thiols in antioxidant systems. *Free Radical Biology and Medicine* **2019**, *140*, 14-27.

32. Guthrie, F. XIII. —On some derivatives from the olefines. *Quarterly Journal of the Chemical Society of London* **1860**, *12* (1), 109-126.

33. Sawyer, T. W.; McNeely, K.; Louis, K.; Lecavalier, P.; Song, Y.; Villanueva, M.; Clewley, R. Comparative toxicity of mono-and bifunctional alkylating homologues of sulphur mustard in human skin keratinocytes. *Toxicology* **2017**, *382*, 36-46.

34. Maisonneuve, A.; Callebat, I.; Debordes, L.; Coppet, L. Distribution of [14C] sulfur mustard in rats after intravenous exposure. *Toxicology and applied pharmacology* **1994**, *125* (2), 281-287.

35. Benson, J. M.; Tibbetts, B. M.; Weber, W. M.; Grotendorst, G. R. Uptake, tissue distribution, and excretion of 14C-sulfur mustard vapor following inhalation in F344 rats and cutaneous exposure in hairless guinea pigs. *Journal of Toxicology and Environmental Health, Part A* **2011**, *74* (13), 875-885.

36. Giustarini, D.; Colombo, G.; Garavaglia, M. L.; Astori, E.; Portinaro, N. M.; Reggiani, F.; Badalamenti, S.; Aloisi, A. M.; Santucci, A.; Rossi, R. Assessment of glutathione/glutathione disulphide ratio and S-glutathionylated proteins in human blood, solid tissues, and cultured cells. *Free Radical Biology and Medicine* **2017**, *112*, 360-375.

37. Müller-Dott, K.; Thiermann, H.; Steinritz, D.; Popp, T. Effect of sulfur mustard on melanogenesis in vitro. *Toxicology Letters* **2020**, *319*, 197-203.

38. Brown, R.; Rice, P. Histopathological changes in Yucatan minipig skin following challenge with sulphur mustard. A sequential study of the first 24 hours following challenge. *International journal of experimental pathology* **1997**, *78* (1), 9-20.

**Chapter 4**

**Metal Micronutrients: Their Importance and Deficiency Symptoms – A Review**

**4.1 Introduction**

The organic elements, C, H, O, N, and S, are those most associated with the human body. However, the majority of the known elements exist in the body in some amount and many play vital roles. Approximately 50 elements are found within the body at some measurable quantity, but only about 26 of these 50 are considered essential (1,2). These physiologically essential elements may be broken down into three categories: organic/bulk elements (96%), macro-minerals (3-4%), and trace elements or metal micronutrients (0.02%) (Figure 4.1) (1-4).

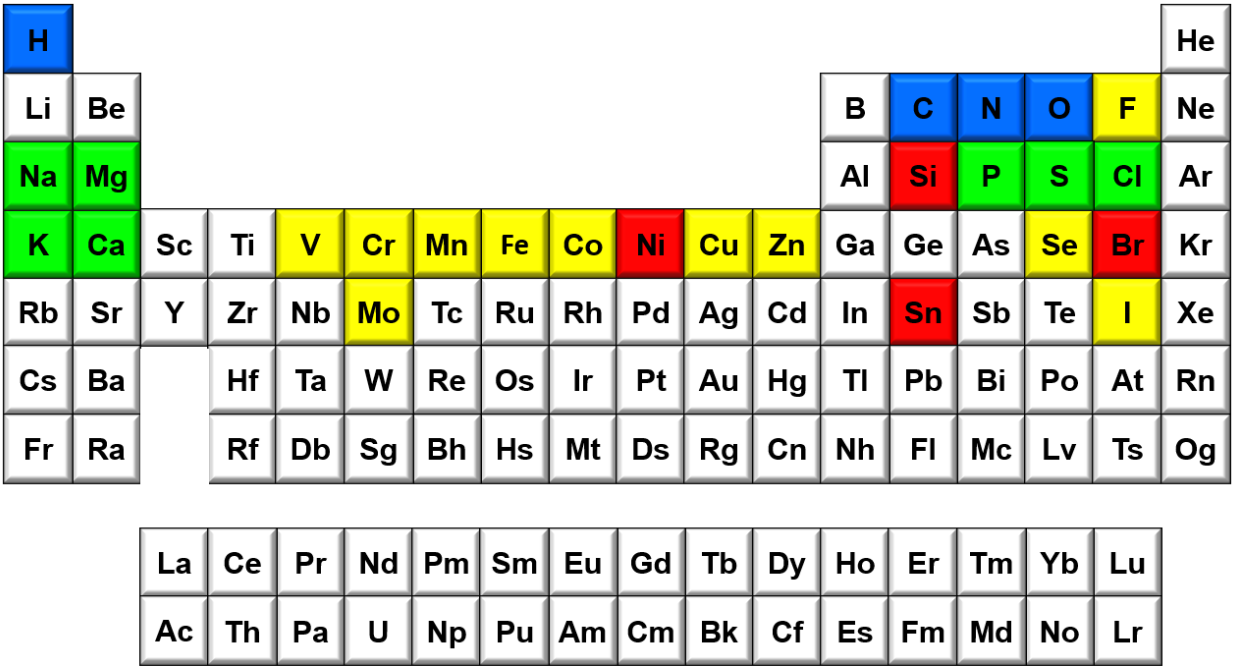


*Figure 4.1 26 Essential elements in the human body divided amongst 3 categories: Organic/Bulk (Blue), Macro-Minerals (Green), Trace Elements (Yellow & Red).*

**Elements colored in red are considered "essential" by some publications but not by others*

The organic/bulk elements are carbon, oxygen, nitrogen and hydrogen; and are all found in amounts well over 1 kilogram in an average 70-kilogram (155 pound) adult (3). The elements classified as macro-minerals are found in ranges from 1 kilogram to 10s of grams: sodium,

potassium, magnesium, calcium, sulfur, phosphorus and chlorine (2,3). The final category of "trace elements" is comprised of about 11 elements: vanadium, molybdenum, manganese, iodine, chromium, selenium, cobalt, nickel, copper, iron, selenium, fluorine, and zinc; and the amounts found in the human body range from several grams (iron ~5g, zinc ~2g) to hundreds of milligrams (copper ~70-100mg) to milligrams (cobalt ~1-2mg) (1-6). There are no concrete definitions for in which category each element truly belongs. For example, sulfur is occasionally classified under the "bulk" element category, iron and zinc are considered by some too high in quantity to be considered "trace", and nickel is often not classified as essential (1-5).

For this dissertation only five of the trace elements will be examined: nickel, manganese, copper, cobalt, and zinc. All five of these elements are known to have high affinities for sulfur and, with the exception of nickel, play vital roles in normal physiological processes. Too much or too little of each can cause physiological problems (7,8). They are found in the body, of course, not as elemental metals, but cations, usually divalent. Although the focus of this chapter is on what happens when the body becomes deficient in these elements, it should be noted that excess of any trace elements can have deadly consequences. Excess zinc for example can cause copper deficiency and reduced immune function; whereas excess copper can cause liver injury, dementia, and even death (1,2).

In the past it had been very difficult to accurately determine the amount of each trace element in the body, and some were at such low detectable levels they could be considered "ultra-trace", such as with nickel (4). However, with the advances in neutron activation analysis and inductively coupled plasma mass spectroscopy (ICP-MS), all these elements can now be detected with much higher precision and accuracy (9,10). For the five elements concerned the expected amounts for a 70-kilogram adult man are as follows: zinc ~2g, copper ~70-100mg, manganese

~16-40mg, nickel ~15mg, and cobalt ~1-2mg (2,6). Along with the amounts of each element, it is helpful to understand where these elements are physiologically concentrated along with their most abundant form.

Zinc is found is all organs of the body, but in the highest concentration as follows: liver > muscle > kidney > pancreas > heart (9). Zinc is most abundantly found in the $Zn^{2+}$ form and its transport controlled by two classes of proteins, zinc transporters (ZnTs) and zinc importer proteins (ZIPs) (11,12). The family of ZnT proteins are responsible for moving zinc out of the cytosol and round the body, while ZIPs are responsible of importing the zinc into the cytosol (12).

Copper was found to have the highest concentrations in the liver, brain, and heart; while still a high concentration was found in the kidney, just slightly lower than the previous organs (9). Only about 10% of copper is found in the plasma or blood, the remining 90% is stored or utilized in the organs (13). Nearly all functional copper is found in the $Cu^{2+}$ ionic form. However, it is important to remember that the $Cu^{+}$ form is readily accessible and conversion between Cu(I) and Cu(II) is often an important part of its function as an enzyme cofactor. The polypeptide chain ceruloplasmin (CP, α-2-globulin) dominates copper transport and is responsible for over 90% of copper transportation (1,13,14).

Manganese falls in the middle of the pack with anywhere from 16-40mg found in the body, with women tending to have more than men (2,9). Manganese is primarily located in the mitochondria and Golgi apparatus; with the highest concentrations in organs being: liver > kidney > pancreas > lung > heart > spleen (2,9,20). With oxidation states ranging from $Mn^{3-}$ to $Mn^{7+}$ it is more versatile than the others; however, the two most common oxidation states in the body are $Mn^{2+}$ and $Mn^{3+}$ (20,48). Manganese is absorbed through digestion and gets transported from the gut to the bloodstream as $Mn^{3+}$ in the Mn-transferrin complex then is converted to $Mn^{2+}$ to be utilized

by enzymes such as manganese superoxide dismutase (MnSOD) (2,48,59). Once absorbed into the blood, manganese is transported throughout the body by zinc transporters ZIP8 and ZnT10, as well as albumin and α2-macro-globulin; since it also crosses the blood-brain barrier a special transporter enzyme known as divalent metal transporter 1 (DMT1) carries manganese into the brain (48,49,51).

Of all trace elements, nickel is the most mysterious, in fact there is very little published literature about nickel's role in the human body, which is why it is often not considered an essential element. Nickel is known to have the highest concentrations in the lungs and thyroid, followed closely by the kidney, brain, and liver (15). Only ten nickel dependent enzymes have been characterized between all archaea, bacteria, plants, and primitive eukaryotes, but none of these enzymes have been identified yet in humans. If a human version of one of these nickel-containing enzyme exists, nickel is often replaced with zinc or the human version does not require a metal ion (42). If it is an essential element for humans, the functional form of nickel is presumably $Ni^{2+}$. While its exact mechanism of transport is unknown, the primary routes of absorption are food or through the lungs and into the blood stream (16).

Cobalt has the lowest concentration of all essential trace elements. It is primarily found in the heart, kidney, liver, and spleen; but it can also be found in blood serum, heart, and pancreas (9,17). Cobalt is almost exclusively found within Vitamin $B_{12}$, this vitamin is unique because it involves the corrin ring allowing for cobalt to exists in three different oxidation states ($Co^{+}$, $Co^{2+}$, and $Co^{3+}$) (17,18). Although all three oxidation states of cobalt are found in the body, the $Co^{3+}$ form is the most common (18). Like its periodic neighbor nickel, little is known about how cobalt is transported throughout the body.

Concentration and distribution are interesting, but function of these metals is more important. Some information about these five metals: manganese, copper, nickel, cobalt and zinc are summarized and highlighted in Table 4.1, for easy access.

*Table 4.1 Summarization of Select Trace Elements, Their Concentrations, Locations, Key Enzymatic Functionality, and Deficiency Symptoms.*

| Metal | Amount Present [a] | Functional Form | Primary Location | Key Proteins or Enzymes | Deficiency Symptoms |
|---|---|---|---|---|---|
| Zinc | 2.3g, $7.82 \times 10^{-4}$ M | $Zn^{2+}$ | Liver, Muscle, Kidney, Heart | Cu,Zn Superoxide Dismutase (SOD1, SOD3), Zinc Finger Proteins (ZFPs) | Oxidative Stress, Chronic Inflammation, Recurrent Infections, Diarrhea, Delayed Wound Healing, & Impaired Cognitive Function |
| Copper | 70mg, $2.45 \times 10^{-5}$ M | $Cu^{+}$, $Cu^{2+}$ | Liver, Brain, Heart | Cu,Zn Superoxide Dismutase (SOD1, SOD3), Lysyl Oxidase (LOX) | Oxidative Stress, Defects in the Elastin-Collagen Connection, Delayed Wound Healing, & Anemia |
| Manganese | $\geq$ 40mg, $1.62 \times 10^{-5}$ M | $Mn^{2+}$, $Mn^{3+}$ | Liver, Kidney, Pancreas | Mn Superoxide Dismutase (MnSOD), Glutamine Synthase, Prolidase | Dermatitis, Impaired Cognitive Function, Decreased Levels of Clotting, Connective Tissue Issues |
| Nickel | 15mg, $5.68 \times 10^{-6}$ M | $Ni^{2+}$ | Lung, Thyroid, Kidney, Liver, Brain | N/A | Decreased Levels of Iron Absorption |
| Cobalt | 1-2mg, $5.66 \times 10^{-7}$ M | $Co^{3+}$, $Co^{2+}$, $Co^{+}$ | Liver, Kidney, Heart | Vitamin $B_{12}$, Methionine Aminopeptidase | Fatigue/Weakness, Short-Term Memory Loss, Diarrhea, & Poor Vision |

[a] *Amounts present are average under the assumption of an average adult weighing 70kg, and concentrations are under the assumption a normal 70kg man contains 45 liters of fluid.*

These trace elements may be very low in concertation, but our bodies would literally die without them. More than 50% of all known enzymes require a metal ion to function at some point in their catalytic cycle (3). Of the five metals being examined, zinc is not only found in the highest

concentration but perhaps plays the most versatile and widespread role in physiological functions. In fact, out of any of the micronutrients classified as “essential” zinc is known to play a larger physiological function than any of the others. Zinc has been shown to have a vital role in over 300 enzymatic functions and bind to more than 3000 proteins (3,11). For example, one key functionality of zinc is in the regulation of DNA replication and transcription via Zinc Finger Proteins (ZFPs). ZFPs are so important to the human body that it is estimated that 3% of all genes in the human genome involve a zinc finger (19). In terms of the immune system, the concentration of zinc within cells can act as a signaling mechanism for pro-inflammation cytokines such as: IL-1β, IL-6, and TNF-α (20). When combined zinc and copper unlock the functionality of Cu,Zn Superoxide Dismutase (SOD1), one of the key free radical scavengers of the body (21).

Along with free radical scavenging, copper plays many pivotal roles from cell signaling to cellular proliferation. Although there are many more that could be cited, copper can be associated with two key enzymatic functions. The first is in cytochrome c oxidase, the final step in the electron transport chain (22,25). Another enzyme that requires copper to function is lysyl oxidase (LOX), a key component of the crosslinking of collagen and elastin (22). When new collagen and elastin are required by the body there is usually a wound involved. Along with its role in LOX, copper is a known modulator for angiogenesis, the process by which new blood vessels are formed (23,24). Copper being the modulator for such an important process as angiogenesis has actually made it a target for cancer research, as without the growth of new blood vessels tumors would starve and cancer could not replicate (23,25).

Manganese plays vital roles in the body specifically with the free radical protection of the mitochondria, in the enzyme MnSOD; other enzymes it found bound to include pyruvate

carboxylase, glutamine synthase, glycosyltransferase, and prolidase (48,51,53). MnSOD is the mitochondria's lead protectant against oxidative damage by converting superoxide to hydrogen peroxide and oxygen gas (53). Glutamine synthase is the most abundant manganese containing enzyme in the body, and plays the key role of detoxifying the brain of ammonia, and the regulation of glutamate (48). The glycosyltransferase is responsible for the production of bone and collagen, while prolidase is responsible for collagen synthesis and cellular growth (51).

Unlike manganese, copper, and zinc, very little is known about the enzymatic functionality of nickel. In fact, across all types of life, archaea, bacteria, and eukarya there are only 10 known nickel-containing enzymes (26). Of these 10 enzymes, only glyoxalase I is found in humans; however, humans use zinc as its metal ion instead of nickel (27). To date, there are no known human enzymes requiring nickel ions to function. Although the understanding is poor, there is still a biological function for nickel, at least in organisms such as plants and bacteria. It has been shown to play a role in cellular membrane and lipid synthesis, been tied to iron uptake, and red blood cell production (28). Though nickel is utilized in these processes, how it is utilized remains undetermined.

Cobalt is synonymous with Vitamin $B_{12}$ (cobalamin) and approximately 85% of all physiological cobalt is bound in Vitamin $B_{12}$ (29). While cobalamin plays important roles in cognitive function and DNA metabolism; cobalt also exists in the enzyme methionine aminopeptidase, a key enzyme in the regulation of protein turnover (30,31).

As these trace elements are found in the body in such small quantities, deficiencies are rare but do occur. Less is known on the short term symptoms of deficiency as most research is often focused on long term deficiency. Further, it should also be noted that since many of these trace elements are highly interconnected a slight deficiency in one can led to a decrease in another.

Deficiency in these trace elements is so rare that more is known about the toxicity of excesses; people are more likely to suffer from metal poisoning than deficiency, specifically with nickel.

It is known that short term zinc deficiencies can lead to oxidative stress, chronic inflammation, diarrhea, delayed wound healing, recurrent infections, impaired cognitive function, hair loss, and skeletal system issues (21,33,36). Most copper deficiency is short lived as long-term copper deficiency is infrequent due to low daily requirements. However, short term copper deficiency results in: oxidative stress, defects in collagen-elastin connections, anima, impaired immunity, irregular heartbeats, and delayed wound healing (32,37,38). Manganese deficiency can last for months, but upon supplementation symptoms disappear rapidly. The symptoms of deficiency can include: transient dermatitis, impaired cognitive function, connective tissue issues, decreased levels of clotting, and increased pain sensitivity. (4,51-52). Cobalt deficiency is possibly the most unusual as the body requires so little of the element. Known symptoms of deficiency include fatigue or weakness, short-term memory loss, diarrhea, and poor or temporary loss of vision (39,40). A deficiency is nickel is so uncommon that the only effect noted in literature is that low levels of nickel lead to poor iron absorption, which in turn can lead to anemia (28,41).

When focusing on the three most researched of these trace elements, manganese, copper and zinc, it is obvious they all play pivotal roles in wound healing, especially if there is a burn wound involved. (32-34). This is of particular interest as a key result of sulfur mustard exposure, specifically of liquid exposure, are blistering wounds (burns) that are difficult and slow to heal.

Most literature on wound healing and specifically burn wounds, revolves around thermal burns, as they are the most common. However, a few studies do exist comparing chemical burns caused by sulfur mustard to thermal burns. Two separate studies conducted using porcine skin compared the transcriptional changes occurring in sulfur mustard burns and thermal burns (46,47). In both

studies it was determined that was significant overlap in both up-regulated and down-regulated transcription profiles. One study found that at least 67% of the down-regulated transcripts were common in both sulfur mustard and thermal burns; while at least 77% of up-regulated transcripts were shared (46). Both studies also concluded that 7 of the 10 most common significantly changed biological functions of both mustard and thermal burn wounds overlap, these include: cellular movement, tissue development, cellular growth and proliferation, tissue morphology, hematological system development and function, cell-to-cell signaling and integration, and immune response (46,47). Although there are noted specific biological differences in response to sulfur mustard and thermal burns, these burn types are similar enough that information learned about trace elements in thermal burns also may apply to mustard burns.

Some work has found that there are massive drops in serum levels of manganese, copper, and zinc following a thermal burn wound, and these low levels can persist from weeks to months even with metal supplementation (32,33,43,50). There is an inverse correlation between serum levels of copper and the size of the thermal burn area, and much of the copper stores in the body are lost to exudation during the healing process (32,43). A study conducted on patients burned over 33% BSA (total body surface area affect by burn) found that exudative losses of copper was 10-40% and zinc was 10% each, of the body's total content (43). Both copper and zinc play direct roles in the formation of granulation tissue, the stabilization of new collagen production, angiogenesis, and keeping the levels of reactive oxygen species (ROS) under control (34,35). Copper plays a key role in at least three separate wound healing enzymes: it directly binds to angiogenin which induces blood vessel formation, it stabilizes hypoxia-inducible factor-1α which induces vascular endothelial growth, and directly binds to LOX which stabilizes collagen fibrils (24,44). The key enzymes dependent of zinc for functionality include alkaline phosphatase

which is an associated with angiogenesis, DNA polymerase which are needed for cell proliferation, and the family of matrix metalloproteinases (MMPs). Specific zinc MMPs include collagenases, important for collagen degradation, stromelysins, crucial for connective tissue remodeling, and gelatinases A & B, which cleave gelatin (45). There is not much literature on the direct role of manganese in wound or burn healing; however, it is known to play roles in both collagen formation and cartilage growth (51). While the copper enzyme LOX helps stabilize collagen fibrils, the manganese enzyme prolidase helps aid in new collagen synthesis; and if there were also damage to cartilage during an injury, then manganese would be needed in the enzyme glycosyltransferase (44, 51). Without sufficient levels of manganese, copper or zinc, wounds would take a long time to heal; published literature has shown that supplementation with manganese, copper and zinc allows for a decrease in wound healing time (33-35,50).

The slow healing wounds of sulfur mustard is not well understood, but the importance of manganese, copper and zinc to healing are. The loss of manganese, copper, and zinc in burn healing might potentially be exacerbated by the further depletion due to binding to sulfur mustard reaction products; thus causing even slower healing times than normal.

Beyond just the overlap of symptoms, it is interest to compare how much sulfur mustard exposure is required for toxic effects relative to the metal micronutrient concentrations. The levels of sulfur mustard exposure that are toxic have been established. The effects of sulfur mustard exposure are broken down into 3 exposure routes and 2 exposure limit levels ($ECt_{50}/ED_{50}$ and $LCt_{50}/LD_{50}$). ECt/ED are those dosages where health effects are first observed and the LCt/LD are the dosages where 50% of exposed die. The three exposure routes are: inhalation of vapors, skin absorption of vapors, and skin absorption of liquid. For the inhalation

of vapors the $ECt_{50}$ is 25 mg•min/$m^3$ and the $LCt_{50}$ is 1,000 mg•min/$m^3$, while for skin absorption of vapors the $ECt_{50}$ is 50 mg•min/$m^3$ and the $LCt_{50}$ is 10,000 mg•min/$m^3$.

It is not completely straightforward to convert these numbers into amounts of mustard that actually end up in the lungs. However, it appears that five to eight liters/min of air pass through the lungs of the average adult. Assuming the lower level of 5 L, the $ECt_{50}$ levels imply that just 125 µg of sulfur mustard, presumably mostly localized to lung tissue, is enough to show health effects and that 5 mg is enough to kill half of those exposed. Determining the levels of vapor that actually react with the skin is even more problematic, but since we have values for direct exposure, we can ignore this.

For the final route of exposure of skin absorption of liquid, the $ED_{50}$ is 600 mg/70kg and the $LD_{50}$ is 1,400 mg/70kg. It appears that, in rats, about 50-70% of the applied cutaneous dose of radiolabeled mustard is taken up and excreted in the urine or feces over the course of a week or so (55). The remainder of the dose persists in the body for longer time periods (56). These studies were further supported by Maisonneuve *et al.* that found when intravenous dosages of sulfur mustard in rats (10 mg/kg) were administered, more than 80% of sulfur mustard or its metabolites/conjugates were excreted via urine within 96 hours (57). Benson *et al.* found that urine is the primary excretion method post sulfur mustard exposure, regardless of inhalation or cutaneous exposure, and that this excretion plateaued around 60 hours for inhalation and 160 hours for cutaneous exposures (58). In other words, virtually all the doses can be expected to enter the body and react. The exact fate of mustard that is delivered cutaneously does not appear to have been determined, but the metabolites excreted in urine that result from reactions following intraperitoneal administration have been determined. It seems likely that cutaneous exposure leads to similar reactions. Since urinary excretion is much higher than fecal or the

longer persisting metabolites, this allows us to estimate what happens to most of the dose. While a precise number is not available, it seems that at least half of the mustard reacts with two sulfur nucleophiles. Often these subsequently go on to be modified by β-lyase or to oxidize to sulfoxides or sulfones, but these processes take time and thus we believe that a reasonable estimate of the levels of alkylation products in the body that contain three sulfurs is half of the $ED_{50}$ or 300 mg/70kg and half of the $LD_{50}$ or 700 mg/70kg. The molecular weight of mustard is 159.089 g/mol, so these dosages correspond to approximately 1.9 and 4.4 mmol, making the further approximation that the body is entirely water.

Under normal physiological conditions that same 70 kg adult has just 1.7 to 3.4 μmol (1-2mg) of cobalt, 1.1 mmol (70mg) of copper, and 0.26 mmol (15mg) of nickel that could bind to these products. The 35 mmol (2300mg) of zinc is the only metal that might saturate the resulting ligand and not be depleted. Although not discussed here, a similar point could be made about iron. A key question then is the relative binding affinity of these metals. We address that in part in Chapter 6, but also refer to the work of Podlaha and Podlahová who found in a similar system the binding affinity followed the order of $Mn^{2+} \approx Fe^{2+} < Co^{2+} < Ni^{2+} < Cu^{2+}$. Subsequent work found an affinity for $Zn^{2+}$ nearly three orders of magnitude less than the affinity of $Cu^{2+}$ and roughly similar to that of $Co^{2+}$ (54) and work by Kotek *et al.* found an even higher affinity for $Cu^{+}$.. More specifically, the $K_d$ for Cu(II) is micromolar and for Cu(I) it is picomolar (59). Although this is far from proof at this point, it seems plausible that significant amounts of the body's copper might form complexes with the levels of ligand that would result from physiologically relevant levels of sulfur mustard exposure and that local depletion of other metals might also result.

## 4.2 References


1. Fraga, C. G. Relevance, essentiality and toxicity of trace elements in human health. *Molecular aspects of medicine* **2005**, *26* (4-5), 235-244.

2. Zoroddu, M. A.; Aaseth, J.; Crisponi, G.; Medici, S.; Peana, M.; Nurchi, V. M. The essential metals for humans: a brief overview. *Journal of inorganic biochemistry* **2019**, *195*, 120-129.

3. Maret, W. The metals in the biological periodic system of the elements: concepts and conjectures. *International journal of molecular sciences* **2016**, *17* (1), 66.

4. Wada, O. What are trace elements? *Journal of the Japan Medical Association* **2004**, *129* (5), 601-615.

5. Bhattacharya, P. T.; Misra, S. R.; Hussain, M. Nutritional aspects of essential trace elements in oral health and disease: an extensive review. *Scientifica* **2016**, *2016*.

6. Emsley, J. *Nature's building blocks: an AZ guide to the elements*; Oxford University Press, 2011.

7. Suzuki, K.; Yamasaki, K. The stability of some metal complexes incorporating oxygen or sulphur as donor atoms. *Journal of Inorganic and Nuclear Chemistry* **1962**, *24* (9), 1093-1103.

8. Kennedy, B.; Lever, A. Studies of the metal–sulfur bond. Complexes of the pyridine thiols. *Canadian Journal of Chemistry* **1972**, *50* (21), 3488-3507.

9. Yukawa, M.; Suzuki-Yasumoto, M.; Amano, K.; Terai, M. Distribution of trace elements in the human body determined by neutron activation analysis. *Archives of Environmental Health: An International Journal* **1980**, *35* (1), 36-44.

10. Haraguchi, H. Metallomics: the history over the last decade and a future outlook. *Metallomics* **2017**, *9* (8), 1001-1013.

11. Choi, S.; Liu, X.; Pan, Z. Zinc deficiency and cellular oxidative stress: prognostic implications in cardiovascular diseases. *Acta Pharmacologica Sinica* **2018**, *39* (7), 1120-1132.

12. Lee, S. R. Critical role of zinc as either an antioxidant or a prooxidant in cellular systems. *Oxidative medicine and cellular longevity* **2018**, *2018*.

13. Pavelková, M.; Vysloužil, J.; Kubová, K.; Vetchý, D. Biological role of copper as an essential trace element in the human organism. Biologická role mědi jako základního stopového prvku v lidském organismu. *Ceska Slov Farm* **2018**, *67* (4), 143-153.

14. Linder, M. C.; Wooten, L.; Cerveza, P.; Cotton, S.; Shulze, R.; Lomeli, N. Copper transport. *The American journal of clinical nutrition* **1998**, *67* (5), 965S-971S.

15. World Health Organization, W. Air quality guidelines 2nd edition Regional Office for Europe, Chapter 6.10 - Nickel. 2000.

16. Genchi, G.; Carocci, A.; Lauria, G.; Sinicropi, M. S.; Catalano, A. Nickel: Human health and environmental toxicology. *International journal of environmental research and public health* **2020**, *17* (3), 679.

17. Czarnek, K.; Terpiłowska, S.; Siwicki, A. K. Selected aspects of the action of cobalt ions in the human body. *Central European Journal of Immunology* **2015**, *40* (2), 236-242.

18. Osman, D.; Cooke, A.; Young, T. R.; Deery, E.; Robinson, N. J.; Warren, M. J. The requirement for cobalt in vitamin B12: A paradigm for protein metalation. *Biochimica et Biophysica Acta (BBA)-Molecular Cell Research* **2021**, *1868* (1), 118896.

19. Klug, A. The discovery of zinc fingers and their applications in gene regulation and genome manipulation. *Annual review of biochemistry* **2010**, *79*, 213-231.

20. Wang, C.; Zhang, R.; Wei, X.; Lv, M.; Jiang, Z. Metalloimmunology: the metal ion-controlled immunity. *Advances in immunology* **2020**, *145*, 187-241.

21. Livingstone, C. Zinc: physiology, deficiency, and parenteral nutrition. *Nutrition in Clinical Practice* **2015**, *30* (3), 371-382.

22. Wazir, S. M.; Ghobrial, I. Copper deficiency, a new triad: anemia, leucopenia, and myeloneuropathy. *Journal of community hospital internal medicine perspectives* **2017**, *7* (4), 265-268.

23. Lelièvre, P.; Sancey, L.; Coll, J.-L.; Deniaud, A.; Busser, B. The multifaceted roles of copper in cancer: A trace metal element with dysregulated metabolism, but also a target or a bullet for therapy. *Cancers* **2020**, *12* (12), 3594.

24. Soncin, F.; Guitton, J.-D.; Cartwright, T.; Badet, J. Interaction of human angiogenin with copper modulates angiogenin binding to endothelial cells. *Biochemical and biophysical research communications* **1997**, *236* (3), 604-610.

25. Babak, M. V.; Ahn, D. Modulation of intracellular copper levels as the mechanism of action of anticancer copper complexes: Clinical relevance. *Biomedicines* **2021**, *9* (8), 852.

26. Treviño, R. E.; Shafaat, H. S. Protein-based models offer mechanistic insight into complex nickel metalloenzymes. *Current Opinion in Chemical Biology* **2022**, *67*, 102110.

27. Boer, J. L.; Mulrooney, S. B.; Hausinger, R. P. Nickel-dependent metalloenzymes. *Archives of biochemistry and biophysics* **2014**, *544*, 142-152.

28. Begum, W.; Rai, S.; Banerjee, S.; Bhattacharjee, S.; Mondal, M. H.; Bhattarai, A.; Saha, B. A comprehensive review on the sources, essentiality and toxicological profile of nickel. *RSC advances* **2022**, *12* (15), 9139-9153.

29. Nordberg, G. F.; Fowler, B. A.; Nordberg, M. The Handbook on the Toxicology of Metals 3E. 2005.

30. Fenech, M. Folate (vitamin B9) and vitamin B12 and their function in the maintenance of nuclear and mitochondrial genome integrity. *Mutation Research/Fundamental and Molecular Mechanisms of Mutagenesis* **2012**, *733* (1-2), 21-33.

31. Kobayashi, M.; Shimizu, S. Cobalt proteins. *European Journal of Biochemistry* **1999**, *261* (1), 1-9.

32. Żwierełło, W.; Styburski, D.; Maruszewska, A.; Piorun, K.; Skórka-Majewicz, M.; Czerwińska, M.; Maciejewska, D.; Baranowska-Bosiacka, I.; Krajewski, A.; Gutowska, I. Bioelements in the treatment of burn injuries–The complex review of metabolism and supplementation (copper, selenium, zinc, iron, manganese, chromium and magnesium). *Journal of Trace Elements in Medicine and Biology* **2020**, *62*, 126616.

33. Al-Kaisy, A.; Sahib, A. S.; Al-Biati, H. Effect of zinc supplement in the prognosis of burn patients in Iraq. *Annals of Burns and Fire Disasters* **2006**, *19* (3), 115.

34. Lin, P.-H.; Sermersheim, M.; Li, H.; Lee, P. H.; Steinberg, S. M.; Ma, J. Zinc in wound healing modulation. *Nutrients* **2017**, *10* (1), 16.

35. Wilkinson, H. N.; Guinn, B.-A.; Hardman, M. J. Combined Metallomics/Transcriptomics Profiling Reveals a Major Role for Metals in Wound Repair. *Frontiers in Cell and Developmental Biology* **2021**, *9*.

36. Chasapis, C. T.; Loutsidou, A. C.; Spiliopoulou, C. A.; Stefanidou, M. E. Zinc and human health: an update. *Archives of toxicology* **2012**, *86* (4), 521-534.

37. Altarelli, M.; Ben-Hamouda, N.; Schneider, A.; Berger, M. M. Copper deficiency: causes, manifestations, and treatment. *Nutrition in Clinical Practice* **2019**, *34* (4), 504-513.

38. Danks, D. Copper deficiency in humans. *Annual review of nutrition* **1988**, *8* (1), 235-257.

39. Langan, R. C.; Goodbred, A. J. Vitamin B12 deficiency: recognition and management. *American family physician* **2017**, *96* (6), 384-389.

40. Serin, H. M.; Arslan, E. A. Neurological symptoms of vitamin B12 deficiency: analysis of pediatric patients. *Acta Clinica Croatica* **2019**, *58* (2), 295.

41. Anke, M.; Grun, M.; Groppel, B.; Kronemann, H. The Biological Importance of Nickel. In *ArchiV Fur Tierernahrung-Archives of Animal Nutrition*, 1983; Akademie Verlag Gmbh Muhlenstrasse 33-34, D-13187 Berlin, Germany: Vol. 33, pp 118-118.

42. Maroney, M. J.; Ciurli, S. Nonredox nickel enzymes. *Chemical reviews* **2014**, *114* (8), 4206-4228.

43. Berger, M. M.; Shenkin, A. Trace element requirements in critically ill burned patients. *Journal of Trace Elements in Medicine and Biology* **2007**, *21*, 44-48.

44. Mirastschijski, U.; Martin, A.; Jorgensen, L. N.; Sampson, B.; Ågren, M. S. Zinc, copper, and selenium tissue levels and their relation to subcutaneous abscess, minor surgery, and wound healing in humans. *Biological trace element research* **2013**, *153* (1), 76-83.

45. Lansdown, A. B.; Mirastschijski, U.; Stubbs, N.; Scanlon, E.; Ågren, M. S. Zinc in wound healing: theoretical, experimental, and clinical aspects. *Wound repair and regeneration* **2007**, *15* (1), 2-16.

46. Price, J. A.; Rogers, J. V.; McDougal, J. N.; Shaw, M. Q.; Reid, F. M.; Graham, J. S. Transcriptional changes in porcine skin at 7 days following sulfur mustard and thermal burn injury. *Cutaneous and ocular Toxicology* **2009**, *28* (3), 129-140.

47. Rogers, J. V.; McDougal, J. N.; Price, J. A.; Reid, F. M.; Graham, J. S. Transcriptional responses associated with sulfur mustard and thermal burns in porcine skin. *Cutaneous and ocular toxicology* **2008**, *27* (3), 135-160.

48. Michalke, B.; Halbach, S.; Nischwitz, V. Speciation and toxicological relevance of manganese in humans. *Journal of Environmental Monitoring* **2007**, *9* (7), 650-656.

49. Sachse, B.; Kolbaum, A. E.; Ziegenhagen, R.; Andres, S.; Berg, K.; Dusemund, B.; Hirsch-Ernst, K. I.; Kappenstein, O.; Mueller, F.; Roehl, C. Dietary manganese exposure in the adult population in Germany—What does it mean in relation to health risks? *Molecular nutrition & food research* **2019**, *63* (16), 1900065.

50. Bang, R.; Al-Sayer, H.; Al-Bader, A.; Mattappallil, A.; Dashti, H. Serum zinc, selenium, manganese and magnesium in zinc-altered diet and burn wound healing. *Trace Elements & Electrolytes* **2007**, *24* (3).

51. Winslow, J. W.; Limesand, K. H.; Zhao, N. The functions of ZIP8, ZIP14, and ZnT10 in the regulation of systemic manganese homeostasis. *International journal of molecular sciences* **2020**, *21* (9), 3304.
52. Santamaria, A. Manganese exposure, essentiality & toxicity. *Indian Journal of Medical Research* **2008**, *128* (4), 484.

53. Smith, M. R.; Fernandes, J.; Go, Y.-M.; Jones, D. P. Redox dynamics of manganese as a mitochondrial life-death switch. *Biochemical and biophysical research communications* **2017**, *482* (3), 388-398.

54. Procházková, O.; Podlahová, J.; Podlaha, J. Metal complexes of thiopolycarboxylic acids. VI. Zinc and cadmium. *Collection of Czechoslovak Chemical Communications* **1973**, *38* (4), 1120-1127.

55. Hambrook, J.; Harrison, J.; Howells, D.; Schock, C. Biological fate of sulphur mustard (1, 1'-thiobis (2-chloroethane)): urinary and faecal excretion of 35S by rat after injection or cutaneous application of 35S-labelled sulphur mustard. *Xenobiotica* **1992**, *22* (1), 65-75

56. Hambrook, J.; Howells, D.; Schock, C. Biological fate of sulphur mustard (1, 1′-thiobis (2-chloroethane)): uptake, distribution and retention of 35S in skin and in blood after cutaneous application of 35S-sulphur mustard in rat and comparison with human blood in vitro. *Xenobiotica* **1993**, *23* (5), 537-561

57. Maisonneuve, A.; Callebat, I.; Debordes, L.; Coppet, L. Biological fate of sulphur mustard in rat: toxicokinetics and disposition. *Xenobiotica* **1993**, *23* (7), 771-780

58. Benson, J. M.; Tibbetts, B. M.; Weber, W. M.; Grotendorst, G. R. Uptake, tissue distribution, and excretion of 14C-sulfur mustard vapor following inhalation in F344 rats and cutaneous exposure in hairless guinea pigs. *Journal of Toxicology and Environmental Health, Part A* **2011**, *74* (13), 875-885.

59. Kotek, J.; Klierova, H.; Doležal, J.; Kopanica, M. The use of complexing agents in the polarographic analysis of inorganic compounds: XVI. The study of chelating agents with sulphur donor atoms. *Journal of Electroanalytical Chemistry and Interfacial Electrochemistry* **1971**, *31* (2), 451-462.

## Chapter 5: Synthesis of Sulfur Mustard Byproduct Analogs

### 5.1 Introduction

It is common in the older literature to see work done directly with sulfur mustard; it is not unique in terms of posing health hazards in the laboratory. However, since it is listed as a Schedule 1 chemical under the Chemical Weapons Convention by the Organization for the Prohibition of Chemical Weapons, it does pose some unique regulatory challenges. Rather than working with mustard itself, it was decided that chemical analogs that mimic those which would be found in the body after sulfur mustard exposure would be synthesized through routes that do not require mustard gas itself.

Sulfur mustard can react with a variety of nucleophiles, but the main biological fate of it is to react with the thiols of cysteine, either free cysteine, cysteine in a protein, a peptide, or glutathione (4-6). These are largely broken down into S,S′-(Thiodi-2,1-ethanediyl)bis[L-cysteine] (Figure 5.1) (6,7). Unfortunately, this compound has extremely low solubility in water (1).

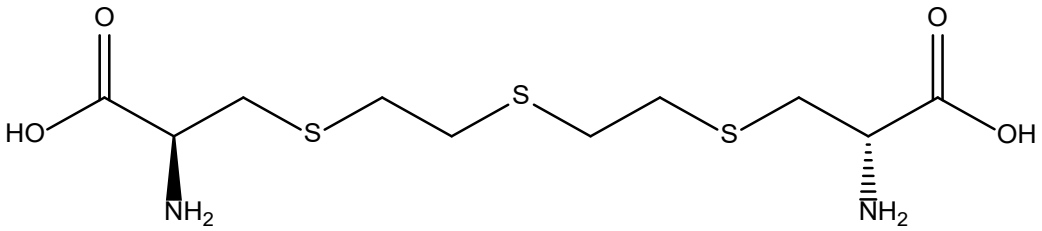


*Figure 5.1 S,S'-(Thiodi-2,1-ethanediyl)bis[L-cysteine].*

There were two main requirements when synthesizing the correct analog: the compound must be soluble in water at physiological pH of 7.4 and it must mimic as closely as possible a compound that could be found physiologically. For these reasons the following three compounds were synthesized: 3,6,9-trithiaundecane-1,11-dicarboxylic acid (**1**, Figure 5.2), 2,5,8-trithianone-1,9-

dicarboxylic acid (**2**, Figure 5.4), and 2,5,8-trithianonane-1,9-diamide (**3**, Figure 5.7). It should be noted that 3,6,9-trithiaundecane-1,11-dicarboxylic acid (**1**) shares the exact same carbon and sulfur backbone as the reaction product of mustard with cysteine. It differs only in the absence of the amine moieties. The cysteine reaction product is presumably insoluble because the zwitterionic form is neutral, reducing solubility, but the charges lead to strong interactions in the solid. It was anticipated that both 2,5,8-trithianone-1,9-dicarboxylic acid (**2**) and 3,6,9-trithiaundecane-1,11-dicarboxylic acid (**1**) should be very soluble when ionized and much less so when protonated.

Both the 2,5,8-trithianone-1,9-dicarboxylic acid (CAS 34183-42-1) and 3,6,9-trithiaundecane-1,11-dicarboxylic acid (CAS 89868-17-7) had been synthesized before and the procedures used here were modified from Ford *et al.* and Addison *et al.* respectively (2,3). Ford *et al.* refluxed bis(2-mercaptoethyl) sulfide with potassium hydroxide and chloroacetic acid in an unspecified alcohol; the work up consisted of distilling of the alcohol, diluting with ice and then acidifying to 'Congo Red' with concentrated hydrochloric acid (2). The key differences in the synthetic procedure used here are the use of iodoacetic acid as opposed to chloroacetic acid and a modified work-up. The solution was extracted instead of distilled, sulfuric acid was used instead of hydrochloric, and Congo Red was not used as an indicator. Addison *et al.* reacted bis(2-mercaptoethyl) sulfide, sodium borohydride, and potassium hydroxide with bromopropionic acid in ethanol at RT; the workup consisted of removing all solvent, dissolving in water, extracting with ether, and acidifying with sulfuric acid (3). This synthesis was modified to use 3-iodopropionic acid, no sodium borohydride, was refluxed, and had a modified work-up. The reaction solution itself was acidified using hydrochloric acid and simply filtered. The compound

2,5,8-trithianonane-1,9-diamide is a novel compound and was synthesized via a similar route (Scheme 5.1).

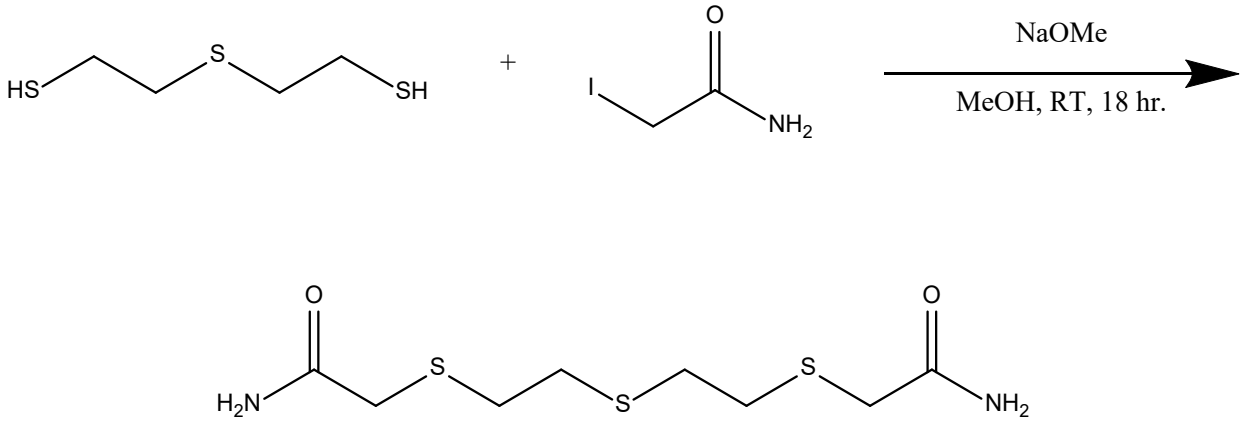


*Scheme 5.1 Synthesis of 2,5,8-Trithianonane-1,9-diamide.*

**5.2 List of Chemicals**

1. Bis (2-mercaptoethyl) sulfide (CAS# 3570-55-6): >97%, TCI America
2. Iodoacetic Acid Sodium Salt (CAS# 305-53-3): 99%, Sigma Aldrich
3. 3-Iodopropionic Acid (CAS# 141-76-4): >98%, TCI America
4. 2-Iodoacetamide (CAS# 144-48-9), 98%, Bean Town Chemical
5. Ethanol (CAS# 64-17-5): 200 Proof, Koptec
6. Methanol (CAS# 67-56-1): ACS Grade, EMD Millipore
7. Dichloromethane (CAS# 75-09-2): >99.5%, VWR BDH Chemicals
8. Sulfuric Acid (CAS# 7664-93-9): 18M ACS Reagent Grade, Ward's Science
9. Hydrochloric Acid (CAS# 7647-01-0): ACS Grade, EMD Millipore
10. Potassium Hydroxide (CAS# 1310-58-3): ACS Grade, Fisher Scientific
11. Sodium Methoxide (CAS# 124-41-4): 5M, TCI America
12. Sodium Hydroxide (CAS# 1310-73-2): ACS Grade, VWR

13. Cobalt (II) Chloride Hexahydrate (CAS# 7791-13-1): Reagent Grade, JT Baker Chemical

14. Deuterium Oxide “100%” (CAS# 7789-20-0): 99.96% D, Cambridge Isotopes Laboratories Inc.

15. Dimethyl Sulfoxide-D6 “100%” (CAS# 2206-27-1): 99.96% D, Cambridge Isotopes Laboratories Inc.

### 5.3 Synthesis and Results

**Synthesis of 3,6,9-Trithiaundecane-1,11-dicarboxylic Acid (3,3’-[thiobis(2,1-ethanediylthio)]bis-propanoic Acid, TTDPA) Compound 1 (Figure 5.3)**

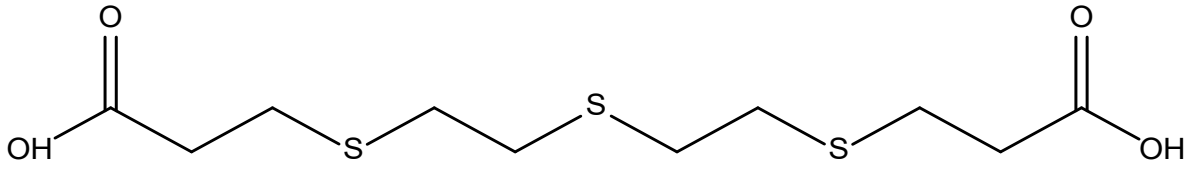


*Figure 5.2 3,6,9-Trithiaundecane-1,11-dicarboxylic Acid.*

A reflux apparatus consisting of a cooling condenser, and addition funnel was assembled and flushed with $N_2$ for 30 minutes. Potassium hydroxide (6.79g, 121mmol) was dissolved in ethanol (200 proof, 300mL), the apparatus was lowered into an oil bath (110°C) and stirred vigorously under a stream of $N_2$ until dissolved. Neat bis(2-mercaptoethyl) sulfide (8.497g, 55.06mmol) was added dropwise and stirred vigorously for 15 minutes. 3-iodopropionic acid (14.8g, 263mmol, 2.2eq) and potassium hydroxide (8.85g, 158mmol, 0.6 eq.) were dissolved in ethanol/water (200 proof, 100mL/ 18MΩ, 25mL), and added dropwise to the potassium hydroxide solution while refluxed and stirred vigorously over a 25-minute period. The flask was then wrapped in foil to prevent light exposure and the solution refluxed and stirred for 24 hours under nitrogen. The resulting golden-brown solution was cooled to room temperature and then acidified to pH 1 via the incremental addition of hydrochloric acid (4M, 50mL). The solution was filtered and the white solid washed with ethanol (200 proof, 50mL) and hydrochloric acid (1M, 150mL). This solid was dissolved in boiling water (18MΩ, 2L) and filtered again, the filtered solution was

cooled to 4°C for 24 hours. The solid was filtered and then dried under high vacuum for 48 hours, and nitrogen for an additional 72 hours. 3,6,9-Trithiaundecane-1,11-dicarboxylic acid (14.053g, 85.6%): M.P. 167-168°C (lit. 164°C) (3). 1H NMR (400MHz, $D_2O$) δ 2.41 (t, 4H), δ 2.72 (t, 4H), δ 2.78 (d, 8H) (Figure 5.6). Elemental analysis, performed by Atlantic MicroLabs $C_{10}H_{18}O_4S_3$ calculated: C, 40.25; H, 6.08; S, 32.23. Found C, 40.10; H, 6.06; S 32.06.

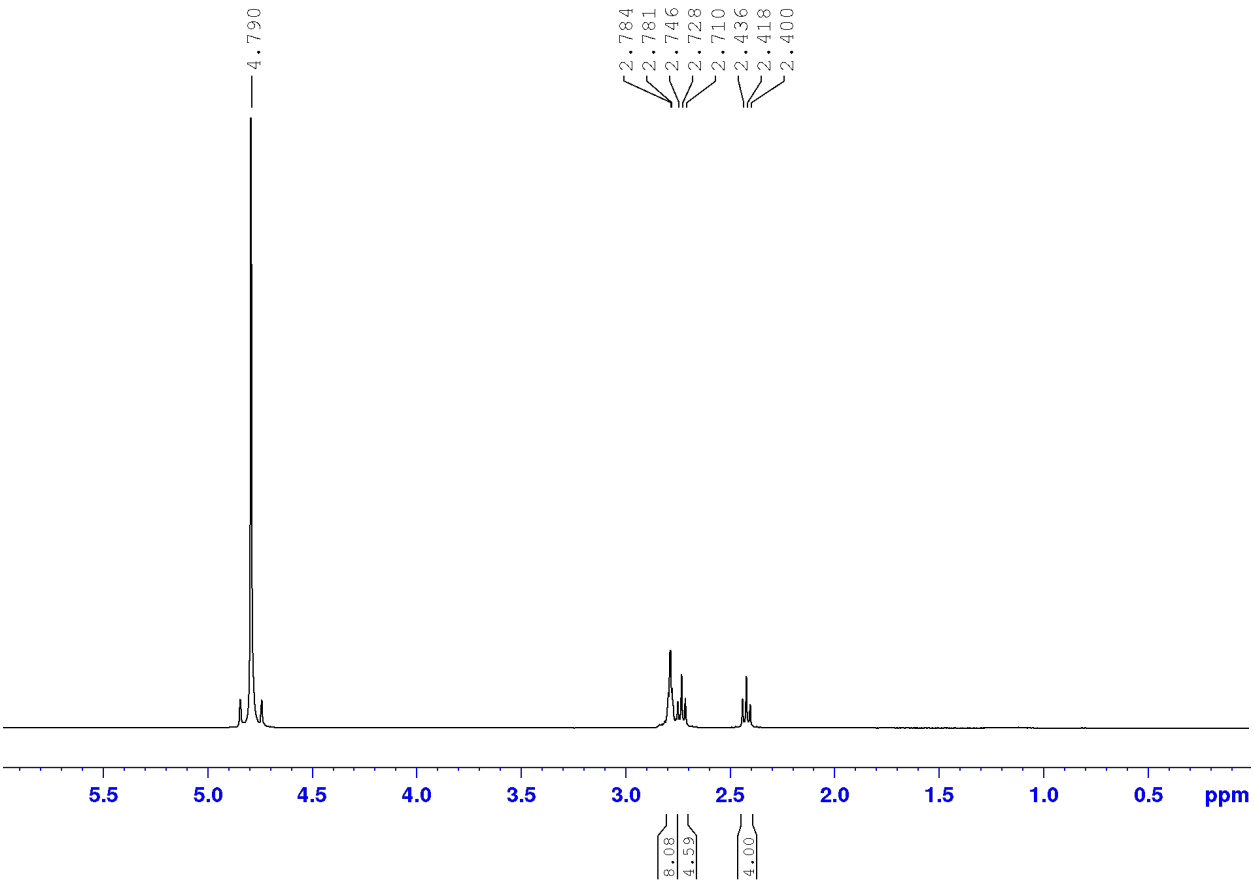


*Figure 5.3 400MHz 1H NMR in $D_2O$ of 3,6,9-Trithiaundecane-1,11-dicarboxylic Acid.*

**Synthesis of 2,5,8-Trithianone-1,9-dicarboxylic Acid (2,2'-[thiobis(2,1-ethanediylthio)]bis-Acetic acid, TTDAA) Compound 2 (Figure 5.4)**

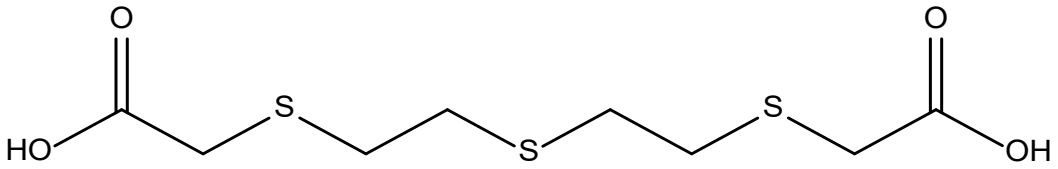


*Figure 5.4 2,5,8-Trithianone-1,9-dicarboxylic Acid.*

A round bottom fitted with an addition funnel was flushed with $N_2$ for 30 minutes. Potassium hydroxide (17g, 302mmol, 5.8eq) was dissolved in ethanol (200 proof, 200mL) under a stream of $N_2$ for 15 minutes. Neat bis(2-mercaptoethyl) sulfide (4g, 25.9mmol, 1 eq) was added dropwise and stirred vigorously for 20 minutes. A solution of iodoacetic acid sodium salt (11.4g, 54.8mmol, 2.12 eq) was dissolved in ethanol (200 proof, 40mL), and added dropwise to the potassium hydroxide solution over a 15-minute period. The reaction apparatus was wrapped in foil to prevent photochemical reaction of the alkyliodide. The reaction was stirred vigorously at room temperature (RT) for 18 hours. Solvent was removed via rotary evaporation, resulting in a white solid which was dissolved in water (18MΩ, 200mL), extracted with dichloromethane (50mL, 4x), and the aqueous layer was acidified to pH 1 via the incremental addition of sulfuric acid (6M, 30mL). This solid was then filtered and washed with 50mL cold water (18MΩ). The resulting white solid dissolved in 1L of boiling water (18MΩ) and cooled at 4°C for 18 hours. Crystalline like solid was filtered, dried under high vacuum for 24 hours.

2,5,8-Trithianone-1,9-dicarboxylic Acid (4.93g, 70.9%): M.P. 115°C (lit. 109-114°C) (2). 1H NMR (400MHz, $D_2O$) δ 2.75 (d, 8H), δ 3.16 (s, 4H) (Figure 5.5). Elemental analysis, performed by Atlantic MicroLabs $C_8H_{14}O_4S_3$ calculated: C, 35.54; H, 5.22; S, 35.57. Found C, 35.33; H, 5.30; S 35.51.

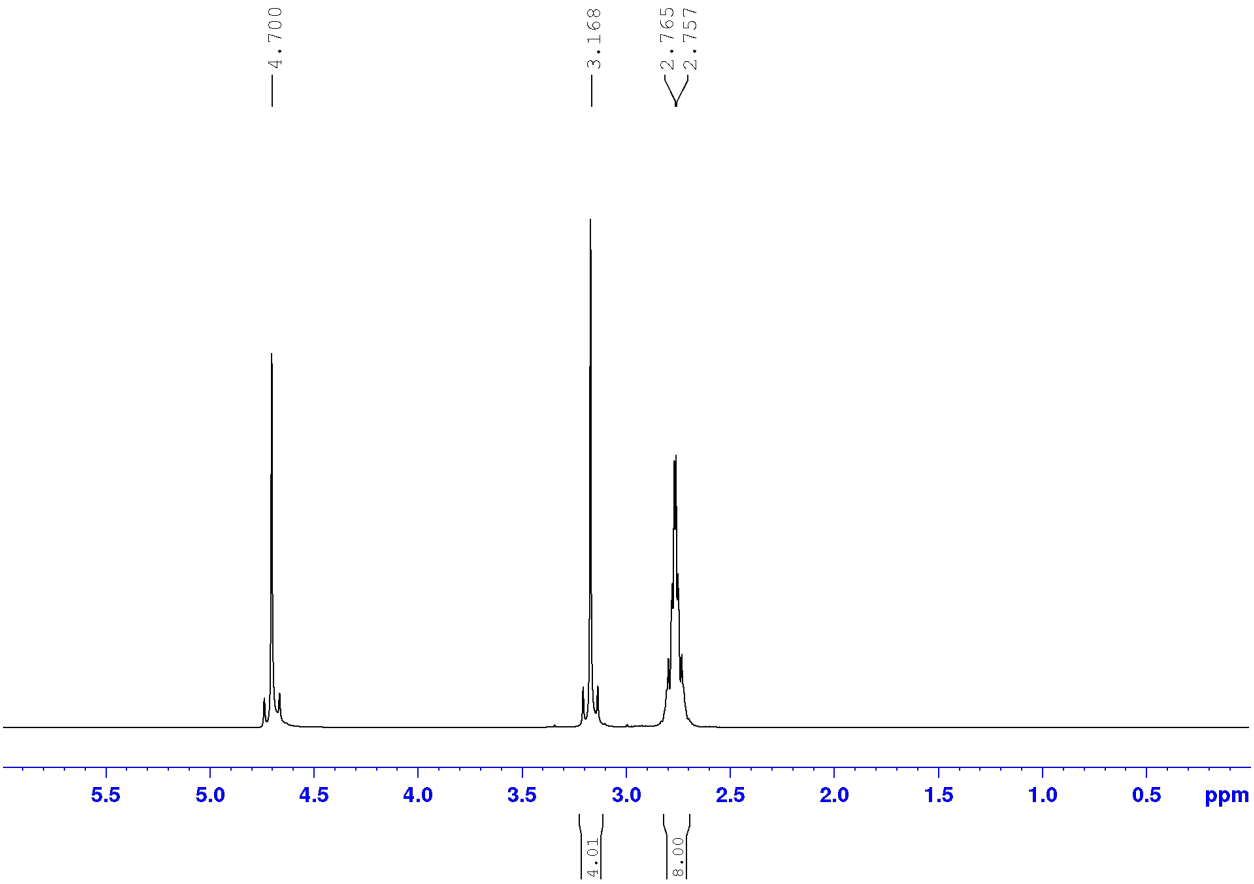


*Figure 5.5 400MHz 1H NMR in $D_2O$ of 2,5,8-Trithianone-1,9-dicarboxylic Acid.*

Larger crystals of **2** were accidently obtained while attempting to crystalize the complex with cobalt. After refluxing equimolar amounts of TTDAA and cobalt (II) chloride hexahydrate in water for 3 hours it was allowed to cool to RT overnight. Crystals large enough for diffraction were found, albeit without any cobalt, and sent the University of Oklahoma crystallographic service. Crystal data $C_8H_{14}O_4S_3$, M = 270.37, triclinic, *a* = 5.0818(2), *b* = 9.9284(3), *c* = 11.8728(4) Å, α = 100.7017(12) °, β = 95.1509(12) °, γ = 95.8971(11) °, Vol. = 581.86(4) $Å^3$, Z = 2, Z' = 1, $D_c$ = 1.543 $Mg/m^3$, F (000) = 284, λ = 0.71073 Å (Figure 5.6). All crystal data and structure refinement for compound **2** are summarized in Table 5.1.

*Table 5.1 Crystal Data, Collection Data, and Refinement Summarization for 2,5,8-Trithianone-1,9-dicarboxylic Acid.*

| Crystal data | |
|---|---|
| Chemical formula | $C_8H_{14}O_4S_3$ |
| $M_r$ | 270.395 |
| Crystal system, space group | Triclinc, P-1 |
| Temperature (K) | 100 |
| $a$, $b$, $c$ (Å) | 5.082, 9.928, 11.873 |
| $V$ (Å$^3$) | 581.87 |
| $Z$ | 2 |
| Radiation type | Mo $K\alpha$ |
| μ (mm$^{-1}$) | 0.628 |
| Crystal size (mm) | 0.050 x 0.148 x 0.306 |
| Data collection | |
| Diffractometer | D8 Quest κ-geometry, Bruker Photon II cmos |
| Absorption correction | semi-empirical from equivalents |
| $T_{min}$, $T_{max}$ | 0.642,0.747 |
| No. of measured, independent and observed [$I > 2\sigma(I)$] reflections | 55217, 5125, 4301 |
| $R_{int}$ | 0.0476 |
| $(\sin \theta/\lambda)_{max}$ (Å$^{-1}$) | 0.0288 |
| Refinement | |
| $R[F^2 > 2\sigma(F^2)]$, $wR(F^2)$, $S$ | 0.0288, 0.0810, 1.008 |
| No. of reflections | 5125 |
| No. of parameters | 142 |
| No. of restraints | 0 |
| H-atom treatment | H-atom parameters constrained |
| $\Delta\rho_{max}$, $\Delta\rho_{min}$ (e Å$^{-3}$) | 0.498, -0.305 |

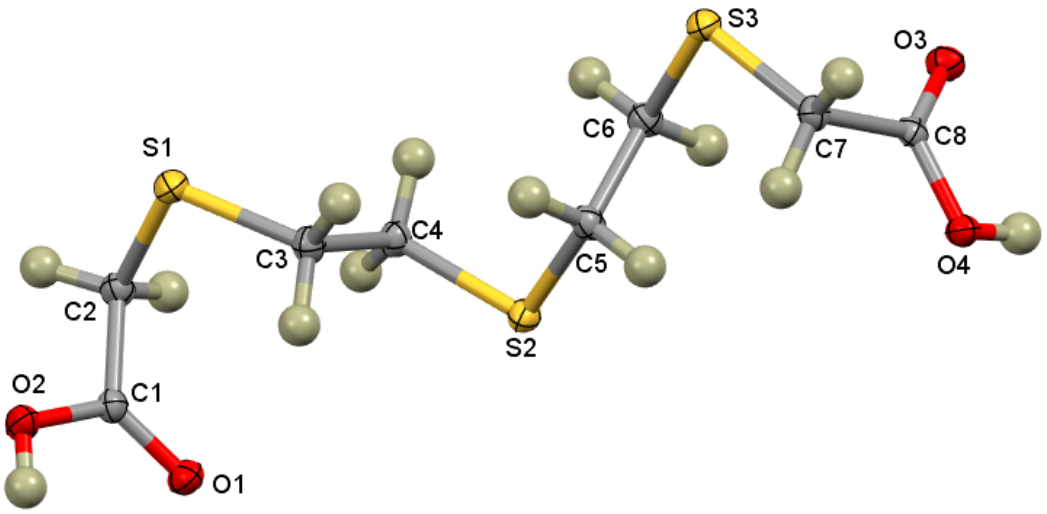


*Figure 5.6 Thermal Ellipsoid Plot of 2,5,8-Trithianone-1,9-dicarboxylic Acid.*

**Synthesis of 2,5,8-Trithianonane-1,9-diamide (2,2'-[thiobis(2,1-ethanediylthio)]bis-Acetamide, TTDAce) Compound 3 (Figure 5.7)**

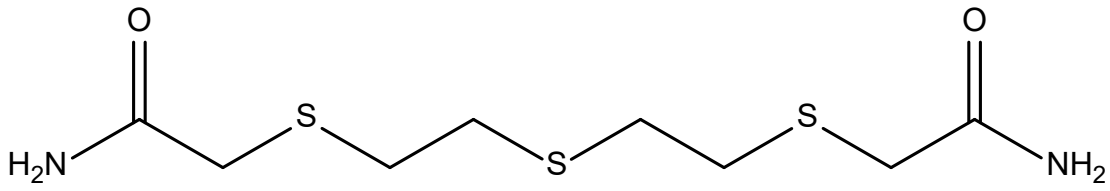


*Figure 5.7 2,5,8-Trithianonae-1,9-diamide.*

A round bottom fitted with an addition funnel was flushed with $N_2$ for 30 minutes. Methanol (HPLC grade, 20mL) and then a solution of sodium methoxide (5M, 10mL, 50mmol, 3.85 eq.) was added and stirred vigorously. Neat bis(2-mercaptoethyl) sulfide (2g, 13mmol) was added dropwise and stirred vigorously for 20 minutes. A solution of 2-iodoacetamide (5.32g, 28.8mmol, 2.2eq) in methanol (HPLC grade, 15mL) was added dropwise over a 6-minute period. The reaction was stirred vigorously at RT for 18 hours. The solution was acidified to pH 1 via incremental addition of hydrochloric acid (4M, 10mL). The resulting white solid was filtered and washed with methanol (HPLC grade, 50mL), then dissolved in sodium hydroxide (2M, 5mL) and diluted with water (18MΩ) to a final volume of 50mL. The solvent was removed via rotary evaporation, and the remaining white solid was recrystallized by first dissolving in boiling water (18MΩ, 300mL) and then cooling to 4°C for 24 hours before filtering. 2,5,8-Trithianonane-1,9-diamide (2.37g, 67.9%): M.P. 155°C. 1H NMR (400MHz, $(CD_3)_2SO$) δ 2.75 (s, 8H), δ 3.09 (s, 4H). δ 7.01 (s, 1H), δ 7.43 (s, 1H) (Figure 5.8). Elemental analysis, performed by Atlantic MicroLabs $C_8H_{16}N_2O_2S_3$ calculated: C, 35.80; H, 6.01; N, 10.44; S, 35.83. Found C, 35.88; H, 6.11; N, 10.41; S 35.67.

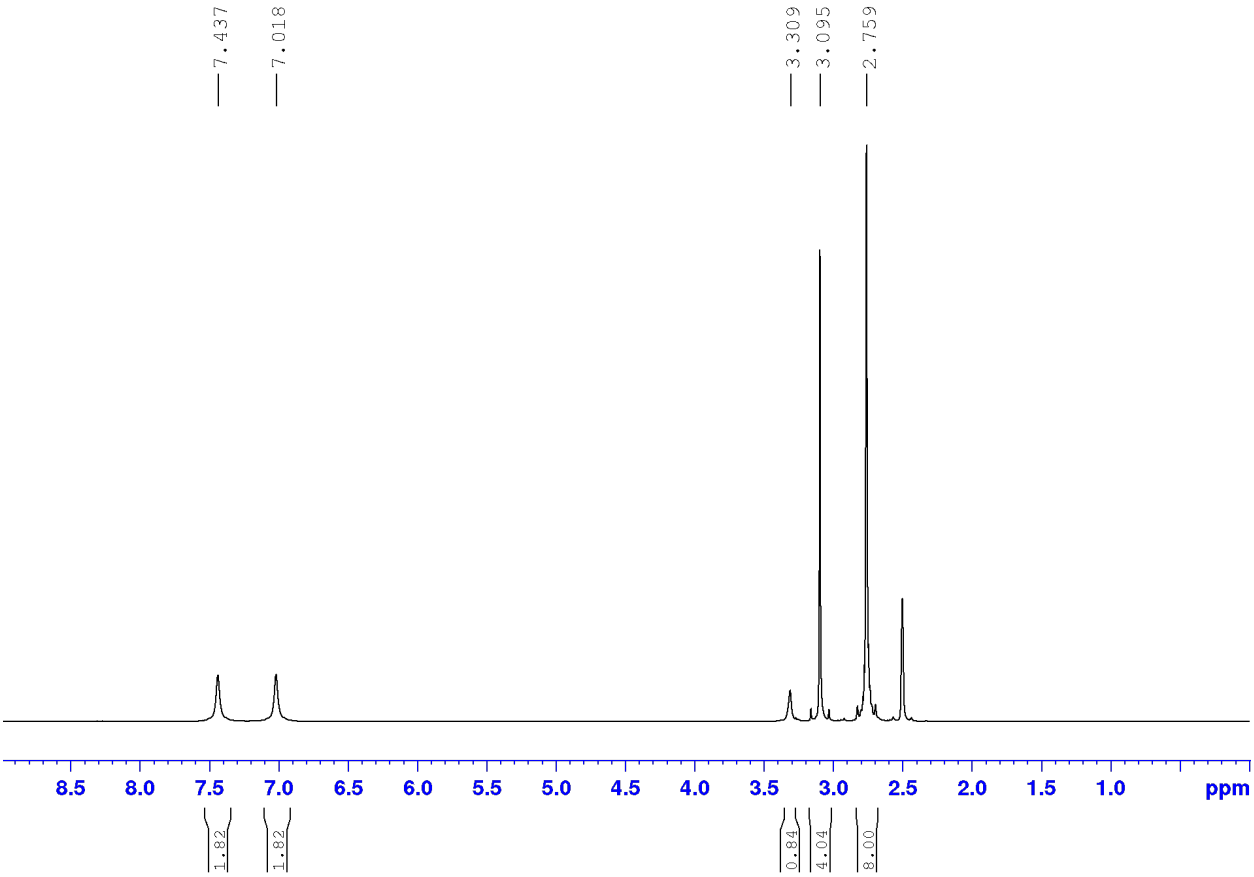


*Figure 5.8 400MHz 1H NMR in $(CD_3)_2SO$ of 2,5,8-Trithianonane-1,9-diamide.*

The crystals used for diffraction were obtained from the last step of synthesis, with no further recrystallization. Crystal data $C_8H_{14}O_4S_3$, M = 270.37, triclinic, *a* = 5.0818(2), *b* = 9.9284(3), *c* = 11.8728(4) Å, α = 100.7017(12) °, β = 95.1509(12) °, γ = 95.8971(11) °, Vol. = 581.86(4) $Å^3$, Z = 2, Z' = 1, $D_c$ = 1.543 $Mg/m^3$, F (000) = 284, λ = 0.71073 Å (Figure 5.9). All crystal data collection and structure refinement details are summarized in Table 5.2. Expanded crystal lattices of varying orientation are given to show the hydrogen bonding between the ligands, and how the interact with each other to form the overall lattice (Figure 5.10).

*Table 5.2 Crystal Data, Collection Data, and Refinement Summarization for 2,5,8-Trithianonane-1,9-diamide.*

| Crystal data | |
|---|---|
| Chemical formula | $C_{16}H_{32}N_4O_4S_6$ |
| $M_r$ | 536.81 |
| Crystal system, space group | Triclinic, P-1 |
| Temperature (K) | 293 |
| $a$, $b$, $c$ (Å) | 5.1052(1), 9.0197(2), 26.6367(8) |
| $V$ (Å$^3$) | 1218.92(5) |
| $Z$ | 2 |
| Radiation type | Cu $K\alpha$ |
| μ (mm$^{-1}$) | 5.445 |
| Crystal size (mm) | 0.55 × 0.23 × 0.17 |
| Data collection | |
| Diffractometer | XtaLAB Synergy, Dualflex, HyPix |
| Absorption correction | Multi-scan (*CrysAlis PRO*; Rigaku OD, 2021) |
| $T_{min}$, $T_{max}$ | 0.278, 0.396 |
| No. of measured, independent and observed [$I > 2\sigma(I)$] reflections | 21322, 4594 , 4594 |
| $R_{int}$ | 0.0759 |
| $(\sin \theta/\lambda)_{max}$ (Å$^{-1}$) | 0.0439 |
| Refinement | |
| $R[F^2 > 2\sigma(F^2)]$, $wR(F^2)$, $S$ | 0.0847, 0.2614, 1.146 |
| No. of reflections | 4594 |
| No. of parameters | 271 |
| No. of restraints | 0 |
| H-atom treatment | H-atom parameters constrained |
| $\Delta\rho_{max}$, $\Delta\rho_{min}$ (e Å$^{-3}$) | 1.51, -0.58 |

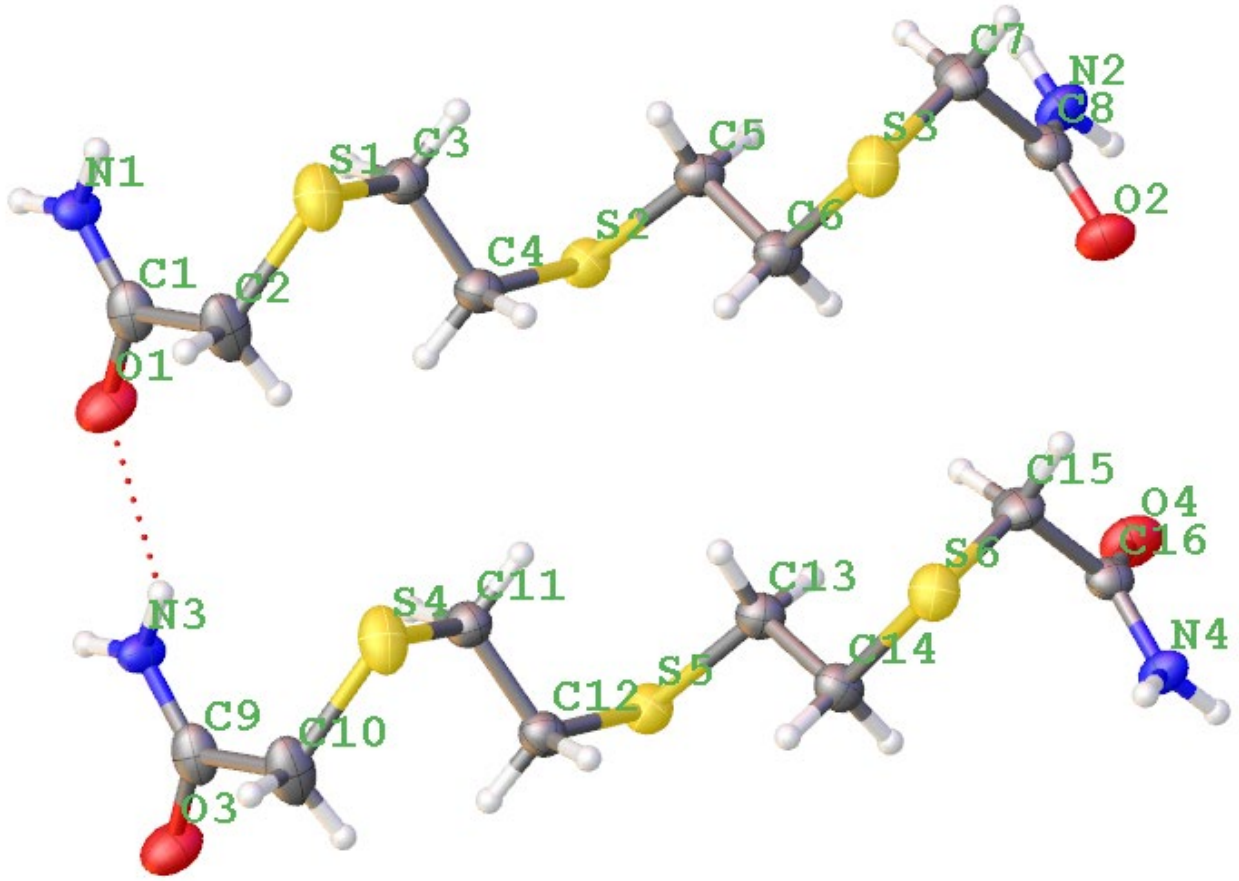


*Figure 5.9 Thermal Ellipsoid Plot of 2,5,8-Trithianonane-1,9-diamide.*

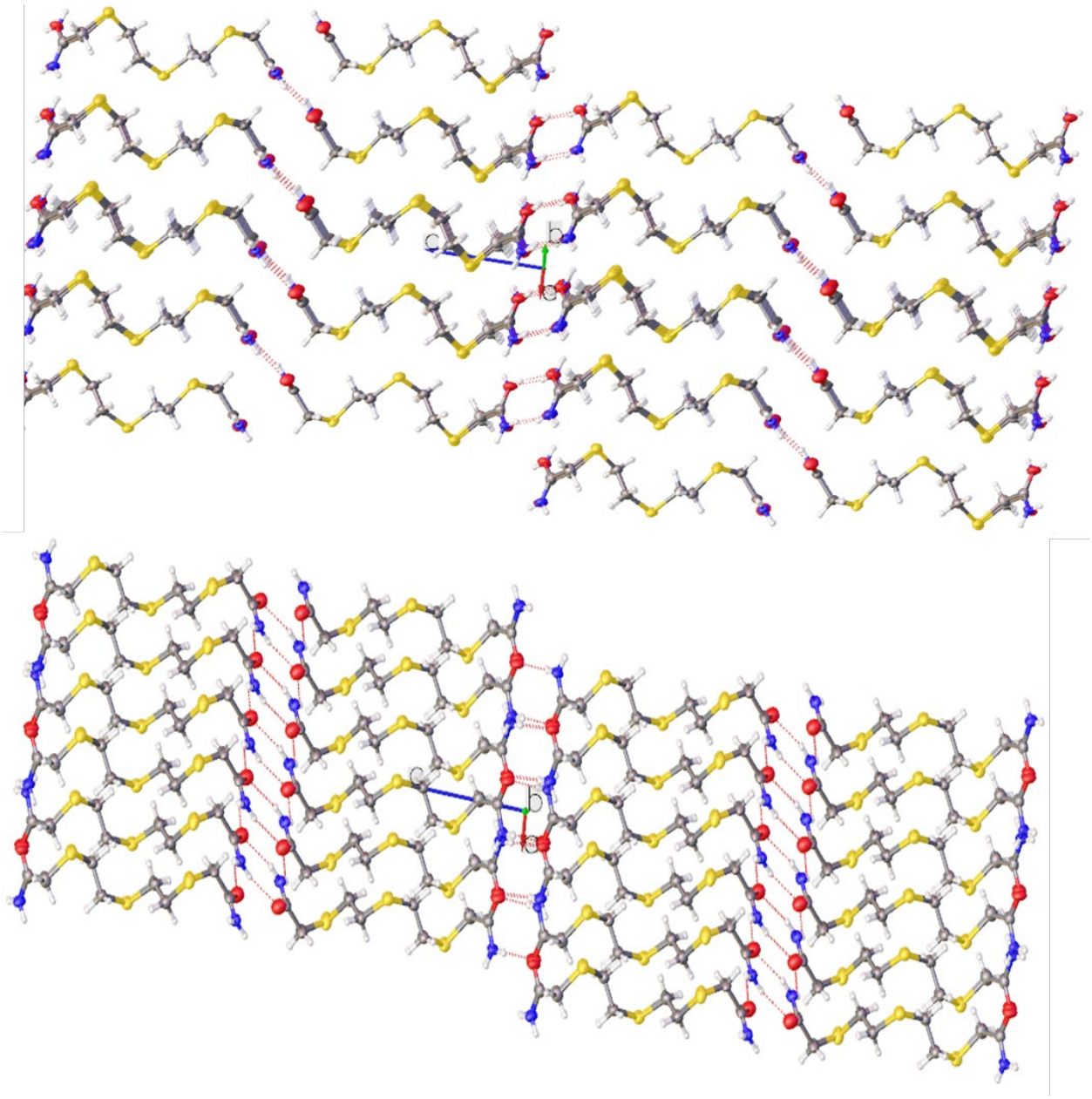


*Figure 5.10 Expanded Crystal Lattice of 2,5,8-Trithianonane-1,9-diamide in Various Orientations.*

## 5.4 Discussion

With the successful crystallization of compound 2 and compound 3, both molecules' crystal structures were analyzed for comparison. Both structures exhibited similar bond lengths and angels between all three C-S-C bonds, summarized in table 5.3. These similarities in physical bond properties and angles would allow for these differing compounds to behave in similar manner, despite their different functional groups (-COOH vs -$CONH_2$). Both compounds also appear to share similar hydrogen bonding in their unit cells, with the proton of the functional group on one molecule bonding the oxygen on the opposing functional group of the second molecule (Figure 5.11).

*Table 5.3 Comparison of Bond Length and Angles of 2,5,8-Trithianone-1,9-dicarboxylic Acid (TTDAA) and 2,5,8-Trithianonane-1,9-diamide (TTDAce) Crystals.*

| Bond Lengths (Å) | | |
|---|---|---|
| Molecule | TTDAA | TTDAce |
| Atoms | Bond Length (Å) | Bond Length (Å) |
| S(1) - C(3) | 1.815(7) | 1.819(4) |
| S(1) - C(2) | 1.819(7) | 1.803(5) |
| S(2) - C(4) | 1.812(9) | 1.816(4) |
| S(2) - C(5) | 1.814(1) | 1.822(4) |
| S(3) - C(7) | 1.797(9) | 1.793(4) |
| S(3) - C(6) | 1.815(9) | 1.824(4) |
| Bond Angles (°) | | |
| Molecule | TTDAA | TTDAce |
| Atoms | Bond Angle (°) | Bond Angle (°) |
| C(3)-S(1)-C(2) | 101.96(4) | 101.9(2) |
| C(4)-S(2)-C(5) | 101.32(4) | 100.06(18) |
| C(7)-S(3)-C(6) | 100.25(4) | 101.86(19) |

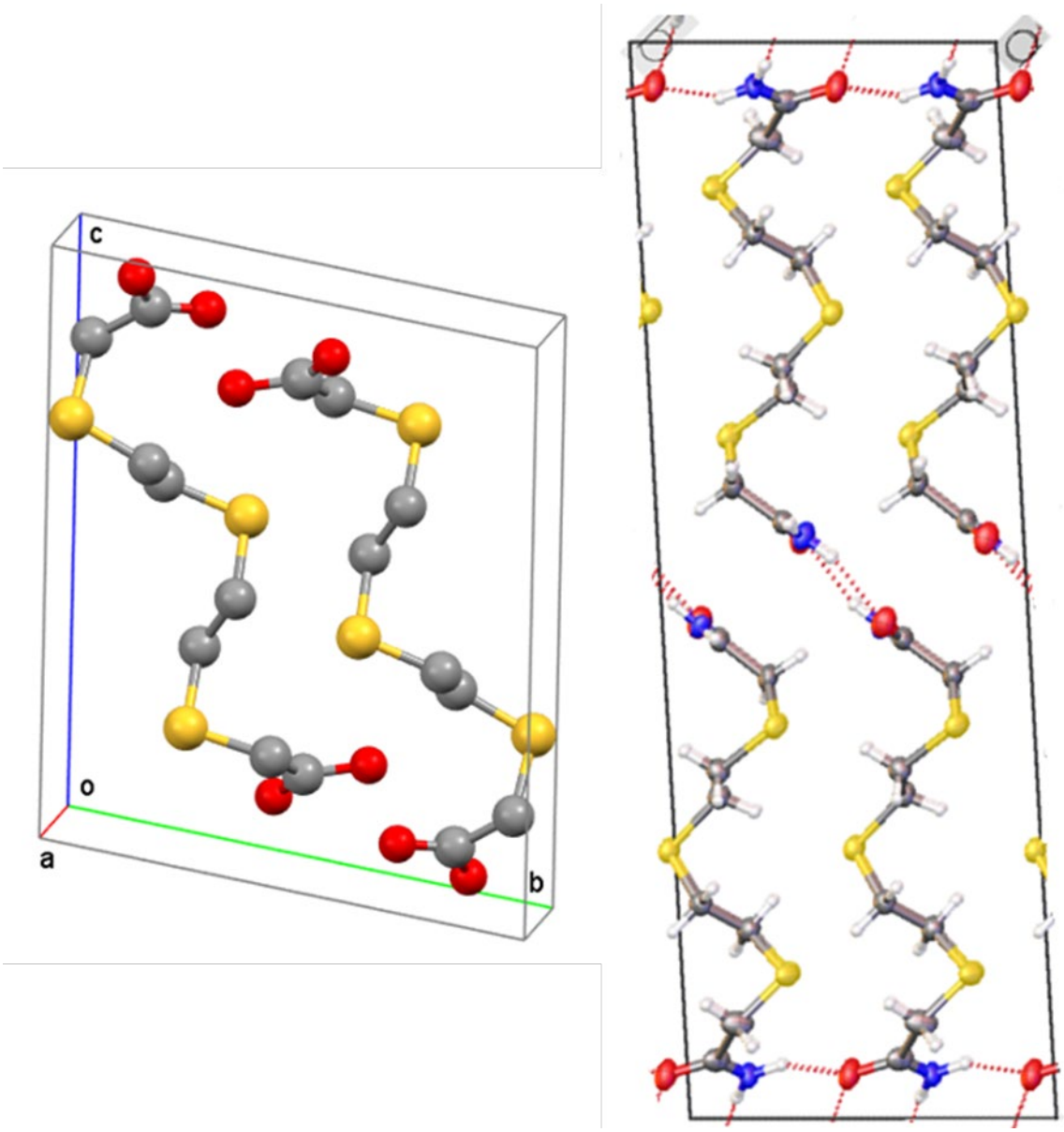


*Figure 5.11 Unit Cell Comparison Showing Hydrogen Bonding within the Unit Cell of Two Molecules of 2,5,8-Trithianone-1,9-dicarboxylic Acid (TTDAA) and 2,5,8-Trithianonane-1,9-diamide (TTDAce) Crystals, Left and Right Respectively.*

Although three compounds were synthesized, compound **3** (2,2'-[thiobis(2,1-ethanediylthio)]bis-acetamide) was not soluble under physiological conditions; in fact, it was not soluble in water under any circumstance regardless of the pH. As anticipated, compound **2** (2,2'-[thiobis(2,1-ethanediylthio)]bis-acetic acid) and compound **1** (3,3'-[thiobis(2,1-ethanediylthio)]bis-propanoic acid acid) were both soluble in water at physiological pH. Both compounds have the potential tridentate sulfur ligand expected in compounds resulting after sulfur mustard exposure; however, compound **1** met this criterion of mimicking such compounds more completely than compound **2**. As noted above, the propionic group of compound **1** more closely matches the backbone of the cysteine than that of compound **2**'s acetic group. Thus, as a whole compound **1** mimics the product that would result in the crosslinking of two cysteine residues. As a result, only compound **1** was selected to move forward for more detailed studies of its complexation with metals and precipitation, detailed in Chapter 6. Attempts were made to crystallize complexes of all three ligands with various transition metals. Fortuitously, crystals of compound **1** complexed with metals were obtained, although the free ligand without a metal never crystallized in a form suitable for diffraction data collection. Similarly, crystals of **2** and **3** in complex with a metal were not obtained.

## 5.5 Reference


1. Stein, W. H.; Moore, S.; Bergmann, M. Chemical Reactions of Mustard Gas and Related Compounds. 1 I. The Transformations of Mustard Gas in Water. Formation and Properties of Sulfonium Salts Derived from Mustard Gas. *The Journal of organic chemistry* **1946**, *11* (6), 664-674.

2. Ford, G.; Pettit, L.; Sherrington, C. The synthesis of some new ligands containing sulphur and arsenic as donor atoms and a study of their complexes with the proton, silver and some divalent metal ions. *Journal of Inorganic and Nuclear Chemistry* **1971**, *33* (12), 4119-4127.

3. Addison, A. W.; Rao, T. N.; Wahlgren, C. G. Synthesis of some benzimidazole-and benzothiazole-derived ligand systems and their precursory diacids. *Journal of heterocyclic chemistry* **1983**, *20* (6), 1481-1484.

4. Sawyer, T. W.; McNeely, K.; Louis, K.; Lecavalier, P.; Song, Y.; Villanueva, M.; Clewley, R. Comparative toxicity of mono-and bifunctional alkylating homologues of sulphur mustard in human skin keratinocytes. *Toxicology* **2017**, *382*, 36-46.

5. Maisonneuve, A.; Callebat, I.; Debordes, L.; Coppet, L. Distribution of [14C] sulfur mustard in rats after intravenous exposure. *Toxicology and applied pharmacology* **1994**, *125* (2), 281-287.

6. Rall, D. P.; Pechura, C. M. Veterans at risk: The health effects of mustard gas and lewisite. **1993**.

7. Davison, C.; Rozman, R. S.; Smith, P. K. Metabolism of bis-β-chloroethyl sulfide (sulfur mustard gas). *Biochemical pharmacology* **1961**, *7* (1), 65-74.

## Chapter 6: Binding and Crystallization of Analogs of Sulfur Mustard Alkylation Products with Metal Micronutrients

### 6.1 Introduction

Of the three ligands successfully synthesized in Chapter 5, 3,6,9-Trithiaundecane-1,11-dicarboxylic acid (TTDPA) was selected as the primary ligand of study (Figure 6.1). Its

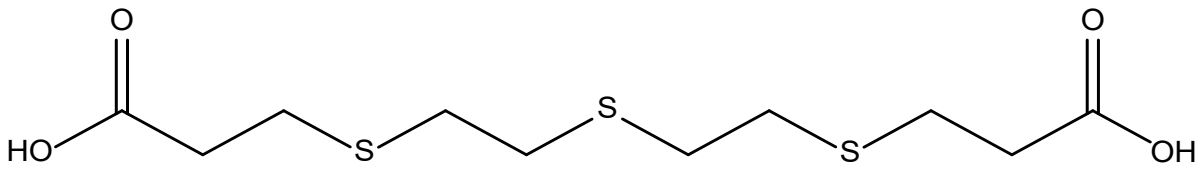


*Figure 6.1 3,6,9-Trithiaundecane-1,11-dicarboxylic acid (TTDPA).*

solubility at physiological pH and replication of the carbon and sulfur backbone formed when two cysteine residues, minus the amino groups, are cross-linked by sulfur mustard make it an ideal model. Complexes of TTDPA with various metals were analyzed via Inductively Coupled Plasma Mass Spectroscopy (ICP-MS), Ultraviolet-Visible Spectroscopy (UV-Vis), and X-ray crystallography. The ultimate goal was to explore the relationship between the binding of TTDPA and these metals (particularly copper and zinc), in the hopes of characterizing the strength and geometry of chelation of metals by this ligand (Figure 6.2).

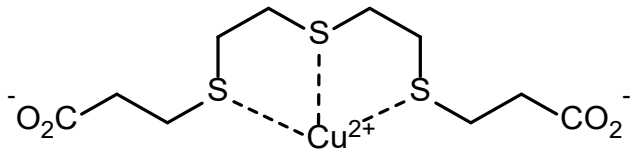


*Figure 6.2 Possible binding of 3,6,9-Trithiaundecane-1,11-dicarboxylic acid with a copper (II) cation.*

The drop in free metal micronutrient concentration due to complex formation could explain sulfur mustard symptoms that are not easily explained by current hypotheses, such as: slow healing wounds, loss of vision, nausea, vomiting, and others.

## 6.2 List of Chemicals

1. 3,6,9-Trithiaundecane-1,11-dicarboxylic acid (TTDPA): Synthesized in our lab (Compound 5.2).
2. Copper (II) Chloride • 2 $H_2O$ (CAS# 10125-13-0): ACS Reagent, Sigma Aldrich
3. Cobalt (II) Chloride • 6 $H_2O$ (CAS#7791-13-1): Reagent Grade, JT Baker
4. Nickel (II) Chloride Anhydrous (CAS# 7791-20-0): Bean Town Chemical
5. Zinc (II) Chloride Anhydrous (CAS# 7646-85-7): 98%, Sigma Aldrich
6. Manganese (II) Chloride • 4 $H_2O$ (CAS# 7773-01-5): ≥99% trace metal basis, Sigma
7. Nitric Acid (CAS# 7697-37-2): 47-49%, JT Baker
8. Hydrochloric Acid (CAS# 7647-01-0): ACS Grade, EMD Millipore
9. Sodium Hydroxide (CAS# 1310-73-2): ACS Grade, VWR
10. Qualitative Filter Paper: VWR Grade, 7.5cm, 5µm particle retention, medium flow rate & porosity, VWR
11. Syringe Filter: Laboratory Grade, 25mm, 0.2µm PTFE Membrane, VWR
12. Corning 96-Well Plate (Product # 3635): 96-Well UV-Transparent Flat Bottom Plate, Acrylic Base

### 6.3 Experimental Methods

The experimental design and set-up revolved around the UV-Vis and mass studies; all other data was a byproduct of that experimentation. The hope was to obtain a picture of the affinity of the tridentate sulfur ligand for metals by mixing a master solution of TTDPA at pH 7.4 with various metal salts, determining the amount of precipitate, and measuring changes in the ultraviolet and visible spectrum of the metals remaining in solution.

A solution of 3,6,9-trithiaundecane-1,11-dicarboxylic acid (TTDPA) (0.1M) at pH 7.4 was made by dissolving purified TTDPA in water and adjusting the pH using sodium hydroxide (10M) and hydrochloric acid (10M) until all TTDPA was dissolved and pH measured 7.4. Master metal solutions (0.2M) were made of the following metals: copper (II) chloride • 2 $H_2O$, cobalt (II) chloride • 6 $H_2O$, nickel (II) chloride anhydrous, zinc (II) chloride anhydrous, and manganese (II) chloride • 4 $H_2O$.

Two types of filters were used: filter paper with 5µm particle retention and syringe filters with 0.2µm PTFE membranes. The paper filters were prepared by first labeling with pencil, washing with water (80mL, 18MΩ) on a Buchner funnel, then dried in a vacuum oven for 24 hours at 75°C, 10 torr and tare weight was determined before use. Similarly, the syringe filters were labeled on the outside with laboratory marker, washed with water (2mL, 18MΩ), and dried under the same conditions as the paper filters before taring. Varying ratios, ranging from a 5-fold excess of TTDPA in relation to metal ion (5:1) to 5-fold excess of metal ion to TTDPA (1:5), of TTDPA and a metal salt were combined together in 20mL glass test tubes (Table 6.1). These solutions were mixed by pipetting up and down 5 times using a 2 ml sterile disposable glass Pasteur pipette and allowed to sit at room temperature for 30 minutes.

*Table 6.1 Experimental Design and Final Molar Concentrations for TTDPA and Metal Ions.*

| Sample | Vol. 0.1M TTDPA (mL) | Vol. 0.2M Metal (mL) | Vol. Water (mL) | [TTDPA] mM | [$Metal^{2+}$] mM |
|---|---|---|---|---|---|
| 5 : 1 | 3.00 | 0.30 | 11.70 | 0.0200 | 0.0040 |
| 3 : 1 | 3.00 | 0.50 | 11.50 | 0.0200 | 0.0067 |
| 1 : 1 | 3.00 | 1.50 | 10.50 | 0.0200 | 0.0200 |
| 1 : 3 | 3.00 | 4.50 | 7.50 | 0.0200 | 0.0600 |
| 1 : 5 | 3.00 | 7.50 | 4.50 | 0.0200 | 0.1001 |

*The sample numbers correspond to the ratio of TTDPA to metal ions. For example, 5:1 indicates a 5-fold molar excess of ligand, while 1:5 indicates a 5-fold excess of metal ions, lastly 1:1 indicates an equimolar amount of each ligand and metal.

These solutions were then filtered either through a 5µm particle filter paper or a 0.2µm PTFE syringe filter. The samples processed via filter paper were conducted in the following manner. A vacuum filtration apparatus was assembled using a 250mL vacuum Erlenmeyer filtering flask and a ceramic Buchner funnel of appropriate size for the filter paper. Vacuum was applied and the sample was then pipetted from the 20mL glass test tube onto the filter, to avoid any precipitate being caught on the sides of the funnel. The filter was then removed to be dried; while the filtrate was then transferred to a labeled 20mL borosilicate test tube. The entire apparatus was rinsed with water (50mL, 18MΩ) between each trial of the same ratio, and dissembled and rinsed thoroughly with house DI water between each varying ratio. For samples processed via syringe filter most aspects were the same as those of the filter paper experiment. Instead of vacuum filtration, each sample was pulled up into a 1mL syringe, then a syringe filter was attached and the sample was filtered. The filter was removed and this was repeated, 1mL at a time, until the entire sample had been filtered. The filtrate was directly collected into a labeled 20mL borosilicate test tube; and the filter was rinsed with water (0.8mL, 18MΩ) before being set aside to dry. The filter, paper or syringe, were then dried in a vacuum oven for 24 hours at 75°C, 10 torr, and weighed again to measure the captured precipitate.

Meanwhile, 250µL of each filtrate was transferred to a 96-well UV-transparent acrylic plate and the spectra examined. The data was collected on a Tecan Safire Plate Reader, from 230-1000nm, with a measurement occurring every 1 nm, and 10 scans occurring at each nm. The UV-Vis analysis was conducted for all mixtures of TTDPA with copper, nickel, and cobalt; manganese and zinc were not analyzed as it is not UV-Vis absorbent. All data shown is the averaged spectra of two separate trials where each sample was measured in triplicate; making each point on the spectra shown here the average of 6 data points. Two trials of TTDPA: $CuCl_2$ were filtered through 5µm particle retention filter paper, and one trails was filtered through 0.2µm PTFE syringe filters.

The remaining filtrate was allowed to slowly evaporate at room temperature in a fume hood. After about 1-1.5 weeks small crystals began to from in the copper containing test tubes (see photos in appendix). Two distinct types of crystals emerged, a green crystal and a clear crystal, often in the same test tube. These crystal forms were separated carefully. As described further below, diffraction data was collected on a XtaLab Synergy, Dualflex, HyPix diffractometer with a Cu Kα X-ray source. The separate types of crystal were also analyzed by combustion elemental analysis at Atlantic MicroLabs.

The dried filters were collected from the vacuum oven and allowed to cool to room temperature for 30 minutes before being weighed. Once the weight was obtained, the captured precipitate was collected by simply folding the filter paper over a weigh boat and collecting what fell off the filter. The precipitate was dry at this point and did not stick to the paper, so almost all of the precipitate fell off the filter. Some dried precipitates, after removal from the filter paper, were prepared for ICP-MS by placing ~1mg of solid in a sterile 50mL polypropylene conical vial (VWR) and adding 1.5mL of concentrated nitric acid to dissolve it. This was diluted in less than

a minute to 50mL with the addition of water (18MΩ). Then a further 1:10 dilution with water was performed on a portion of this solution, into a sterile 15mL polypropylene conical vial (VWR). Each sample was analyzed for the concentration of its respective metal, using a Thermo Scientific iCap Q ICP-MS with ASX-560 autosampler instrument.

### 6.4 Results

A combination of different techniques was used to obtain the maximum amount of information. UV-Vis was used to determine the amount of free metal ions left in solution after mixing with TTPDA, X-ray diffraction was used to solve the structure of obtained crystals, elemental analysis was used to confirm the elemental composition of the separate crystals, and ICP-MS was used to determine the ratio of complexes in the precipitate. The crystal structure and ICP-MS data were then combined to determine how much of the precipitate was captured in relation to how much was expected to theoretically form if all material formed a complex and precipitated.

Each ratio of ligand and metal was mixed in a glass test tube, mixed, and allowed to react for 30 minutes. The solutions were then filtered and the precipitates and supernatant separated. Along with each filtered supernatant, a solution of metal was made at the nominal concentration matching that sample, assuming that no metal was removed by precipitation and filtration, and measured alongside the mixtures. None of the observed peaks in the UV-Vis experimentation can be attributed to the plate background, water, or TTDPA by itself as none of these absorb at these wavelengths (Graph 6.1). Of the four metals examined, only copper showed any measurable changes in spectra, although all five metals showed the visible formation of precipitates before filtering.

In the first mixture where TTDPA is in a 5-fold molar excess in ratio to copper (II) chloride (5:1), there was a visible decrease in intensity around 815nm where $Cu^{2+}$ has its $\lambda_{max}$ (Graph 6.2) in comparison the copper chloride solution at the same nominal concentration. As the spectra gets closer to the UV region the mixture absorbs more strongly than the metal solution by itself. This leads to the assumption that this is due to a complex formed between TTDPA and $Cu^{2+}$, and some of it remains soluble at low concentrations.

The second molar ratio of (3:1) where TTDPA is in a 3-fold molar excess in ratio to copper (II) chloride, there is an even more visible decrease in intensity at 815nm (Graph 6.3) relative the copper chloride at the same nominal concentration. Note that the TTDPA ligand was mixed to the same concentration in all of these samples. This decrease in adsorption at 815nm is interpreted as meaning that there is a complex formed between TTDPA and $Cu^{2+}$ causing a measurable decrease in the concentration of free copper in the mixture. Like the 5:1 mixture there also appears to be an increase in absorbance in the UV region, presumably caused by the soluble complex of TTDPA and $Cu^{2+}$.

In the mixture (1:1) where both TTDPA and $Cu^{2+}$ are in an equimolar ratio the most distinguishable changes in the UV-Vis spectra are observed (Graph 6.4). Judging from the absorbance at 815nm, there is almost a complete removal of unbound $Cu^{2+}$ in the sample when compared to a solution of $Cu^{2+}$ by itself at that same nominal concentration. A peak appears with an absorption maxima at approximately 365nm presumably due to a soluble complex of TTDPA and $Cu^{2+}$. This peak cannot be attributed to unbound TTDPA, as it is not UV-Vis active at this wavelength. The other mixtures (1:3, 1:5) represent $Cu^{2+}$ being in a 3-fold and 5-fold excess in relation to TTDPA. The spectra for these mixtures also show the measurable decrease in $Cu^{2+}$ at 815nm. However, this decrease is not as significant as the decrease observed in the 1:1 mixture

(Graphs 6.5 and 6.6). This is expected since there is significantly more $Cu^{2+}$ in these solutions in comparison. The peak at 365nm we attribute to the complex formed between TTDPA and $Cu^{2+}$ is still prevalent but the shape changes, possibly due to the higher concentrations of $Cu^{2+}$ in the sample.

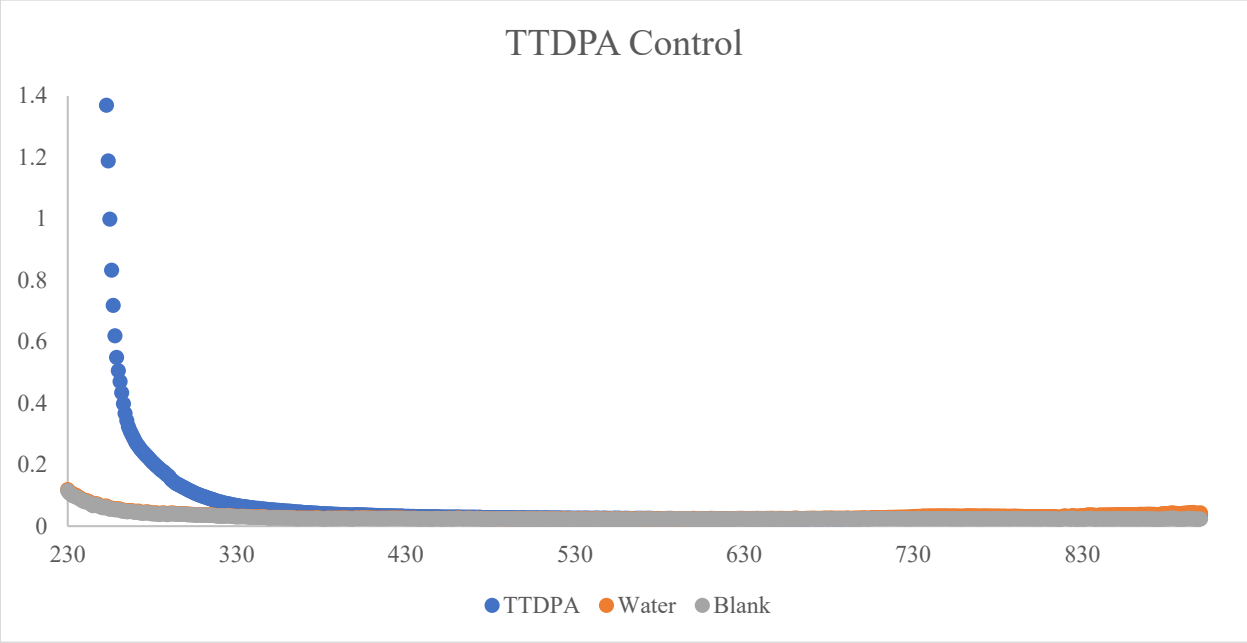


*Graph 6.1 Control Spectra of TTDPA 0.0003M (blue), Water 18MΩ (orange), and an empty tray (gray).*

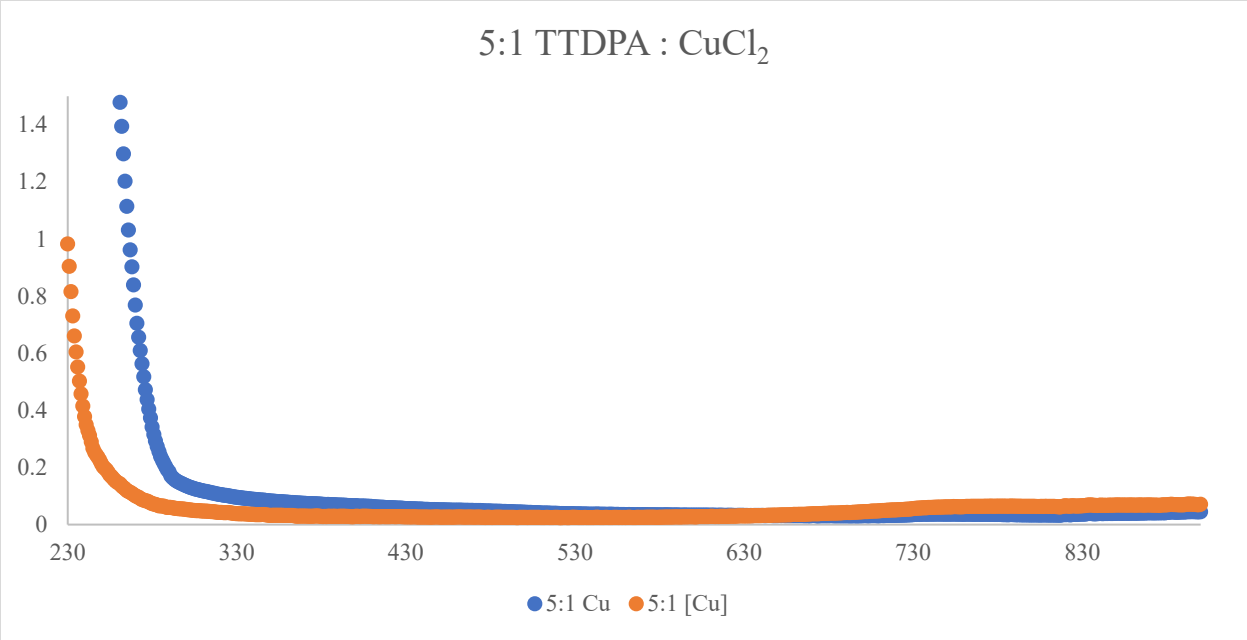


*Graph 6.2 UV-Vis Spectra of 5:1 TTDPA:$CuCl_2$ Filtered (blue) through 5µm Filter Paper Compared to $CuCl_2$ at Matching Nominal Concentration (0.0006M) (orange).*

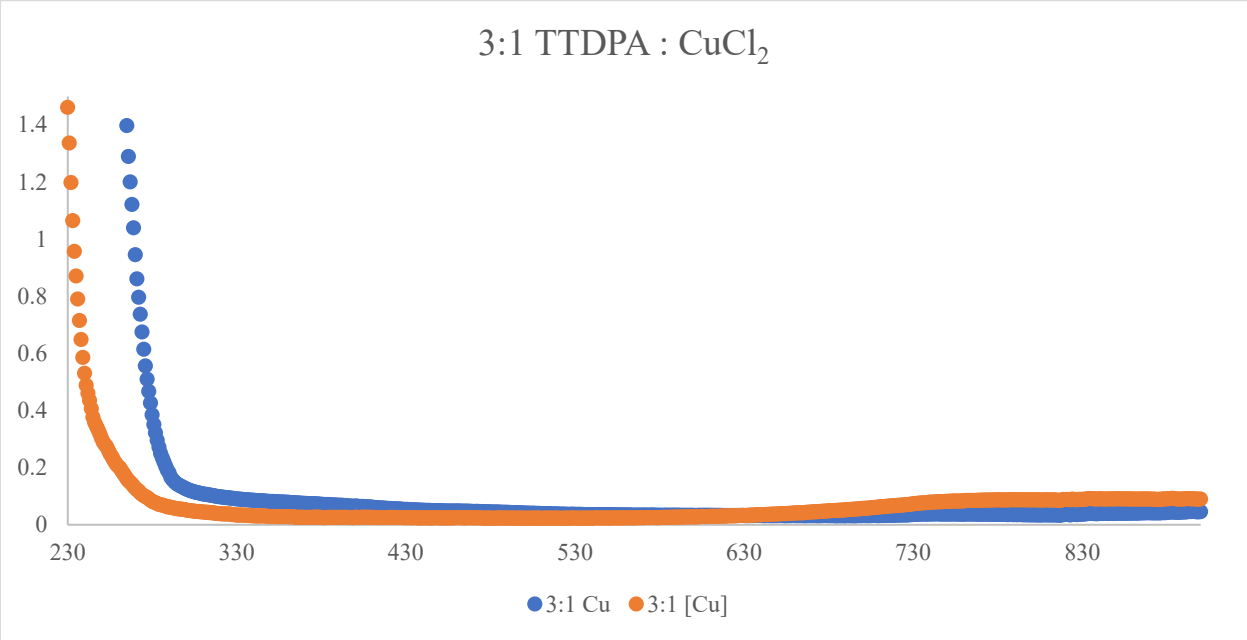


*Graph 6.3 UV-Vis Spectra of 3:1 TTDPA:$CuCl_2$ Filtered (blue) through 5µm Filter Paper Compared to $CuCl_2$ at Matching Nominal Concentration (0.001M) (orange).*

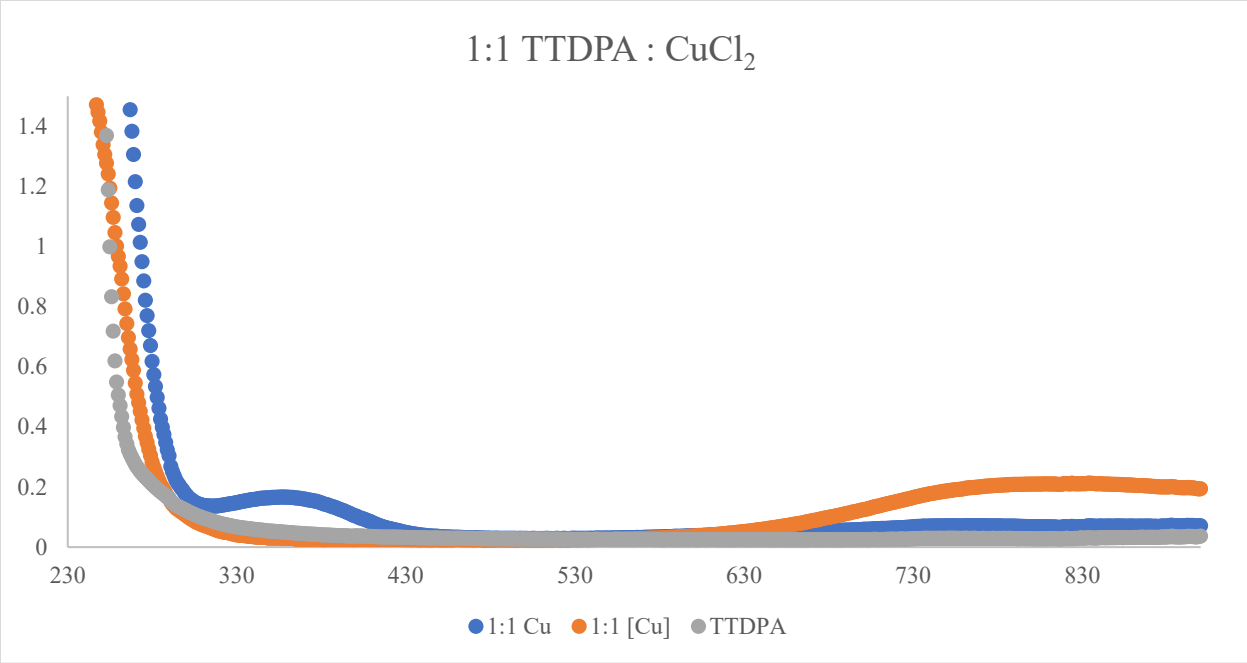


*Graph 6.4 UV-Vis Spectra of 1:1 TTDPA: $CuCl_2$ Filtered (blue) through 5µm Filter Paper Compared to $CuCl_2$ at Matching Nominal Concentration (0.003M) (orange) and TTDPA (0.003M) Alone at Matching Nominal Concentration (gray).*

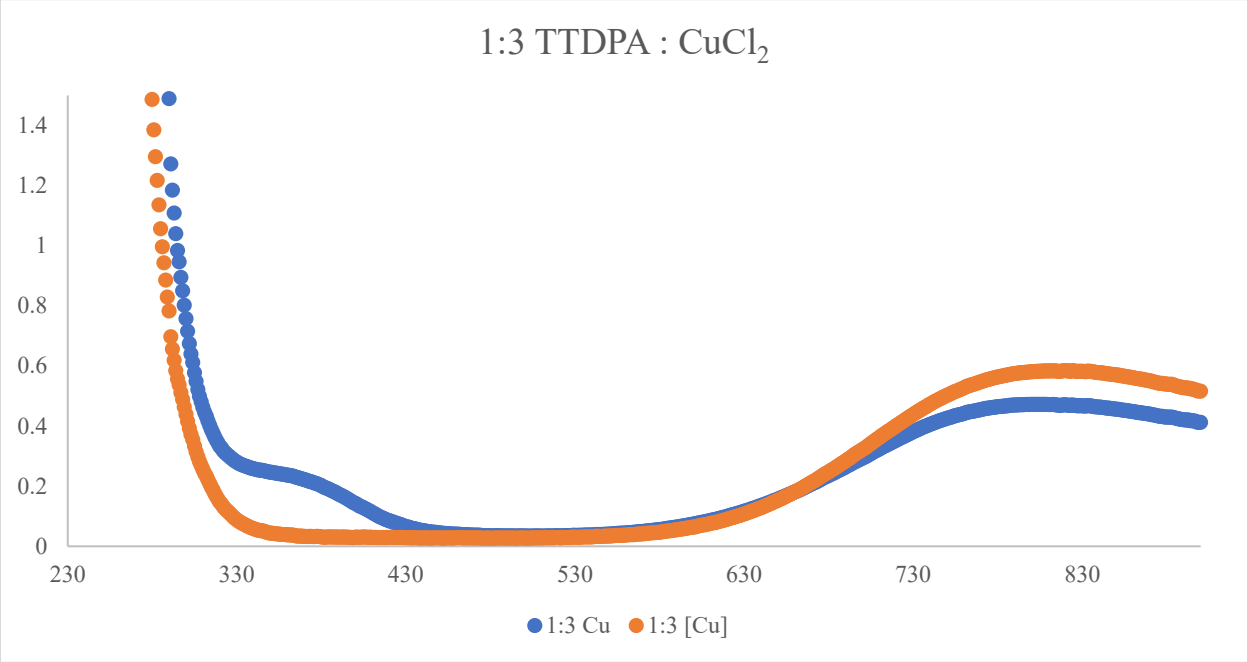


*Graph 6.5 UV-Vis Spectra of 1:3 TTDPA: $CuCl_2$ Filtered (blue) through 5µm Filter Paper Compared to $CuCl_2$ at Matching Nominal Concentration (0.009M) (orange).*

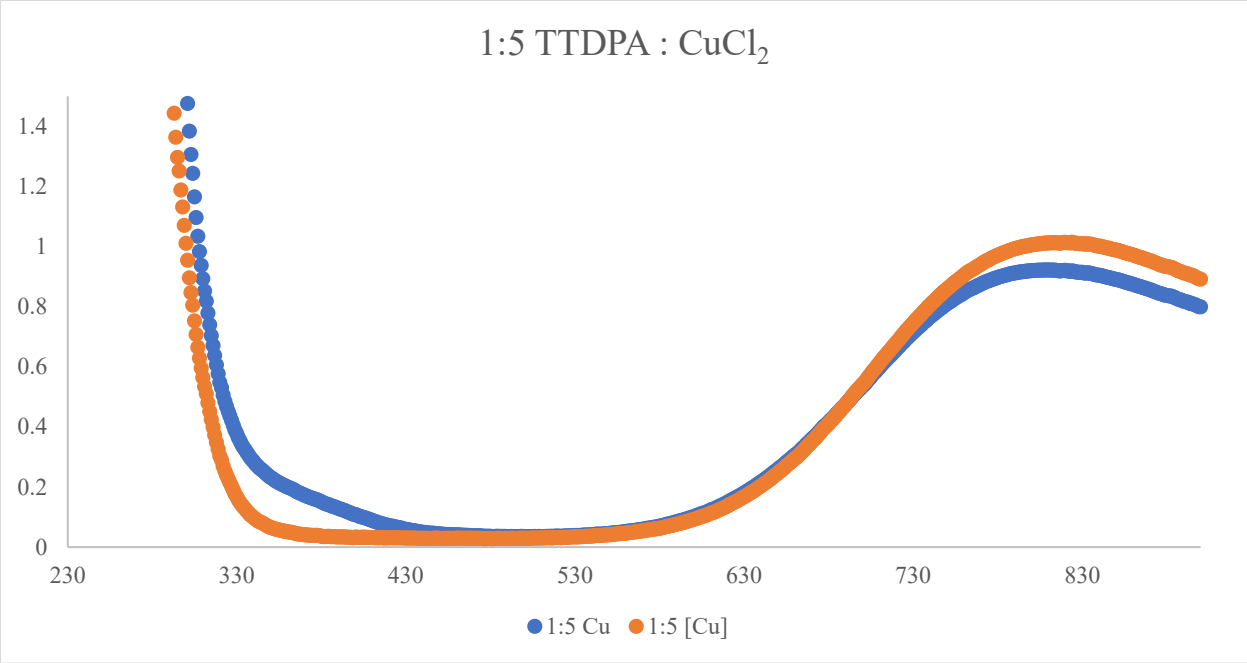


*Graph 6.6 UV-Vis Spectra of 1:5 TTDPA: $CuCl_2$ Filtered (blue) through 5µm Filter Paper Compared to $CuCl_2$ at Matching Nominal Concentration (0.0015M) (orange).*

This line of experimentation was repeated using the 0.2µm PTFE syringe filters, as to be certain that no smaller particles of the precipitated complex was passing through the filter of the 5µm paper. Each mixture ratio was again performed in triplicate; however, only one trial of this experiment was conducted, since the results matched that of the 5µm filter paper. For all mixtures (5:1, 3:1, 1:1, 1:3, and 1:5) the resulting UV-Vis spectra of the 0.2µm PTFE filters showed the same trends and changes in intensity around the 815nm of $Cu^{2+}$, as well as the growth of the complex peak at 365nm (Graphs 6.7-6.11).

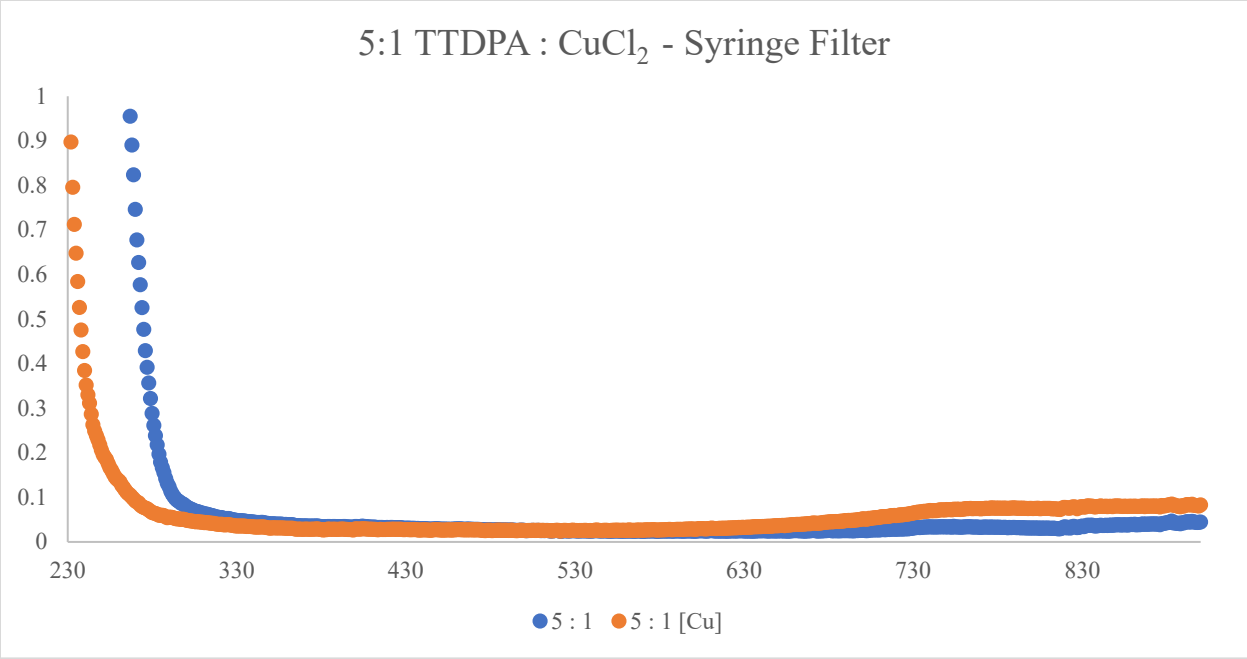


*Graph 6.7 UV-Vis Spectra of 5:1 TTDPA: $CuCl_2$ Filtered (blue) through 0.2µm PTFE Syringe Filter Compared to $CuCl_2$ (0.00006M) Alone at Matching Nominal Concentration (orange).*

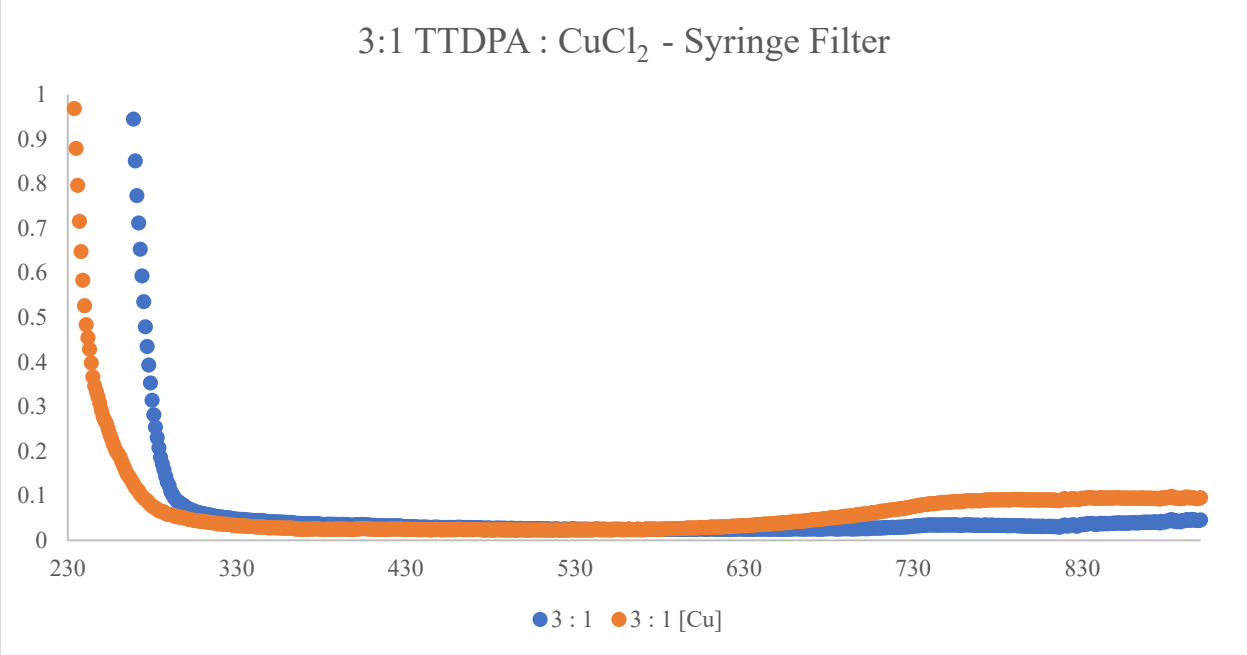


*Graph 6.8 UV-Vis Spectra of 3:1 TTDPA: $CuCl_2$ Filtered (blue) through 0.2µm PTFE Syringe Filter Compared to $CuCl_2$ (0.0001M) Alone at Matching Concentration (orange).*

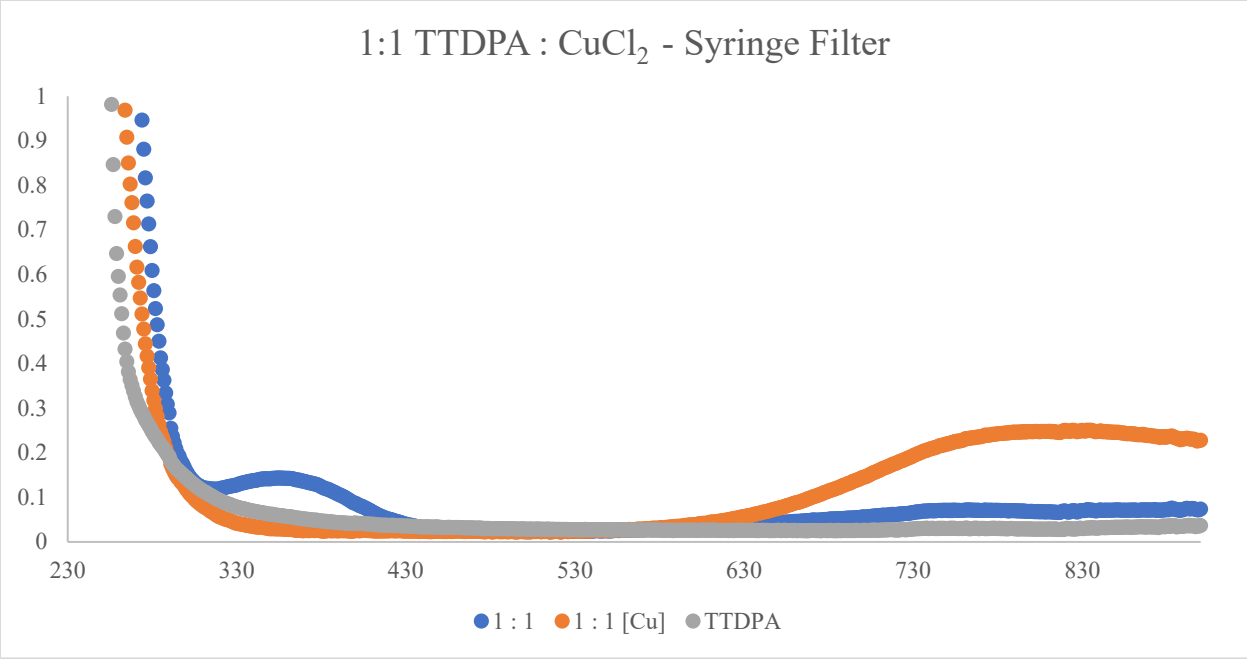


*Graph 6.9 UV-Vis Spectra of 1:1 TTDPA: $CuCl_2$ Filtered (blue) through 0.2µm PTFE Syringe Filter Compared to $CuCl_2$ (0.003M) Alone (orange) at Matching Nominal Concentration and TTDPA Alone at Matching Nominal Concentration (gray).*

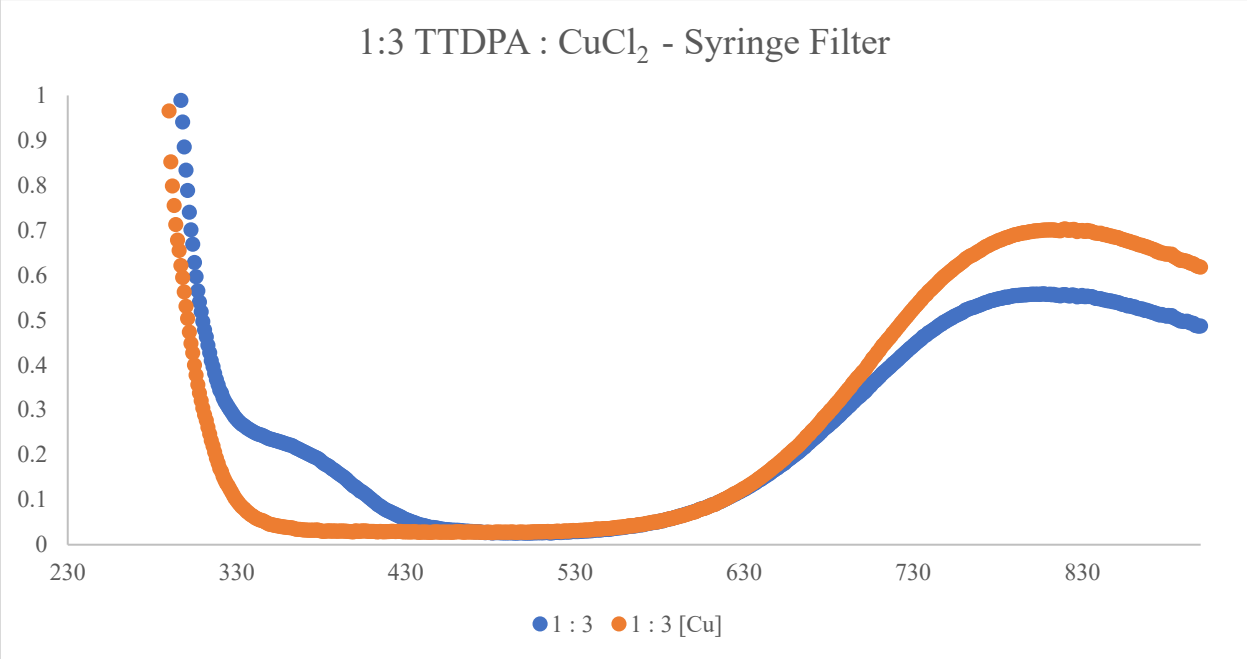


*Graph 6.10 UV-Vis Spectra of 1:3 TTDPA: $CuCl_2$ Filtered (blue) through 0.2µm PTFE Syringe Filter Compared to $CuCl_2$ (0.009M) Alone at Matching Concentration (orange).*

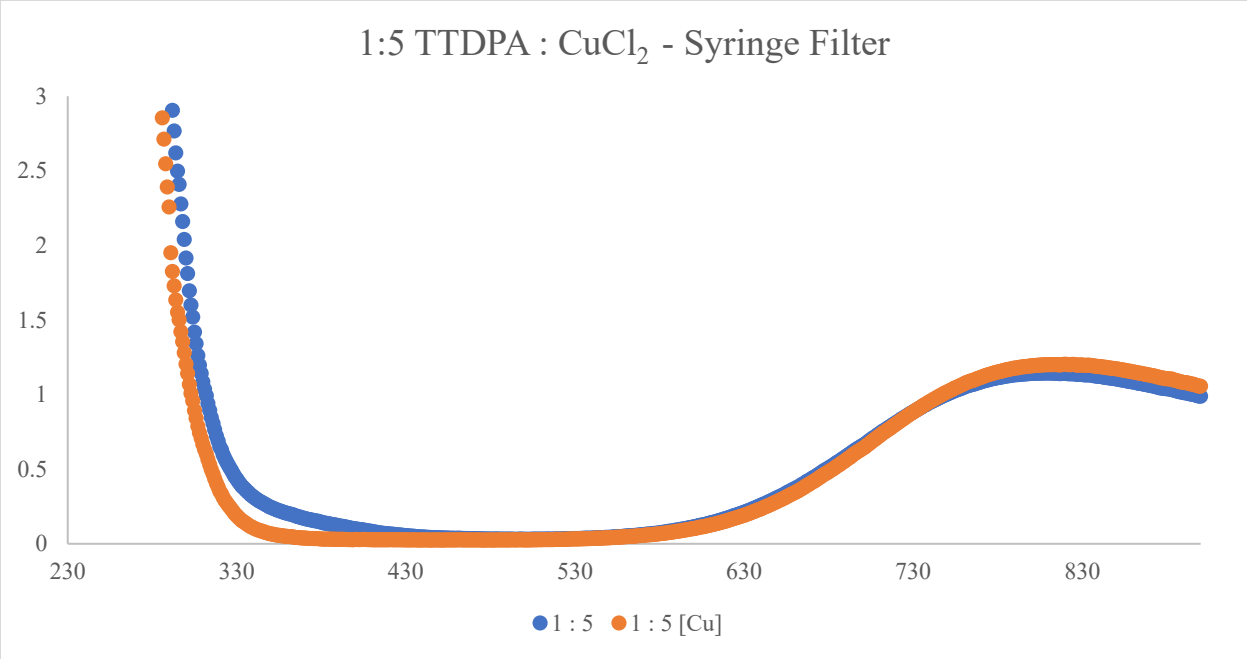


*Graph 6.11 UV-Vis Spectra of 1:5 TTDPA: $CuCl_2$ Filtered (blue) through 0.2µm PTFE Syringe Filter Compared to $CuCl_2$ (0.0015M) Alone at Matching Concentration (orange).*

To be certain that the UV-Vis spectra for all mixtures were the same regardless of the filter type or size used, the spectra were all overlayed (Graphs 6.12-6.16). The spectra were nearly identical for mixtures 5:1, 3:1, and 1:1; however, with mixture 1:3 and 1:5 it appears that there was more unbound $Cu^{2+}$ in the samples that were filtered using the 0.2µM PTFE filters.

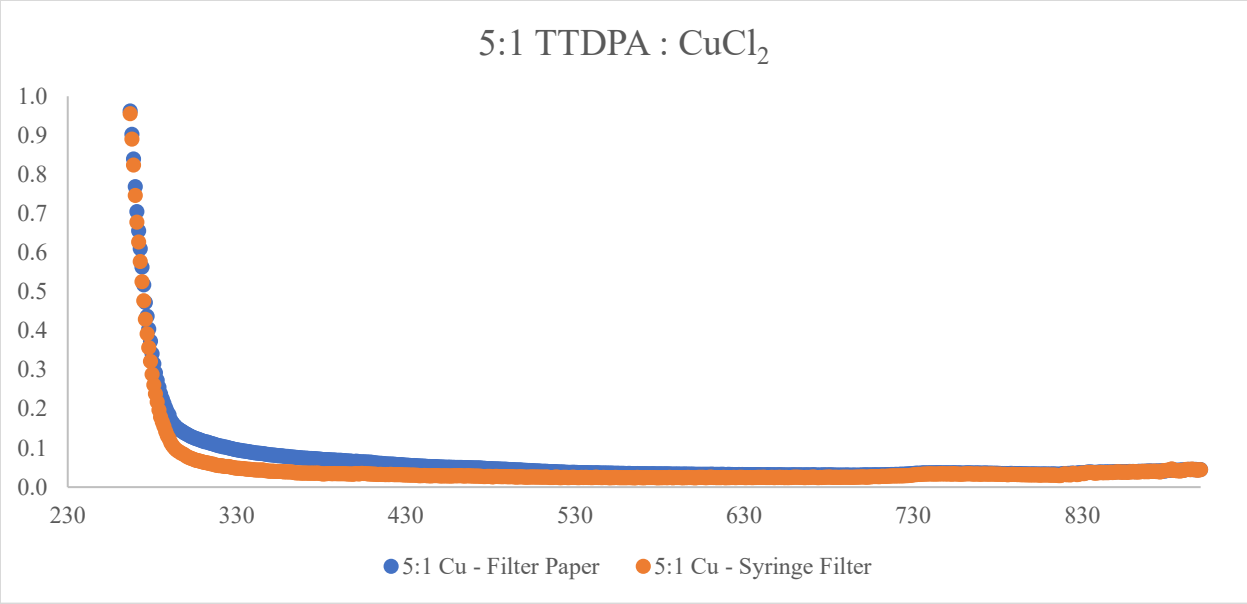


*Graph 6.12 UV-Vis Spectra of 5:1 TTDPA: $CuCl_2$ Filtered (blue) through 5µm Filter Paper Compared to 0.2µm PTFE Syringe Filter (orange).*

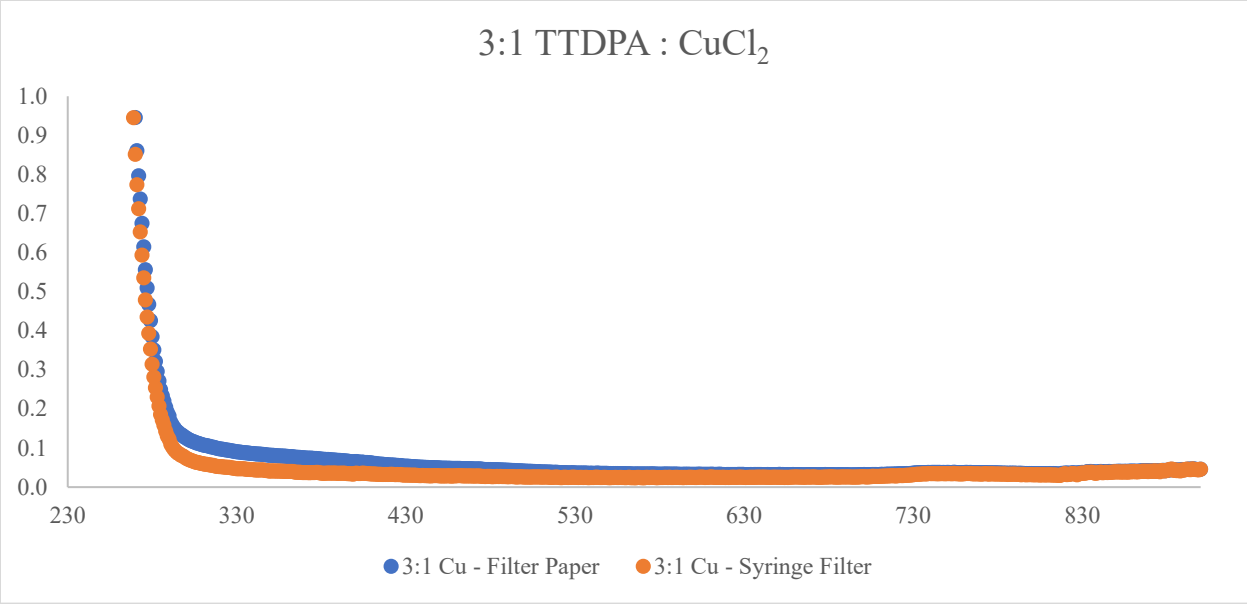


*Graph 6.13 UV-Vis Spectra of 3:1 TTDPA: $CuCl_2$ Filtered (blue) through 5µm Filter Paper Compared to 0.2µm PTFE Syringe Filter (orange).*

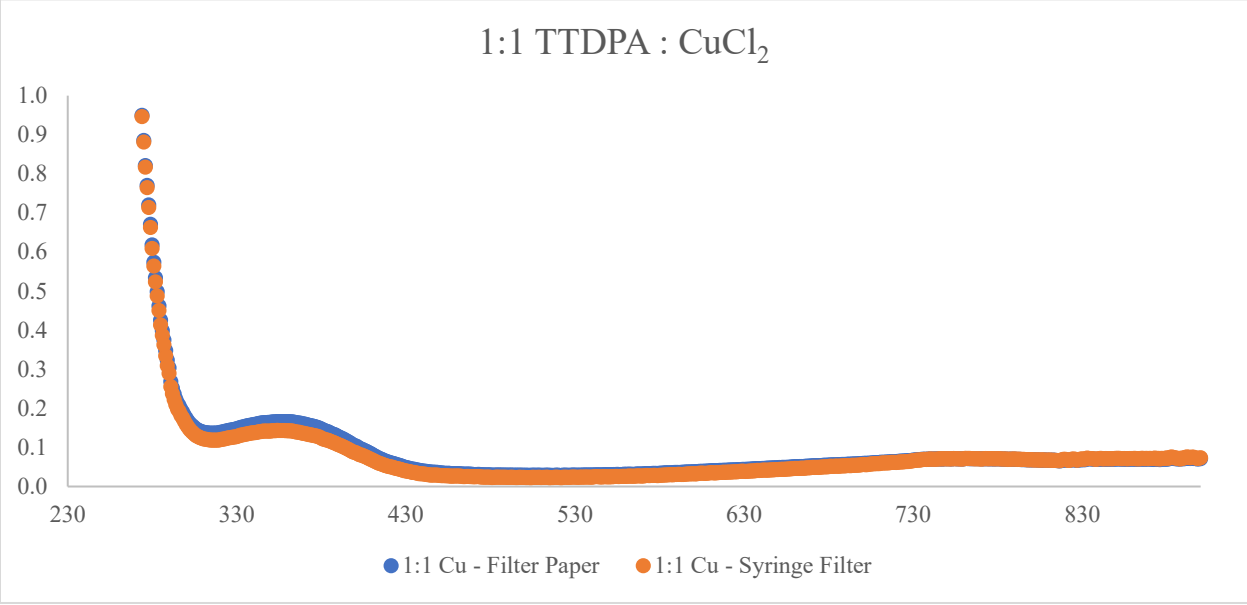


*Graph 6.14 UV-Vis Spectra of 1:1 TTDPA: $CuCl_2$ Filtered (blue) through 5µm Filter Paper Compared to 0.2µm PTFE Syringe Filter (orange).*

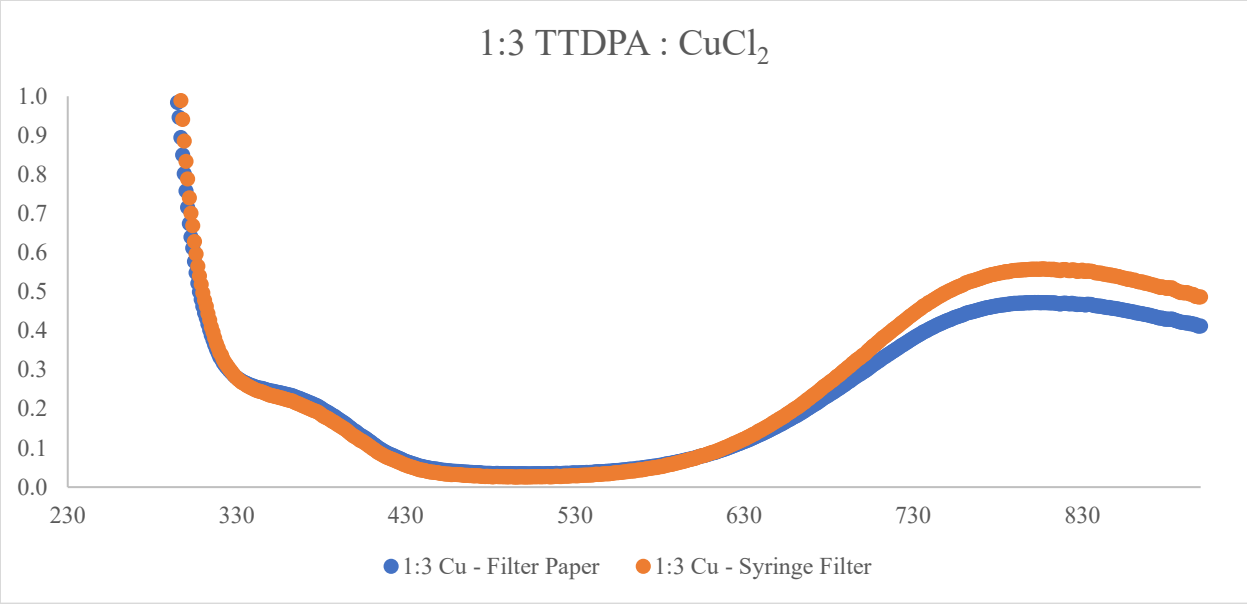


*Graph 6.15 UV-Vis Spectra of 1:3 TTDPA: $CuCl_2$ Filtered (blue) through 5µm Filter Paper Compared to 0.2µm PTFE Syringe Filter (orange).*

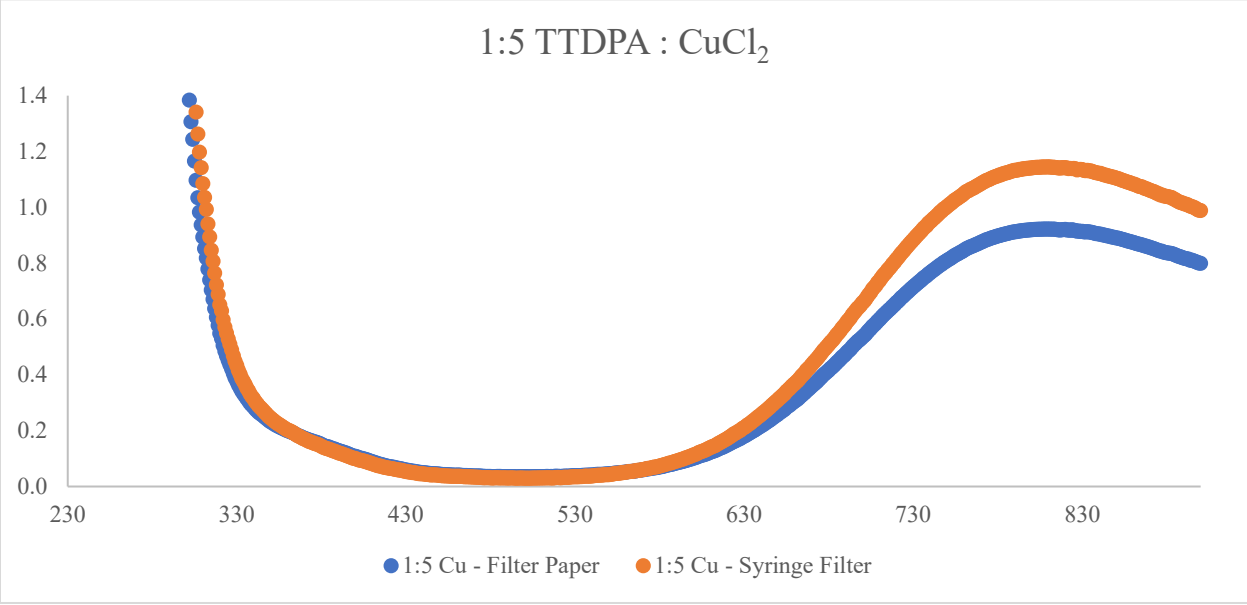


*Graph 6.16 UV-Vis Spectra of 1:5 TTDPA: $CuCl_2$ Filtered (blue) through 5µm Filter Paper Compared to 0.2µm PTFE Syringe Filter (orange).*

After many failed attempts at crystal growth, it was decided to let the test tubes filled with filtered supernatant sit and slowly evaporate. The filtrate of the ligand and copper that was allowed to evaporate yielded large crystals after about 1.5 weeks. A control was also set up with metal solutions and TTDPA that were also filtered and set out to evaporate alongside the mixtures; these control solutions never yielded any crystal formation. Unfortunately, the only samples that produced crystals were the TTDPA: $Cu^{2+}$ samples, but all of the ratios of ligand to copper did form crystals.

In fact, there were two distinct types of crystals formed, a green crystal and a clear crystal that turned slightly blue upon drying (Figure 6.3). The structure of both types of crystals were solved using a Rigaku XtaLAB Synergy X-Ray Diffractometer and refined using OLEX2 (Tables 6.2 and 6.3). Although the TTDPA: $Cu^{2+}$ filtrates were the only samples to produce crystals, many other filtrates using other metals produced flocculant precipitates that were colorful and did not match the physical characteristics of either the ligand or metal independent of each other (see Appendix for crystal growth tubes and all crystal data).

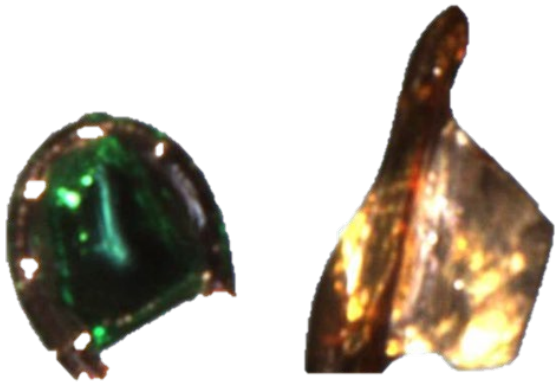

*Figure 6.3 Images of Crystals Used for Data Collection.*

The solved structures revealed the distinguishing characteristics of these crystals (Figures 6.4 and 6.9). The expanded unit cells are included to show simplest repeating pattern in the crystal structure (Figures 6.5 and 6.10) The green crystals (L-CuCl) had two copper ions per TTDPA ligand, whereas the clear crystals (μCl-bis-(Cu-L)) only had one copper ion per TTDPA ligand. In the green L-CuCl structure one copper ion was bound to the sulfur atoms as predicted, but the second copper ion was bound to the carboxylate groups. The L-CuCl is interesting in that the $Cu^{2+}$ bound to the sulfurs was also coordinated to a single, unshared, chloride and was tetrahedral. The second $Cu^{2+}$ coordinated to both oxygens of two carboxylate groups, each carboxylate contributed by a different TTDPA. In addition, each copper is modeled as bound to hydroxide and another $Cu^{2+}$, which is in turn binding to two other carboxylates and a hydroxide. Thus, these adjacent coppers both have a coordination number of six and are octahedral, with an average bond length of 2.622Å which coincides with other published values. (Figure 6.10) (7). When the expanded crystal structure was studied, it appeared that the carboxylate bound copper is what produced the intermolecular bonding to form the lattice structure. In addition to the hydroxides directly bound to the $Cu^{2+}$ there were also 12 waters of hydration per 4 TTDPA molecules found in the crystal; or in other words each TTDPA molecule has 3 waters of hydration associated with it. The formula of the L-CuCl structure is given as $C_{40}H_{92}O_{32}S_{12}Cu_8Cl_4$ and modeled $C_{40}H_{64}O_{32}S_{12}Cu_8Cl_4^{4+} \bullet 4OH^- \bullet 12H_2O$.

Under current structural assumptions the crystals are completely charge balanced. However, if the central copper ions in μCl-bis-(Cu-L) or L-CuCl are $Cu^+$ it is theoretically possible the protonation states assigned are incorrect. However, since the copper used in the experiments was in the $Cu^{2+}$ form and it is not obvious how an electron could be gained to create $Cu^+$, this seems very unlikely. One other complicating factor should be mentioned. The presence of copper ions

in the molecule itself could be a source of error, as analyzing copper containing molecules with X-rays from a copper source, the only one available to us, can be problematic.

In the μCl-bis-(Cu-L) structure the unit cell contained two separate TTDPA ligands each with their own copper, but the two coppers were bridged together by a single chlorine atom. Though a single chloride bridge between two coppers is rare, there is literature supporting the presence of this type of binuclear chloride bridge between two copper (II) atoms (1-3). Some literature on this single chloride bridged copper atoms report an average Cu-Cl bond length of 2.48Å and a Cu-Cl-Cu bond angle of 174.2°. A second study of these Cu-Cl-Cu bonds found an angle of 107.5° and bond distances of 2.340Å and 2.966Å for the Cu-Cl bond lengths (3). For our μCl-bis-(Cu-L) structure we found an average Cu-Cl bond length of 2.26Å and a Cu-Cl-Cu bond angle of 176.7°. Views of the entire crystal lattice structure of each complex have been oriented along all three axes, a, b, and c, and are shown in Figures 6.6-6.8, 6.11-6.13. Electron density map ($F_O - F_C$, 0.235 $eÅ^{-3}$) of the clear crystals shows no missing density that could otherwise be associated with water bound to the structure; and the map for the green crystal shows no missing density either. (Figure 6.14 and 6.15).

*Table 6.2 Crystal Data, Collection Data, and Refinement Summary for μCl-bis-(Cu-L) – Clear Crystal.*

| Crystal data - μCl-bis-(Cu-L) – Clear Crystal. | |
|---|---|
| Chemical formula | $C_{20}H_{33}O_8S_6Cu_2Cl$ |
| $M_r$ | 756.421 |
| Crystal system, space group | Orthorhombic, $Pca2_1$ |
| Temperature (K) | 293 |
| *a*, *b*, *c* (Å) | 12.1018(2), 9.9499(2), 24.4174(4) |
| *V* (Å$^3$) | 2940.14(9) |
| *Z* | 4 |
| Radiation type | Cu *K*α |
| μ (mm$^{-1}$) | 8.8 |
| Crystal size (mm) | 0.13 × 0.077 × 0.06 |
| | |
| Data collection | |
| Diffractometer | XtaLAB Synergy, Dualflex, HyPix |
| Absorption correction | Multi-scan (*CrysAlis PRO*; Rigaku OD, 2021) |
| $T_{min}$, $T_{max}$ | 0.799, 1.00 |
| No. of measured, independent and observed [$I > 2\sigma(I)$] reflections | 29441, 5657, 5657 |
| $R_{int}$ | 0.0538 |
| $(\sin \theta/\lambda)_{max}$ (Å$^{-1}$) | 0.0371 |
| | |
| Refinement | |
| $R[F^2 > 2\sigma(F^2)]$, $wR(F^2)$, $S$ | 0.0421, 0.1350, 1.073 |
| No. of reflections | 5657 |
| No. of parameters | 335 |
| No. of restraints | 1 |
| H-atom treatment | H-atom parameters constrained |
| $\Delta\rho_{max}$, $\Delta\rho_{min}$ (e Å$^{-3}$) | 0.48, -0.63 |

*Table 6.3 Crystal Data, Collection Data, and Refinement Summary for L-CuCl – Green Crystal.*

| Crystal data – L-CuCl – Green Crystal | |
|---|---|
| Chemical formula | $C_{40}H_{92}O_{32}S_{12}Cu_8Cl_4$ |
| $M_r$ | 2120.176 |
| Crystal system, space group | Monoclinic, $P2_1/c$ |
| Temperature (K) | 293 |
| $a$, $b$, $c$ (Å) | 25.5617(3), 10.72810(10), 14.7307(2) |
| $V$ (Å$^3$) | 3967.92(8) |
| $Z$ | 2 |
| Radiation type | Cu $K\alpha$ |
| μ (mm$^{-1}$) | 7.145 |
| Crystal size (mm) | 0.19 × 0.16 × 0.05 |
| | |
| Data collection | |
| Diffractometer | XtaLAB Synergy, Dualflex, HyPix |
| Absorption correction | Multi-scan (*CrysAlis PRO*; Rigaku OD, 2021) |
| $T_{min}$, $T_{max}$ | 0.578, 1.000 |
| No. of measured, independent and observed [$I > 2\sigma(I)$] reflections | 58507, 8400, 8400 |
| $R_{int}$ | 0.0565 |
| $(\sin \theta/\lambda)_{max}$ (Å$^{-1}$) | 0.0300 |
| | |
| Refinement | |
| $R[F^2 > 2\sigma(F^2)]$, $wR(F^2)$, $S$ | 0.0619, 0.1824, 1.023 |
| No. of reflections | 8400 |
| No. of parameters | 457 |
| No. of restraints | 2 |
| H-atom treatment | H-atom parameters constrained |
| $\Delta\rho_{max}$, $\Delta\rho_{min}$ (e Å$^{-3}$) | 1.94, -0.86 |

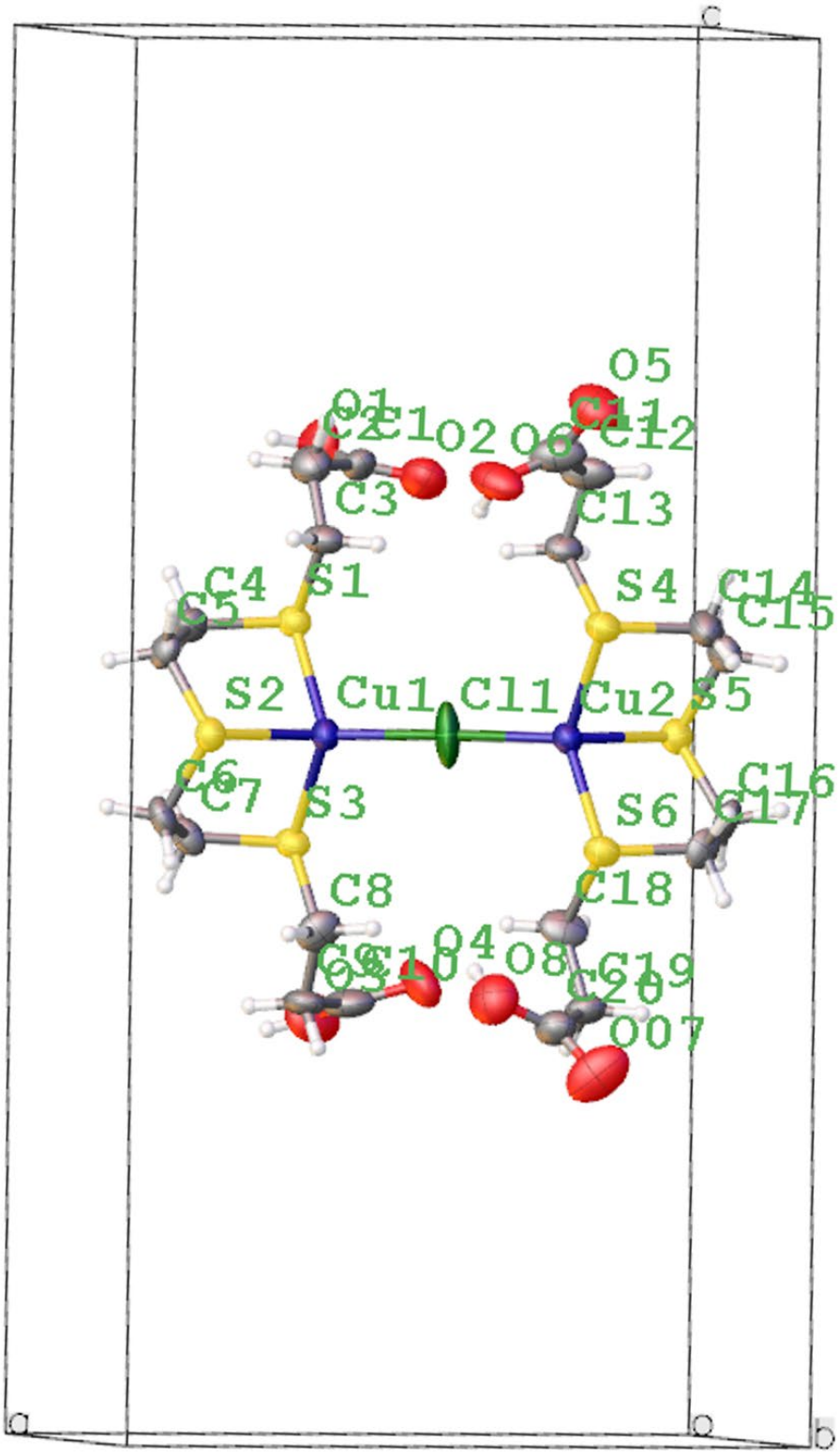


*Figure 6.4 Solved Crystal Structure of μCl-bis-(Cu-L) inside the unit cell– Clear Crystal.*

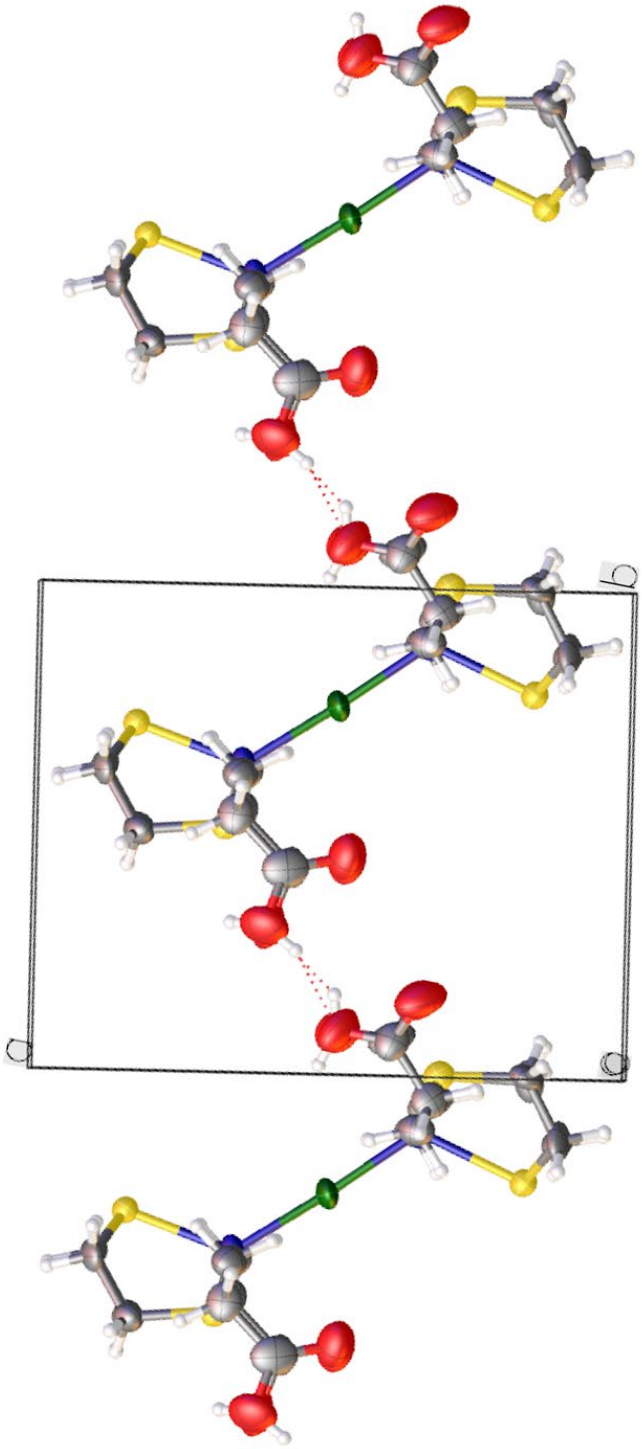

*Figure 6.5 Expanded Lattice Structure of μCl-bis-(Cu-L) in Relation to the Unit Cell – Clear Crystal.*

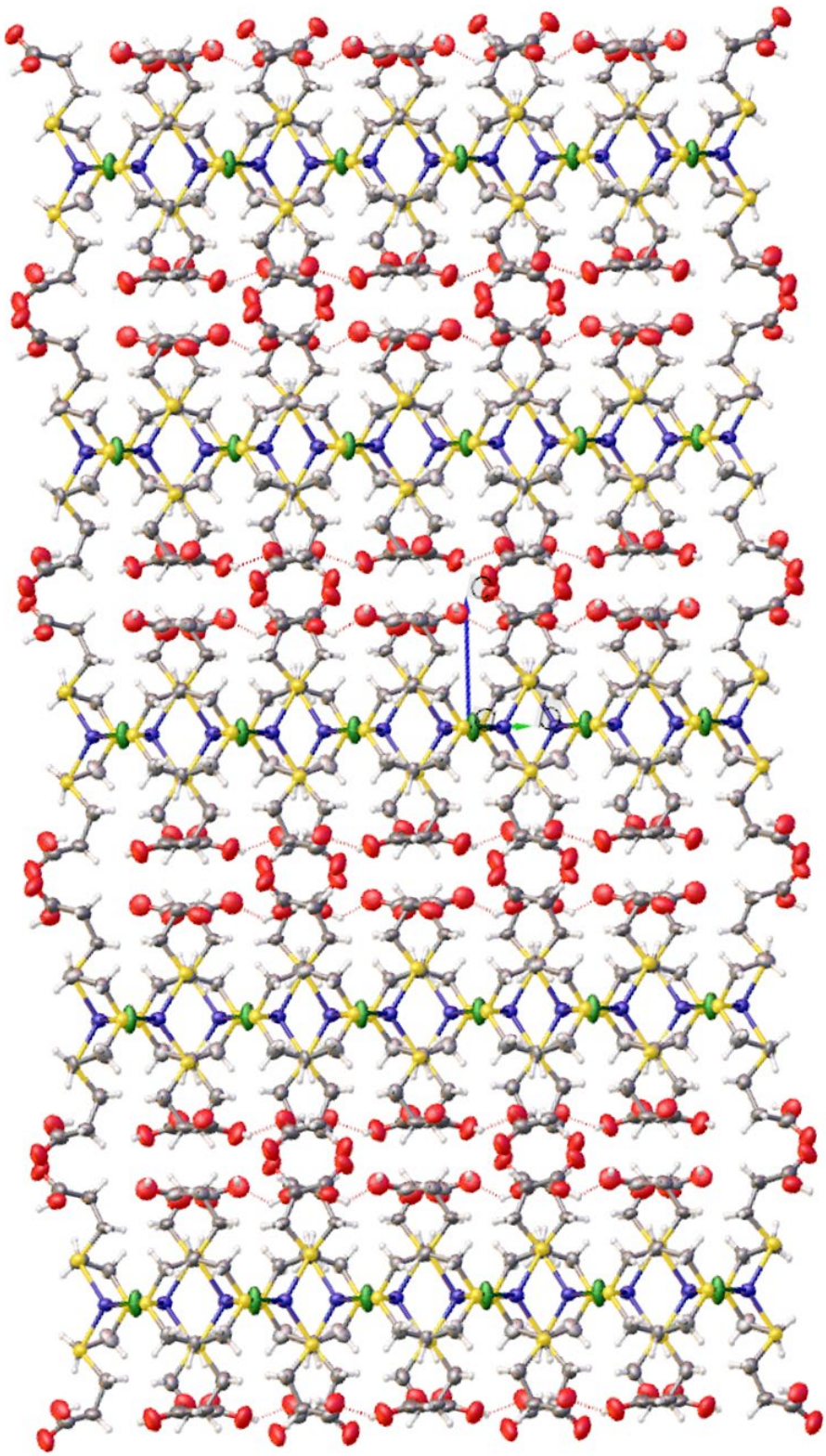

*Figure 6.6 Full Lattice Structure of μCl-bis-(Cu-L) (Clear Crystal) Looking down the A axis – Clear Crystal.*

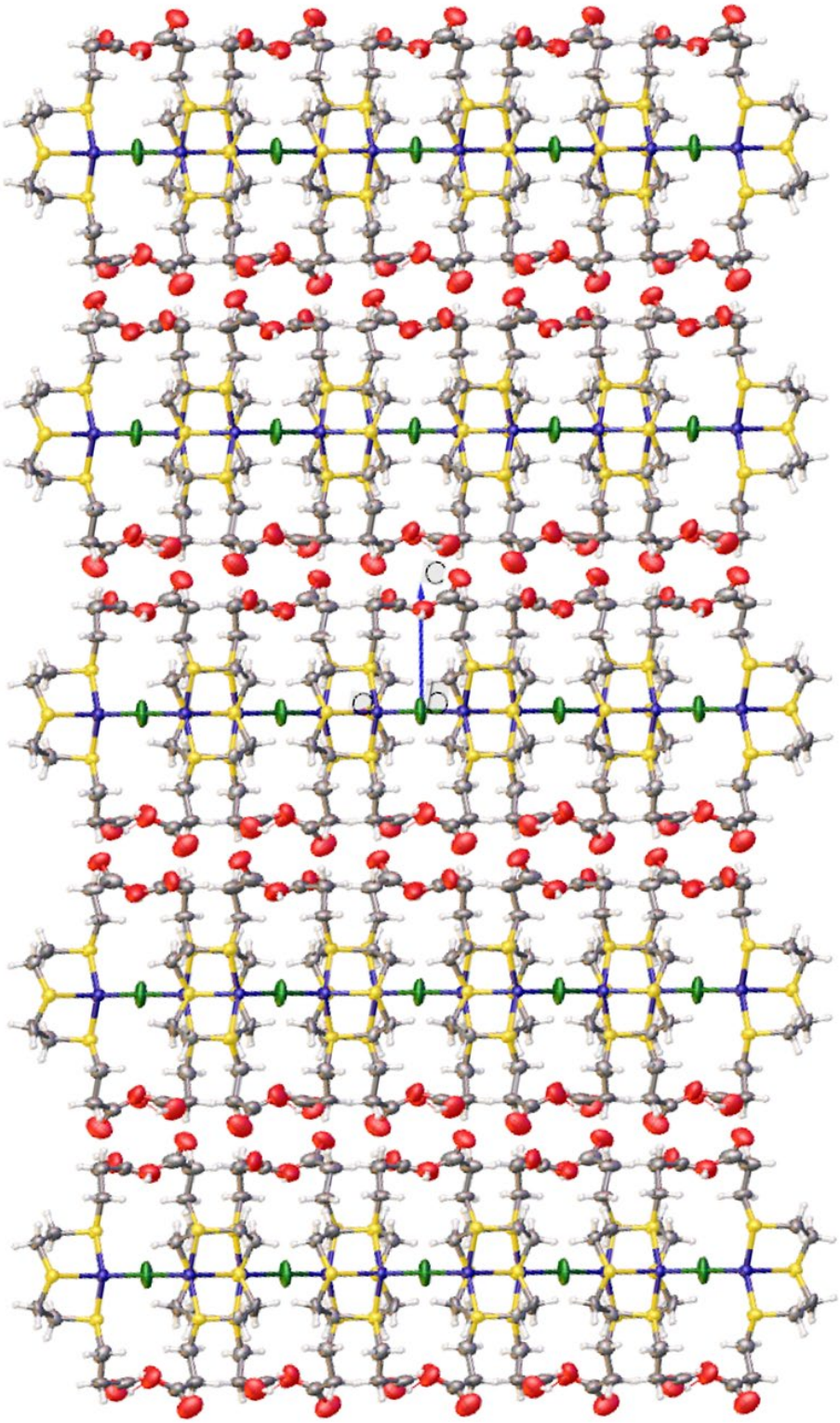


*Figure 6.7 Full Lattice Structure of μCl-bis-(Cu-L) (Clear Crystal) Looking down the B axis – Clear Crystal.*

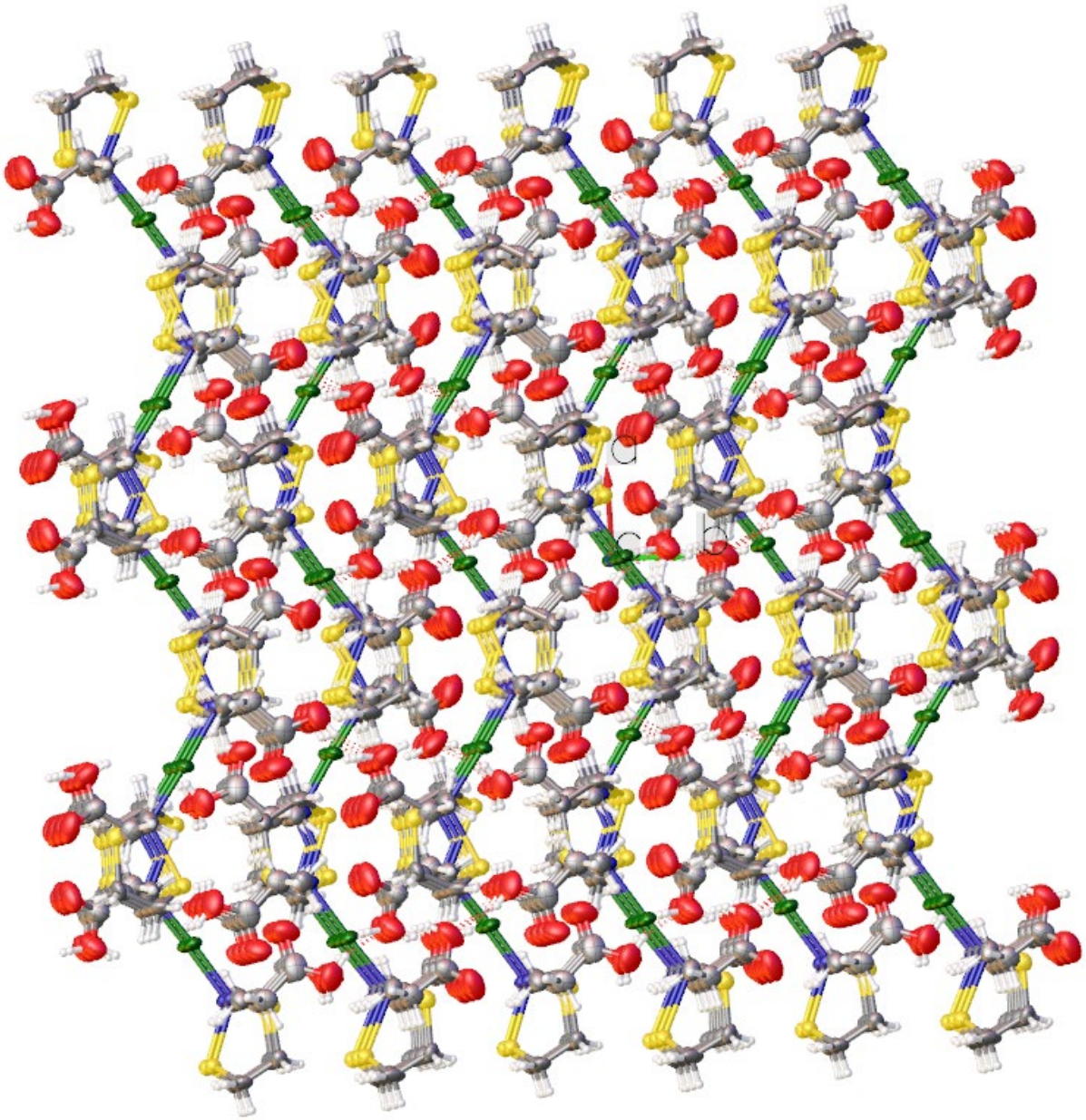

*Figure 6.8 Full Lattice Structure of μCl-bis-(Cu-L) (Clear Crystal) Looking down the C axis – Clear Crystal.*

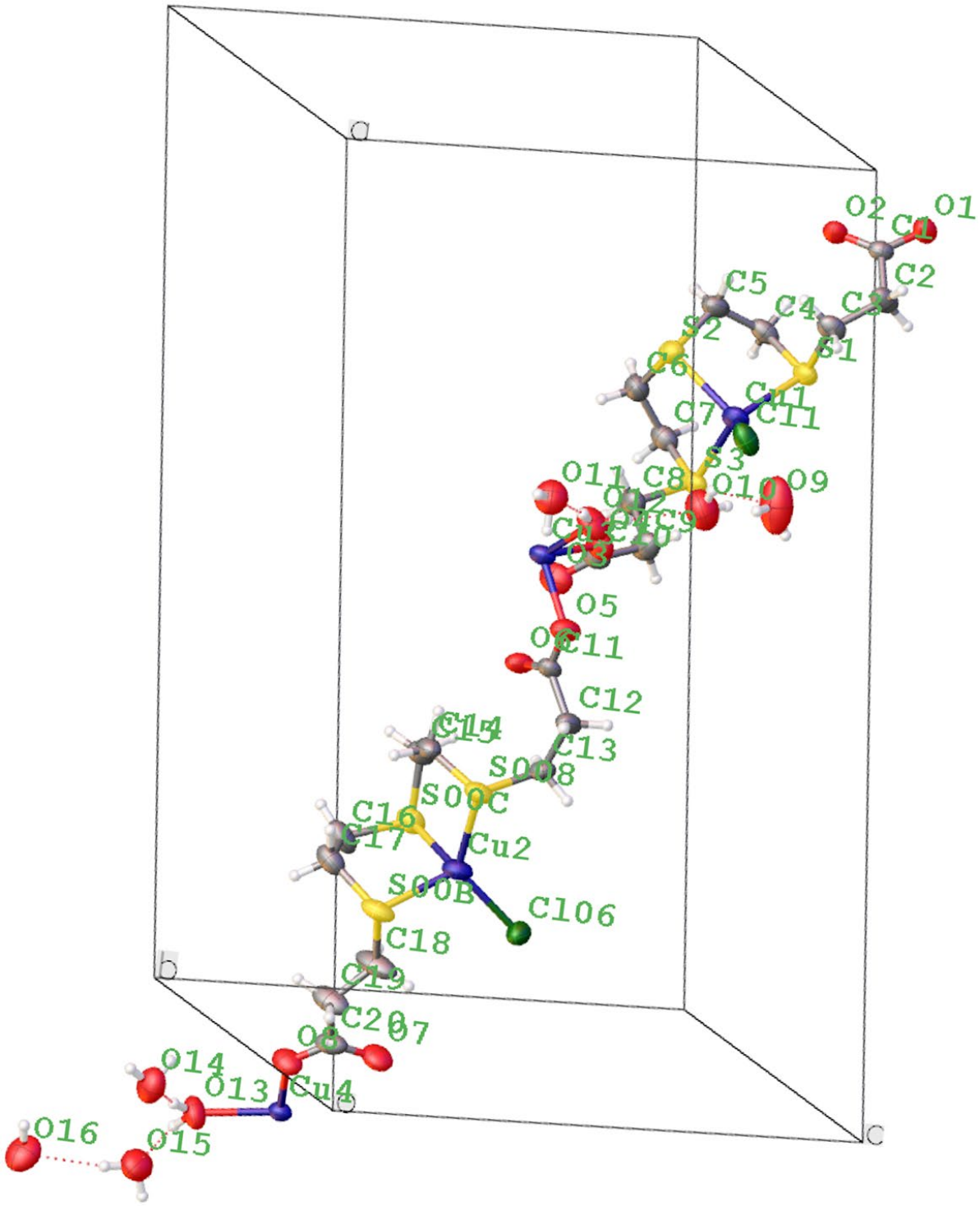


*Figure 6.9 Solved Crystal Structure of L-CuCl inside the unit cell– Green Crystal.*

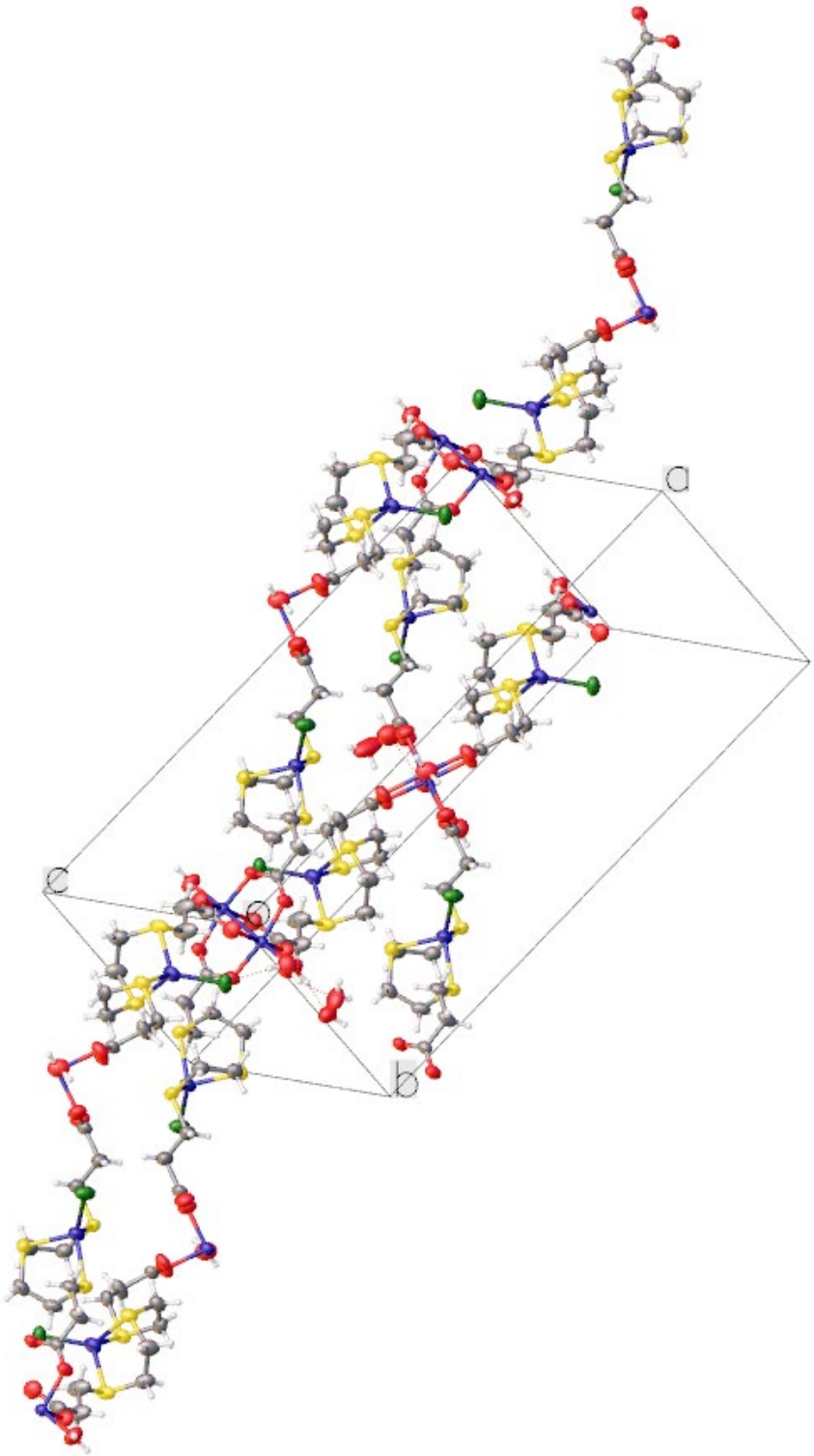

*Figure 6.10 Expanded Lattice Structure L-CuCl inside the Unit Cell – Green Crystal.*

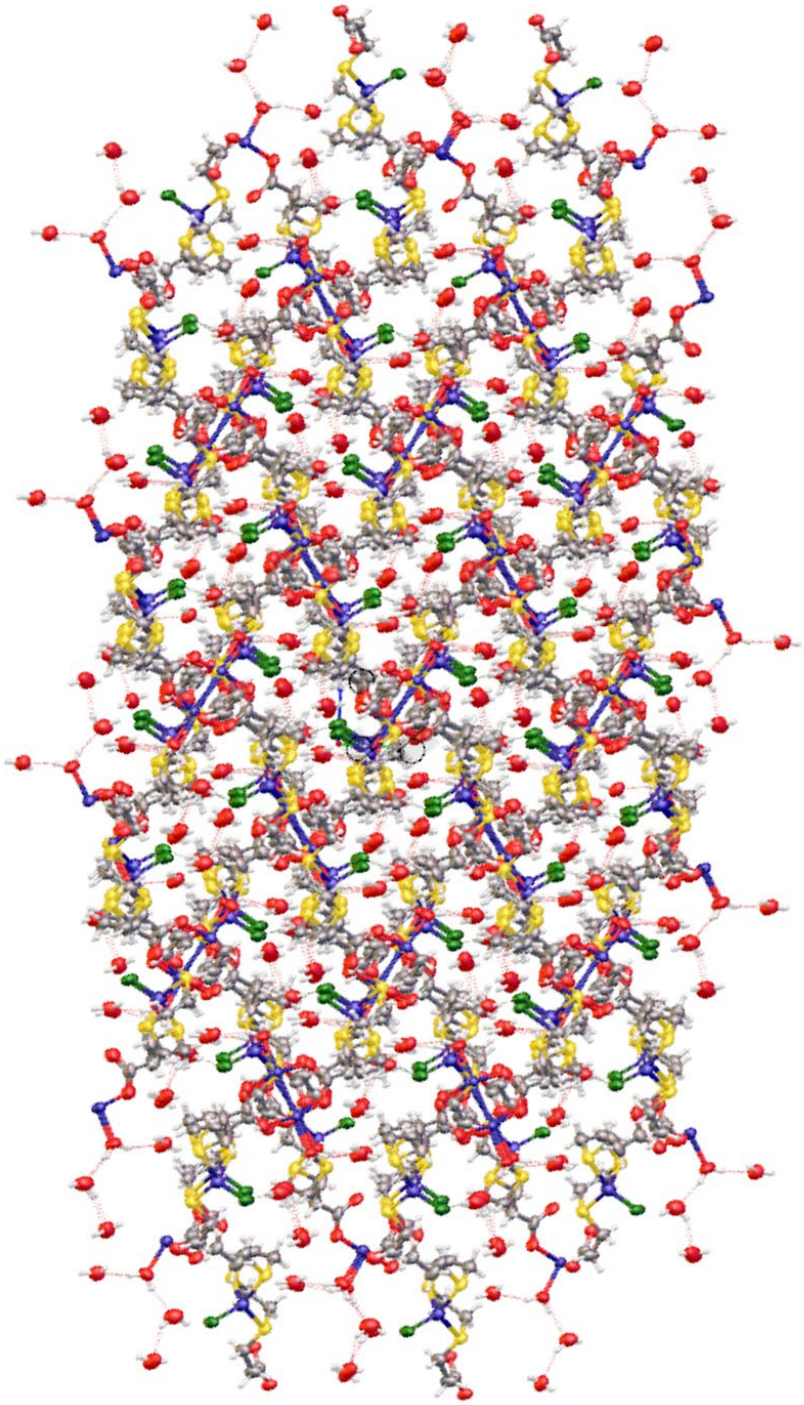

*Figure 6.11 Full Lattice Structure of L-CuCl Looking down the A axis – Green Crystal.*

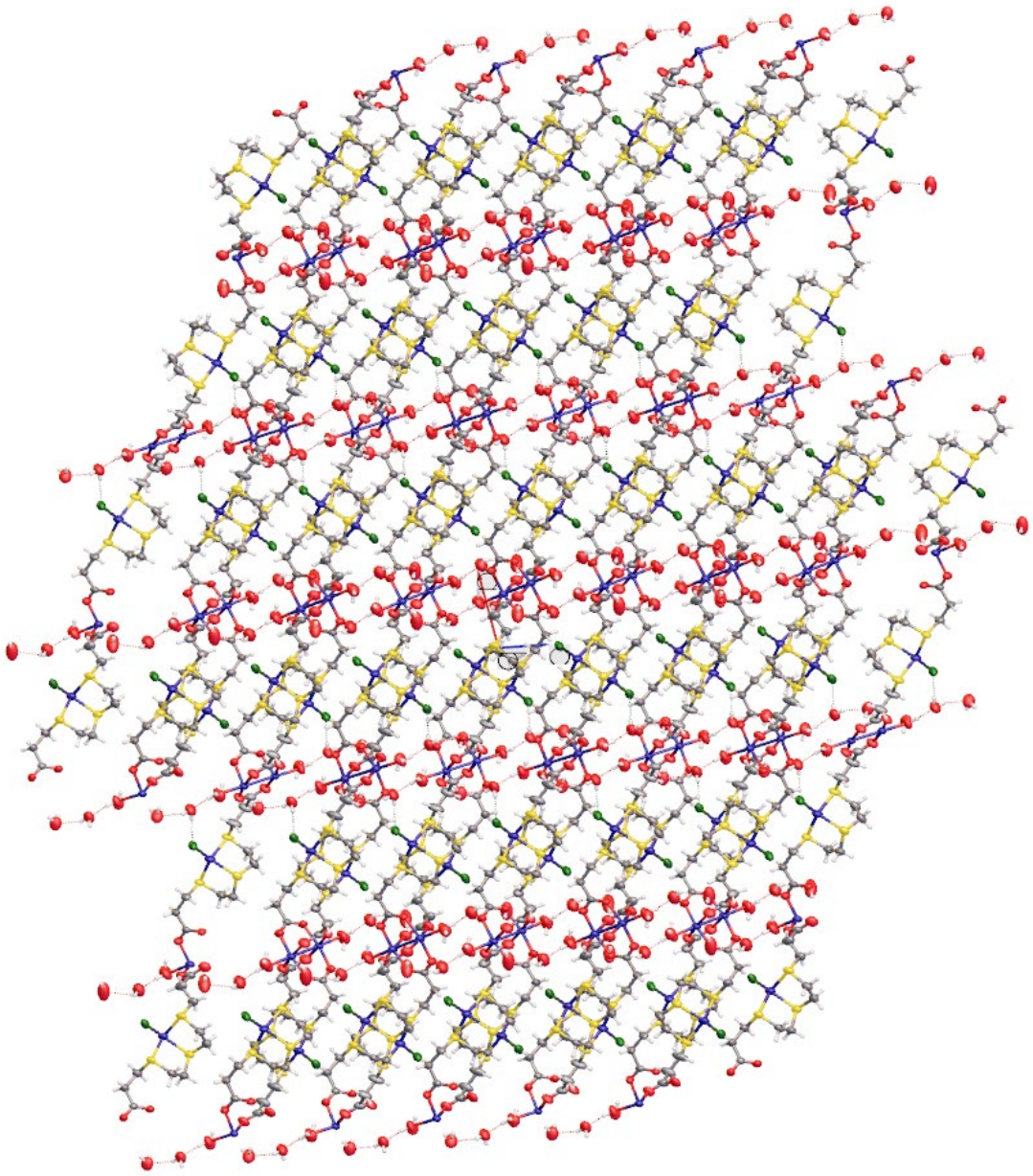

*Figure 6.12 Full Lattice Structure of L-CuCl Looking down the B axis – Green Crystal.*

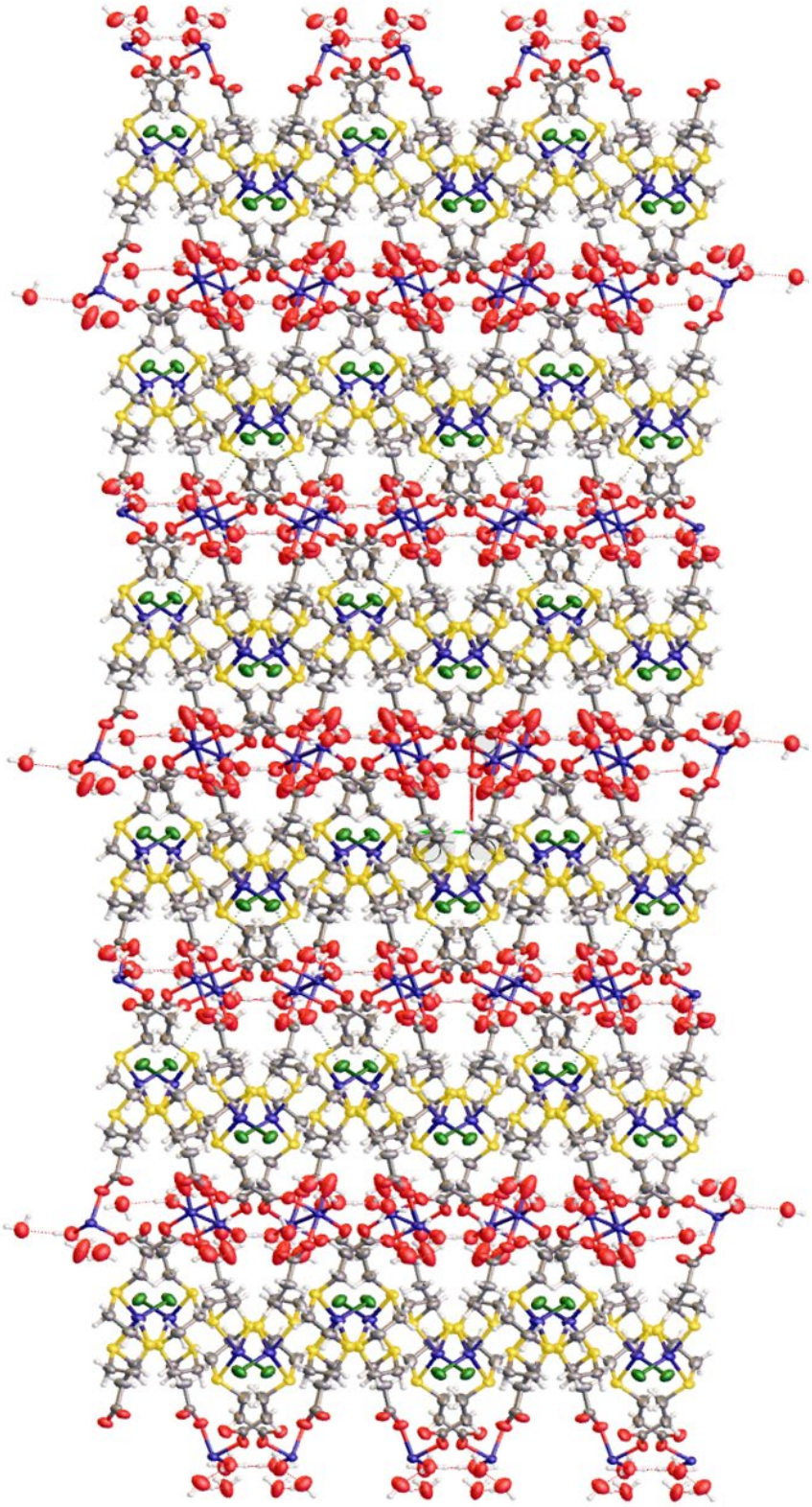

*Figure 6.13 Full Lattice Structure of L-CuCl Looking down the C axis – Green Crystal.*

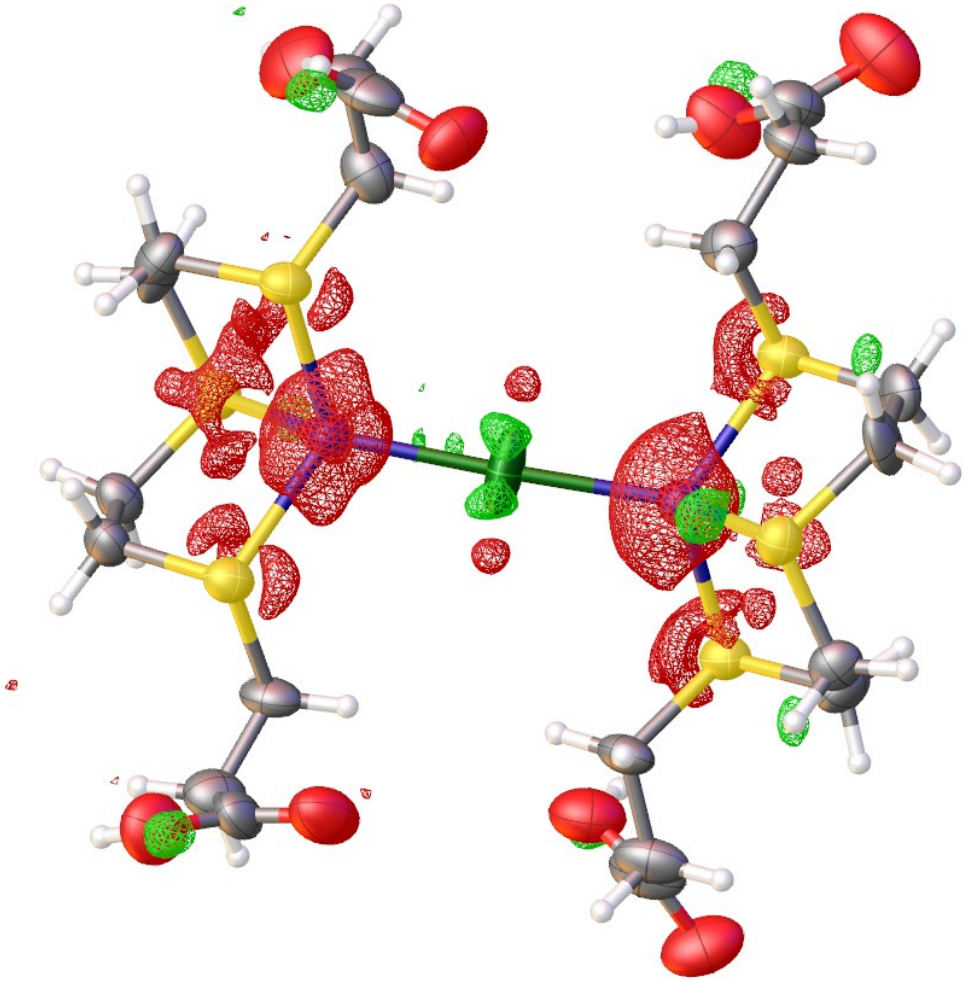

*Figure 6.14 Electron Density Map ($F_O$-$F_C$, 0.235 eÅ$^{-3}$) of the μCl-bis-(Cu-L) - Clear Crystal.*

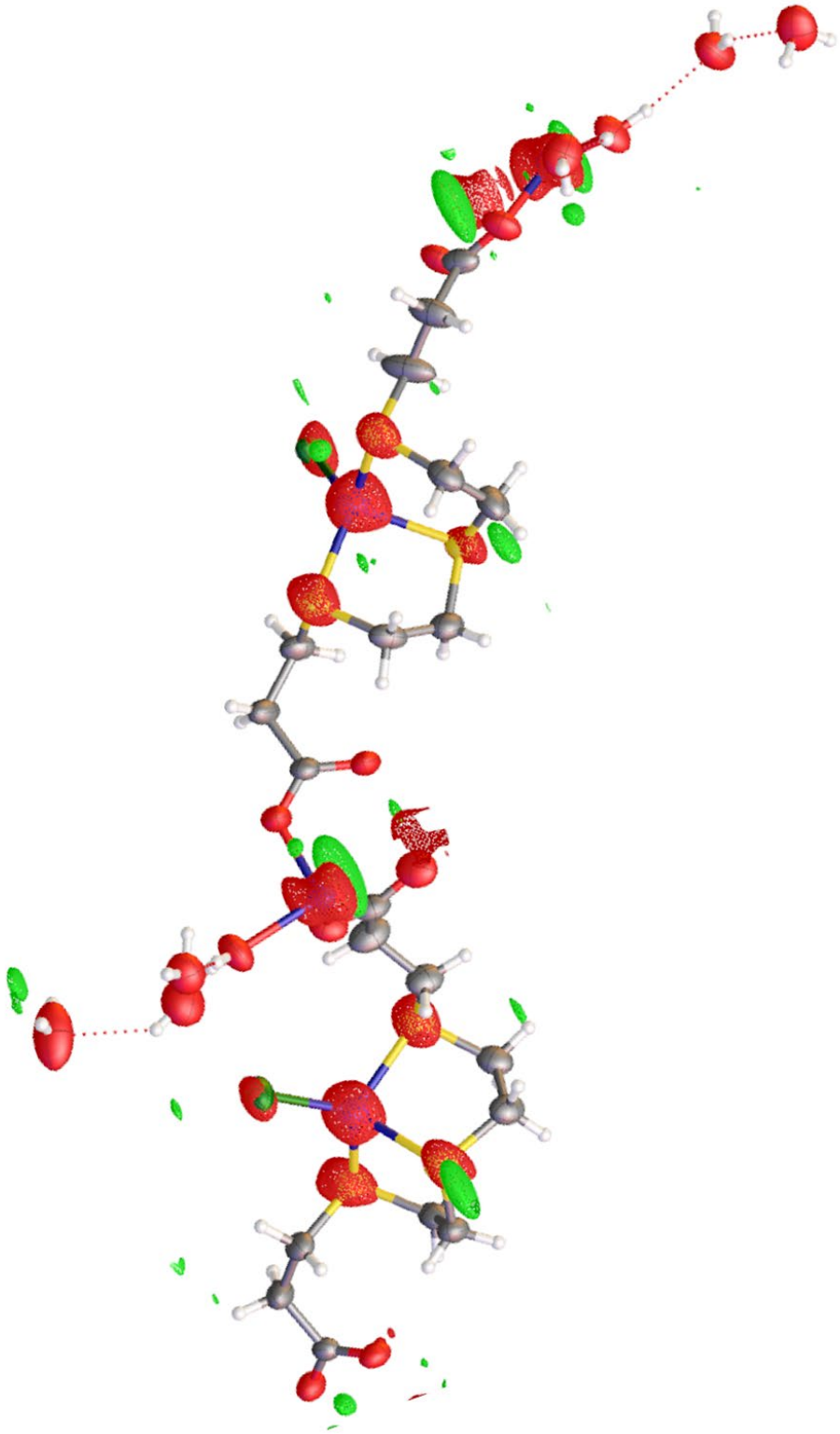

*Figure 6.15 Electron Density Map ($F_O$-$F_C$, 0.235 eÅ$^{-3}$) of the L-CuCl - Green Crystal.*

The bond lengths and angles of the central sulfur-carbon bonds were analyzed and compared between the two different structures of the ligand-copper complex (Table 6.4) as well as to the unbound structures of TTDAA and TTDAce (Table 6.5). Though TTDAA and TTDAce are not the same as the TTDPA ligand at the ends of the ligands, they are identical in the critical center section that resembles the alkylation product of sulfur nucleophiles with sulfur mustard. When comparing bond lengths and angles it appears that TTDPA when bound to a single copper has shorter S-C bonds and more open angles between the C-S-C bonds than the two metal free ligands. The bond lengths between the S-Cu are also shorter in the clear crystals than the green crystals, as well as containing a slightly shorter Cu-Cl bond.

*Table 6.4 Comparison of Bond Length and Angles of μCl-bis-(Cu-L) (Clear) and L-CuCl (green).*

| Bond Lengths (Å) | | |
|---|---|---|
| Molecule | μCl-bis-(Cu-L) | L-CuCl |
| Atoms | Bond Length (Å) | Bond Length (Å) |
| C(3) - S(1) | 1.816(7) | 1.816(5) |
| C(4) - S(1) | 1.793(6) | 1.811(5) |
| C(5) - S(2) | 1.813(7) | 1.811(5) |
| C(6) - S(2) | 1.811(7) | 1.809(6) |
| C(7) - S(3) | 1.822(6) | 1.807(6) |
| C(8) - S(3) | 1.832(9) | 1.830(5) |
| S(1) - Cu(1) | 2.3072(19) | 2.3336(12) |
| S(2) - Cu(1) | 2.3480(6) | 2.3820(14) |
| S(3) - Cu(1) | 2.2998(18) | 2.3258(15) |
| Cu(1) - Cl(1) | 2.2561(6) | 2.2896(14) |
| Bond Angles (°) | | |
| Molecule | μCl-bis-(Cu-L) | L-CuCl |
| Atoms | Bond Angle (°) | Bond Angle (°) |
| C(3)-S(1)-C(4) | 103.7(4) | 104.5(2) |
| C(5)-S(2)-C(6) | 105.22(15) | 103.6(3) |
| C(7)-S(3)-C(8) | 103.1(4) | 99.4(3) |
| S(1)-Cu(1)-S(2) | 93.08(6) | 92.04(5) |
| S(2)-Cu(1)-S(3) | 93.37(6) | 91.12(5) |
| S(1)-Cu(1)-S(3) | 113.03(3) | 112.32(5) |

*Table 6.5 Comparison of Bond Length and Angles of μCl-bis-(Cu-L) vs L-Cu-Cl with Unbound Ligands 2,5,8-Trithianone-1,9-dicarboxylic Acid (TTDAA) and 2,5,8-Trithianonane-1,9-diamide (TTDAce).*

| Bond Lengths (Å) | | | | |
|---|---|---|---|---|
| Molecule | TTDAA | TTDAce | μCl-bis-(Cu-L) | L-CuCl |
| Atoms | Bond Length (Å) | Bond Length (Å) | Bond Length (Å) | Bond Length (Å) |
| S(1) - C(3) | 1.815(7) | 1.817(4) | 1.816(7) | 1.816(5) |
| S(1) - C(2) | 1.819(7) | 1.793(4) | 1.793(6) | 1.811(5) |
| S(2) - C(4) | 1.812(9) | 1.815(4) | 1.813(7) | 1.811(5) |
| S(2) - C(5) | 1.814(1) | 1.813(4) | 1.811(7) | 1.809(6) |
| S(3) - C(7) | 1.797(9) | 1.805(4) | 1.832(9) | 1.830(5) |
| S(3) - C(6) | 1.815(9) | 1.815(4) | 1.822(6) | 1.807(6) |
| Bond Angles (°) | | | | |
| Molecule | TTDAA | TTDAce | μCl-bis-(Cu-L) | L-CuCl |
| Atoms | Bond Angle (°) | Bond Angle (°) | Bond Angle (°) | Bond Angle (°) |
| C(3)-S(1)-C(2) | 101.96(4) | 101.83(2) | 103.7(4) | 104.5(2) |
| C(4)-S(2)-C(5) | 101.32(4) | 100.41(2) | 105.22(15) | 103.6(3) |
| C(7)-S(3)-C(6) | 100.25(4) | 101.7(2) | 103.1(4) | 99.4(3) |

Some of these crystals were collected and separated based on their color, green or clear, rinsed multiple times with water (18MΩ), dried via evaporation, and sent to Atlantic MicroLabs for elemental analysis via combustion. The theoretical (on the basis of the crystal structure defined formula of ($C_{40}H_{64}O_{32}S_{12}Cu_8Cl_4^{4+} \bullet 4OH^- \bullet 12H_2O$) and found elemental analysis data for the green crystals matched well (Table 6.6). The clear crystals (with an apparent formula of $C_{20}H_{33}O_8S_6Cu_2Cl$ based on the crystal structure) proved to be somewhat more complicated. As seen in Table 6.7 there is disagreement. As Table 6.8 shows, adding 3 hypothetical waters of hydration brings the calculated and found percentages into better agreement, but according to the crystal structure there is not any water and, indeed, no room for any water (Figure 6.14). It is possible that there was water present in more macroscopic voids and cracks of the material sent for elemental analysis. It is likely that the carboxylate groups are largely, but not totally,

deprotonated, based on the need to maintain charge balance in the solid. The theoretical, calculated, and solvent adjusted data for the clear crystal is summarized in Tables 6.7 and 6.8. Although not perfect for μCl-bis-(Cu-L), the elemental analysis data still strongly supports that the crystal structures of both forms have been correctly solved and refined.

*Table 6.6 Elemental Analysis of L-CuCl (green crystal) based on formula derived from X-Ray Data.*

| Atom | Number Present | Mass | Theoretical | Found |
|---|---|---|---|---|
| C | 40 | 480.40 | 22.66% | 23.06% |
| H | 92 | 92.74 | 4.37% | 4.40% |
| O | 32 | 512.00 | 24.15% | N/A |
| S | 12 | 384.84 | 18.15% | 18.57% |
| Cl | 4 | 141.80 | 6.69% | 6.55% |
| Cu | 8 | 508.40 | 23.98% | N/A |
| $C_{40}H_{64}O_{32}S_{12}Cu_8Cl_4^{4+} \bullet 4OH^- \bullet 12H_2O$ | | 2120.176 | | |

*Table 6.7 Elemental Analysis of μCl-bis-(Cu-L) (clear crystal) based on formula derived from X-Ray Data.*

| Atom | Number Present | Mass | Theoretical | Found |
|---|---|---|---|---|
| C | 20 | 240.20 | 31.75% | 28.93% |
| H | 33 | 33.26 | 4.40% | 4.60% |
| O | 8 | 128.00 | 16.92% | N/A |
| S | 6 | 192.42 | 25.44% | 23.66% |
| Cl | 1 | 35.45 | 4.69% | 4.39% |
| Cu | 2 | 127.10 | 16.80% | N/A |
| $C_{20}H_{33}O_8S_6Cu_2Cl$ | | 756.434 | | |

***This formula assumes that 3 of 4 carboxylate groups are unprotonated and there is no molecular water in the sample.*

*Table 6.8 Elemental Analysis of μCl-bis-(Cu-L) based on formula derived from X-Ray data and three hypothetical waters.*

| Atom | Number Present | Mass | Theoretical | Found |
|---|---|---|---|---|
| C | 20 | 240.2 | 29.64% | 28.93% |
| H | 39 | 39.312 | 4.85% | 4.60% |
| O | 11 | 176 | 21.72% | N/A |
| S | 6 | 192.42 | 23.74% | 23.66% |
| Cl | 1 | 35.45 | 4.37% | 4.39% |
| Cu | 2 | 127.1 | 15.68% | N/A |
| $C_{20}H_{33}O_8S_6Cu_2Cl \bullet 3H_2O$ | | 810.482 | | |

**This calculation assumes there are 3 unprotonated carboxylate groups, one protonated carboxylate, and 3 water molecules per complex.*

These masses were then used to examine how much precipitate was actually captured, the water was excluded from the mass of the crystals as the precipitate samples were dried under vacuum and heat. For determination of the ratio of complex formation in the precipitate select samples of TTDPA: $CuCl_2$, 3:1, 1:1, and 1:3, were prepared and analyzed via ICP-MS (Table 6.9). When the TTDPA was in excess the μCl-bis-(Cu-L) product (clear crystal) made up about ~87% of the total mass of the precipitate. However, at the 1:1 and 1:3 ratios that number dropped to about 68% for both samples, with the other 32% being the L-CuCl product (green crystal). This would appear to indicate that there seems to be a limit on to how much of each product is formed, and that the L-CuCl product is the secondary product, hitting a plateau of formation around the equimolar ratio of TTDPA: $Cu^{2+}$.

*Table 6.9 Determine of Mass Percentages of μCl-bis-(Cu-L) (clear crystal) and L-CuCl (green crystal) Products in TTDPA: $Cu^{2+}$ Precipitate Samples.*

| Sample | Measured Copper (ppm) | Copper (mg) | μCl-bis-(Cu-L) | L-CuCl |
|---|---|---|---|---|
| 3 to 1 | 336 | 0.1714 | 86.8% | 13.2% |
| 1 to 1 | 379 | 0.1933 | 68.5% | 31.5% |
| 1 to 3 | 440 | 0.2244 | 68% | 32% |

Once the precipitate of each sample was dried on its respective filter, it was cooled to room temperature for 30 minutes and then weighed. The initial mass of the filter was then subtracted from the final mass, yielding the amount of precipitate captured. The mass studies included the addition of TTDPA: $Zn^{2+}$ and TTDPA: $Mn^{2+}$ produced in the same manner as the $Cu^{2+}$ samples. However, TTDPA: $Zn^{2+}$ and TTDPA: $Mn^{2+}$ were each only reacted in 5:1, 1:1, and 1:5 ratios; and, both filtered and weighed only with the 5µm filter paper. There were two separate trials conducted and each mixture was also performed in triplicate, resulting again in a total of 6 data points. For each trial, the triplicate mixtures were then averaged and their standard deviation measured.

The data for trials 1 & 2 of TTDPA: $Cu^{2+}$ filtered through 5µm filter paper yielded relatively similar numbers with the second trial averaging higher total precipitate across all mixtures (Table 6.10,6.11), and their direct comparison between trial averages summarized in Table 6.12. The process was repeated again for the TTDPA: $Cu^{2+}$ trial filtered through 0.2µm PTFE syringe filters (Table 6.13). When results of the filter paper and syringe filter data are compared directly (Table 6.14) shows little deviation between the recorded masses of mixtures of 5:1, 3:1, 1:1, and 3:1; while 1:5 has a slightly higher recorded deviation. One reason for discrepancies between the paper filter and the syringe filters might be leakage at the connection between the filter and the syringe causing a loss of precipitate mass.

The reaction between TTDPA: $ZnCl_2$ was treated the same as the TTDPA: $CuCl_2$ samples, but only in the ratios of 5:1, 1:1, and 1:5 on the 5µm filter paper. There was very little deviation between the triplicate samples of each mixture in their respective trials (Table 6.15,6.16). When compared directly TTDPA: $Zn^{2+}$ (Table 6.17) there is a higher deviation that in the copper trial,

but not in any amount that would arise concern. The highest deviation is in the 1:3 mixture, where the deviation between trials is 3.9mg which equates to less than 4% of the overall mass.

The reaction between TTDPA: $MnCl_2$ was treated the same as the TTDPA: $CuCl_2$ and TTDPA: $ZnCl_2$ samples, but only in the ratios of 5:1, 1:1, and 1:5 on the 5µm filter paper. The manganese trials proved similar to those of nickel and cobalt with the ratios of 5:1 and 1:1 showing a visible precipitate but almost no captured precipitate. The 1:1 ratio did form a fair amount of visible precipitate after filtration, but only after sitting undisturbed for a few days. However, in the 1:5 trial the vast majority of precipitate was captured. (Table 6.18,6.19). When the trials are compared directly TTDPA: $Mn^{2+}$ (Table 6.20) there is little deviation between the trials. The highest is in the 5:1 trial, but the mass changes there were so low it could simply be attributed to error. On the TTDPA: $MnCl_2$ trial of 1:5 that showed the greatest change in mass the deviation was only 1.86% of the overall mass.

*Table 6.10 Recorded Precipitate Mass for TTDPA: $CuCl_2$ Mixtures Filtered through 5µm Filter Paper – Trial 1.*

| Copper w/ TTDPA- Trail 1 | | | | | | |
|---|---|---|---|---|---|---|
| Filter Code | TTDPA: Copper Ratio | Initial Mass (g) | Final Mass (g) 24hr. | Δ Mass (mg) 24 hr. | Avg. Δ (mg) 24 hr. | Std. Dev. 24 hr. |
| A1 | 5:1 Cu - T1 | 0.3283 | 0.3429 | 14.6 | 13.9 | 1.8 |
| A2 | 5:1 Cu - T1 | 0.3138 | 0.3291 | 15.3 | | |
| A3 | 5:1 Cu - T1 | 0.3318 | 0.3437 | 11.9 | | |
| B1 | 3:1 Cu - T1 | 0.3202 | 0.3457 | 25.5 | 24.2 | 2.1 |
| B2 | 3:1 Cu - T1 | 0.3149 | 0.3402 | 25.3 | | |
| B3 | 3:1 Cu - T1 | 0.3315 | 0.3533 | 21.8 | | |
| C1 | 1:1 Cu - T1 | 0.3144 | 0.4015 | 87.1 | 86.9 | 1.3 |
| C2 | 1:1 Cu - T1 | 0.3193 | 0.4048 | 85.5 | | |
| C3 | 1:1 Cu - T1 | 0.3294 | 0.4175 | 88.1 | | |
| D1 | 1:3 Cu - T1 | 0.3195 | 0.3878 | 68.3 | 67.8 | 0.9 |
| D2 | 1:3 Cu - T1 | 0.3204 | 0.3872 | 66.8 | | |
| D3 | 1:3 Cu - T1 | 0.3151 | 0.3835 | 68.4 | | |
| E1 | 1:5 Cu - T1 | 0.3323 | 0.3871 | 54.8 | 52.3 | 2.3 |
| E2 | 1:5 Cu - T1 | 0.3302 | 0.3805 | 50.3 | | |
| E3 | 1:5 Cu - T1 | 0.3208 | 0.3727 | 51.9 | | |

*Table 6.11 Recorded Precipitate Mass for TTDPA: $CuCl_2$ Mixtures Filtered through 5µm Filter Paper – Trial 2.*

| Copper w/ TTDPA - Trial 2 | | | | | | |
|---|---|---|---|---|---|---|
| Filter Code | TTDPA: Copper Ratio | Initial Mass (g) | Final Mass (g) 24hr. | Δ Mass (mg) 24 hr. | Avg. Δ (mg) 24 hr. | Std. Dev. 24 hr. |
| A1p | 5:1 Cu - T2 | 0.3276 | 0.3469 | 19.3 | 17.2 | 3.2 |
| A2p | 5:1 Cu - T2 | 0.3191 | 0.3379 | 18.8 | | |
| A3p | 5:1 Cu - T2 | 0.3187 | 0.3322 | 13.5 | | |
| B1p | 3:1 Cu - T2 | 0.3197 | 0.3468 | 27.1 | 29.4 | 2.5 |
| B2p | 3:1 Cu - T2 | 0.3227 | 0.3548 | 32.1 | | |
| B3p | 3:1 Cu - T2 | 0.3248 | 0.3537 | 28.9 | | |
| C1p | 1:1 Cu - T2 | 0.3291 | 0.4117 | 82.6 | 87.1 | 6.7 |
| C2p | 1:1 Cu - T2 | 0.3210 | 0.4048 | 83.8 | | |
| C3p | 1:1 Cu - T2 | 0.3189 | 0.4137 | 94.8 | | |
| D1p | 1:3 Cu - T2 | 0.3169 | 0.4001 | 83.2 | 85.0 | 1.9 |
| D2p | 1:3 Cu - T2 | 0.3059 | 0.3908 | 84.9 | | |
| D3p | 1:3 Cu - T2 | 0.3164 | 0.4033 | 86.9 | | |
| E1p | 1:5 Cu - T2 | 0.3279 | 0.4011 | 73.2 | 71.6 | 1.4 |
| E2p | 1:5 Cu - T2 | 0.3142 | 0.3855 | 71.3 | | |
| E3p | 1:5 Cu - T2 | 0.3127 | 0.3831 | 70.4 | | |

*Table 6.12 Comparison of Trial 1 and Trail 2 Masses of Mass for TTDPA: $CuCl_2$ Mixtures Filtered through 5µm Filter Paper.*

| Copper w/ TTDPA- T1 vs T2 | | | |
|---|---|---|---|
| TTDPA: Copper Ratio | Δ Mass (mg) 24 hr. T1 | Δ Mass (mg) 24 hr. T2 | Std. Dev. T1 & T2 |
| 5:1 Cu - Avg. | 13.9 | 17.2 | 2.3 |
| 3:1 Cu - Avg. | 24.2 | 29.4 | 3.7 |
| 1:1 Cu - Avg. | 86.9 | 87.1 | 0.1 |
| 1:3 Cu - Avg. | 67.8 | 85.0 | 12.1 |
| 1:5 Cu - Avg. | 52.3 | 71.6 | 13.6 |

*Table 6.13 Precipitate Mass for TTDPA: $CuCl_2$ Mixtures Filtered through 0.2µm PTFE Syringe Filter.*

| Copper w/ TTDPA- Syringe Filter | | | | | | |
|---|---|---|---|---|---|---|
| Filter Code | TTDPA: Copper Ratio | Initial Mass (g) | Final Mass (g) 24hr. | Δ Mass (mg) 24 hr. | Avg. Δ (mg) 24 hr. | Std. Dev. 24 hr. |
| A1 | 5:1 Cu - S | 3.2445 | 3.2592 | 14.70 | 16.2 | 1.9 |
| A2 | 5:1 Cu - S | 3.2375 | 3.2558 | 18.30 | | |
| A3 | 5:1 Cu - S | 3.2354 | 3.2509 | 15.50 | | |
| B1 | 3:1 Cu - S | 3.2391 | 3.2681 | 29.00 | 30.9 | 3.1 |
| B2 | 3:1 Cu - S | 3.2430 | 3.2775 | 34.50 | | |
| B3 | 3:1 Cu - S | 3.2446 | 3.2737 | 29.09 | | |
| C1 | 1:1 Cu - S | 3.2518 | 3.3401 | 88.30 | 88.4 | 0.8 |
| C2 | 1:1 Cu - S | 3.2296 | 3.3173 | 87.70 | | |
| C3 | 1:1 Cu - S | 3.2389 | 3.3281 | 89.20 | | |
| D1 | 1:3 Cu - S | 3.2404 | 3.3151 | 74.70 | 75.1 | 0.4 |
| D2 | 1:3 Cu - S | 3.2428 | 3.3179 | 75.10 | | |
| D3 | 1:3 Cu - S | 3.2456 | 3.321 | 75.40 | | |
| E1 | 1:5 Cu - S | 3.2419 | 3.3007 | 58.80 | 55.2 | 3.1 |
| E2 | 1:5 Cu - S | 3.2411 | 3.2945 | 53.40 | | |
| E3 | 1:5 Cu - S | 3.2337 | 3.2871 | 53.40 | | |

*Table 6.14 Comparison of 5µm Filter Paper Averages with 0.2µm PTFE Syringe Filter Averages for Precipitate Masses of TTDPA: $CuCl_2$.*

| Copper w/ TTDPA- Filter Paper vs. Syringe Filter | | | |
|---|---|---|---|
| TTDPA: Copper Ratio | Δ Mass (mg) Filter Paper | Δ Mass (mg) 24 hr. Syringe Filter | Std. Dev. 24 hr. Paper vs Syringe |
| 5:1 Cu - Avg. | 15.6 | 16.2 | 0.4 |
| 3:1 Cu - Avg. | 26.8 | 30.9 | 2.9 |
| 1:1 Cu - Avg. | 87.0 | 88.4 | 1.0 |
| 1:3 Cu - Avg. | 76.4 | 75.1 | 1.0 |
| 1:5 Cu - Avg. | 62.0 | 55.2 | 4.8 |

*Table 6.15 Recorded Precipitate Mass for TTDPA: $ZnCl_2$ Mixtures Filtered through 5µm Filter Paper – Trial 1.*

| Zinc w/ TTDPA - Trial 1 | | | | | | |
|---|---|---|---|---|---|---|
| Filter Code | TTDPA: Zinc Ratio | Initial Mass (g) | Final Mass (g) 24hr. | Δ Mass (mg) 24 hr. | Avg. Δ (mg) 24 hr. | Std. Dev. 24 hr. |
| Z1 | 5:1 Zn - T1 | 0.3205 | 0.3462 | 25.7 | 24.7 | 0.9 |
| Z2 | 5:1 Zn - T1 | 0.3123 | 0.3366 | 24.3 | | |
| Z3 | 5:1 Zn - T1 | 0.3148 | 0.3389 | 24.1 | | |
| Z4 | 1:1 Zn - T1 | 0.3139 | 0.4045 | 90.6 | 95.1 | 5.6 |
| Z5 | 1:1 Zn - T1 | 0.3233 | 0.4167 | 93.4 | | |
| Z6 | 1:1 Zn - T1 | 0.3109 | 0.4123 | 101.4 | | |
| Z7 | 1:5 Zn - T1 | 0.3214 | 0.4209 | 99.5 | 101.6 | 4.2 |
| Z8 | 1:5 Zn - T1 | 0.3089 | 0.4153 | 106.4 | | |
| Z9 | 1:5 Zn - T1 | 0.3266 | 0.4255 | 98.9 | | |

*Table 6.16 Recorded Precipitate Mass for TTDPA: $ZnCl_2$ Mixtures Filtered through 5µm Filter Paper – Trial 2.*

| Zinc w/ TTDPA - Trial 2 | | | | | | |
|---|---|---|---|---|---|---|
| Filter Code | TTDPA: Zinc Ratio | Initial Mass (g) | Final Mass (g) 24hr. | Δ Mass (mg) 24 hr. | Avg. Δ (mg) 24 hr. | Std. Dev. 24 hr. |
| Z'1 | 5:1 Zn - T2 | 0.3106 | 0.3328 | 22.2 | 22.9 | 2.1 |
| Z'2 | 5:1 Zn - T2 | 0.3186 | 0.3439 | 25.3 | | |
| Z'3 | 5:1 Zn - T2 | 0.3150 | 0.3363 | 21.3 | | |
| Z'4 | 1:1 Zn - T2 | 0.3259 | 0.4238 | 97.9 | 97.1 | 1.2 |
| Z'5 | 1:1 Zn - T2 | 0.3114 | 0.4092 | 97.8 | | |
| Z'6 | 1:1 Zn - T2 | 0.3254 | 0.4211 | 95.7 | | |
| Z'7 | 1:5 Zn - T2 | 0.3101 | 0.4143 | 104.2 | 107.1 | 4.5 |
| Z'8 | 1:5 Zn - T2 | 0.3263 | 0.4386 | 112.3 | | |
| Z'9 | 1:5 Zn - T2 | 0.3102 | 0.4149 | 104.7 | | |

*Table 6.17 Comparison of Trial 1 and Trail 2 Masses of Mass for TTDPA: $ZnCl_2$ Mixtures Filtered through 5µm Filter Paper.*

| Zinc w/ TTDPA- T1 vs T2 | | | |
|---|---|---|---|
| TTDPA: Zinc Ratio | Δ Mass (mg) 24 hr. T1 | Δ Mass (mg) 24 hr. T2 | Std. Dev. 24 hr. T1 & T2 |
| 5:1 Zn - Avg. | 24.7 | 22.9 | 1.2 |
| 1:1 Zn - Avg. | 95.1 | 97.1 | 1.4 |
| 1:5 Zn - Avg. | 101.6 | 107.1 | 3.9 |

*Table 6.18 Recorded Precipitate Mass for TTDPA: $MnCl_2$ Mixtures Filtered through 5µm Filter Paper – Trial 1.*

| Manganese w/ TTDPA - Trial 1 | | | | | | |
|---|---|---|---|---|---|---|
| Filter Code | TTDPA: Manganese Ratio | Initial Mass (g) | Final Mass (g) 24hr. | Δ Mass (mg) 24 hr. | Avg. Δ (mg) 24 hr. | Std. Dev. 24 hr. |
| M1 | 5:1 Mn - T1 | 0.3209 | 0.3299 | 9 | 5.6 | 3.0 |
| M2 | 5:1 Mn - T1 | 0.3111 | 0.3144 | 3.3 | | |
| M3 | 5:1 Mn - T1 | 0.3088 | 0.3133 | 4.5 | | |
| M4 | 1:1 Mn - T1 | 0.3161 | 0.3202 | 4.1 | 2.5 | 1.4 |
| M5 | 1:1 Mn - T1 | 0.3192 | 0.3211 | 1.9 | | |
| M6 | 1:1 Mn - T1 | 0.3143 | 0.3157 | 1.4 | | |
| M7 | 1:5 Mn - T1 | 0.3195 | 0.4183 | 98.8 | 95.4 | 4.3 |
| M8 | 1:5 Mn - T1 | 0.3225 | 0.4131 | 90.6 | | |
| M9 | 1:5 Mn - T1 | 0.3241 | 0.4209 | 96.8 | | |

*Table 6.19 Recorded Precipitate Mass for TTDPA: $MnCl_2$ Mixtures Filtered through 5µm Filter Paper – Trial 2.*

| Manganese w/ TTDPA - Trial 2 | | | | | | |
|---|---|---|---|---|---|---|
| Filter Code | TTDPA: Manganese Ratio | Initial Mass (g) | Final Mass (g) 24hr. | Δ Mass (mg) 24 hr. | Avg. Δ (mg) 24 hr. | Std. Dev. 24 hr. |
| N1 | 5:1 Mn - T2 | 0.3198 | 0.3259 | 6.1 | 4.5 | 2.9 |
| N2 | 5:1 Mn - T2 | 0.3171 | 0.3234 | 6.3 | | |
| N3 | 5:1 Mn - T2 | 0.3141 | 0.3152 | 1.1 | | |
| N4 | 1:1 Mn - T2 | 0.3166 | 0.3209 | 4.3 | 2.3 | 1.8 |
| N5 | 1:1 Mn - T2 | 0.3139 | 0.3158 | 1.9 | | |
| N6 | 1:1 Mn - T2 | 0.3211 | 0.3218 | 0.7 | | |
| N7 | 1:5 Mn - T2 | 0.3077 | 0.4076 | 99.9 | 98.0 | 1.7 |
| N8 | 1:5 Mn - T2 | 0.3197 | 0.4171 | 97.4 | | |
| N9 | 1:5 Mn - T2 | 0.3163 | 0.4129 | 96.6 | | |

*Table 6.20 Comparison of Trial 1 and Trail 2 Masses of Mass for TTDPA: $MnCl_2$ Mixtures Filtered through 5µm Filter Paper.*

| Manganese w/ TTDPA- T1 vs T2 | | | |
|---|---|---|---|
| TTDPA: Manganese Ratio | Δ Mass (mg) 24 hr. T1 | Δ Mass (mg) 24 hr. T2 | Std. Dev. 24 hr. T1 & T2 |
| 5:1 Mn - Avg. | 5.6 | 4.5 | 0.8 |
| 1:1 Mn - Avg. | 2.5 | 2.3 | 0.1 |
| 1:5 Mn - Avg. | 95.4 | 98.0 | 1.8 |

The next step was to convert the recorded masses into a percentage of the expected mass. The molecular weight off the complexes were determined from the empirical formula obtained via X-Ray diffraction of the clear and green crystals. For TTDPA: $CuCl_2$ complexes the masses were 756.43 g/mol for the µCl-bis-(Cu-L) product and 2091.95 g/mol for the L-CuCl product, solvent water was removed from the masses for these calculations as the samples were dried in a vacuum oven (24 hours, 75°, 10 torr). To then ascertain the complex masses for TTDPA: $ZnCl_2$ and TTDPA: $MnCl_2$, since there was not crystal data, the mass of the copper complex was used. Simply the mass of the copper atoms was replaced by the mass of the zinc or manganese atom

and the mass recalculated (Table 6.21). The total theoretical yield was then calculated based on 100% precipitation of complex from solution where the 5:1 solution yielded only clear crystal complex and the 1:5 solution yielded only 100% green crystal complex. The total masses of ratios of 3:1, 1:1, and 1:3 were calculated based on the percent make-up of the clear and green crystal complexes, obtained from the ICP-MS data (Table 6.22). It should be noted that the assumption that 5:1 was 100% clear crystal product, and 1:5 was 100% green crystal product are mostly not accurate; in that, there is a small percentage of green crystal product in the 5:1 and a much higher percentage of clear crystal product in the 1:5.

*Table 6.21 Determination of complex mass assuming molecular formulas based on copper X-ray crystal data.*

| Crystal Product Mass | | |
|---|---|---|
| Metal | Clear | Green |
| Copper | 756.43 | 2091.952 |
| Zinc | 756.0984 | 2091.289 |
| Manganese | 735.214 | 2049.52 |

**All formulas excluded any molecular water even if present in crystal, because samples were dried in a vacuum oven, and X represents: Cu, Zn, or Mn.*

*Table 6.22 Total possible amount of precipitate formation based of ratios of ICP-MS data and masses derived from those of Table 6.21.*

| Total Possible Precipitate 1:1 (mg) - Based of ICP Data | | | | | | |
|---|---|---|---|---|---|---|
| Sample/Metal | mol. Complex | % Clear | % Green | Copper | Zinc | Manganese |
| 5 : 1 | 0.00006 | 100.0% | 0.0% | 45.4 | 45.4 | 44.1 |
| 3 : 1 | 0.00010 | 86.8% | 13.2% | 93.3 | 93.3 | 90.9 |
| 1 : 1 | 0.00030 | 68.5% | 31.5% | 353.3 | 353.2 | 345.0 |
| 1 : 3 | 0.00030 | 68.0% | 32.0% | 355.4 | 355.2 | 346.9 |
| 1 : 5 | 0.00030 | 0.0% | 100.0% | 628.0 | 627.8 | 615.2 |

The percentage of recovered mass (captured yield) was calculated by simply dividing the recorded mass by these calculated theoretical masses. The averages for each ratio were also calculated along with the standard deviation between the repetitions of each ratio (Tables 6.23-16.29). All data was averaged together as with the masses to give a better understanding of the trends of precipitate recovery (Table 6.30-6.33). The TTDPA: $Cu^{2+}$ samples filtered through the 5µm filter paper were compared to those same ratios filtered through the 0.2µm PFTE syringe filter (Table 6.34). The increased deviation between samples, specifically at the lower metal concentrations, are not surprising given low levels of precipitate formation and the difficulty in accurately measuring small changes in masses. However, both the 5µm filter paper and the 0.2µm PFTE syringe filter showed consistent precipitate capture; with the exception of the TTDPA: $Cu^{2+}$ 3:1 ratio where the PTFE filter captured a higher percentage of precipitate, and the TTDPA: $Cu^{2+}$ 1:5 where the filter paper captured more than the PTFE filter. Overall, there was not a substantial difference between the 5µm filter paper or the 0.2µm PFTE syringe filter. In the TTDPA: $ZnCl_2$ trials the highest percentage of recovered mass occurred in the 5:1 ratio, which is interesting as the 1:5 ratio showed substantially larger precipitate formation than all other trials. Interestingly the trials for TTDPA: $Mn^{2+}$ showed more captured precipitate for the 5:1 ratio than the 1:1 ratio, although the 1:1 ratio showed more visible precipitate formation.

*Table 6.23 Percentage of Captured Precipitate for TTDPA: $Cu^{2+}$ Trail 1 on 5µm Filter Paper, Measured Against the Expected Mass.*

| Copper 24 Hours Drying Time - Trial 1 | | | | | | |
|---|---|---|---|---|---|---|
| Filter Code | TTDPA : Copper Ratio | Δ Mass (mg) | Theo Total (mg) | % Yield | Avg. % Yield | Std Dev. % |
| A1 | 5:1 Cu - T1 | 14.6 | 45.4 | 32.15% | 30.68% | 3.95% |
| A2 | 5:1 Cu - T1 | 15.3 | 45.4 | 33.69% | | |
| A3 | 5:1 Cu - T1 | 11.9 | 45.4 | 26.20% | | |
| B1 | 3:1 Cu - T1 | 25.5 | 93.3 | 27.32% | 25.93% | 2.23% |
| B2 | 3:1 Cu - T1 | 25.3 | 93.3 | 27.11% | | |
| B3 | 3:1 Cu - T1 | 21.8 | 93.3 | 23.36% | | |
| C1 | 1:1 Cu - T1 | 87.1 | 353.3 | 24.65% | 24.59% | 0.37% |
| C2 | 1:1 Cu - T1 | 85.5 | 353.3 | 24.20% | | |
| C3 | 1:1 Cu - T1 | 88.1 | 353.3 | 24.93% | | |
| D1 | 1:3 Cu - T1 | 68.3 | 355.4 | 19.22% | 19.09% | 0.25% |
| D2 | 1:3 Cu - T1 | 66.8 | 355.4 | 18.80% | | |
| D3 | 1:3 Cu - T1 | 68.4 | 355.4 | 19.25% | | |
| E1 | 1:5 Cu - T1 | 54.8 | 628.0 | 8.73% | 8.33% | 0.36% |
| E2 | 1:5 Cu - T1 | 50.3 | 628.0 | 8.01% | | |
| E3 | 1:5 Cu - T1 | 51.9 | 628.0 | 8.26% | | |

*Table 6.24 Percentage of Captured Precipitate for TTDPA: $Cu^{2+}$ Trail 2 on 5µm Filter Paper, Measured Against the Expected Mass.*

| Copper 24 Hours Drying Time - Trial 2 | | | | | | |
|---|---|---|---|---|---|---|
| Filter Code | TTDPA : Copper Ratio | Δ Mass (mg) | Theo Total (mg) | % Yield | Avg. % Yield | Std Dev. % |
| A1p | 5:1 Cu - T2 | 19.3 | 45.4 | 42.50% | 37.87% | 7.08% |
| A2p | 5:1 Cu - T2 | 18.8 | 45.4 | 41.40% | | |
| A3p | 5:1 Cu - T2 | 13.5 | 45.4 | 29.73% | | |
| B1p | 3:1 Cu - T2 | 27.1 | 93.3 | 29.04% | 31.46% | 2.71% |
| B2p | 3:1 Cu - T2 | 32.1 | 93.3 | 34.39% | | |
| B3p | 3:1 Cu - T2 | 28.9 | 93.3 | 30.96% | | |
| C1p | 1:1 Cu - T2 | 82.6 | 353.3 | 23.38% | 24.64% | 1.90% |
| C2p | 1:1 Cu - T2 | 83.8 | 353.3 | 23.72% | | |
| C3p | 1:1 Cu - T2 | 94.8 | 353.3 | 26.83% | | |
| D1p | 1:3 Cu - T2 | 83.2 | 355.4 | 23.41% | 23.92% | 0.52% |
| D2p | 1:3 Cu - T2 | 84.9 | 355.4 | 23.89% | | |
| D3p | 1:3 Cu - T2 | 86.9 | 355.4 | 24.45% | | |
| E1p | 1:5 Cu - T2 | 73.2 | 628.0 | 11.66% | 11.41% | 0.23% |
| E2p | 1:5 Cu - T2 | 71.3 | 628.0 | 11.35% | | |
| E3p | 1:5 Cu - T2 | 70.4 | 628.0 | 11.21% | | |

*Table 6.25 Percentage of Captured Precipitate for TTDPA: $Cu^{2+}$ on 0.2µm PTFE Syringe Filter, Measured Against the Expected Mass.*

| Copper 24 Hours Drying Time - Syringe Filter | | | | | | |
|---|---|---|---|---|---|---|
| Filter Code | TTDPA : Copper Ratio | Δ Mass (mg) | Theo Total (mg) | % Yield | Avg. % Yield | Std Dev. % |
| A1 | 5:1 Cu - T1 | 14.7 | 45.4 | 32.37% | 35.60% | 4.16% |
| A2 | 5:1 Cu - T1 | 18.3 | 45.4 | 40.29% | | |
| A3 | 5:1 Cu - T1 | 15.5 | 45.4 | 34.13% | | |
| B1 | 3:1 Cu - T1 | 29.0 | 93.3 | 31.07% | 33.07% | 3.37% |
| B2 | 3:1 Cu - T1 | 34.5 | 93.3 | 36.96% | | |
| B3 | 3:1 Cu - T1 | 29.1 | 93.3 | 31.17% | | |
| C1 | 1:1 Cu - T1 | 88.3 | 353.3 | 24.99% | 25.02% | 0.21% |
| C2 | 1:1 Cu - T1 | 87.7 | 353.3 | 24.82% | | |
| C3 | 1:1 Cu - T1 | 89.2 | 353.3 | 25.24% | | |
| D1 | 1:3 Cu - T1 | 74.7 | 355.4 | 21.02% | 21.12% | 0.10% |
| D2 | 1:3 Cu - T1 | 75.1 | 355.4 | 21.13% | | |
| D3 | 1:3 Cu - T1 | 75.4 | 355.4 | 21.22% | | |
| E1 | 1:5 Cu - T1 | 58.8 | 628.0 | 9.36% | 8.79% | 0.50% |
| E2 | 1:5 Cu - T1 | 53.4 | 628.0 | 8.50% | | |
| E3 | 1:5 Cu - T1 | 53.4 | 628.0 | 8.50% | | |

*Table 6.26 Percentage of Captured Precipitate for TTDPA: $Zn^{2+}$ Trail 1 on 5µm Filter Paper, Measured Against the Expected Mass.*

| Zinc 24 Hours Drying Time - Trial 1 | | | | | | |
|---|---|---|---|---|---|---|
| Filter Code | TTDPA : Zinc Ratio | Δ Mass (mg) | Theo Total (mg) | % Yield | Avg. % Yield | Std Dev. % |
| Z1 | 5:1 Zn - T1 | 25.7 | 45.4 | 56.61% | 54.41% | 1.92% |
| Z2 | 5:1 Zn - T1 | 24.3 | 45.4 | 53.53% | | |
| Z3 | 5:1 Zn - T1 | 24.1 | 45.4 | 53.09% | | |
| Z4 | 1:1 Zn - T1 | 90.6 | 353.2 | 25.65% | 26.93% | 1.59% |
| Z5 | 1:1 Zn - T1 | 93.4 | 353.2 | 26.44% | | |
| Z6 | 1:1 Zn - T1 | 101.4 | 353.2 | 28.71% | | |
| Z7 | 1:5 Zn - T1 | 99.5 | 627.8 | 15.85% | 16.18% | 0.66% |
| Z8 | 1:5 Zn - T1 | 106.4 | 627.8 | 16.95% | | |
| Z9 | 1:5 Zn - T1 | 98.9 | 627.8 | 15.75% | | |

*Table 6.27 Percentage of Captured Precipitate for TTDPA: $Zn^{2+}$ Trail 2 on 5µm Filter Paper, Measured Against the Expected Mass.*

| Zinc 24 Hours Drying Time - Trial 2 | | | | | | |
|---|---|---|---|---|---|---|
| Filter Code | TTDPA : Zinc Ratio | Δ Mass (mg) | Theo Total (mg) | % Yield | Avg. % Yield | Std Dev. % |
| Z'1 | 5:1 Zn - T2 | 22.2 | 45.4 | 48.90% | 50.52% | 4.62% |
| Z'2 | 5:1 Zn - T2 | 25.3 | 45.4 | 55.73% | | |
| Z'3 | 5:1 Zn - T2 | 21.3 | 45.4 | 46.92% | | |
| Z'4 | 1:1 Zn - T2 | 97.9 | 353.2 | 27.72% | 27.50% | 0.35% |
| Z'5 | 1:1 Zn - T2 | 97.8 | 353.2 | 27.69% | | |
| Z'6 | 1:1 Zn - T2 | 95.7 | 353.2 | 27.09% | | |
| Z'7 | 1:5 Zn - T2 | 104.2 | 627.8 | 16.60% | 17.06% | 0.72% |
| Z'8 | 1:5 Zn - T2 | 112.3 | 627.8 | 17.89% | | |
| Z'9 | 1:5 Zn - T2 | 104.7 | 627.8 | 16.68% | | |

*Table 6.28 Percentage of Captured Precipitate for TTDPA: $Mn^{2+}$ Trail 1 on 5µm Filter Paper, Measured Against the Expected Mass Based.*

| Manganese 24 Hours Drying Time - Trial 1 | | | | | | |
|---|---|---|---|---|---|---|
| Filter Code | TTDPA : Manganese Ratio | Δ Mass (mg) | Theo Total (mg) | % Yield | Avg. % Yield | Std Dev. % |
| M1 | 5:1 Mn - T1 | 9 | 44.1 | 20.39% | 12.69% | 6.81% |
| M2 | 5:1 Mn - T1 | 3.3 | 44.1 | 7.48% | | |
| M3 | 5:1 Mn - T1 | 4.5 | 44.1 | 10.19% | | |
| M4 | 1:1 Mn - T1 | 4.1 | 345.0 | 1.19% | 0.72% | 0.42% |
| M5 | 1:1 Mn - T1 | 1.9 | 345.0 | 0.55% | | |
| M6 | 1:1 Mn - T1 | 1.4 | 345.0 | 0.41% | | |
| M7 | 1:5 Mn - T1 | 98.8 | 615.2 | 16.06% | 15.51% | 0.69% |
| M8 | 1:5 Mn - T1 | 90.6 | 615.2 | 14.73% | | |
| M9 | 1:5 Mn - T1 | 96.8 | 615.2 | 15.73% | | |

*Table 6.29 Percentage of Captured Precipitate for TTDPA: $Mn^{2+}$ Trail 2 on 5µm Filter Paper, Measured Against the Expected Mass.*

| Manganese 24 Hours Drying Time - Trial 2 | | | | | | |
|---|---|---|---|---|---|---|
| Filter Code | TTDPA : Manganese Ratio | Δ Mass (mg) | Theo Total (mg) | % Yield | Avg. % Yield | Std Dev. % |
| N1 | 5:1 Mn - T2 | 6.1 | 44.1 | 13.82% | 10.19% | 6.67% |
| N2 | 5:1 Mn - T2 | 6.3 | 44.1 | 14.27% | | |
| N3 | 5:1 Mn - T2 | 1.1 | 44.1 | 2.49% | | |
| N4 | 1:1 Mn - T2 | 4.3 | 345.0 | 1.25% | 0.67% | 0.53% |
| N5 | 1:1 Mn - T2 | 1.9 | 345.0 | 0.55% | | |
| N6 | 1:1 Mn - T2 | 0.7 | 345.0 | 0.20% | | |
| N7 | 1:5 Mn - T2 | 99.9 | 615.2 | 16.24% | 15.92% | 0.28% |
| N8 | 1:5 Mn - T2 | 97.4 | 615.2 | 15.83% | | |
| N9 | 1:5 Mn - T2 | 96.6 | 615.2 | 15.70% | | |

*Table 6.30 Average Percentage of Captured Precipitate for TTDPA: $Cu^{2+}$ on 5µm Filter Paper, Measured Against the Expected Mass.*

| Copper w/ TTDPA- Average | | | | |
|---|---|---|---|---|
| TTDPA : Copper Ratio | Mass (mg) | Theo. Mass (mg) | Avg. % Yield | Std Dev. % |
| 5:1 Cu - Avg. | 15.6 | 45.4 | 34.28% | 6.47% |
| 3:1 Cu - Avg. | 26.8 | 93.3 | 28.70% | 3.76% |
| 1:1 Cu - Avg. | 87.0 | 353.3 | 24.62% | 1.23% |
| 1:3 Cu - Avg. | 76.4 | 355.4 | 21.50% | 2.67% |
| 1:5 Cu - Avg. | 62.0 | 628.0 | 9.87% | 1.71% |

*Table 6.31 Percentage of Captured Precipitate for TTDPA: $Cu^{2+}$ on 0.2µm PTFE Syringe Filter, Measured Against the Expected Mass.*

| Copper w/ TTDPA- Average – Syringe | | | | |
|---|---|---|---|---|
| TTDPA : Copper Ratio | Mass (mg) | Theo. Mass (mg) | Avg. % Yield | Std Dev. % |
| 5:1 Cu - Avg. | 16.2 | 45.4 | 35.60% | 4.16% |
| 3:1 Cu - Avg. | 30.9 | 93.3 | 33.07% | 3.37% |
| 1:1 Cu - Avg. | 88.4 | 353.3 | 25.02% | 0.21% |
| 1:3 Cu - Avg. | 75.1 | 355.4 | 21.12% | 0.10% |
| 1:5 Cu - Avg. | 55.2 | 628.0 | 8.79% | 0.50% |

*Table 6.32 Average Percentage of Captured Precipitate for TTDPA: $Zn^{2+}$ on 5µm Filter Paper, Measured Against the Expected Mass.*

| Zinc w/ TTDPA- Average | | | | |
|---|---|---|---|---|
| TTDPA : Zinc Ratio | Mass (mg) | Theo. Mass (mg) | Avg. % Yield | Std Dev. % |
| 5:1 Zn - Avg. | 23.8 | 45.4 | 52.46% | 3.82% |
| 1:1 Zn - Avg. | 96.1 | 353.2 | 27.22% | 1.07% |
| 1:5 Zn - Avg. | 104.3 | 627.8 | 16.62% | 0.78% |

*Table 6.33 Average Percentage of Captured Precipitate for TTDPA: $Mn^{2+}$ on 5µm Filter Paper, Measured Against the Expected Mass.*

| Manganese w/ TTDPA- Average | | | | |
|---|---|---|---|---|
| TTDPA : Manganese Ratio | Mass (mg) | Theo. Mass (mg) | Avg. % Yield | Std Dev. % |
| 5:1 Mn - Avg. | 5.1 | 44.1 | 11.44% | 6.18% |
| 1:1 Mn - Avg. | 2.4 | 345.0 | 0.69% | 0.43% |
| 1:5 Mn - Avg. | 96.7 | 615.2 | 15.72% | 0.53% |

*Table 6.34 Average Percentage of Captured Precipitate for TTDPA: $Cu^{2+}$ Comparison of 5µm Filter Paper vs. 0.2µm PTFE Syringe Filter.*

| Copper w/ TTDPA- Average Paper vs. Syringe | | | |
|---|---|---|---|
| TTDPA : Copper Ratio | Avg. % Yield - Paper | Avg. % Yield - Syringe | Std Dev. % |
| 5:1 Cu - Avg. | 34.3% | 35.6% | 0.93% |
| 3:1 Cu - Avg. | 28.7% | 33.1% | 3.09% |
| 1:1 Cu - Avg. | 24.6% | 25.0% | 0.28% |
| 1:3 Cu - Avg. | 21.5% | 21.1% | 0.27% |
| 1:5 Cu - Avg. | 9.9% | 8.8% | 0.76% |

The formation of the complex between copper II cations and the TTDPA ligand can be viewed as a series of linked equilibria. The first step in this model is the formation of a copper-monochloride complex.

$$Cu^{2+} + Cl^- \rightleftharpoons Cu^{2+}\text{–}Cl^-$$

$$Cl^- + Cu^{2+}\text{–}Cl^- \rightleftharpoons Cl^-\text{–}Cu^{2+}\text{–}Cl^-$$

$$Cl^- + Cl^-\text{–}Cu^{2+}\text{–}Cl^- \rightleftharpoons \begin{matrix} & Cl^- & \\ & | & \\ Cl^-\text{–}Cu^{2+}\text{–}Cl^- & & \end{matrix}$$

$$Cl^- + \begin{matrix} & Cl^- & \\ & | & \\ Cl^-\text{–}Cu^{2+}\text{–}Cl^- & & \end{matrix} \rightleftharpoons \begin{matrix} & Cl^- & \\ & | & \\ Cl^-\text{–}Cu^{2+}\text{–}Cl^- & & \\ & | & \\ & Cl^- & \end{matrix}$$

This complex can subsequently be removed by reaction with another chloride and formation of a copper-dichloride complex, which can in turn form a copper-trichloride complex which can further lead to a copper-tetrachloride complex. The stability of these complexes has been previously determined. At the concentrations used here the copper-monochloride complex would comprise approximately 1 to 15% of the total copper, the copper-dichloride concentration would range from negligible to approximately 2% of the total copper, and the tri- and tetrachloro complexes would all be negligible in the concentrations used in our experiments (10).

The reaction of the copper-monochloride species with the TTDPA ligand (L) to form a complex is the one of greatest interest. The stability of this complex will determine whether or not the formation of a similar complex with the thiol alkylation products of sulfur mustard is of any significance in the human body. The TTDPA ligand was used in these experiments was in the form with both carboxylates ionized. The soluble complex formed would then have a single net negative charge.

$L^{2-} + Cu^{2+}–Cl^{-} \rightleftharpoons [L\text{-}Cu\text{-}Cl]^{-}$

Further complicating analysis of our results, this putative complex then goes on to precipitate in two different forms. The first form is the μCl-bis-(Cu-L), a clear crystal.

$2[L\text{-}Cu\text{-}Cl]^{-} + H^{+} \rightleftharpoons$ μCl-bis-(Cu-L) + $Cl^{-}$

In the clear crystal, there are two coppers which share a bridging chloride. To maintain overall charge neutrality, a single proton is assumed to be shared amongst the four carboxylates of the two ligands. This is modeled in the crystal structure by partial occupancy.

The second form, L-CuCl, is a green crystal in which the carboxylates interact with additional coppers. This carboxylate-copper interaction is of less interest to us here as it will not occur in

the forms of the ligand to be found in a human exposed to sulfur mustard, but we need to take it into account.

$4[\text{L-Cu-Cl}]^- + 4Cu^{2+} + 4HO^- + 12H_2O \rightleftharpoons$ L-CuCl

In the green crystal there are four ligands in the unit cell, each with a copper-monochloride bound to the tridentate sulfur ligand. There are four additional coppers, each coordinated to two carboxylates. We therefore modeled 12 waters of hydration and 4 hydroxides, to maintain charge balance. The hydroxides are modeled as interacting with the coppers that are also interacting with the carboxylates. This means that there is a net negative charge in this region of the structure and a net positive charge on the copper-monochloride complex. However, the hydroxides and waters of hydration form a network of hydrogen bonds, so the negative charge is presumably spread more diffusely throughout the crystal.

We unfortunately do not have enough data to calculate the $K_{sp}$ for these two crystal forms. Similarly, we cannot calculate the equilibrium constant for the formation of the soluble complex. Nevertheless, the decrease in absorbance at 815nm allows us to estimate the reduction of copper in solution, from the result of copper binding to TTDPA and/or precipitation. Much of the complex formed precipitates out of solution and we have measured this by weighing. However, the fact that two different complexes form in amounts that depend on the copper concentration again complicates analysis. But several striking points reveal themselves. First and foremost, the amount of precipitate captured goes up steadily as the concentration of copper increases when copper is the limiting factor (5:1 or 3:1) or when copper and TTDPA were equal (1:1). However, when copper was in excess (1:3 or 1:5) the amount of precipitate actually declines. (Recall that the concentration of the ligand is a constant across all these trials.) This is not true for the zinc experiments (Table 6.32), where the amount of precipitate goes up with increasing metal. The

manganese (Table 6.33) has more noise at lower concentrations, but precipitation also appears to go up as metal concentration increases. Also interestingly, the ICP data tells that that, as one would expect, the amount of the green crystal form in the precipitate increases as copper goes from limiting (3:1) to equimolar (1:1), but then does not increase further as copper is available in excess (1:3).

The other interesting point is that a new peak appears around 365nm in the copper filtrate. We think it is reasonable to assume that this is due to the soluble complex. Unfortunately, the new peak sits on the shoulder of a peak for copper itself and, more importantly, we have no idea of what the extinction coefficient is, so we cannot calculate a concentration. However, we do observe that the relative amount of this material in solution is very small when is limiting (5:1 and 3:1), climbs appreciably when ligand and copper are equimolar (1:1), climbs further when copper is in excess (1:3), but then actually drops as copper further increases (1:5).

This seems paradoxical. There is less ligand and copper precipitating at the greatest excess of copper, the peak that is thought to be the soluble complex decreases, and the amount of the crystal form with the most copper does not appear to increase in the precipitate. This may imply that excess copper allows the formation of other soluble complexes that do not have a clear spectroscopic signature. It is tempting to speculate that this might be complexes where different sulfurs a given ligand interact with two or even three different coppers, but further experimentation will be required to determine if this is the case.

## 6.5 Discussion

Through the use of multiple techniques, UV-Vis spectroscopy, elemental analysis, ICP-MS, and small molecule X-Ray crystallography, it can be determined the successful complexation of various metals to TTDPA has occurred. Although copper and TTDPA showed the most promising data other metals such as zinc and manganese showed measurable complex formation. Although all metals appeared to form visible complexes that precipitated out of solution, copper, zinc, and in-part manganese were the only metals that produced any measurable data.

These findings are further supported by literature published in 1970 by Podlaha *et al.* in a study focusing on the binding of TTDAA and various metals including copper, nickel, cobalt, and zinc (4,5). What they determined was that all complexes formed a 1:1 ratio of metal atom to ligand, they also noted the formation of green crystals in their TTDAA: $CuCl_2$ solutions as well as the formation of a UV-Vis peak around 365nm. Although studying a similar ligand, we now know that it is is possible for more than one type of complex to be formed, and the green crystals they described may be similar to ours where one copper atom is bound to the sulfurs and the other is bound to the carboxylate groups. Podlaha *et al.* also published binding constants for TTDAA: $Cu^{2+}$ (4). They published a K value of 2290 for TTDAA:$Cu^{2+}$.

When comparing the recovered mass of precipitate versus the expected mass of precipitate both copper and zinc fell within acceptable percentages for all ratios in the trial, leading to the conclusion that a complex between the TTDPA and the metal ion had in fact occurred. With manganese only the highest ratio of metal (1:5) produced any measurable precipitate. This could be that although a complex does form, manganese does not bind tightly to TTDPA, so only when the metal ion is in mass excess will a complex form.

The confirmation of complex formation between copper and TTDPA was further established by measurable changes in the UV-Vis spectra of the samples. Upon the mixture of these two compounds a decreased in the copper absorption can be measured, along with the formation of a new peak, that only appears once the compounds are combined. Unfortunately, complex formation with zinc could not also be supported via UV-Vis, since zinc is not UV-Vis active.

The crystal structure of 2,5,8-trithianone-1,9-dicarboxylic acid ((2,2'-[thiobis(2,1-ethanediylthio)]bis-acetic acid, TTDAA) with copper (II) was published by Nanda *et al.* in 1996 (CSD Entry TORZAB, deposition 1274320). A similar paper was published in 1980 by Drew *et al.* which showed the complexes formed by 1,11-diamino-3,6,9-trithiaundecane (Figure 6.16, 6.17) with copper and nickel (6). They were able to successfully crystalize and solve the structures of the copper (CSD Entry BRUCUA, deposition 1115496) and nickel (CSD Entry BRUCUB, deposition 1115497) complexes, but found different results than the complex presented in this dissertation. In the diamino complex the amine groups played a chelating role to both the copper and nickel ions; and in the TTDAA structure (6.18) it was shown that the carboxylate groups also played a role in complex formation and stability. In contrast to these hexadentate structures, in our tetradentate structures only the sulfurs are chelating to the central metal atoms and not the carboxylates. This is a key difference, as the carboxylate groups not participating in metal binding means that this type of chelation could still occur within in the body with larger molecules alkylated by sulfur mustard where the carboxylates and amine groups of cysteine are involved in amide bonds. The complex stability in our structures also results in differing bond lengths and angles between the copper sulfur atoms, resulting in a more open structure with shorter Cu-S bond lengths and significantly wider S-Cu-S angles (Table 6.35).

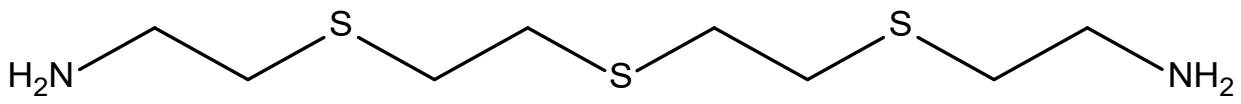


*Figure 6.16 Structure of ligand 1,11-diamino-3,6,9-trithiaundcane.*

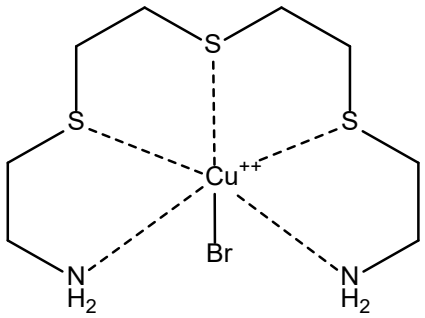


*Figure 6.17 Structure of 1,11-diamino-3,6,9-trithiaundcane bound to $Cu^{2+}$ as published by Drew et al (6).*

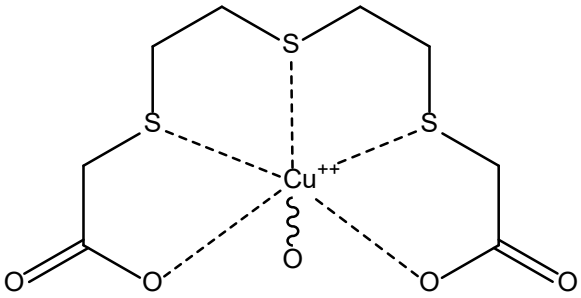


*Figure 6.18 Structure of 2,5,8-trithianone-1,9-dicarboxylic acid bound to $Cu^{2+}$ as published by Namda et al (9).*

*Table 6.35 Comparison of bond lengths and angles of our structures versus those of Drew et al. and Nanda et al.*

| Bond Lengths (Å) | | | | |
|---|---|---|---|---|
| Molecule | μCl-bis-(Cu-L) | L-CuCl | Cu-Diamino | Cu-carboxylate |
| Atoms | Bond Length (Å) | Bond Length (Å) | Bond Length (Å) | Bond Length (Å) |
| S(1) - Cu(1) | 2.3072(19) | 2.3336(12) | 2.340(6) | 2.596(1) |
| S(2) - Cu(1) | 2.3480(6) | 2.3820(14) | 2.576(9) | 2.357(1) |
| S(3) - Cu(1) | 2.2998(18) | 2.3258(15) | 2.340(6) | 2.459(1) |
| Bond Angles (°) | | | | |
| Molecule | μCl-bis-(Cu-L) | L-CuCl | Cu-Diamino | Cu-carboxylate |
| Atoms | Bond Angle (°) | Bond Angle (°) | Bond Angle (°) | Bond Angle (°) |
| S(1)-Cu(1)-S(2) | 93.08(6) | 92.04(5) | 86.8(2) | 86.42(3) |
| S(2)-Cu(1)-S(3) | 93.37(6) | 91.12(5) | 86.8(2) | 88.52(2) |
| S(1)-Cu(1)-S(3) | 113.03(3) | 112.32(5) | 92.9(2) | 99.34(4) |

Through the process of slow evaporation, all ratios of copper and TTDPA produced crystals, both clear and green in a varying ratio. In the solutions that started with lower copper concentrations more clear crystals were present, and in rations where copper was in excess (1:5) the green crystals appeared first and in larger amounts. This is understandable as there is an excess of copper and carboxylate groups do have an affinity for copper ions, as the copper concertation drops then the clear crystals with only the copper bound to the sulfurs would begin to form.

Again, the structures solved here prove successful complex formation between the thiol alkylation products of sulfur mustard and copper requires only the three sulfurs and not amines, carboxylates, or other functional groups. Obviously, complexes that involve additional functional groups can form as the structures of Nanda *et al.* and Drew *et al.* show (6,9). But additional interactions only would serve to strengthen the interaction with copper. Our work shows definitively that a stable complex with copper is possible even if such additionally stabilizing interactions are not present.

Some of the crystals were separated, dried, and sent for elemental analysis. The elemental analysis matched what was calculated for the green crystals based of the molecular formation derived from the crystal structure. The clear crystals did not match perfectly from crystal structure to elemental analysis, however with some assumptions about molecular water and protonation of carboxylate groups the numbers converge. Although the exact oxidation state of the bound copper ion was not experimentally determined, it is likely that all copper ions are $Cu^{2+}$. If any $Cu^{+}$ formed, it would rapidly be reoxidized to $Cu^{2+}$ by atmospheric oxygen.

For the precipitate that did not crystalize, but was dried for precipitate mass determination, some was collected and sent for ICP-MS analysis to determine how much copper was in the precipitate. What was discovered was a ratio of both the clear and green crystal complexes. When TTDPA is in excess (3:1) the majority of the precipitate was indicative of the clear crystals (87% μCl-bis-(Cu-L) vs 13% L-CuCl). However, when TTDPA and copper were in equimolar ratio or when copper was in excess (1:1 or 1:3) then the majority of the precipitate was still that of μCl-bis-(Cu-L) but with a much higher percentage of L-CuCl complex present (68% μCl-bis-(Cu-L) vs 32% L-CuCl). This analysis matches the way the crystals grew in solution as well, with green forming first and in higher ratios when excess copper was present in solution.

Although the vast majority of analysis revolved around copper, the insight learned can be applied to the other metals studied as well. It is possible that the other transition metals, zinc, nickel, cobalt, and manganese, would behave similarly to copper. Further research could be conducted into ICP-MS analysis of these other TTDPA-metal complex precipitates to observe the metal to sulfur ratio in the samples. There is also the potential that if done on a much larger scale there

could be a measurable amount of precipitate captured for all TTDPA-metal complexes regardless of the ratio of TTDPA to metal.

### 6.6 References


1. Kumar, S. B.; Mahendrasinh, Z.; Ankita, S.; Mohammedayaz, R.; Pragna, P.; Suresh, E. A binuclear chloride bridged copper (II) complex with a modified ligand structure and different coordination environment and mononuclear cobalt (II) complexes with a pyridylpyrazole ligand: Synthesis, structure and cytotoxic activity. *Polyhedron* **2012**, *36* (1), 15-20.

2. Melnik, M.; Kabešov, M.; Koman, M. Mac škov, Ľ.; Garaj, J.; Holloway, C. E.; Valent, A. Copper (II) Coordination Compounds: Classification and Analysis of Crystallographic and Structural Data III. *Dimeric Compounds. J. Coord. Chem* **1998**, *45*, 147-359.

3. Kumar, S. B.; Mahendrasinh, Z.; Ankita, S.; Mohammedayaz, R.; Pragna, P.; Suresh, E. A binuclear chloride bridged copper (II) complex with a modified ligand structure and different coordination environment and mononuclear cobalt (II) complexes with a pyridylpyrazole ligand: Synthesis, structure and cytotoxic activity. *Polyhedron* **2012**, *36* (1), 15-20.

4. Podlaha, J.; Podlahová, J. Metal complexes of thiopolycarboxylic acids. IV. diethylenetrithiodiacetic acid. *Inorganica Chimica Acta* **1971**, *5*, 420-424.

5. Procházková, O.; Podlahová, J.; Podlaha, J. Metal complexes of thiopolycarboxylic acids. VI. Zinc and cadmium. *Collection of Czechoslovak Chemical Communications* **1973**, *38* (4), 1120-1127.

6. Drew, M. G.; Rice, D. A.; Richards, K. M. Bivalent metal complexes of 1, 11-diamino-3, 6, 9-trithiaundecane and the crystal structures of adducts with nickel (II) and copper (II) bromides. *Journal of the Chemical Society, Dalton Transactions* **1980**, (12), 2503-2508.

7. Hakimi, M.; Rezaei, H.; Moeini, K.; Mardani, Z.; Eigner, V.; Dušek, M. Formation of a copper–copper bond in coordination of a cyclotriphosphazene ligand toward Cu (II): Structural, spectral and docking studies. *Journal of Molecular Structure* **2020**, *1207*, 127804.

8. Lee, D.-H.; Hatcher, L. Q.; Vance, M. A.; Sarangi, R.; Milligan, A. E.; Narducci Sarjeant, A. A.; Incarvito, C. D.; Rheingold, A. L.; Hodgson, K. O.; Hedman, B. Copper (I) Complex O2-Reactivity with a N3S Thioether Ligand: a Copper− Dioxygen Adduct Including Sulfur Ligation, Ligand Oxygenation, and Comparisons with All Nitrogen Ligand Analogues. *Inorganic chemistry* **2007**, *46* (15), 6056-6068.

9. Nanda, K. K.; Addison, A. W.; Sinn, E.; Thompson, L. K. Helical antiferromagnetic copper (II) chains with a collagen structural motif. *Inorganic chemistry* **1996**, *35* (21), 5966-5967.

10. Meng, Y.; Bard, A. J. Measurement of temperature-dependent stability constants of Cu (I) and Cu (II) chloride complexes by voltammetry at a Pt ultramicroelectrode. *Analytical chemistry* **2015**, *87* (6), 3498-3504.

## Chapter 7

## Conclusion

Sulfur mustard has been used as a chemical weapon for over a century and was one of the most prolifically used weapons of World War I. However, the physiologic effects of this weapon are still not fully understood. The majority of symptoms can be explained by the three leading hypotheses for its mode of action, DNA-alkylation, peptide alkylation, and inflammation. While these three do a good job covering the broad symptoms, there are still commonly reported symptoms that remain unexplained (Chapter 3).

Research conducted in our laboratory has shown that there is an interaction between synthesized molecules that mimic sulfur mustard byproducts and the key metal micronutrients (Chapter 6). Interestingly the unexplained symptoms correspond with symptoms of metal micronutrient deficiency; specifically, those of zinc, copper, nickel, cobalt, and manganese. These metals play key roles in antioxidant protection and much research has focused on their roles in burn wound healing. While not exactly the same, the body seems to heal thermal burns in broadly the same way it does chemical burns. When a victim is deficient in these metal micronutrients, specifically zinc and copper, it can lead to delayed and slowed wound healing (Chapter 4). While slow healing wounds were one of the first ever reported symptoms of exposure to sulfur mustard, it is one of the main symptoms that has no current explanation. The results presented here make plausible the hypothesis that exposure to sulfur mustard causes localized deficiency in these key metal micronutrients thereby slowing the healing time. The idea that these ligand-metal interactions are strong enough to capture metal micronutrients from the cell is reinforced by Dubrovskii *et al.* who reported the use of $Cu^{2+}$ in an affinity column to separate out globin peptides monoalkylated by sulfur mustard (1). Their results supports the idea that the stable

complex formed between the sulfur mustard alkylation products and metal ions is strong enough to remove free ions from the cell; thereby causing a localized depletion effect.

It is possible that interaction between the product of mustard and metal not only can be used to explain many of the symptoms of exposure simply because of metal depletion, but such interaction could also lead to an increased toxicity of the metals. Toxicity of complexes similar to those formed by sulfur mustard alkylation products is supported by Smet *et al.* who reported that hexathia-macrocylic ligand copper complexes are toxic to cells (2). Indeed, these hexathia-macrocylic ligands were not significantly toxic to cells on their own; but, when combined with copper and exposed to cells, cell death increased. Copper alone caused an increase of cellular death around 20%, and when the ligand was introduced, that magnitude increased to around 40% and in some cases upwards of 70%. While copper alone is toxic to the cells, when these thioethers compounds are introduced the toxicity dramatically increases.

This research has led to a new hypothesis of the effects of sulfur mustard exposure on the human body. A study similar to that of Smet *et al.* could be conducted using the ligands synthetized in our lab. By exposing cells to these ligands and monitoring their toxicity; then, combining these ligands with metal ions and exposing the cells again and monitoring their toxicity. If an increased toxic effect is noticed then it would be worth exploring this in live animal studies. Such experimentation could include the monitoring of metal micronutrient levels in rats before, during, and after exposure to sulfur mustard to determine effect. A similar study would be conducted by supplementing the diet of sulfur mustard exposed rats with higher levels of these metal micronutrients and monitoring their healing progress. Controls would include normal rats, and rats which were purposely made deficient in the metal micronutrients.

A separate application of this research could be the expansion of metal affinity columns as published by Dubrovskii. Where affinity columns could be developed using metal ions ($Cu^{2+}$, $Mn^{2+}$, or $Zn^{2+}$) to capture different alkylation products of sulfur mustard exposure. This idea could potentially lead to the discovery of new adducts that have not been previously found or a new purification method to help better study the byproducts of sulfur mustard exposure.

Overall, the research conducted over the course of this dissertation has many applications and could potentially lead to a new understanding of how sulfur mustard effects the body from unexplained exposure symptoms to increased toxicity effects.

## 7.1 References


1. Dubrovskii, Y. A.; Gladilovich, V.; Krasnov, I.; Podolskaya, E.; Murashko, E.; Babakov, V. Isolation of alkylated rat hemoglobin adducts using metal-affinity chromatography. *Russian Journal of Bioorganic Chemistry* **2012**, *38* (1), 41-45.
2. Smet, P.; Pauwels, T.; Dierickx, P. The effect of hexaaza-and hexathia–macrocyclic ligands on transition metal cytotoxicity in human hepatoma-derived cultured cells. *Human & Experimental Toxicology* **2002**, *21* (8), 421-427.

# Chapter 8

# Other Experimentation

## 8.1 Introduction

This chapter is designed to include the remaining experimentation that was conducted over the entirety of this project. These experiments proved inconsequential to the final results and conclusions or the designated products could not be successfully synthesized. Many of these synthetic routes and experiments proved useful for knowledge building as well as streamlining experimental design for later work.

There were 7 different desired compounds, shown in Table 8.1, that were either successfully or unsuccessfully synthesized, but they can be divided into 4 separate categories. These categories include: affinity column project, biological markers, reagents, and biological simulants. The affinity column project category was designated due to an abandoned endpoint of this research. The original hope was to develop an affinity column that would trap biological byproducts of sulfur mustard exposure, making them easier to separate and study. This goal was abandoned for a variety of reasons, such as compounds having insufficient solubility or precipitation upon metal binding. Nonetheless there was a compound that developed for this category: Compound A. The second category of biological markers refers to compounds that are known to be present in the body following sulfur mustard exposure. In fact, these compounds can often be used to determine the level of exposure a person experienced; and include Compound B and Compound C. The category of biological simulants was designed to enhance the conclusion of this research by reproducing experiments with a compound that could be potentially isolated from the body following sulfur mustard exposure. However, the resulting compounds would probably never be actually isolated from the body (Compound E), had too low a solubility to be of any practical use (Compound F), or was never successfully synthesized (Compound H). The final category of

reagents only contains one product (Compound D), which was hypothesized to replace actual sulfur mustard as the starting material in many published reactions, allowing for those synthetic routes to be followed. However, this product was never properly synthesized so that idea was scrapped.

*Table 8.1 Letter Code and Compound Name of Other Proposed Compounds.*

| Letter Code | Compound Name |
|---|---|
| A | 1,9-Diphenyl-2,5,8-Trithianonane (DPTT) |
| B | Glutathione-Ethylthioethyl-Glutathione (GSH-ETE-GSH) |
| C | Thiodiglycol Sulfoxide |
| D | Bis (2-bromoethyl) Sulfoxide |
| E | 3,3′-(((thiobis(ethane-2,1-diyl)) bis(sulfanediyl)) bis(methylene)) dibenzoic acid (3,3′-TMBA) |
| F | 1,11-Diamino-3,6,9-trithiaundecane (DATT) |
| G | S,S′-(thiodi-2,1-ethanediyl) bis-BOC-L-Cysteine Methyl Ester (BOCC) |

**8.2 List of Chemicals**

16. Bis (2-mercaptoethyl) sulfide (CAS# 3570-55-6): >97%, TCI America
17. Benzyl Chloride (CAS# 100-44-7): 99%, Sigma Aldrich
18. Thiodiglycol (CAS# 111-48-8): ≥99%, Sigma Aldrich
19. Pyridine (CAS# 110-86-1): ≥99% ACS Reagent, Sigma Aldrich
20. Methane Sulfonyl Chloride (CAS# 124-63-0): 99.5+%, Sigma Aldrich
21. L-Glutathione reduced (CAS#70-18-8): ≥98% Bioreagent, Sigma Aldrich
22. Thionyl Bromide (CAS#507-16-4): 97%, Sigma Aldrich
23. 3-Chlorobenzoic Acid (CAS# 3179-77-4): 97%, Alfa Aesar
24. 2-Bromoethlamine Hydrobromide (CAS# 2576-47-8): 98-101%, Chem Impex Inter.
25. BOC-3-iodo-L-alanine methyl ester (CAS# 93267-04-0): 98%, Alfa Aesar
26. Ethanol (CAS# 64-17-5): 200 Proof, Koptec

27. Methanol (CAS# 67-56-1): ACS Grade, EMD Millipore
28. Isopropyl Alcohol (CAS# 67-63-0): HPLC Grade, EM Science
29. Toluene (CAS# 108-88-3): ≥99.5%, VWR Chemicals BDH
30. Acetonitrile (CAS# 75-05-8): HPLC Grade, VWR Chemicals BDH
31. Hydrogen Peroxide (CAS# 7732-18-5): 30-32%, Avantor
32. Sodium Hypochlorite (Bleach) (CAS# 7681-52-9): 6%, Great Value
33. Dichloromethane (CAS# 75-09-2): >99.5%, VWR BDH Chemicals
34. Sodium Methoxide (CAS# 124-41-4): 5M, TCI America
35. Sodium Hydroxide (CAS# 1310-73-2): ACS Grade, VWR
36. Magnesium Sulfate (CAS# 7487-88-9): Fisher Scientific
37. Sodium Bicarbonate (CAS# 144-55-8): ACS Grade, VWR
38. Hydrobromic Acid (CAS#10035-10-6): 47-49%, Bean Town Chemical
39. Nitric Acid (CAS# 7697-37-2): 47-49%, JT Baker
40. Sodium Sulfate (CAS# 7757-82-6): ACS Grade, EMD
41. Hydrochloric Acid (CAS# 7647-01-0): ACS Grade, EMD Millipore
42. Sodium Ethoxide (CAS# 141-52-6): 20%, TCI America
43. Trifluoracetic Acid (CAS# 76-05-1): Biotechnology Grade, VWR
44. Sodium Carbonate (CAS# 497-19-8): ≥99.5%, VWR Chemicals BHD
45. TLC Plates: 250µm Thickness, 60Å pore, Aluminum Back, VWR
46. Chloroform-D “100%” (CAS# 865-49-6): 99.96% D, Cambridge Isotopes Laboratories Inc.
47. Deuterium Oxide “100%” (CAS# 7789-20-0): 99.96% D, Cambridge Isotopes Laboratories Inc.

48. Acetonitrile-D3 “100%” (CAS# 2206-26-0): 99.96% D, Cambridge Isotopes Laboratories Inc.
49. Dimethyl Sulfoxide-D6 “100%” (CAS# 2206-27-1): 99.96% D, Cambridge Isotopes Laboratories Inc.
50. Silver (I) Nitrate (CAS# 7761-88-8): Photographic Grade, Kodak
51. Nickel (II) Nitrate (CAS# 10196-18-6): Reagent Grade, Ward’s Science
52. Sodium Nitrate (CAS# 7632-00-00): 97%, Bean Town Chemical
53. Copper (II) Chloride • 2 $H_2O$ (CAS# 10125-13-0): ACS Reagent, Sigma Aldrich
54. Nickel (II) Chloride Anhydrous (CAS# 7791-20-0): Bean Town Chemical
55. Zinc (II) Chloride Anhydrous (CAS# 7646-85-7): 98%, Sigma Aldrich
56. Cobalt (II) Chloride • 6 $H_2O$ (CAS#7791-13-1): Reagent Grade, JT Baker
57. Sodium Chloride (CAS# 7647-14-5): Lab Grade, VWR
58. Sodium Acetate • 3 $H_2O$ (CAS# 6131-90-4): Lab Grade, EMD
59. Zinc (II) Acetate • 2 $H_2O$ (CAS# 557-34-6): 99.99% Trace Metal Basis, Sigma Aldrich
60. Nickel (II) Acetate • 4 $H_2O$ (CAS# 6018-89-9): Analysis Grade, Acros Organics
61. Copper (II) Acetate • $H_2O$ (CAS# 6046-93-1): Lab Grade, Ward’s Science
62. Cobalt (II) Acetate • 4 $H_2O$ (CAS# 6147-53-1): ≥98%, STREM Chemicals Inc.
63. Sodium Benzoate (CAS# 532-32-1): 99.0-101.0%, JT Baker

### 8.3 Synthetic Routes and Results

**Compound A: 1,9-Diphenyl-2,5,8-Trithianonane (DPTT)**

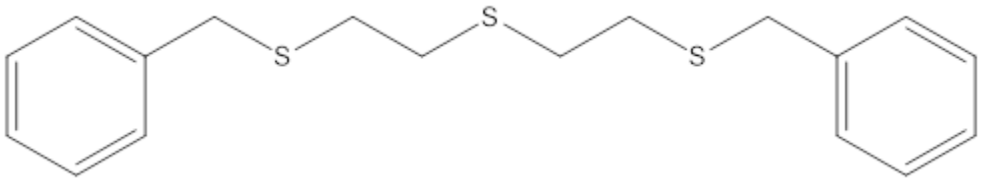


*Figure 8.1 Structure of 1 1,9-Diphenyl-2,5,8-Trithianone (DPTT)*

The synthesis of 1,9-Diphenyl-2,5,8-Trithianonane (DPTT) was adapted from Segawa *et al.* (1), originally published in Japanese and translated to English. A round bottom flask, stir bar, and addition funnel were dried in a 150°C oven for 24 hours. Upon assembly and after being fitted with septa, the apparatus was flushed with nitrogen for 30 minutes. Once cooled to room temperature, the apparatus was lowed into an ethanol bath with circulating cooler and cooled to -30°C. A solution of sodium methoxide in ethanol (5M, 150mL, 750mmol, 2.14 eq.), bis(2-mercaptoethyl) sulfide (5.4g, 350mmol), and toluene (50mL) were added via syringe and stirred as fast as possible while cooling for 30 minutes. At this point the apparatus was ballooned with nitrogen and the continuous stream removed. A solution of benzyl chloride (9.45g, 750mmol, 2.14 eq.) was dissolved in toluene (75mL) and added dropwise over the course of 15 minutes. The reaction was stirred as fast as possible for 10 hours, the flaks was then cooled in a -20°C freezer for 36 hours. The solvent was removed resulting in a white snow-like solid which was dissolved in toluene (125mL). The organic solution was transferred to a separatory funnel and extracted 3 times with and equal volume of sodium hydroxide (0.1M, 125mL), and the aqueous layer discarded after each wash. The organic layer was then dried with magnesium sulfate, filtered, and the solvent removed. The resulting solid was dried for a total of 72 hours under high vacuum. The resulting product 1,9-diphenyl-2,5,8-trithianonane (7.8g, 68.7%): 1H NMR

(400MHz, $CDCl_3$) δ 2.576/2.601 (dd, 8H), δ 3.745 (s, 4H), δ 7.316 (s, 10H) (Figure 8.2). Remaining in the NMR spectra was δ 2.127 (s) which corresponds to water in the sample. Overall, this synthesis was a success and a new route differing from the published paper. Segawa (1) reacted thiodiglycol with thiourea and concentrated hydrochloric acid under reflux then added potassium hydroxide. Refluxed again, then more concentrated hydrochloric acid was added; extracted with diethyl ether and dried with magnesium sulfate. This liquid was then added to ethanol, solid sodium metal, benzyl chloride reacted and then concentrated by removing the solvent. Dissolved in benzene, dried with magnesium sulfate and filtered. The crude product was then obtained via silica column and benzene. The synthetic route developed in this research simplified the number of reaction steps by utilizing different starting materials. However, this molecule was not chosen for final studies as it is not a biologically relevant molecule and is not water soluble. DPTT was used in preliminary UV-Vis studies, those used in further experiments described in Chapter 6.

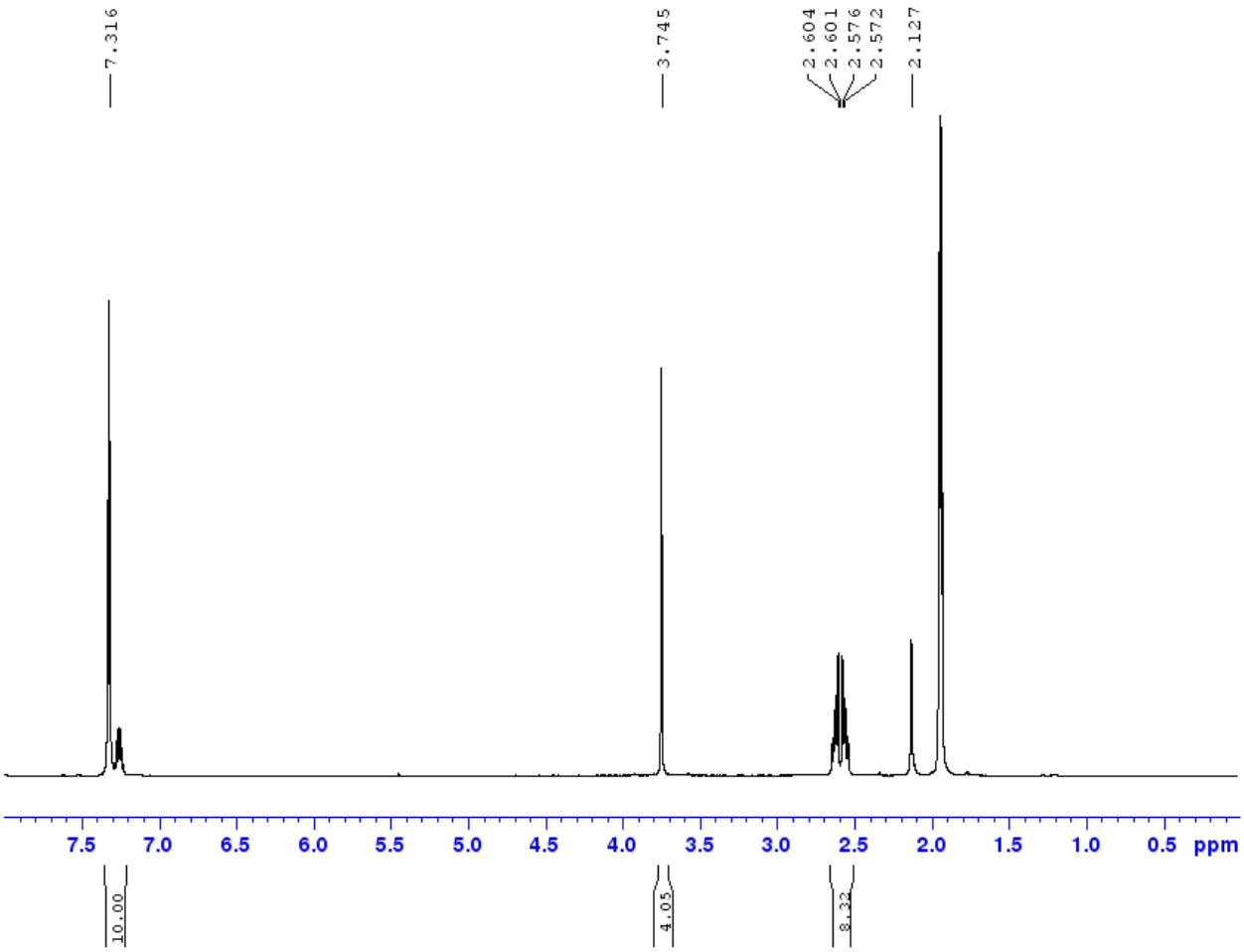


*Figure 8.2 400MHz $^{1}H$ NMR in $CDCl_3$ of 1,9-Diphenyl-2,5,8-Trithianonane (DPTT).*

**Compound B: Glutathione-Ethylthioethyl-Glutathione (GSH-ETE-GSH)**

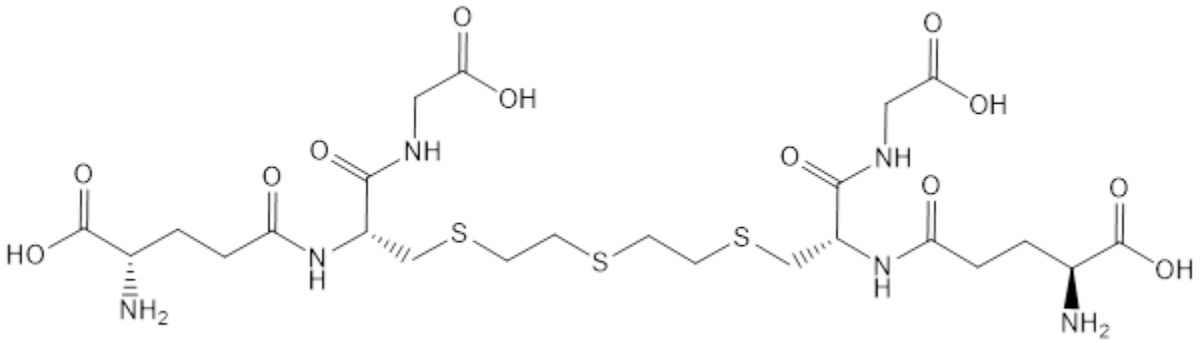


*Figure 8.3 Structure of* Glutathione-Ethylthioethyl-Glutathione (GSH-ETE-GSH).

The attempted synthesis of the molecule glutathione-ethylthioethyl-glutathione (GSH-ETE-GSH) was adapted from Bielmann *et al.* (2). The molecule GSH-ETE-GSH is known to be a biomarker of sulfur mustard exposure as it is a main byproduct of exposure (2,6). The procedure below was inspired by the aforenoted publication; however, the author uses sulfur mustard as the starting reagent, which we wished to avoid. A round bottom and stir bar were dried for 24 hours in a 150°C oven. The round bottom was fitted with a septum and flushed with nitrogen for 30 minutes while cooling. To which cold acetonitrile (25mL, -20°C) was added followed by thiodiglycol (0.21mL, 2.03mmol) and pyridine (0.35mL, 4.26mmol, 2.1 eq.) and stirred as fast as possible. Methane sulfonyl chloride (0.33mL, 4.26mmol, 2.1eq.) was then added dropwise and the reaction was stirred and allowed to warm to room temperature for 3.5 hours. A solution of reduced glutathione (1.31g, 4.26mmol, 2.1eq.) dissolved in sodium bicarbonate (10mL, 10%) was next added dropwise over a 10-minute period. This addition was followed by sodium hydroxide (0.5mL, 10M) to ensure the reaction was under basic conditions, reacted for 7 days, while being monitored via NMR. Following the glutathione addition, two separate layers formed if the reaction were to sit stagnant. After day 7 it was determined that the reaction was unsuccessful as neither the top nor bottom reaction layers seemed to contained the desired

product. The NMR spectra did not show unreacted starting material (lack of δ 1.4), however there was also no evidence of a successful reaction in either the top or bottom layers (Figure 8.4 and 8.5).

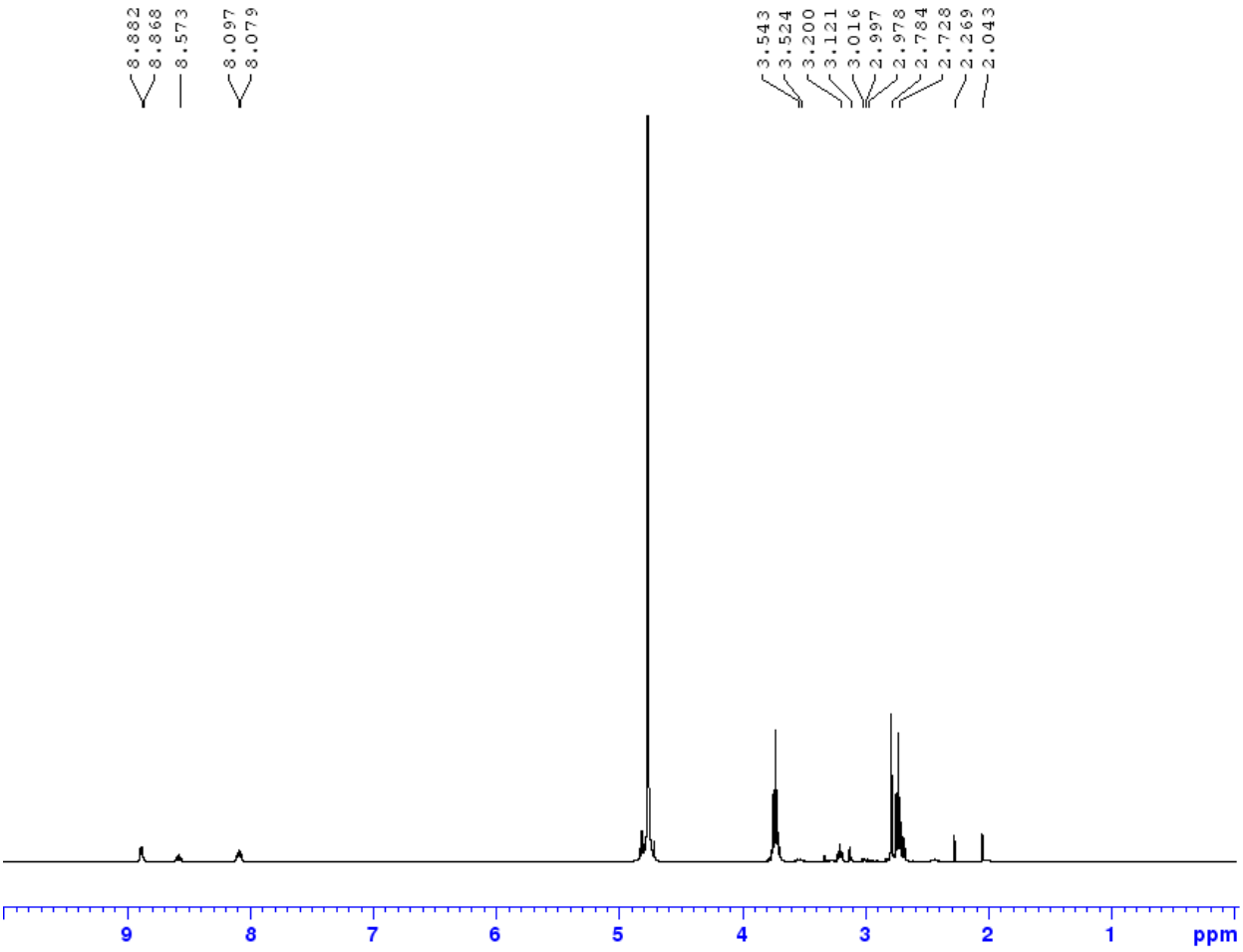


*Figure 8.4 400MHz $^{1}H$ NMR in $D_2O$ of Glutathione-Ethylthioethyl-Glutathione (GSH-ETE-GSH) Day7 Top Layer.*

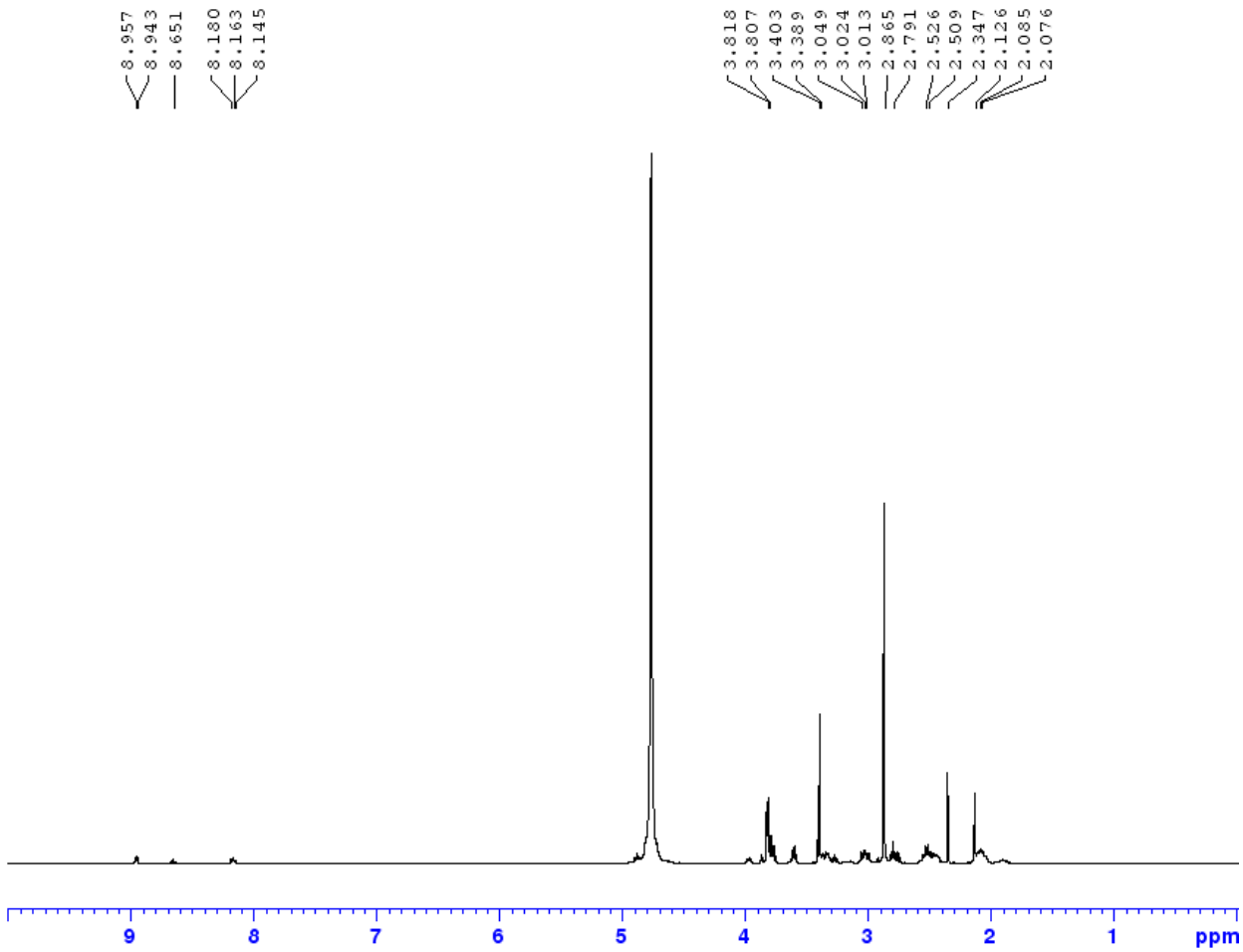


*Figure 8.5 400MHz $^{1}H$ NMR in $D_2O$ of Glutathione-Ethylthioethyl-Glutathione (GSH-ETE-GSH) Day7 Bottom Layer.*

**Compound C: Thiodiglycol Sulfoxide**

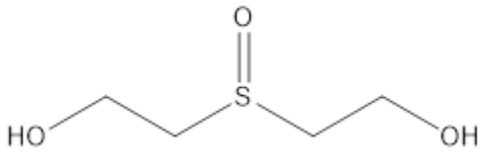


*Figure 8.6 Structure of Thiodiglycol Sulfoxide.*

The idea of synthesizing thiodiglycol sulfoxide came from the knowledge that it is a known degradation product of sulfur mustard; allowing it to be a key test molecule as it is a known biological marker. The synthesis was successful and rather straight forward. A round bottom with septa and stir bar, was placed on ice. To which water (18MΩ, 3mL) and thiodiglycol (2.5g) was added. This was stirred as fast as possible, to which hydrogen peroxide (30%, 5mL) was added dropwise over 10-minute period. The reaction was stirred for 30 minutes, at which point approximately 50% of the solvent was removed. Isopropyl alcohol (25mL) was added and the solution stored overnight at 4°C. The desired product crashed out of solution, was filtered and washed with more isopropyl alcohol. Thiodiglycol sulfoxide reaction product was analyzed via NMR, $^{1}$H NMR (400MHz, $D_2O$) δ 3.21(d, 4H), δ 4.11 (t, 4H) (Figure 8.7).

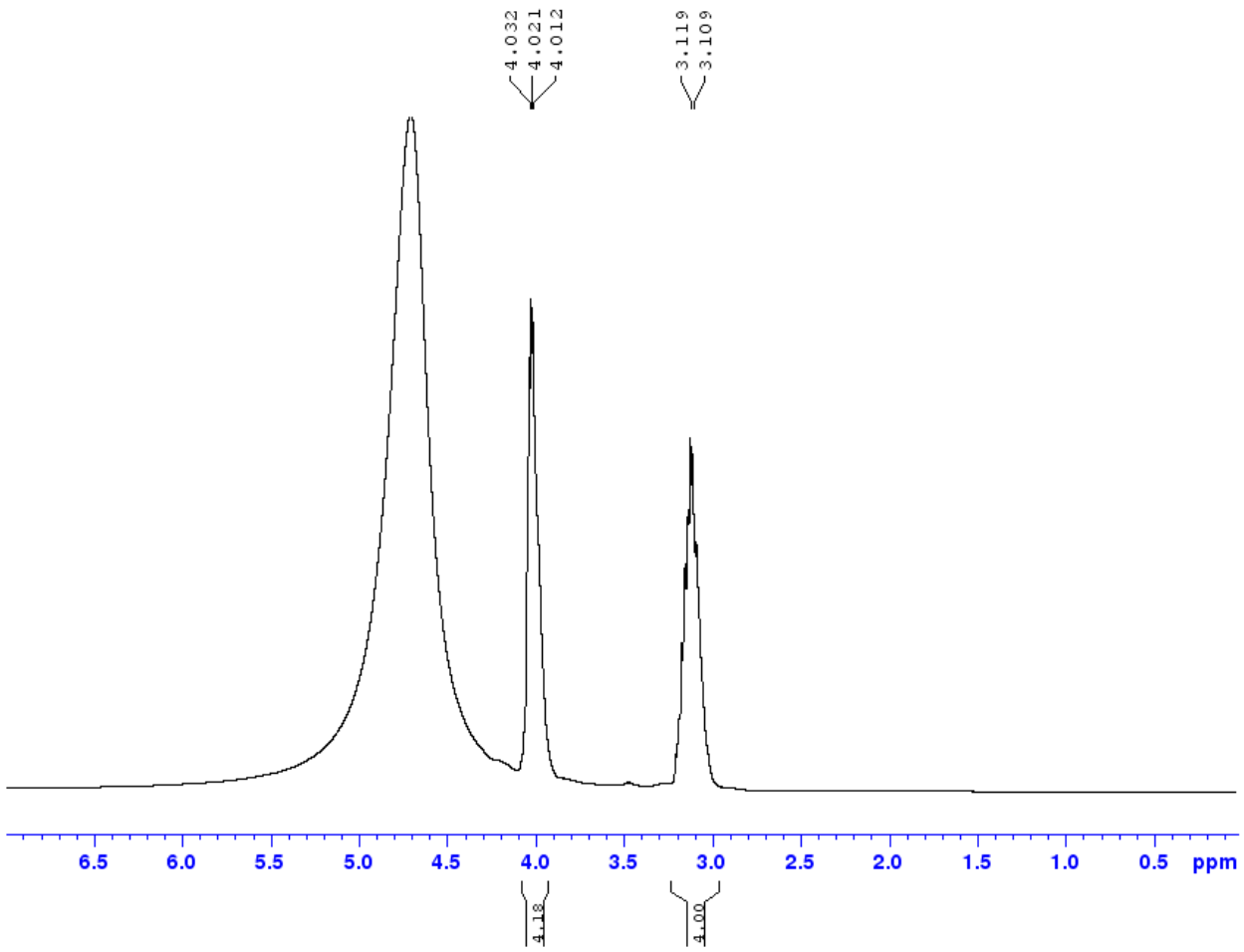


*Figure 8.7 400MHz $^{1}H$ NMR in $D_2O$ of Thiodiglycol Sulfoxide.*

**Compound D: Bis (2-bromoethyl) Sulfoxide**

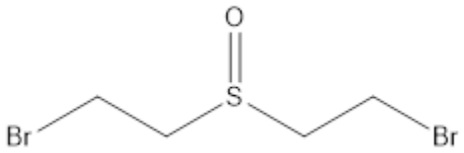


*Figure 8.8 Structure of Bis (2-bromoethyl) Sulfoxide.*

We wished to synthesize bis (2-bromoethyl) sulfoxide, while avoiding, if possible, bromine mustard as a reagent. It could be potentially be used as a starting material in order to make molecules such as the GSH-ETE-GSH product. To mitigate risk, the initial reaction method was based on a paper by Manandhar *et al.* that produced sulfur mustard oxide without having to isolate any sulfur mustard by using a "one-pot" reaction style (3). Three separate synthetic routes were attempted to synthesize bis (2-bromoethyl) sulfoxide but, unfortunately none were successful.

The first synthesis method was the most complex and carried the most risk (Scheme 8.1), synthesizing bromine mustard. A specific reaction apparatus was set up: comprised of an oil bath, three 3-neck round bottoms, a stir bar, an addition funnel, cannula needs, and neutralizing solutions (Figure 8.9). The reaction was carried out in the first round bottom, the second round bottom was filled with water, and the third with a solution of 50% bleach and 2M sodium bicarbonate. A constant stream of nitrogen was blown into the first round bottom, then bubbled via cannula needle into the water of the second, and bubble again through the bleach solution of the third before being vented into the fume hood. The reaction flask (first round bottom) was lowered into the oil bath set to 90°C to which thiodiglycol (6mL, 60mmol) was added. Concentrated hydrobromic acid (29.31mL, 540mmol, 9 eq.) was added dropwise over a 30-minute period via the addition funnel. The reaction was then stirred as fast as possible for 90

minutes. Upon completion two distinct layers had formed and the top layer was transferred to the second round bottom via cannula needle. The reaction flask was then removed from the oil bath and allowed to cool to room temperature before being placed on ice. Once cooled on ice, concentrated nitric acid (37.5mL, 900mmol, 15 eq.) was added dropwise over a 30-minute period via the addition funnel and stirred as fast as possible for 30 minutes. The solution in the reaction flask was then transferred to a separatory funnel and extracted 3x with dichloromethane (75mL) and the organic layers combined after each wash. The dichloromethane was then dried with magnesium sulfate, filtered, and the solvent removed. The result was a dark orange/brown oil that was analyzed via TLC plate in dichloromethane and showed 3 distinct spots. It was believed that these spots corresponded to bromine mustard, bromine mustard sulfoxide (desired product), and bromine mustard sulfone. A flash column of silica was utilized in order to separate these spots by using hexane, ethyl acetate, and dichloromethane and the fractions were analyzed via NMR. Fraction 1: $^{1}$H NMR (400MHz, $CDCl_3$) δ 2.962 (t, 4H), δ 3.110 (t, 1H), δ 3.522 (t, 4H), δ 3.644 (t, 1H), δ 4.014/4.031 (q, 2H) (Figure 8.10). The signals at 2.962 and 3.522 ppm likely correspond to bromide mustard; 3.110 and 3.644 ppm correspond to bromide mustard sulfoxide, and the signal at 4.014/4.031 ppm relates to bromide mustard sulfone. Fraction 2: $^{1}$H NMR (400MHz, $CDCl_3$), upon analysis this fraction was heavy contaminated with multiple peaks that do not match to any known solvents, starting materials, or products (Figure 8.11). Fraction 3: $^{1}$H NMR (400MHz, $CDCl_3$) δ 2.962 (t, 2H), δ 3.525 (t, 2H), δ 4.017/4.035 (q, 8H) (Figure 8.12). The signals at 2.962 and 3.525 ppm correspond to bromide mustard and the signal at 4.017/4.035 ppm relates to bromide mustard sulfone. Fraction 4: $^{1}$H NMR (400MHz, $CDCl_3$) δ 2.206 (s), δ 2.994 (t, 2H), δ 3.558 (t, 2H), δ 4.05/4.068 (q, 1H) (Figure 8.13). The signals at 2.962 and 3.525 ppm correspond to bromide mustard, the signal at 4.017/4.035 ppm relates to bromide mustard

sulfone, and the singlet at 2.206 ppm is water contamination. Although the desired product can be found in the first fraction, this crude product was destroyed and work was not continued on this synthesis method as the crude product was deemed to hazardous to work with; being that bromine mustard was the main product.

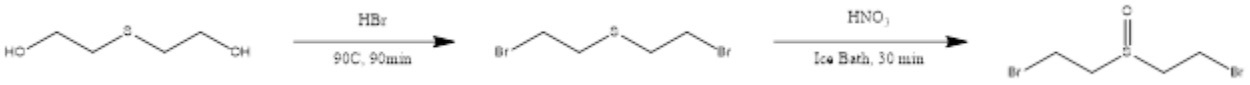


*Scheme 8.1 Bis (2-bromoethyl) sulfoxide synthesis via thiodiglycol and hydrobromic acid.*

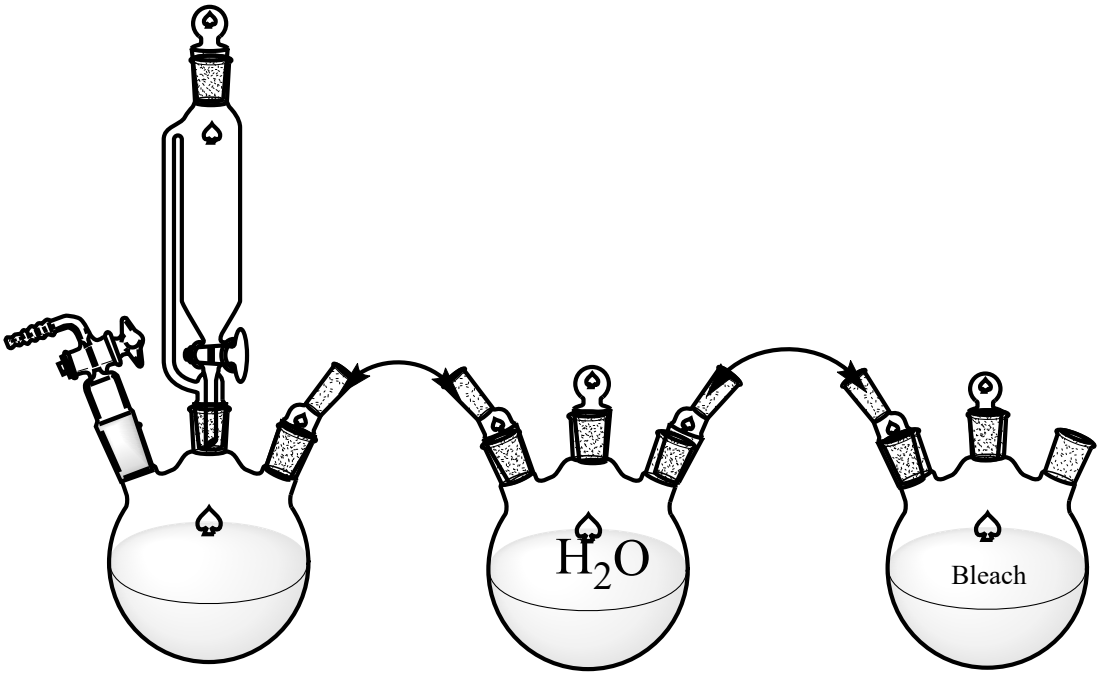


*Figure 8.9 Reaction Apparatus set-up for Scheme 8.1.*

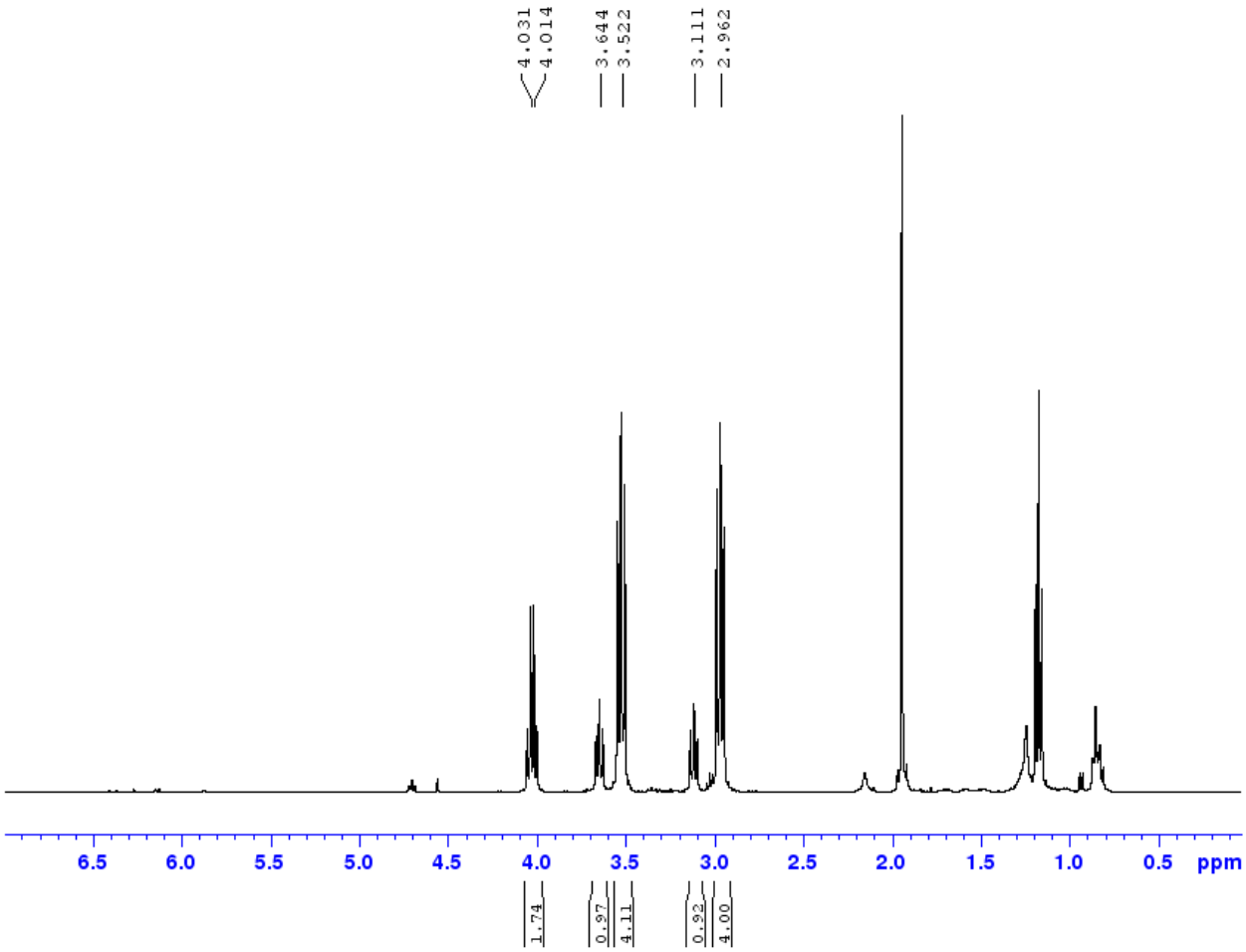


*Figure 8.10 400MHz $^{1}H$ NMR in $CD_3CN$ of bis (2-bromoethyl) sulfoxide – scheme 1 – fraction 1 hexane.*

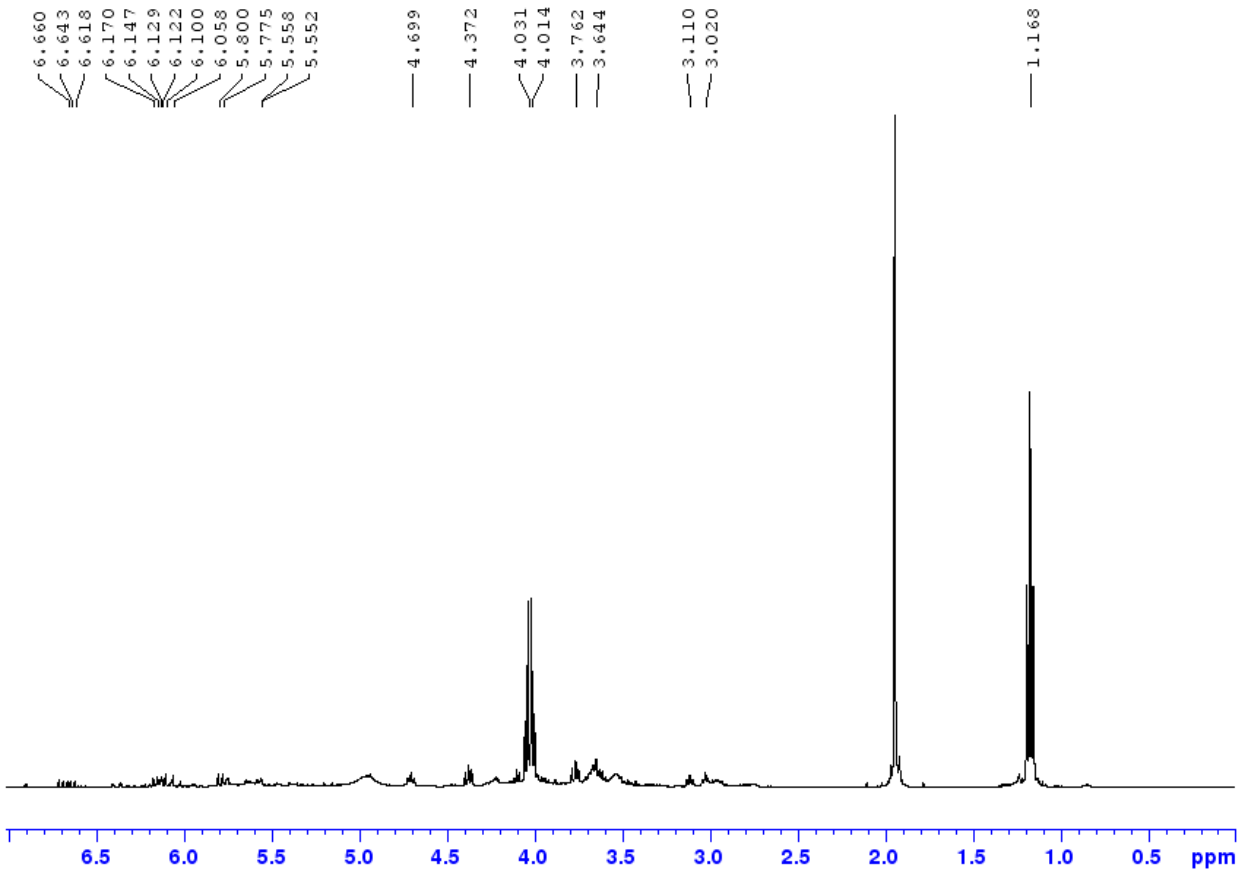


*Figure 8.11 400MHz $^{1}H$ NMR in $CD_3CN$ of bis (2-bromoethyl) sulfoxide – scheme 1 – fraction 2 hexane/ethyl acetate.*

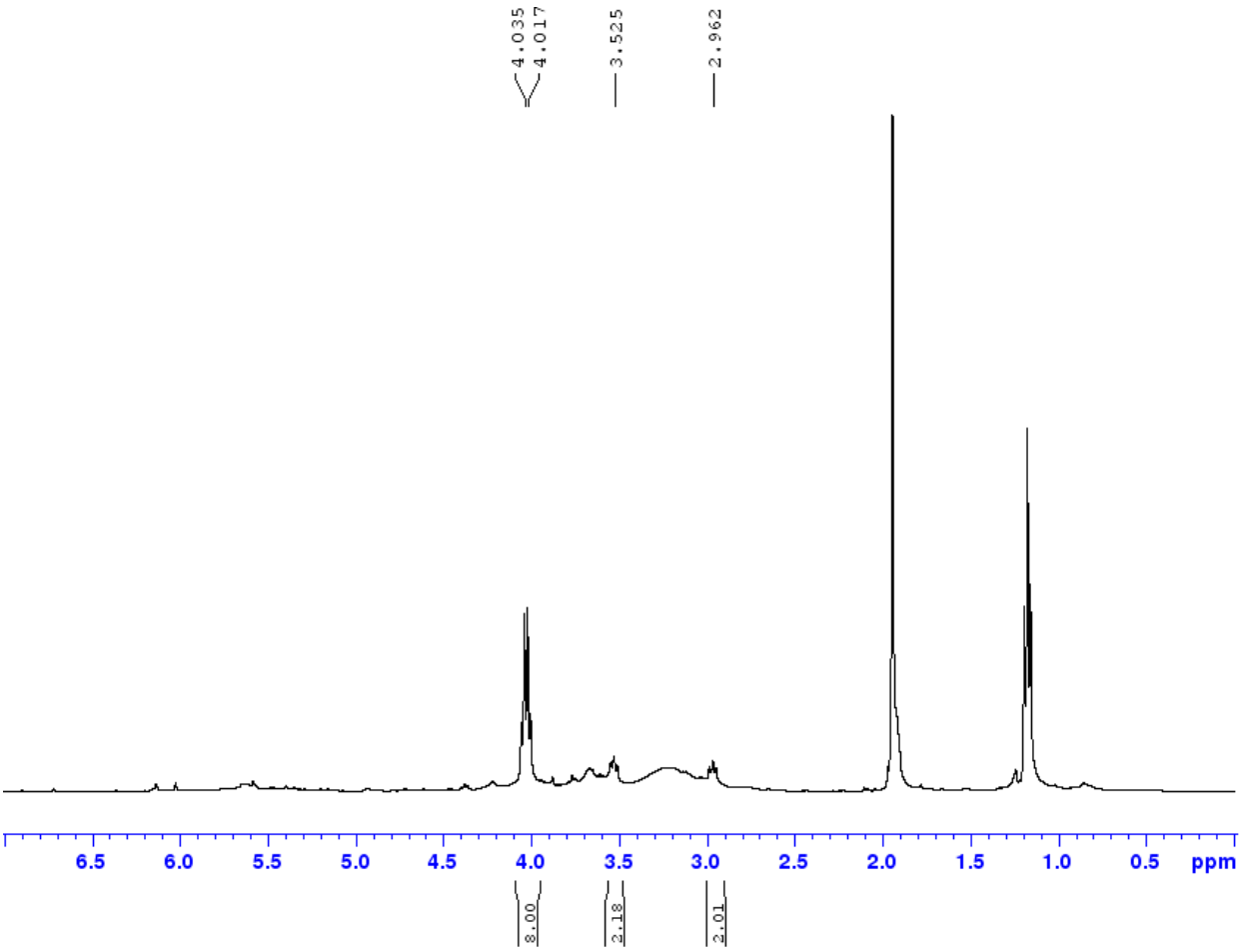


*Figure 8.12 400MHz $^{1}H$ NMR in $CD_3CN$ of bis (2-bromoethyl) sulfoxide – scheme 1 – fraction 3 ethyl acetate.*

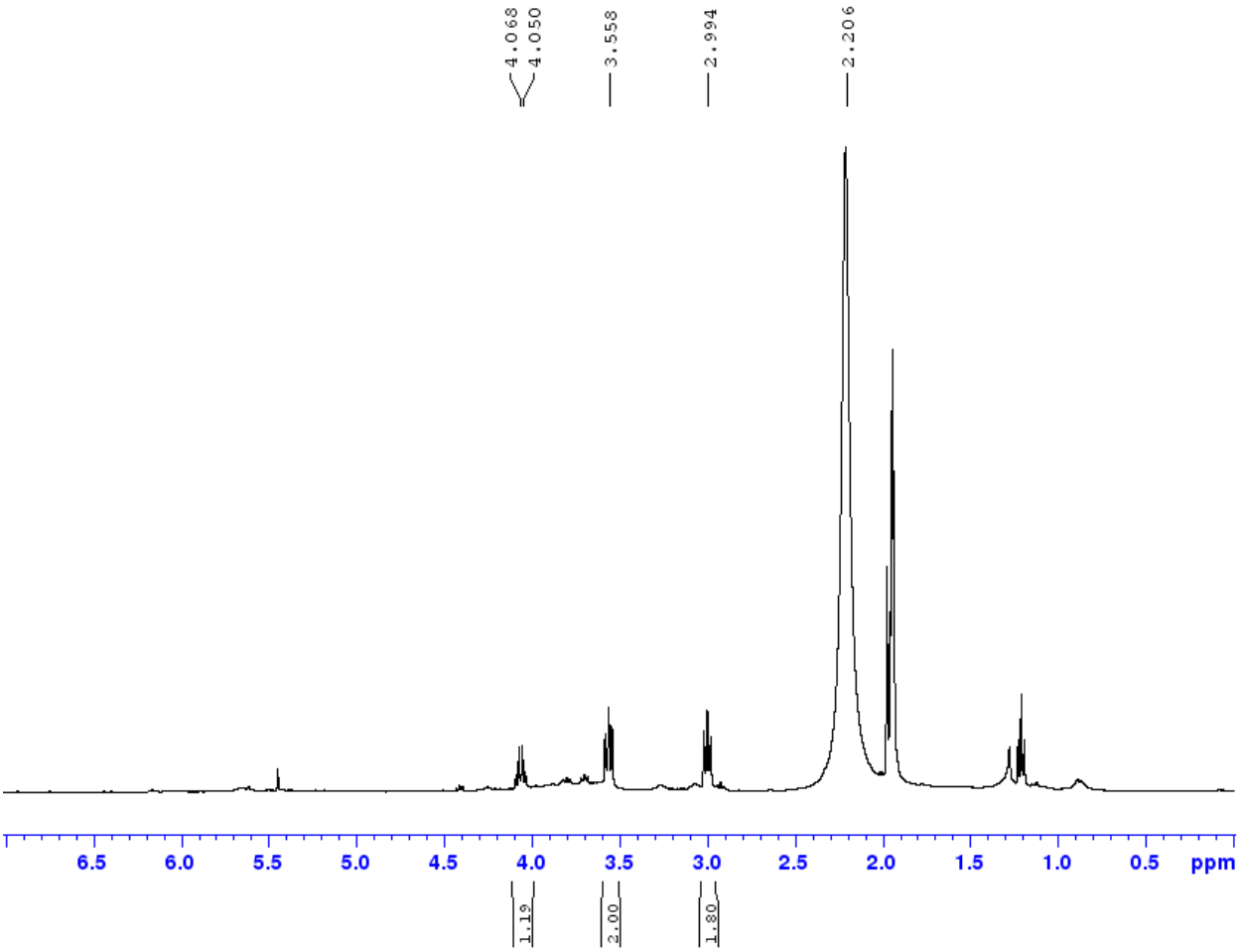


*Figure 8.13 400MHz $^{1}H$ NMR in $CD_3CN$ of bis (2-bromoethyl) sulfoxide – scheme 1 – fraction 4 dichloromethane.*

A second safer synthesis method (Scheme 8.2) was derived using the previously synthesized thiodiglycol sulfoxide as a starting material. In a round bottom fitted with a septum and stir bar, neat thiodiglycol sulfoxide (1.70g, 12mmol) was stirred under nitrogen. Concentrated hydrobromic acid (3.5mL, 30mmol, 2.5 eq.) was added dropwise over a 3-minute period and the reaction was stirred at room temperature for 60 hours; the result was a dark brownish/yellow oil. While the crude product was stirred sodium sulfate was incrementally added (0.1M, 1mL increment, 8mL total) until the solution turned and remained clear. A solution of ethanol and acetonitrile (50/50) was added and the reaction stored at 4°C for 60 hours. No solids formed so

the solvent was removed resulting in a bright orange oil. This crude oil was dissolved in acetone to which a white precipitate formed (sodium sulfate) and an orange solution (product). The bis (2-bromoethyl) sulfoxide reaction was not successful: $^{1}H$ NMR (400MHz, $D_2O$) δ 2.730 (t), δ 2.804 (t), δ 3.119 (t), δ 3.644 (3), δ 3.780 (m), δ 4.081 (t) (Figure 8.14). The signals in this NMR were difficult to decipher and appear as though there is a combination of all three products as well as unreacted starting material. Due to the fact there could be bromine mustard present in the crude sample, it was destroyed and this synthetic route not further researched.

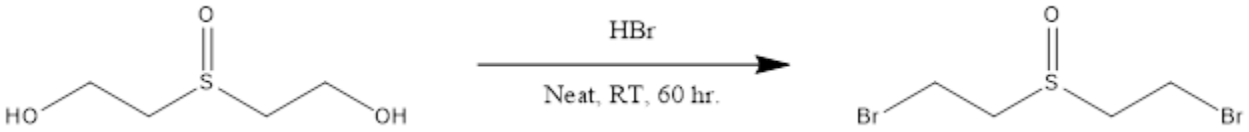


*Scheme 8.2 Bis (2-bromoethyl) sulfoxide synthesis via thiodiglycol sulfoxide and hydrobromic acid.*

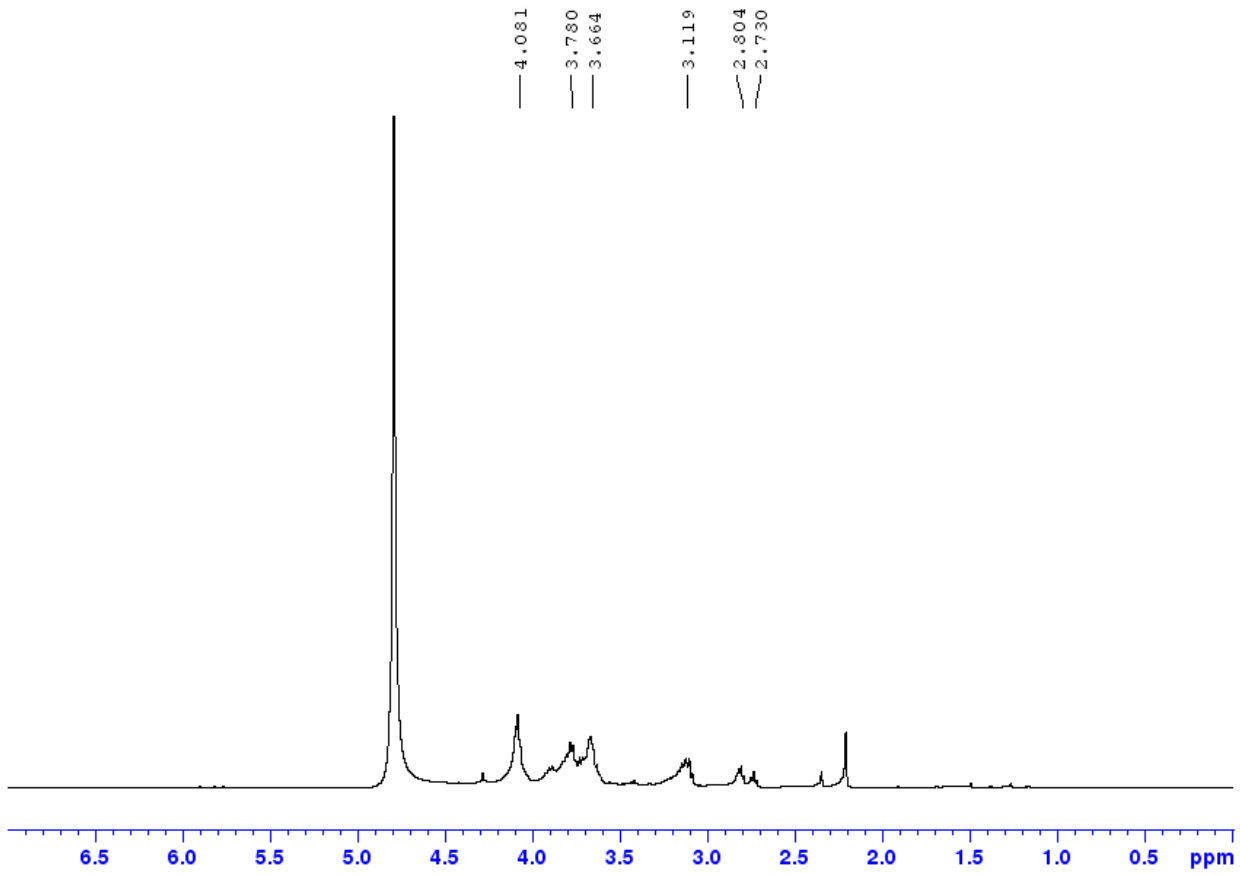


*Figure 8.14 400MHz $^{1}H$ NMR in $D_2O$ of bis (2-bromoetyl) sulfoxide – scheme 2.*

A final synthetic route was proposed for the synthesis of bis (2-bromoethyl) sulfoxide using thiodiglycol sulfoxide and thionyl bromide (Scheme 8.3). A round bottom fitted with a spectrum, and stir bar was flushed with nitrogen. Thiodiglycol sulfoxide (1.85g, 13mmol) was added and stirred. Thionyl bromide (2.3mL, 28.6mmol, 2.2 eq.) was added dropwise over a 2-minute period and the reaction was allowed to stir at room temperature. The reaction was monitored every 24 hours for 96 hours via NMR. The reaction was stopped after 96 hours as NMR showed the product was bromide mustard: $^{1}H$ NMR (400MHz, $CD_3CN$) δ 2.378 (s), δ 2.963 (t, 4H), δ 3.523 (t, 4H) (Figure 8.15). The signal at 2.378 ppm corresponds to water contamination, and the

signals at 2.963 and 3.523 ppm correspond to bromide mustard. Since bromine mustard again was the main product, this reaction was destroyed and no further research was conducted.

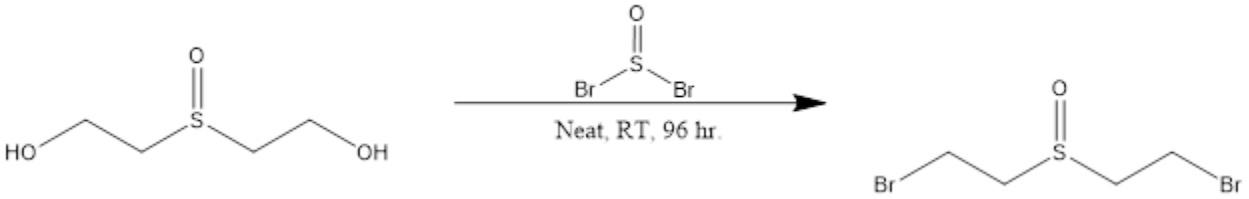


*Scheme 8.3 Bis (2-bromoethyl) sulfoxide synthesis via thiodiglycol sulfoxide and thionyl bromide.*

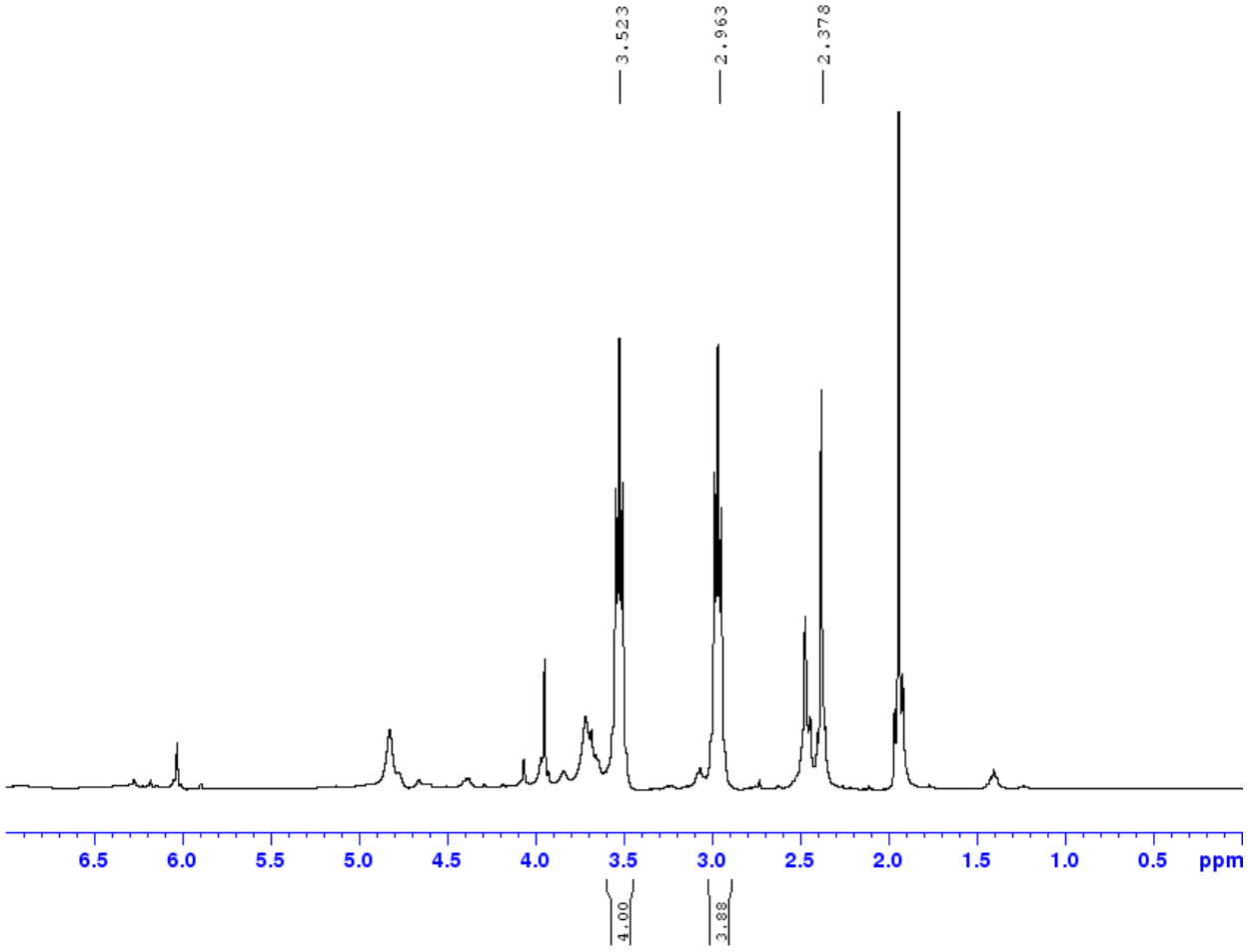


*Figure 8.15 400MHz $^{1}H$ NMR in $CD_3CN$ of bis (2-bromoethyl) sulfoxide – scheme 3.*

After the failure of three separate synthetic routes, it was decided to scrap the idea of synthesizing bis (2-bromoethyl) sulfoxide and focus research efforts onto other molecules that were safer and more easily synthesized.

**Compound E: 3,3′-(((thiobis(ethane-2,1-diyl))bis(sulfanediyl))bis(methylene))dibenzoic acid (3,3′-TMBA)**

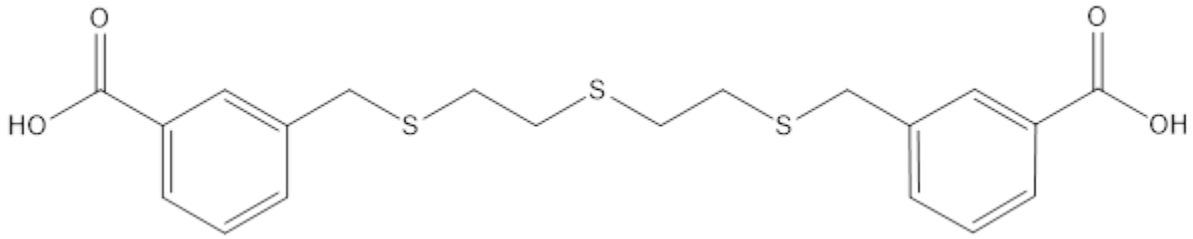


*Figure 8.16 Structure of 3,3′-(((thiobis(ethane-2,1-diyl)) bis(sulfanediyl)) bis(methylene)) dibenzoic acid (3,3′-TMBA).*

The synthesis for 3,3′-(((thiobis(ethane-2,1-diyl)) bis(sulfanediyl)) bis(methylene)) dibenzoic acid (3,3′-TMBA) was successful and that of a novel compound. In a round bottom fitted with a stir bar and septa was flushed with nitrogen. To which bis (2-mercaptoethyl) sulfide (0.833g, 5.4mmol), methanol (40mL) and sodium methoxide (30%, 20mL, 108mmol, 10 eq.) and stirred under nitrogen as fast as possible for 20 minutes at room temperature. A solution of methanol (20mL) and 3-chloromethylbenzoic acid (1.93g, 11.3mmol 1.05 eq.) was added dropwise over a 15-minute period. The reaction stirred for 18 hours under ballooned nitrogen at room temperature. Water (18MΩ, 100mL) was added and the pH of the reaction was lowered to pH 1 by incrementally adding hydrochloric acid (4M, 25mL) while being continually stirred, and a solid began to from once the solution was constantly acidic. The white solid was filtered out washed with hydrochloric acid (0.25M, 100mL), then dissolved in sodium hydroxide (2M, 150mL) to from the sodium salt. The pure product 3,3′-(((thiobis(ethane-2,1-diyl))

bis(sulfanediyl)) bis(methylene)) dibenzoic acid sodium salt (2.09g, 83.6%) was analyzed via NMR: $^{1}$H NMR (400MHz, $D_2O$) δ 2.442 (t, 8H), δ 3.679 (t, 4H), δ 3.24 (t), δ 7.26-7.338 (m, 4H), δ 7.62-7.639 (d, 2H), δ 7.685 (s, 2H) (Figure 8.17). Although this compound was novel and successfully synthesized it was not selected as final molecule for two main reasons. The first reason was it was originally used as a chelating compound during the portion of research that focused on an affinity column. The second reason was that although had good water solubility as the sodium salt, it did not resemble any known molecule that would appear in the body following exposure to sulfur mustard. It was however used for preliminary UV-Vis studies focusing on the binding and precipitation of key metal micronutrients.

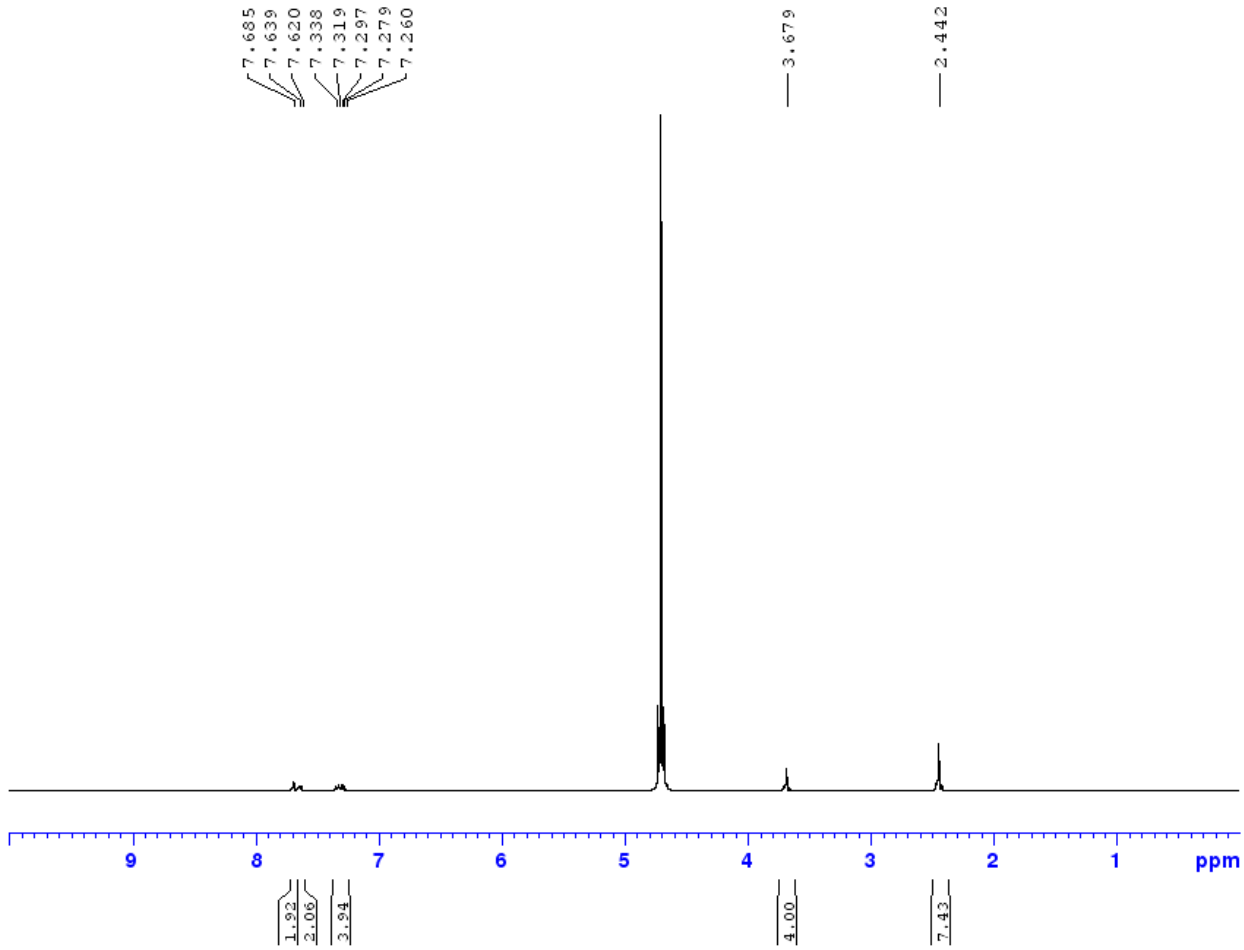


*Figure 8.17 400MHz $^{1}H$ NMR in $D_2O$ of 2,5,8-Trithianonane-1,9-Dibenzoic Acid (TDBA).*

**Compound F: 1,11-Diamino-3,6,9-trithiaundecane (DATT)**

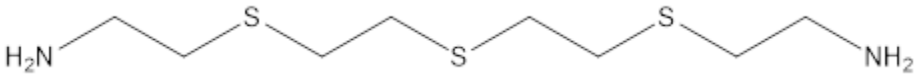


*Figure 8.18 Structure of 1,11-Diamino-3,6,9-trithiaundecane (DATT).*

The synthesis of 1,11-Diamino-3,6,9-trithiaundecane (DATT) was an interesting compound as it would have served as a biological simulant. The compound DATT mimics two partial cysteine residues bound together as if they would have been exposed to sulfur mustard. It is only a partial mimic because the molecule is missing the carboxyl group to make it fully cysteine. The synthetic procedure was adapted from Drew *et al.* (4) with the main difference being apparatus setup and base used. A round bottom was fitted with a chilled reflux condenser, stir bar, capped with septa, and lowered into a 110°C oil bath. Ethanol (200 proof, 40mL, 1.45 eq.) and sodium ethoxide (5M, 15mL, 75mmol) was added and stirred as fast as possible. Once the ethanol began to reflux bis (2-mercaptoehtyl) sulfide (4g, 25.9mmol) was added and refluxed for 15-minutes. At which point the reflux was stopped, 2-bromoethylamine hydrobromide (11g, 53.7mmol, 1.03eq.) slowly, and the reaction brought back to reflux with stirring. The solution was allowed to react for 4 hours, and then cooled to room temperature overnight. A solid (sodium bromide) had formed upon cooling and was filtered out and the solvent removed. The resulting crude product was a thick orange sludge that was dried under nitrogen for 72 hours. This crude product was then recrystallized from a solution of hydrobromic acid in ethanol (5%, 95%), resulting in white crystals and an orange solution. The white crystals were then dried under a combination of nitrogen and high vacuum. The product 1,11-diamino-3,6,9-trithiaundecane (3.07g, 29.4%): $^{1}$H NMR (400MHz, $CD_3CN$) δ 1.18(m), δ 2.87 (t), δ 3.24 (t), δ 3.374 (m), δ 3.569 (s), δ 3.698 (d) (Figure 8.19). The signals at 1.18, 3.569, and 3.698 ppm correspond to unreacted starting material, signals at 3.87, 3.24, and 3.374 ppm can be related to desired product. Although this

reaction was a moderately successful, there was a small amount of unreacted starting material, the overall product had negligible solubility in water. This resulting in the DPTT not being selected as a ligand for further research.

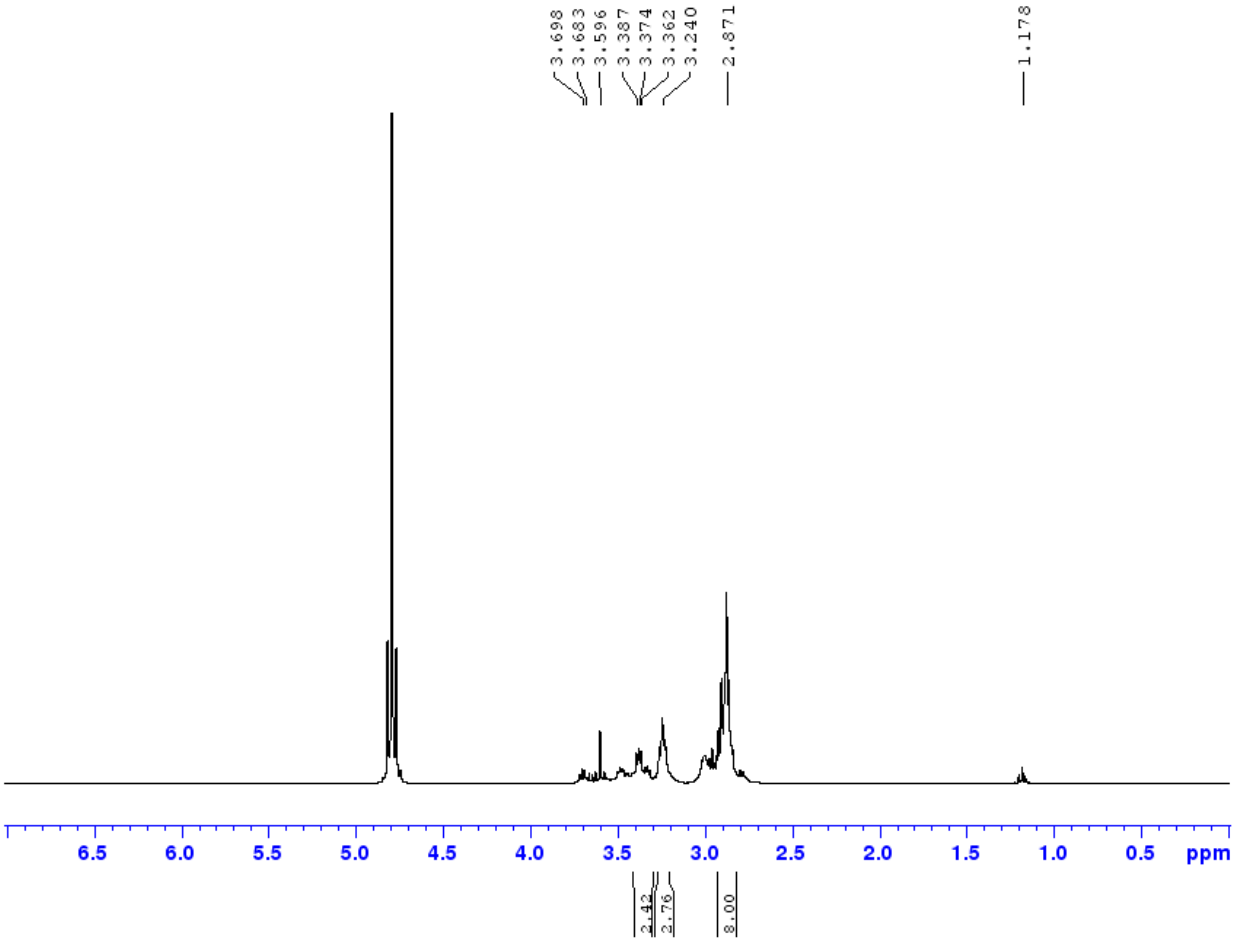


*Figure 8.19 400MHz $^{1}H$ NMR in $D_2O$ of 1,11-Diamino-3,6,9-trithiaundecane.*

**Compound G: S,S′-(thiodi-2,1-ethanediyl) bis-BOC-L-Cysteine Methyl Ester (BOCC)**

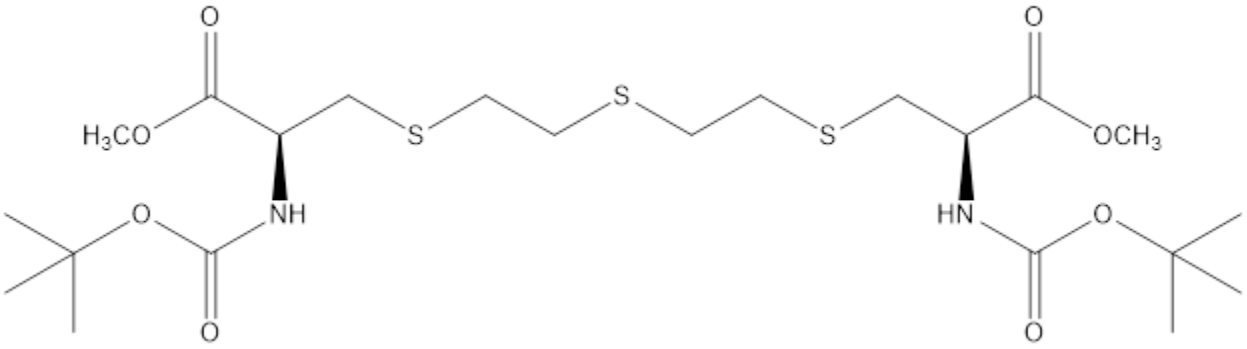


*Figure 8.20 Structure of S,S'-(thiodi-2,1-ethanediyl) bis-BOC-L-cysteine methyl ester (BOCC).*

The synthesis of S,S′-(thiodi-2,1-ethanediyl) bis-BOC-L-cysteine methyl ester (BOCC) was perhaps one of the most ambitious syntheses undertaken, however; if it had been successful it would have been the perfect biological simulant as it would be the result of two cysteine residues reaction with sulfur mustard. Three separate syntheses were tried to successfully synthesize this molecule however none accomplished this goal.

The first synthesis method used a strong base and occurred at room temperature. In a rotund bottom fitted with a septum and stir bar was flushed with nitrogen for 15 minutes. To which water (18MΩ, 75mL), sodium methoxide (5M, 75µL, 5mmol, 3.6 eq.), and bis (2-mercaptoethyl) sulfide (91µL, 0.7mmol) were combined and stirred as fast as possible for 15 minutes. After, BOC-3-Iodo-L-alanine methyl ester (0.5g, 1.52mmol, 1.01 eq.) was added and the reaction stirred for 24 hours. The solvent was removed resulting in a crude solid product of dark orange-brown appearance, which was dried under nitrogen for 48 hours. An attempted recrystallization of the crude product conducted using a boiling solution of water and methanol (25%, 75%), and allowed to cool overnight; resulting in a mainly white solid with faint orange color. This solid was filtered and dried under nitrogen for 24 hours. The product was analyzed via NMR and was very difficult to decipher: $^{1}$H NMR (400MHz, $(CD_3)_2SO$) δ 1.386 (s, 9H), δ 2.734-3.067 (m,

36H), δ 3.317 (s), δ 3.64 (s, 3H), δ 4.139 (s, 1H), δ 7.326 (d, 1H) (Figure 8.21). The signal at 3.317 ppm is contamination by water in the sample. The multiplet of signals between 2.734-3.067 ppm that integrates to 36 protons, shows a mixture of unreacted starting material, possible product, and possible mono-substituted product. Due to the mixture of products and there being so little material to work with no further purification was attempted. The mixture was also only soluble in DMSO which would not bode well for future use since it would not be soluble under physiological conditions.

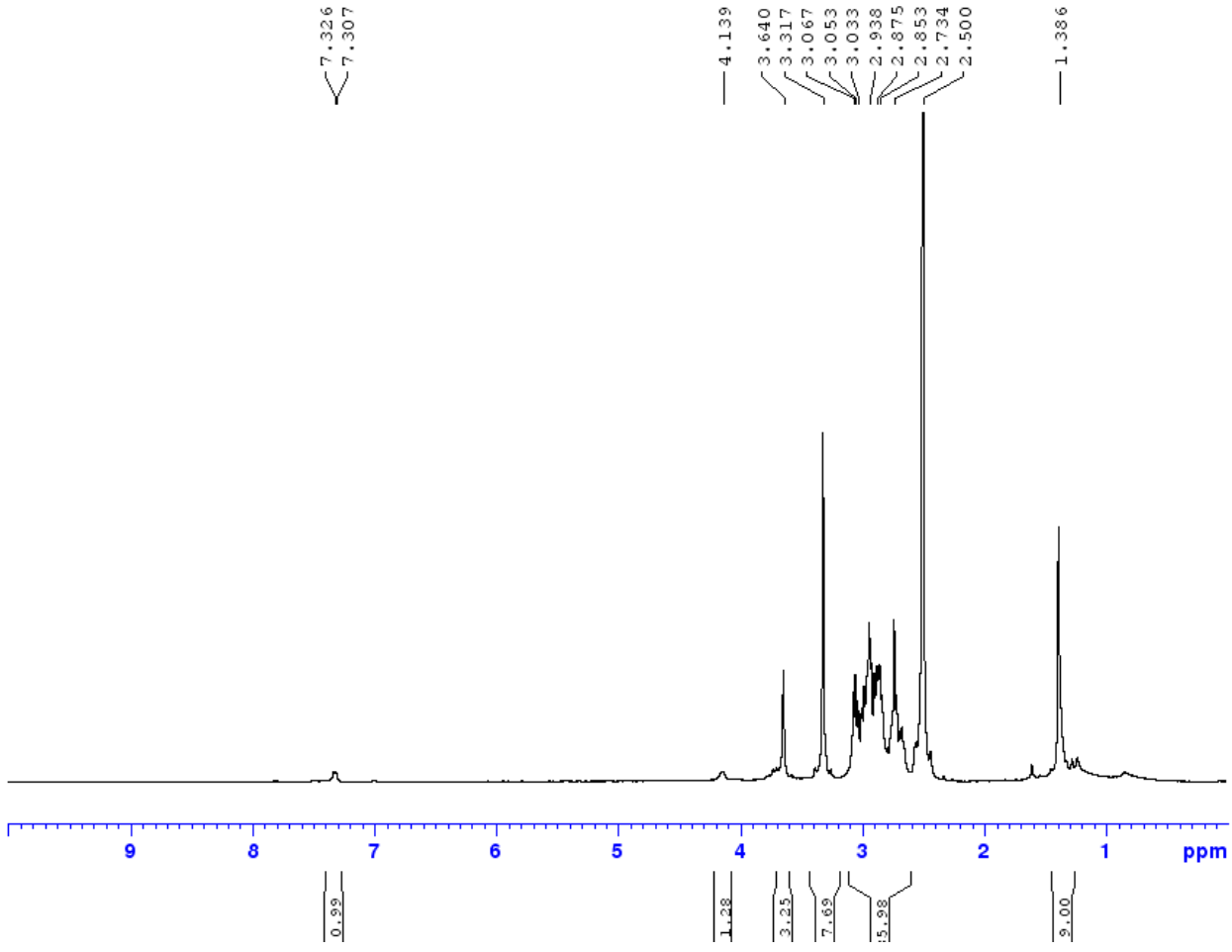


*Figure 8.21 400MHz in $(CD_3)_2SO$ of S,S'-(thiodi-2,1-ethanediyl) bis-BOC-L-Cysteine Methyl Ester (BOCC) – strong base and room temperature.*

The second synthesis method also involved a strong base, but unlike before was refluxed in the hopes of driving the reaction towards the desired product. A round bottom was fitted with a cooled reflux condenser, stir bar, capped with septa, and lowered into a 110°C oil bath. To which a solution of methanol (300mL) and BOC-3-Iodo-L-alanine methyl ester (2.015g, 6.08mmol, 1.05 eq.), stirred as fast as possible and brought to a reflux. Sodium methoxide (5M, 1.75mL, 29mmol, 5 eq.) was added dropwise and refluxed for 10 minutes. After which bis (2-mercaptoethyl) sulfide (0.447g, 2.9mmol) was added dropwise and the apparatus was covered in foil to prevent excess light exposure. The reaction was refluxed for 24 hours, then cooled to room temperature for 3 hours will continuously being stirred. The solvent was then evaporated using a stream of nitrogen for 48 hours, resulting in thick oil. The crude product was tested via TLC plate which showed 2 spots, a flash column was used to separate these spots and fractions analyzed via NMR (spectra not included). This reaction did not work as not fractions showed any signals or integrations that resembled the starting materials or the desired product.

The third and final synthesis method was conducted at room temperature without any base. In a liquid scintillation vial BOC-3-Iodo-L-alanine methyl ester (0.25g, 0.759mmol, 1.05 eq.) was dissolved in methanol (15ml) and stirred for 10 minutes. Bis (2-mercaptoethyl) sulfide (0.056mg, 0.36mmol) was added dropwise over a 5-minute period. The reaction was then allowed to stir as fast as possible for 1 week. The solvent was removed and the resulting solid was dissolved in sodium carbonate (0.1M, 10mL) and stirred. The remaining solid was filtered out and treated with trifluoroacetic acid (TFA) (1mL), in order to cleave the BOC-protecting group, stirred for 1 minute and the TFA removed. This treatment resulted in an oil that was dissolved in methanol (10mL) upon which a solid precipitated out of solution. The solid was separated and dried in a 75°C vacuum oven for 12 hours, while the solvent was removed from the liquid layer and both

analyzed via NMR. The solid was not soluble in $D_2O$ and resulted in a spectrum with no peaks (Figure 8.22), in fact this solid was not soluble even in $(CD_3)_2SO$. The residue left behind by the liquid layer was soluble in $D_2O$ but did not contain an expected signals from the product or starting materials (Figure 8.23).

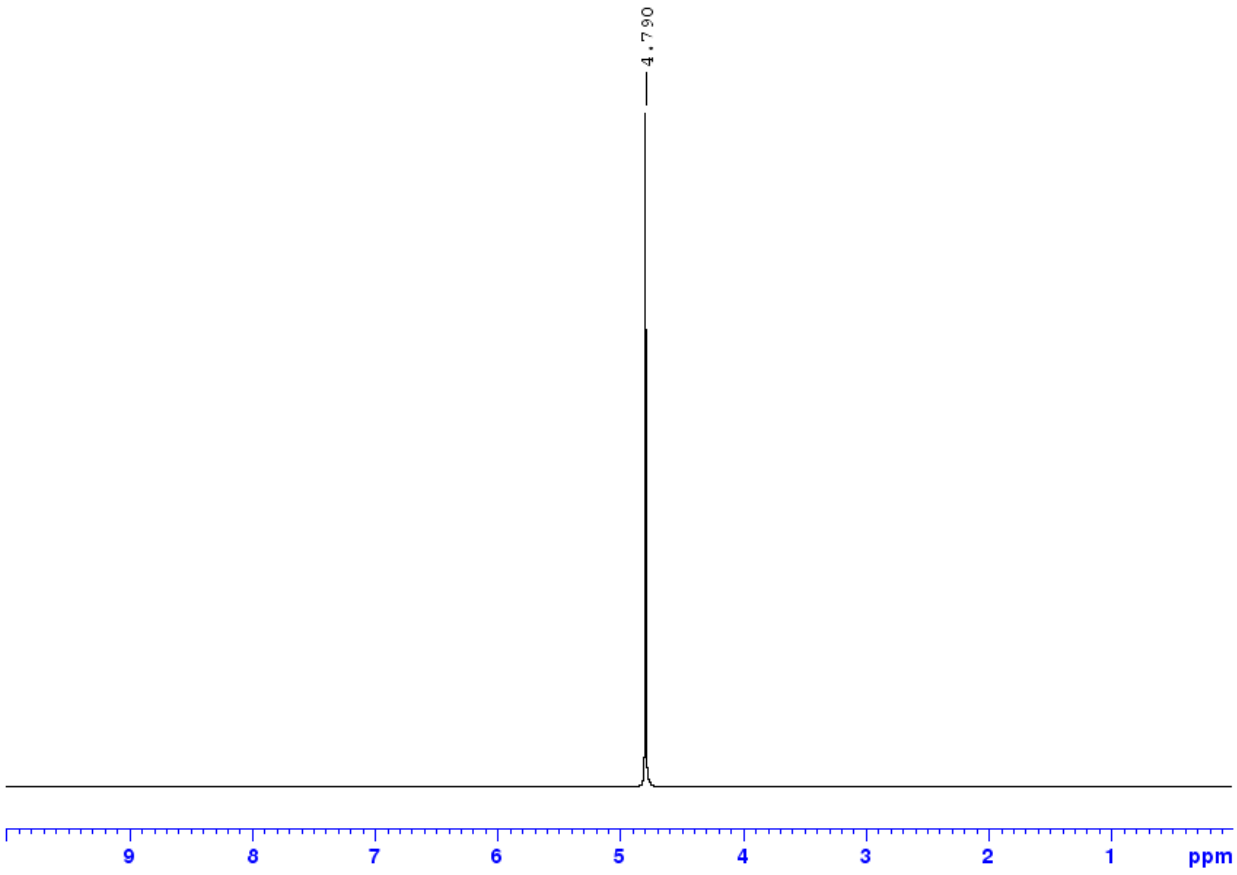


*Figure 8.22 400MHz $^1H$ NMR in $D_2O$ of S,S'-(thiodi-2,1-ethanediyl) bis-BOC-L-Cysteine Methyl Ester (BOCC) – scheme 3 – TFA treated solid.*

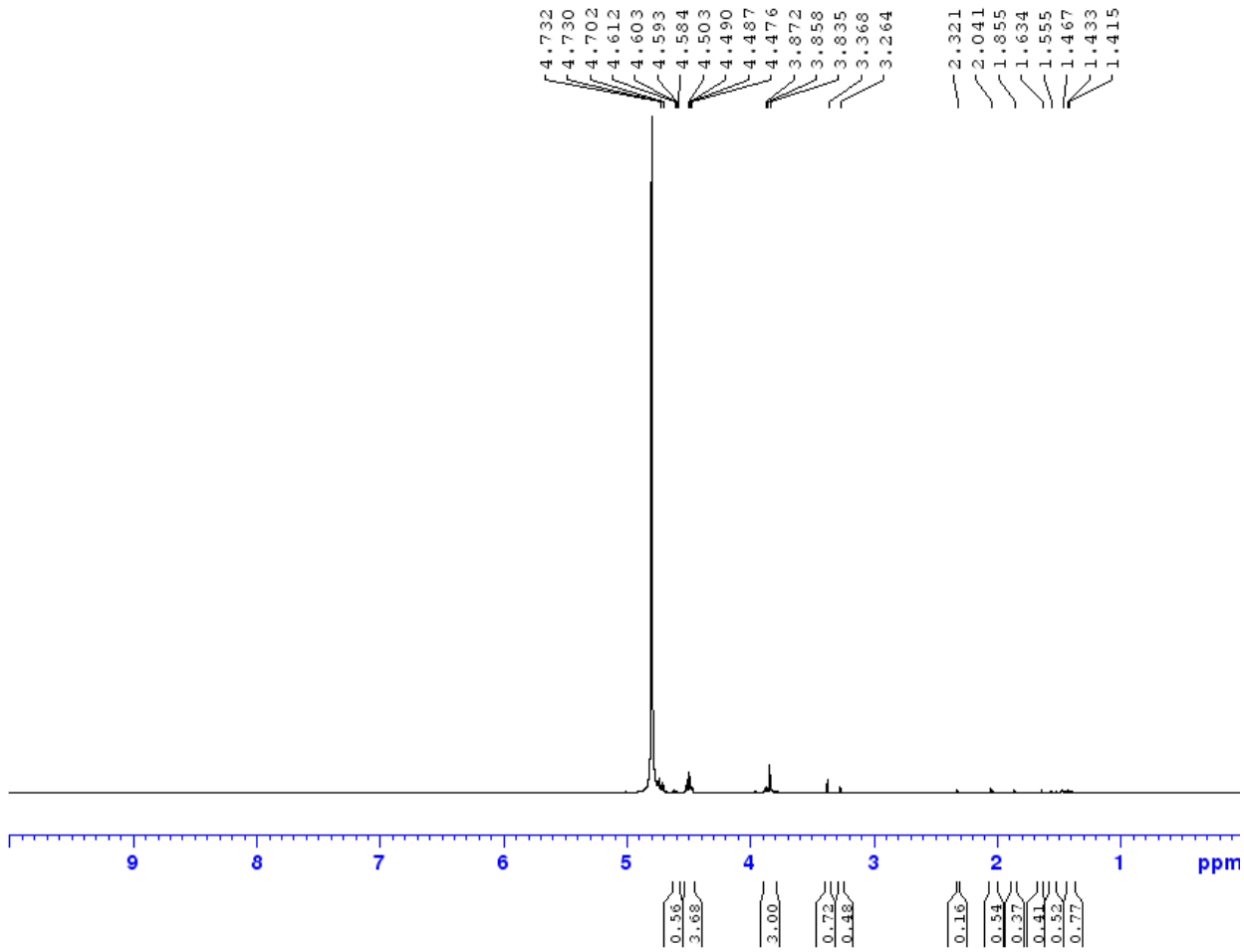


*Figure 8.23 400MHz $^{1}H$ NMR in $D_2O$ of S,S'-(thiodi-2,1-ethanediyl) bis-BOC-L-Cysteine Methyl Ester (BOCC) – scheme 3 – TFA treated liquid.*

Due to the complexity of synthesis and the multiple unsuccessful varying synthesis attempts it was decided to no longer try to synthesize the BOCC compound.

### 8.4 Preliminary UV-Vis Spectrometric Studies

The study of these molecules and their interaction with specific metals using Ultraviolet-Visible Spectroscopy (UV-Vis) was the key to the feasibility and proof of concept for this research. The analytical method of UV-Vis was chosen over other methods such as NMR or Isothermal Titration Calorimetry (ITC) for a few reasons. The reason that NMR was not selected was because NMRs rely on magnetic fields, if the metal concentration in a sample is too high it interferes with the instruments ability to accurately record data. The reason ITC was not selected was the instrumentation available in our laboratory could not hold a steady base line. For these two specific reasons hundreds of trials studying ligand and metal binding were carried out via UV-Vis, with only key studies highlighted.

One of the first ligands studied via UV-Vis was 1,9-diphenyl-2,5,8-trithianonane (DPTT), since this ligand was synthesized to act as a metal chelator, for the since discontinued affinity column, a larger range of metals were tested; some of which are not included as the biological relevant metal micronutrients in this research. The experimental setup proved to be the key basis for all UV-Vis experiments for the duration of this research. First 5 separate stock solution of DPTT, silver (I) nitrate, lead (II) nitrate, nickel (II) nitrate, and sodium nitrate were made in a solution of water/methanol (50/50) and to a final concentration of 0.77mM. The sodium metal was selected as it is known to have no interaction with sulfur, those acting as a control for the other three metals. The experiment was set up so there was a varying ratio of metal to DPTT from the ranges of 5-fold excess of DPTT or a 5-fold excess of metal (Table 8.2). The solutions were mixed and then transferred to a UV transparent 96-well plate and measured form 230-1000nm, with a measurement occurring at every nm.

*Table 8.2 Experimental Design and Final Molar Ratio of DPTT to Metal Salts Used.*

| Sample Ratio | Final Conc. DPTT (μmol) | Final Conc. Metal (μmol) |
|---|---|---|
| 5x [DPTT] : 1x [Metal] | 0.077 | 0.015 |
| 4x [DPTT] : 1x [Metal] | 0.077 | 0.019 |
| 3x [DPTT] : 1x [Metal] | 0.077 | 0.026 |
| 2x [DPTT] : 1x [Metal] | 0.077 | 0.039 |
| 1x [DPTT] : 1x [Metal] | 0.077 | 0.077 |
| 1x [DPTT] : 2x [Metal] | 0.039 | 0.077 |
| 1x [DPTT] : 3x [Metal] | 0.026 | 0.077 |
| 1x [DPTT] : 4x [Metal] | 0.019 | 0.077 |
| 1x [DPTT] : 5x [Metal] | 0.015 | 0.077 |

While this experiment between DPTT, silver, lead, nickel, and sodium proved useful from an experimental design aspect, it provided little usable data for the grand scope of this research. The spectra that resulted from the combination of DPTT and a metal showed no measurable changes at the concentrations used. The concentration would not be increased because DPTT was sparingly soluble in pure water, and the metals are sparling soluble if not insoluble in pure methanol; therefore, the ratio of water to methanol could not be changed or neither DPTT or the metal would be in solution. Between these solubility issues and moving away from the affinity column idea, the study of interaction between DPTT and metals was scrapped.

The next ligand research in regards to metal binding and UV-Vis spectroscopy was 3,3′-(((thiobis(ethane-2,1-diyl))bis(sulfanediyl))bis(methylene))dibenzoic acid (3,3′-TMBA). A slightly modified experimental design was tested with the 3,3′-TMBA compound, which was tested with copper (II) chloride dihydrate, nickel (II) chloride anhydrous, silver (I) nitrate, zinc (II) chloride anhydrous, cobalt (II) chloride hexahydrate, and a control of sodium chloride. The key difference in these 3,3′-TMBA experiments were that the ratio of 3,3′-TMBA to metal was

constantly varied and not held constant like previously. The sodium salt form of 3,3′-TMBA was also used to conduct these experiments as the protonated form was not soluble in water, but the sodium salt form was.

All metal salts and 3,3′-TMBA were made as master solution with a final concentration of 0.1M in straight water. The initial tests were carried out on a smaller scale with all metals and then narrowed down to a select few to conduct on a larger scale monitoring experiment. These experiments were conducted by varying the percentage of volume for each the metal and 3,3′-TMBA (Table 8.3). One important observation that began before analysis via UV-Vis was that in every case of 3,3′-TMBA mixed with a metal, except sodium, a precipitate formed. Because of this, each sample was mixed in a microfuge tube and centrifuged at 14G for 30 second; it was then the supernatant that was transferred into a UV-transparent 96-well plate and measured from 230-1000nm taking a measurement every nm.

*Table 8.3 Initial Experimental Design for 3,3′-TMBA and All Metal Salts.*

| Sample Name | Vol. 3,3-TMBA (µL) | Vol. Metal (µL) | Final Conc. 3,3-TMBA (µmol) | Final Conc. Metal (µmol) |
|---|---|---|---|---|
| 90 / 10 | 90 | 10 | 9 | 1 |
| 80 / 20 | 80 | 20 | 8 | 2 |
| 50 / 50 | 50 | 50 | 5 | 5 |
| 20 / 80 | 20 | 80 | 2 | 8 |
| 10 / 90 | 10 | 90 | 1 | 9 |

After the initial experiment only copper (II) chloride and cobalt (II) chloride were chosen to continue for further analysis. Sodium chloride was used as a control, and there was measurable interaction between the sodium and sulfur, so there was no need to expand its study. Both silver (I) nitrate and nickel (II) chloride showed both the formation of a precipitate and evidence of binding based of change in spectra; however, both metals had too high absorbance, even at dilute

concentration, to produce trustworthy data. Zinc (II) chloride also produced a precipitate but was not used for further study as zinc is not UV-Vis active so there would have been no way to measure any changes in binding using this method. The data for this experimental design was not included as it yielded no true insight aiding research.

Continued analysis with 3,3′-TMBA, copper (II) chloride dehydrate, and cobalt (II) chloride hexahydrate was conducted in a similar manner to that of the initial trials, but with more percentage ratios (Table 8.4). These mixtures were also centrifuged at 14G for 30 seconds and the supernatant measured. The remaining supernatant was discarded and the pelleted precipitate was dried under heat and vacuum for 48 hours. The hope was to redissolve and obtain a UV-Vis spectra of the pellet to compare with that of the supernatant; however, the pellets were never successfully redissolved. The main importance of these pellets was, there was a measure amount of product that precipitated out of solution that could be accurately weighted and duplicated.

*Table 8.4 Full Scale Analysis of 3,3′-TMBA with Copper (II) Chloride and Cobalt (II) Chloride.*

| Sample Name | Vol. 3,3-TMBA (μL) | Vol. Metal (μL) | Final Conc. 3,3-TMBA (μmol) | Final Conc. Metal (μmol) |
|---|---|---|---|---|
| 90 / 10 | 90 | 10 | 9 | 1 |
| 80 / 20 | 80 | 20 | 8 | 2 |
| 70 / 30 | 70 | 30 | 7 | 3 |
| 60 / 40 | 60 | 40 | 6 | 4 |
| 50 / 50 | 50 | 50 | 5 | 5 |
| 40 / 60 | 40 | 60 | 4 | 6 |
| 30 / 70 | 30 | 70 | 3 | 7 |
| 20 / 80 | 20 | 80 | 2 | 8 |
| 10 / 90 | 10 | 90 | 1 | 9 |

The results of these UV-Vis studies showed a strong measurable interaction between 3,3′-TMBA and copper (II) chloride with noticeable changes in the concentration of copper and a shift in the

location of the maximum intensity peak related to copper. The spectra of 3,3′-TMBA and copper (II) chloride show a reduction in the overall intensity of the at the λ-max of copper, leading to the conclusion that a binding between the compound 3,3′-TMBA and copper ions did in fact occur (Graphs 8.1-8.4). The other important development was the shift in the λ-max of copper following the binding of the 3,3′-TMBA compounds, more noticeable in the samples with a lower copper concentration (Graphs 8.3-8.4). Each graph of the binding of 3,3′-TMBA and copper (II) chloride contains the samples spectra from the samples supernatant, the ligand alone, and copper (II) chloride alone at their respective concentrations for that specific sample. Unfortunately, there was a non-measurable interaction between 3,3′-TMBA and cobalt (II) chloride, although noticeable precipitate formation occurred there was not enough strong data from UV-Vis spectra to discern any useful information (data not shown).

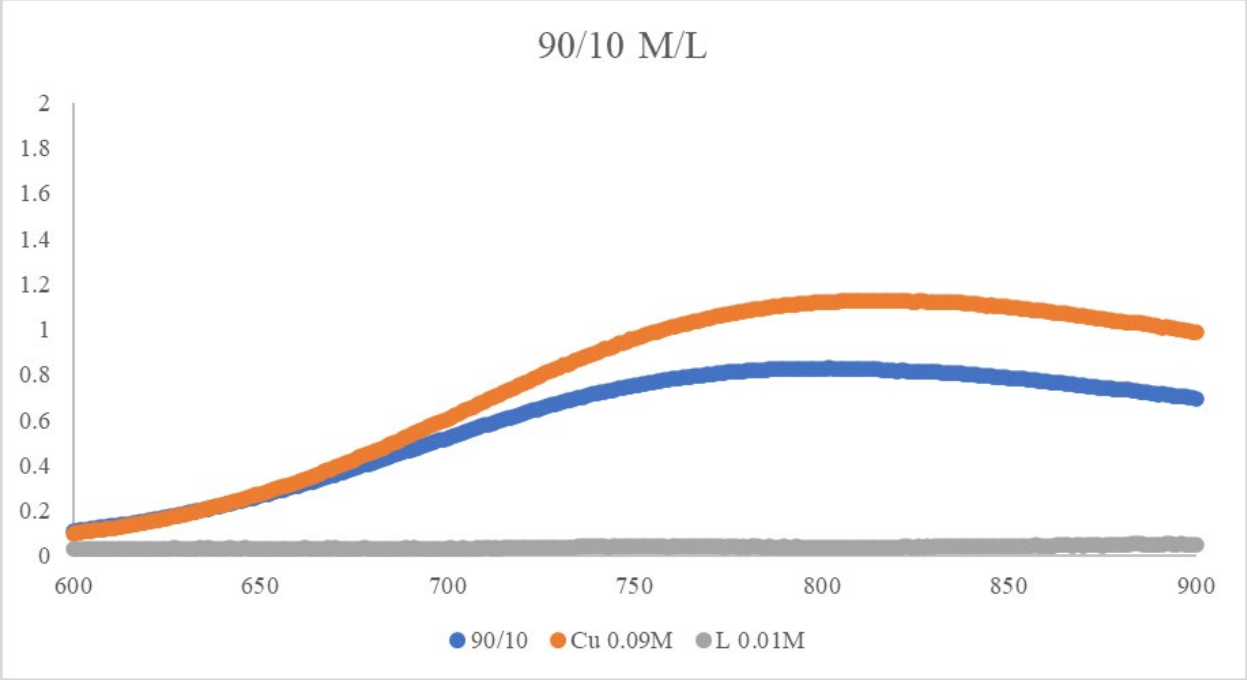


*Graph 8.1 Spectral Comparison of 3,3'-TMBA bound to Copper (II) Chloride at 90% Copper and 10% 3,3'-TMBA with Control Spectra of Copper (II) Chloride and 3,3-TMBA (L) at their Respective Concentrations.*

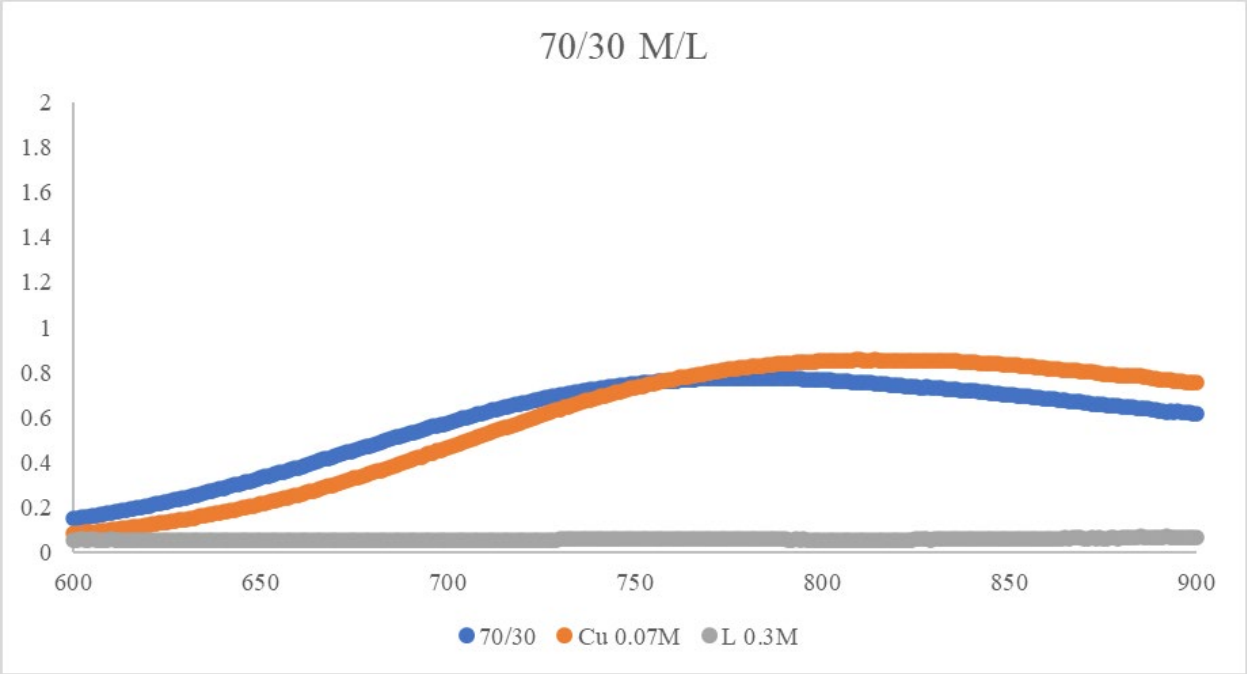


*Graph 8.2 Spectral Comparison of 3,3'-TMBA bound to Copper (II) Chloride at 70% Copper and 30% 3,3'-TMBA with Control Spectra of Copper (II) Chloride and 3,3-TMBA (L) at their Respective Concentrations.*

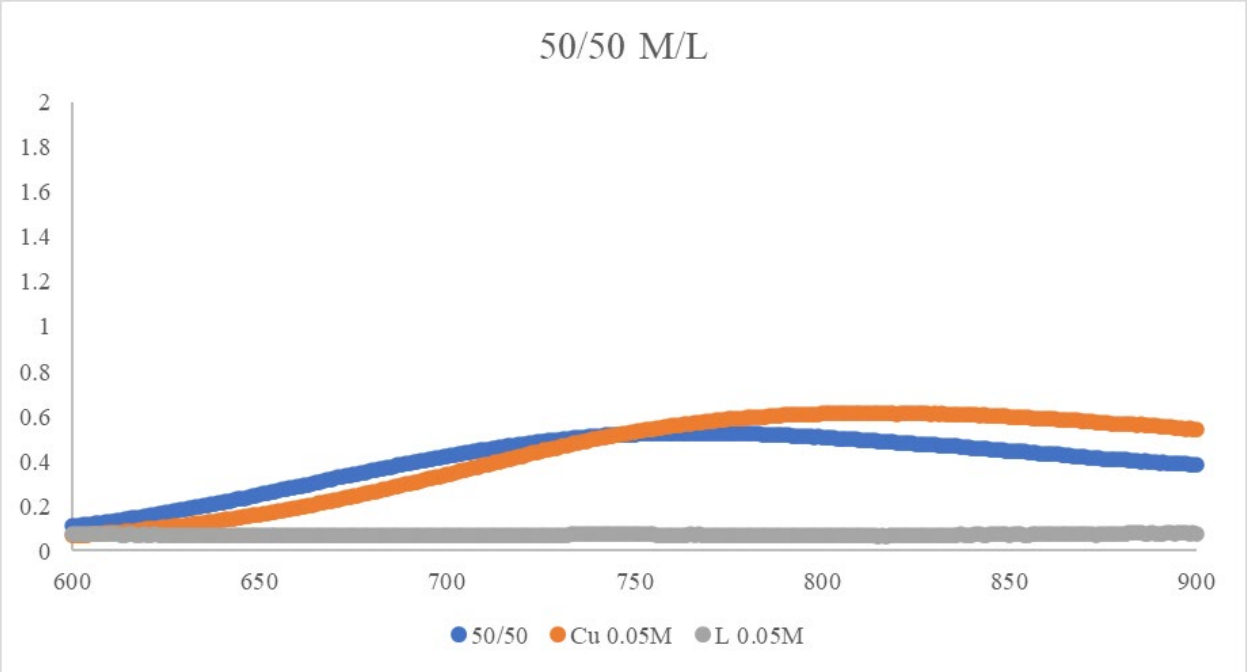


*Graph 8.3 Spectral Comparison of 3,3'-TMBA bound to Copper (II) Chloride at 50% Copper and 50% 3,3'-TMBA with Control Spectra of Copper (II) Chloride and 3,3-TMBA (L) at their Respective Concentrations.*

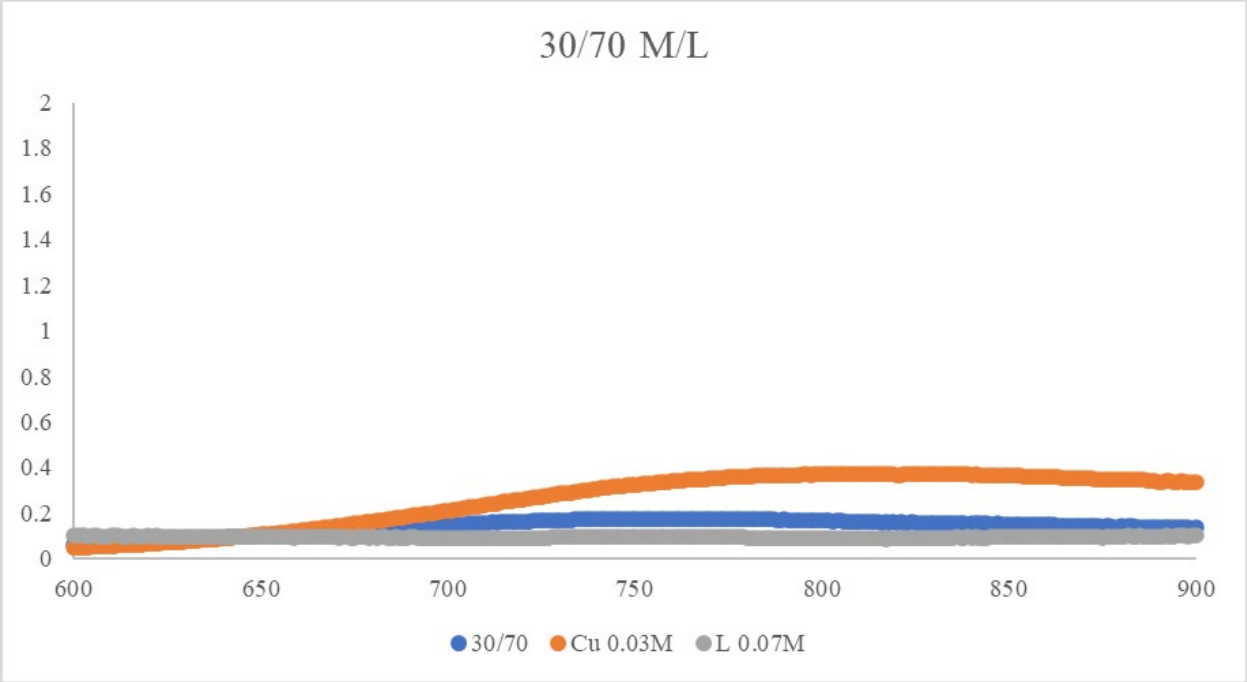


*Graph 8.4 Spectral Comparison of 3,3'-TMBA bound to Copper (II) Chloride at 30% Copper and 70% 3,3'-TMBA with Control Spectra of Copper (II) Chloride and 3,3-TMBA (L) at their Respective Concentrations.*

To ensure that the spectra changes and the precipitation observed were a result of the copper ions binding to the sulfur atoms instead of interacting with carboxylate groups present. A control study was conducted following the exact same parameters as before. Copper (II) chloride dihydrate was reacted with sodium benzoate instead of the 3,3′-TMBA compound. The control experiment revealed that there was no discernable shift in the λ-max of copper nor a significant decrease in absorbance when copper (II) chloride was reacted with sodium benzoate (Graphs 8.5-8.8). Each graph for the solution of sodium benzoate and copper (II) chloride contains the samples spectra, the sodium benzoate alone, and copper (II) chloride alone at their respective concentrations for that specific sample. Although there was some difference in absorbance intensities it was not believed that this was of any significance.

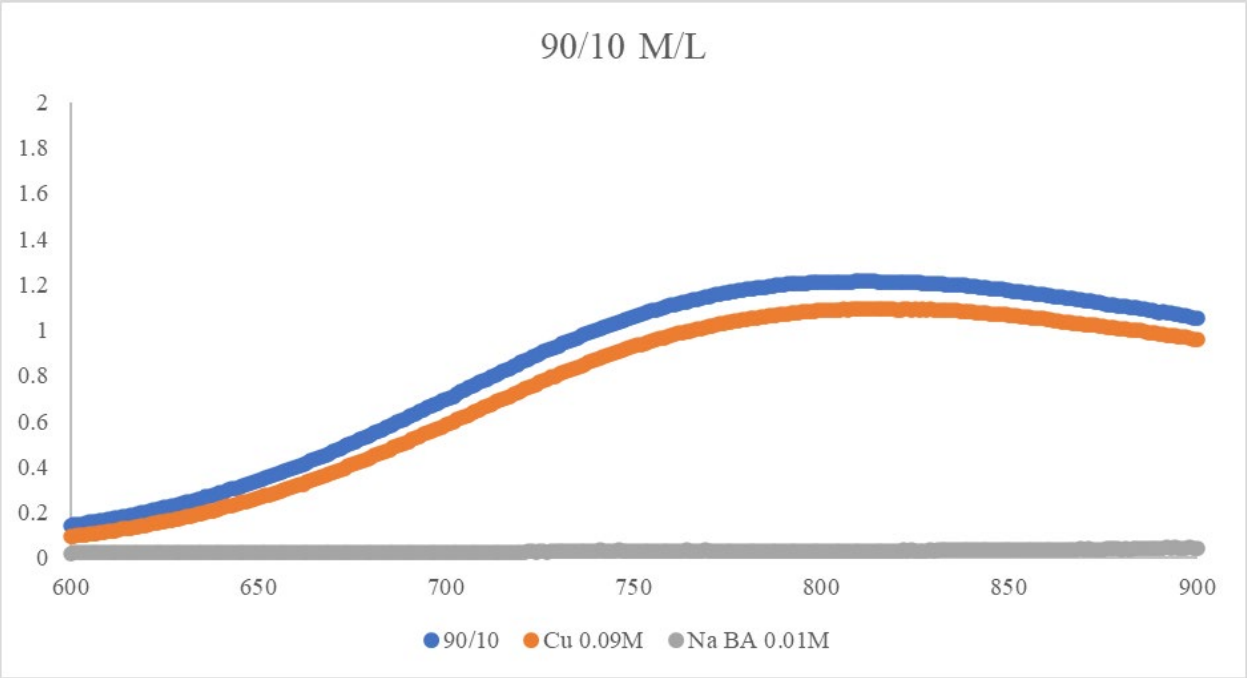


*Graph 8.5 Spectral Comparison of Sodium Benzoate and Copper (II) Chloride at 90% Copper and 10% Sodium Benzoate with Control Spectra of Copper (II) Chloride and Sodium Benzoate (Na BA) at their Respective Concentrations.*

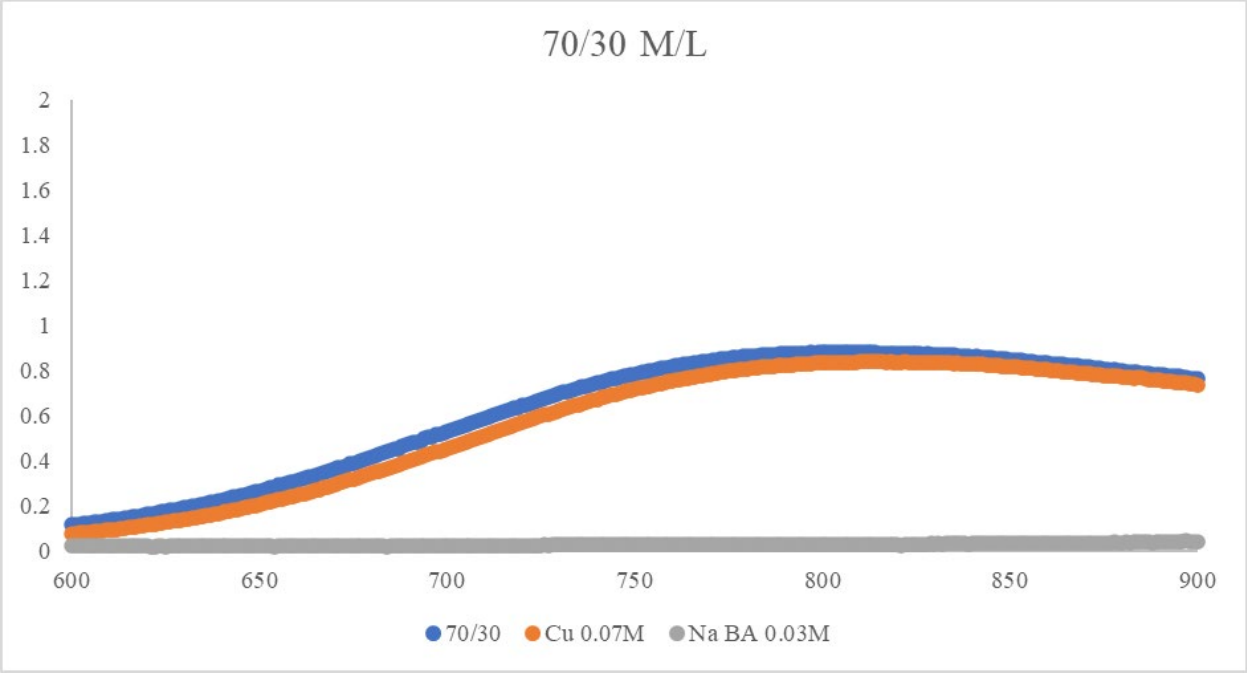


*Graph 8.6 Spectral Comparison of Sodium Benzoate and Copper (II) Chloride at 70% Copper and 30% Sodium Benzoate with Control Spectra of Copper (II) Chloride and Sodium Benzoate (Na BA) at their Respective Concentrations.*

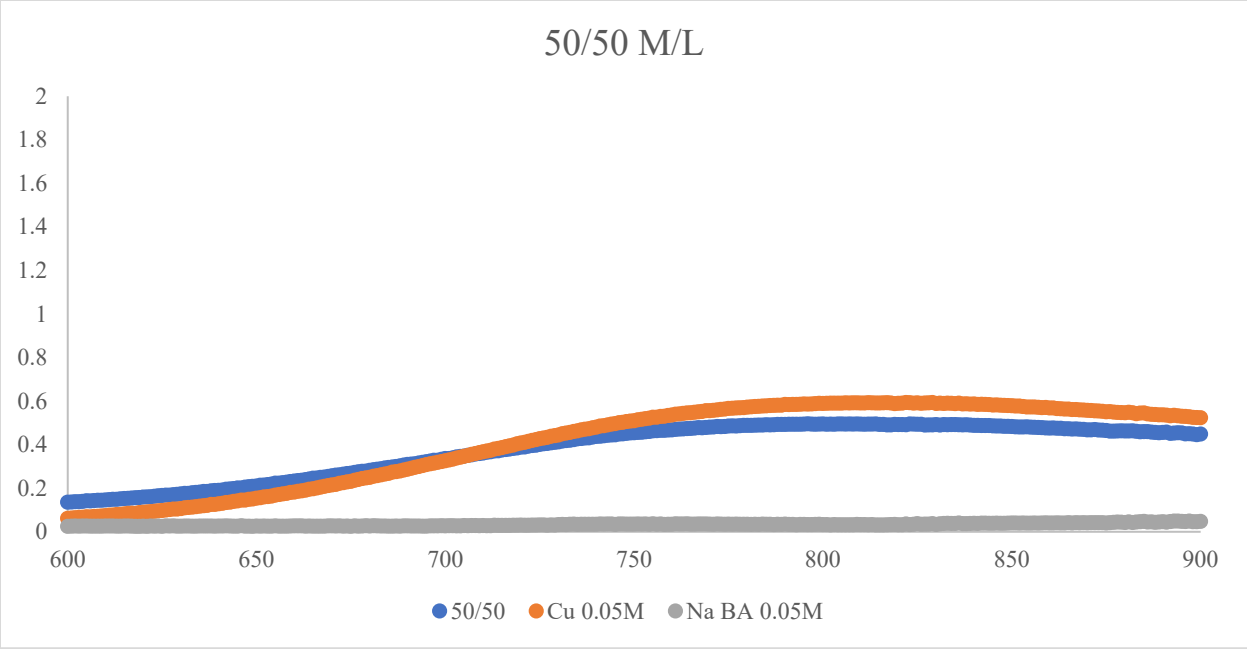


*Graph 8.7 Spectral Comparison of Sodium Benzoate and Copper (II) Chloride at 50% Copper and 50% Sodium Benzoate with Control Spectra of Copper (II) Chloride and Sodium Benzoate (Na BA) at their Respective Concentrations.*

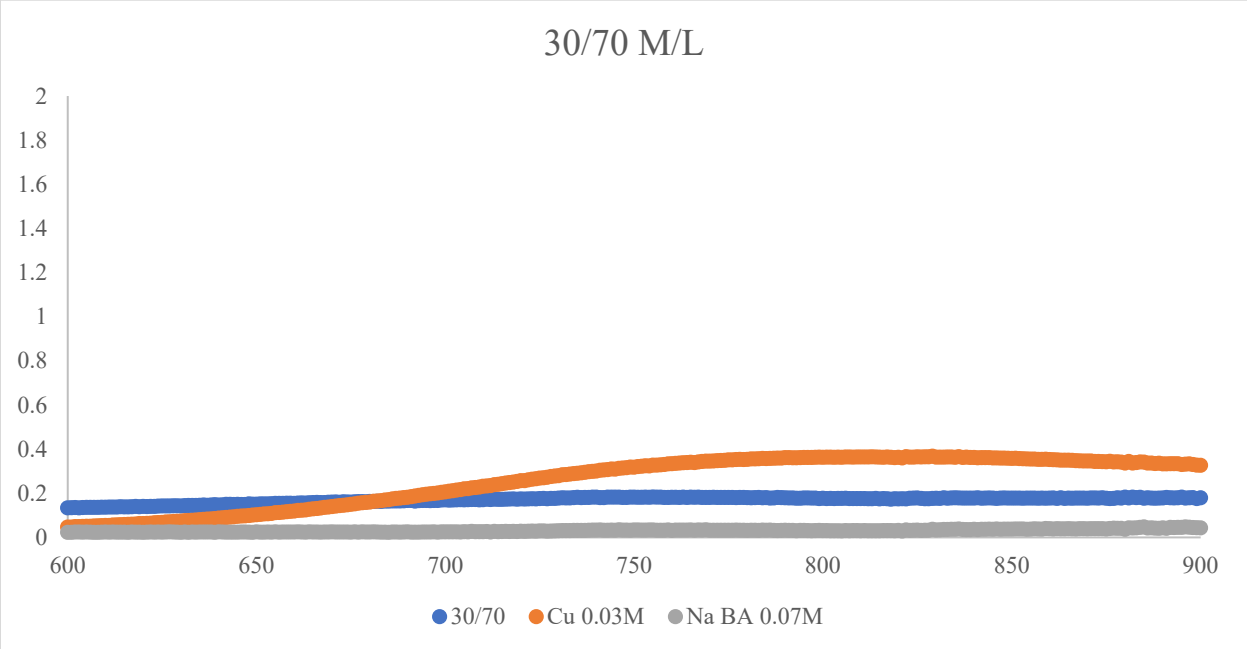


*Graph 8.8 Spectral Comparison of Sodium Benzoate and Copper (II) Chloride at 30% Copper and 70% Sodium Benzoate with Control Spectra of Copper (II) Chloride and Sodium Benzoate (Na BA) at their Respective Concentrations.*

Due to no significant shifts in spectral peaks or decreases in spectral intensity with the sodium benzoate and copper (II) chloride control study; it was concluded that the changes and intensity and λ-max shift of copper was due to the biding of 3,3′-TMBA and no interaction with the carboxylate groups played a role. As the scope of research shifted to focusing on more biologically relevant compounds, 3,3′-TMBA was not included as a key compound as it does not mimic a compound that would be found as a result of sulfur mustard exposure. It however, did provide insight that these sulfur bridged compounds do in fact interact with metal ions without interaction of other functional groups.

The final ligand tested was 2,5,8-Trithianone-1,9-dicarboxylic acid (TTDAA, Compound 2 Ch. 5). Although TTDAA was a successful synthesis and was characterized via NMR, crystallography, and elemental analysis; it was included in this section as the UV-Vis experimentation results were not chosen as a key contributor to the scope of this research (Figure 5.1-5.2). Master solutions (0.1M) were made in water (18MΩ) of TTDAA sodium salt, sodium acetate trihydrate, zinc acetate dihydrate, nickel (II) acetate tetrahydrate, copper (II) acetate monohydrate, and cobalt (II) acetate tetrahydrate. Iron (III) chloride was also tested, but due to complication with using iron it was not selected as a metal for further study. TTDAA was reacted with each metal individually in two separate strategies: first where the concentration of TTDAA was held constant and the concertation of metal ion varied, and the second where the concentration of metal ion was held constant and the concertation of TTDAA was varied (Table 8.5).

*Table 8.5 Initial Extermination Setup of TTDAA and Metals at Constant Concentration Ratios.*

| TTDAA Concentration Held Constant | | | |
|---|---|---|---|
| Sample Name [TTDAA:Metal] | [TTDAA] mM | [Metal] mM | Ratio TTDAA : Metal |
| Metal 1:0 | 33 | 0 | N/A |
| Metal 1:0.25 | 33 | 8.25 | 4 |
| Metal 1:0.5 | 33 | 16.5 | 2 |
| Metal 1:0.75 | 33 | 24.75 | 1.33 |
| Metal 1:1 | 33 | 33 | 1 |
| Metal Ion Concentration Held Constant | | | |
| Sample Name [TTDAA:Metal] | [TTDAA] mM | [Metal] mM | Ratio TTDAA : Metal |
| Metal 0:1 | 0 | 33 | N/A |
| Metal 0.25:1 | 8.25 | 33 | 0.25 |
| Metal 0.5:1 | 16.5 | 33 | 0.5 |
| Metal 0.75:1 | 24.75 | 33 | 0.75 |
| Metal 1:1 | 33 | 33 | 1 |

Since many samples formed a precipitate upon their reaction (Table 8.6), each sample was centrifuged at 14G for 60 seconds and only the supernatant was analyzed. Each supernatant was transferred to a 96-well UV-transparent plate and measured from 230-1000nm, with a measurement every nm. As before with sodium and zinc ions, there was no discernable information to be gathered from the UV-Vis data. Sodium did not with the TTDAA ligand as expected, and zinc is not UV-Vis active so no data could be gathered; however, nearly all of the zinc solutions formed a visible precipitate upon their mixture with TTDAA. None of this data is surprising as all previously studied ligands had yielded similar results. Copper, nickel, and cobalt all showed promising results from these studies. As before, copper showed a shift in the λ-max after the reaction with TTDAA, as well as a change in the intensity of the spectra; this held true regardless with reagent was held at a constant concentration (Graphs 8.9-8.10). The reaction between nickel and TTDAA had the same result as copper, there was a noticeable shift in the λ-maxes for nickel as well as changes in intensity (Graphs 8.11-8.12). The reaction between

TTDAA and cobalt was only carried out under the condition where the cobalt concentration was held constant, and at slightly lower concentrations. Although there was no noticeable shift in the λ-max of cobalt, there was the growth on a peak that only appeared after the reaction of cobalt and TTDAA (Graph 8.13).

*Table 8.6 Precipitate Formation as a Result of the Reaction between TTDAA and Specific Metal Ions at Varying Concentrations.*

| Sample Name [L : M] | [TTDAA] mM | [Metal] mM | Precipitate Formation |
|---|---|---|---|
| Copper 1:0 | 33 | 0 | |
| Copper 1:0.25 | 33 | 8.25 | |
| Copper 1:0.5 | 33 | 16.5 | |
| Copper 1:0.75 | 33 | 24.75 | * |
| Copper 1:1 | 33 | 33 | * |
| Copper 0:1 | 0 | 33 | |
| Copper 0.25:1 | 8.25 | 33 | |
| Copper 0.5:1 | 16.5 | 33 | |
| Copper 0.75:1 | 24.75 | 33 | * |
| Copper 1:1 | 33 | 33 | * |
| Nickel 1:0 | 33 | 0 | |
| Nickel 1:0.25 | 33 | 8.25 | |
| Nickel 1:0.5 | 33 | 16.5 | |
| Nickel 1:0.75 | 33 | 24.75 | * |
| Nickel 1:1 | 33 | 33 | * |
| Nickel 0:1 | 0 | 33 | |
| Nickel 0.25:1 | 8.25 | 33 | |
| Nickel 0.5:1 | 16.5 | 33 | |
| Nickel 0.75:1 | 24.75 | 33 | * |
| Nickel 1:1 | 33 | 33 | * |
| Zinc 1:0 | 33 | 0 | |
| Zinc 1:0.25 | 33 | 8.25 | |
| Zinc 1:0.5 | 33 | 16.5 | + |
| Zinc 1:0.75 | 33 | 24.75 | + |
| Zinc 1:1 | 33 | 33 | + |
| Zinc 0:1 | 0 | 33 | |
| Zinc 0.25:1 | 8.25 | 33 | |
| Zinc 0.5:1 | 16.5 | 33 | + |
| Zinc 0.75:1 | 24.75 | 33 | + |
| Zinc 1:1 | 33 | 33 | + |
| Sodium 1:0 | 33 | 0 | |
| Sodium 1:0.25 | 33 | 8.25 | |
| Sodium 1:0.5 | 33 | 16.5 | |
| Sodium 1:0.75 | 33 | 24.75 | |
| Sodium 1:1 | 33 | 33 | |
| Sodium 0:1 | 0 | 33 | |
| Sodium 0.25:1 | 8.25 | 33 | |
| Sodium 0.5:1 | 16.5 | 33 | |
| Sodium 0.75:1 | 24.75 | 33 | |
| Sodium 1:1 | 33 | 33 | |
| Cobalt 0:1 | 0 | 10 | |
| Cobalt 0.25:1 | 2.5 | 10 | |
| Cobalt 0.5:1 | 5 | 10 | + |
| Cobalt 0.75:1 | 7.5 | 10 | + |
| Cobalt 1:1 | 10 | 10 | * |
| * = Formed Immediately + = Formed within 24 hours | | | |

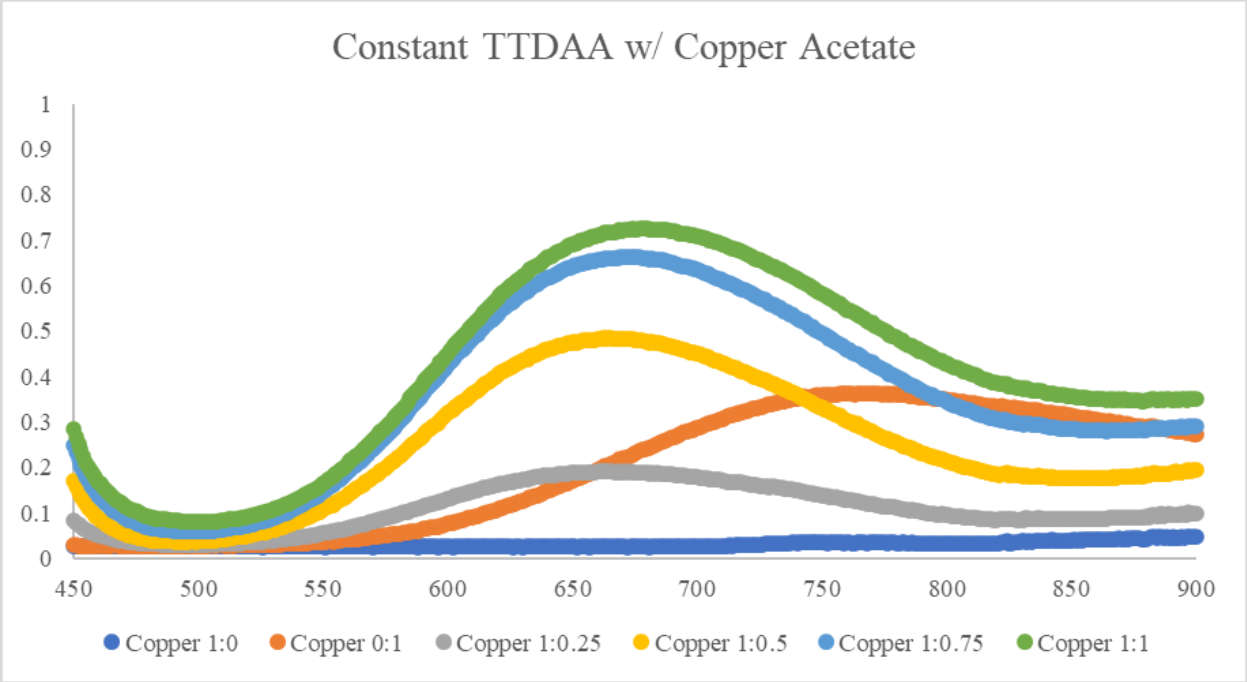


*Graph 8.9 UV-Vis Spectra for the Reaction of TTDAA and Copper (II) Acetate Monohydrate with the Concentration of TTDAA Held Constant.*

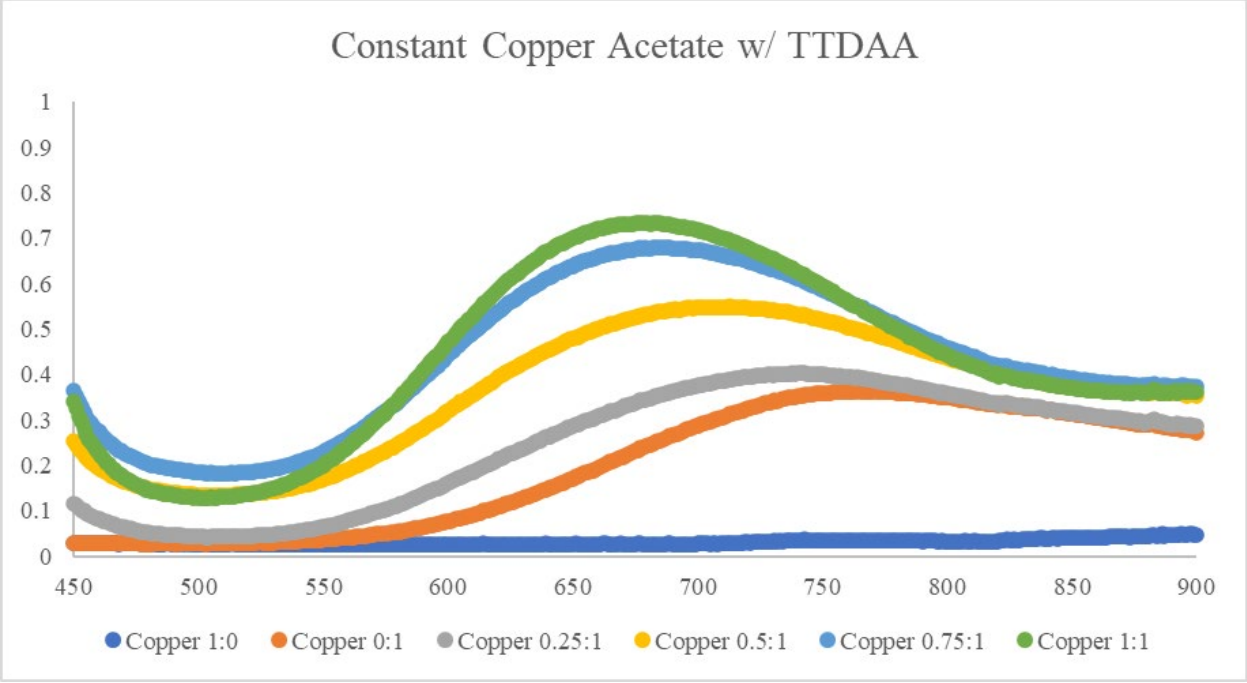


*Graph 8.10 UV-Vis Spectra for the Reaction of TTDAA and Copper (II) Acetate Monohydrate with the Concentration of Copper (II) Acetate Monohydrate Held Constant.*

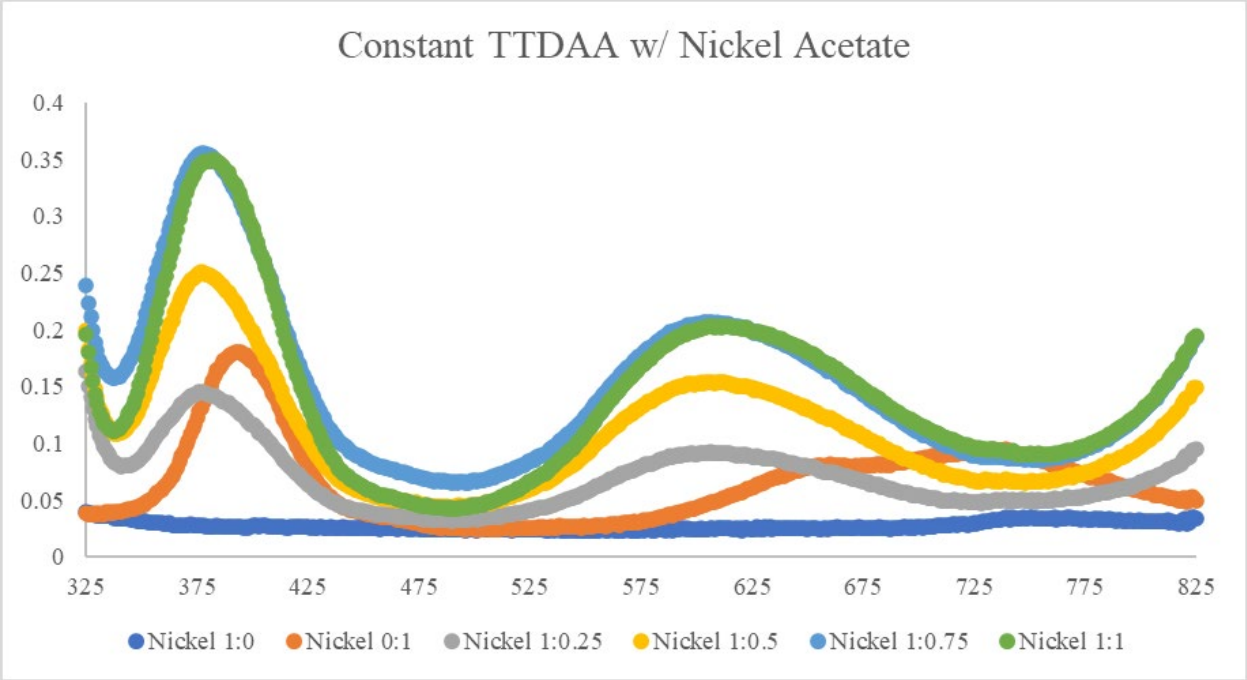


*Graph 8.11 UV-Vis Spectra for the Reaction of TTDAA and Nickel (II) Acetate Tetrahydrate with the Concentration of TTDAA Held Constant.*

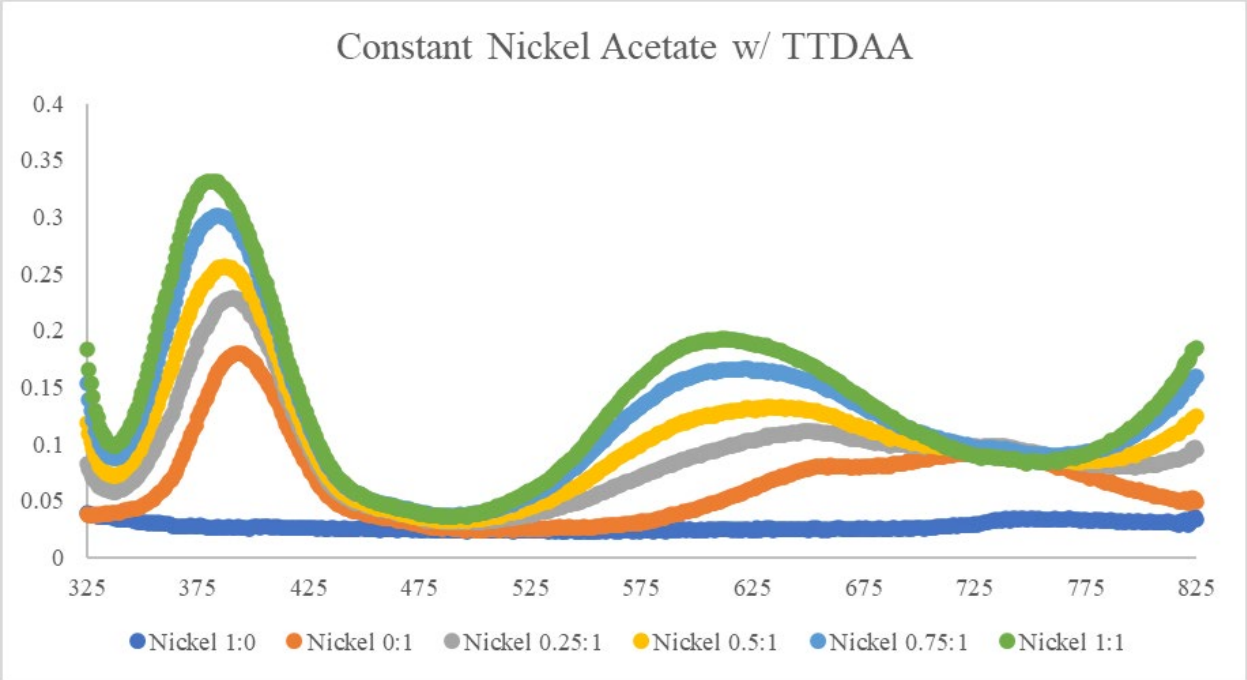


*Graph 8.12 UV-Vis Spectra for the Reaction of TTDAA and Nickel (II) Acetate Tetrahydrate with the Concentration of Nickel (II) Acetate Tetrahydrate Held Constant.*

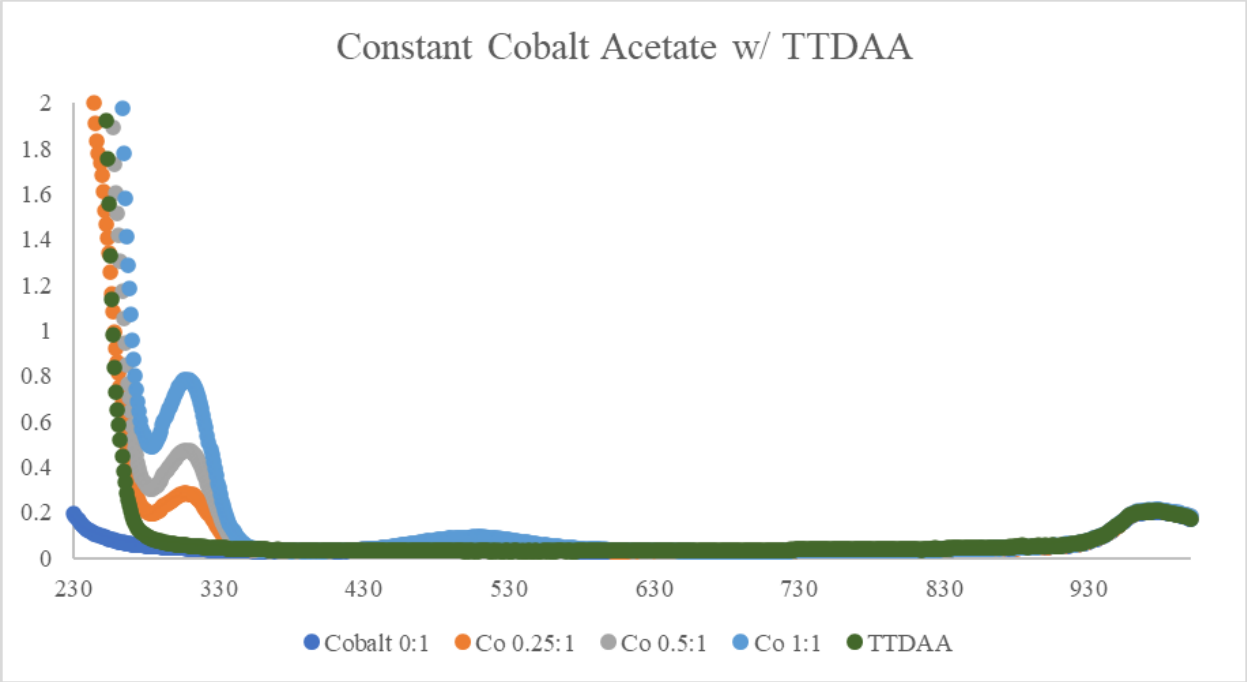


*Graph 8.13 UV-Vis Spectra for the Reaction of TTDAA and Cobalt (II) Acetate Tetrahydrate with the Concentration of Cobalt (II) Acetate Tetrahydrate (Cobalt 0:1) Held Constant.*

Published information exists about the binding of TTDAA and many of the aforementioned metals, which was only discovered after all the research had been conducted. The publication by Podlaha *et al.* did not however include any UV-Vis spectra, which they claimed to have used to obtain their binding constants, and stated that all ligands and ions formed a 1:1 complex ratio (5). Based of the data that was collected for this research, the binding constants published by Podlaha *et al.* could not be replicated even following their published procedure. A titration curve between TTDAA and copper (II) chloride dihydrate was conducted and agreed that the complex formation between TTDAA and copper only formed in the 1:1 manner (Graph 8.14).

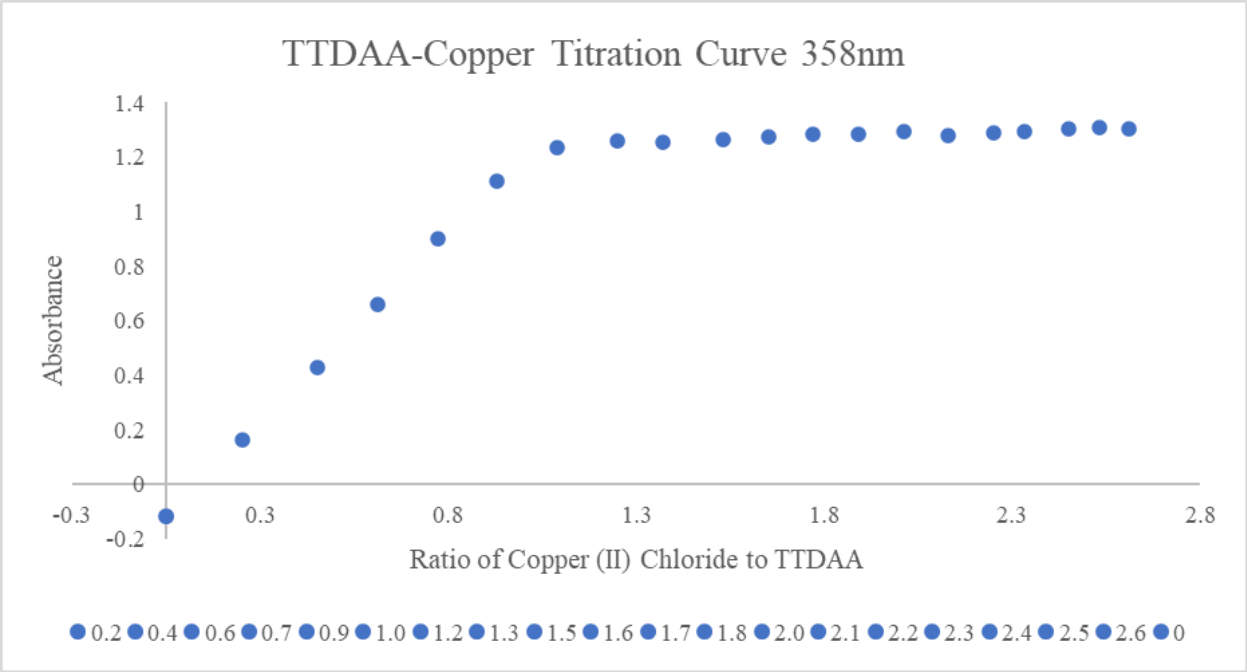


*Graph 8.14 Titration Curve of Copper (II) Chloride and TTDAA at 358nm, with the Concentration of TTDAA Held Constant, and the Concentration of Copper (II) Chloride increasing.*

Beyond experimentation with UV-Vis spectra, there were countless attempts to crystalize the complex of TTDAA and all of the various aforementioned metals. These included methods such as slow evaporation, solvent diffusion, reflux, and boiling solvents. Yet no matter how many attempts or combinations of methods were tired no complexes were successfully crystalized. Although many useful pieces of information were learned from the experimental trials with TTDAA it was not chosen as the final ligand of study. The main reason being that published research already existed on the complex formation between TTDAA and the selected metal micronutrients, so the research conducted would not have been novel (5). The second reason being that the successful synthesis and purification of 3,6,9-Trithiaundecane-1,11-dicarboxylic Acid (TTDPA, Compound 1 Ch. 5) allowed for a molecule to be studied that was more biologically relevant and had no published binding information.

## 8.5 Conclusion

The work conducted in this chapter did not directly contribute to testing the hypothesis that unexplained sulfur mustard symptoms are the result of the depletion of metal micronutrients. This work did however provide large insight to how to conduct and interpret much of the experimentation that was used for that work. Many compounds that were not successfully synthesized gave rise to the opportunity to perform synthetic methods and techniques that would not have been performed otherwise, such as reflux or pH/solvent manipulation. Of the compounds that were successfully synthesized but conducive to the overall goal; allowed for the learning of purification and analyzation techniques such as NMR, elemental analyses, crystallization and many more. Even the practice of trying to operate an ITC instrument, that never worked properly, still yielded valuable experience on experimental design and instrumental troubleshooting.

While the direct conclusion of this research was not achieved from the experiments in this chapter, it was these experiments that shifted the focus of research from the creation of an affinity column to the idea of metal micronutrient depletion. Many of the original compounds (Compounds A and B) were synthesized with the hopes of forming an affinity column it was their behavior with the metal solutions, specifically DPTT, that shifted the idea of focus to biological depletion. Compound 3,3′-TMBA was synthesized as it would be more biologically relevant than DPTT, although both are similar, and when 3,3′-TMBA started to show similar attributes of metal binding and complex precipitation that the idea of metal micronutrient deficiency was made the new end point.

This new end point led to synthesis of TTDAA which was not included in this chapter because of its success in synthesis pathway and crystallization, but the UV-Vis studies performed using it

were included here. Spectrometric analysis of TTDAA and various metal salts really drove home the idea that there was an interaction between these sulfur chains and metal ions in biologically relevant ligands. The observable shifts in spectra that only occurred upon the mixing of TTDAA and a metal showed not only the viability of this concept, but also the success of this specific experimental design. This TTDAA success is what led to the idea of synthesis for more biologically relevant materials (TTDPA and BOCC). Unfortunately, the compound BOCC was never synthesized or purified as it would have been the crown jewel of this research since it is the direct linkage of two cysteine residues following sulfur mustard exposure.

Overall, the research conducted in this chapter served as a launching pad for experimentation that ultimately addressed the proposed idea of sulfur mustard exposure leading to metal micronutrient deficiency. This chapter's research allowed for learning of experimental design, purification techniques, crystallization techniques, instrumental trouble shooting, and vast data analysis. While not directly testing the proposed hypothesis, the research that did would not have been conducted to the level it was without all the failures or partial successes of this preliminary experimentation.

## 8.6 References


1. Segawa, M.; Kobayashi, S.; Tuji, H.; Chayama, K. Selective collection of metal ions with a trithioether derivative and poly-N-isopropylacrylamide. *Bunseki Kagaku* **2004**, *53* (11), 1223-1228.

2. Bielmann, A.; Sambiagio, N.; Wehr, N.; Gerber-Lemaire, S.; Bochet, C. G.; Curty, C. Synthesis of different glutathione–sulfur mustard adducts of verified and potential biomarkers. *RSC advances* **2018**, *8* (42), 23881-23890.

3. Manandhar, E.; Pay, A.; Veress, L. A.; Logue, B. A. Rapid analysis of sulfur mustard oxide in plasma using gas chromatography-chemical ionization-mass spectrometry for diagnosis of sulfur mustard exposure. *Journal of Chromatography A* **2018**, *1572*, 106-111.

4. Drew, M. G.; Rice, D. A.; Richards, K. M. Bivalent metal complexes of 1, 11-diamino-3, 6, 9-trithiaundecane and the crystal structures of adducts with nickel (II) and copper (II) bromides. *Journal of the Chemical Society, Dalton Transactions* **1980**, (12), 2503-2508.

5. Podlaha, J.; Podlahová, J. Metal complexes of thiopolycarboxylic acids. IV. diethylenetrithiodiacetic acid. *Inorganica Chimica Acta* **1971**, *5*, 420-424.

6. Davison, C.; Rozman, R. S.; Smith, P. K. Metabolism of bis-β-chloroethyl sulfide (sulfur mustard gas). *Biochemical pharmacology* **1961**, *7* (1), 65-74.

**Appendix I: Experimental Pictures**

**Pictures of Crystal and Precipitate formation of TTDPA: Metal**

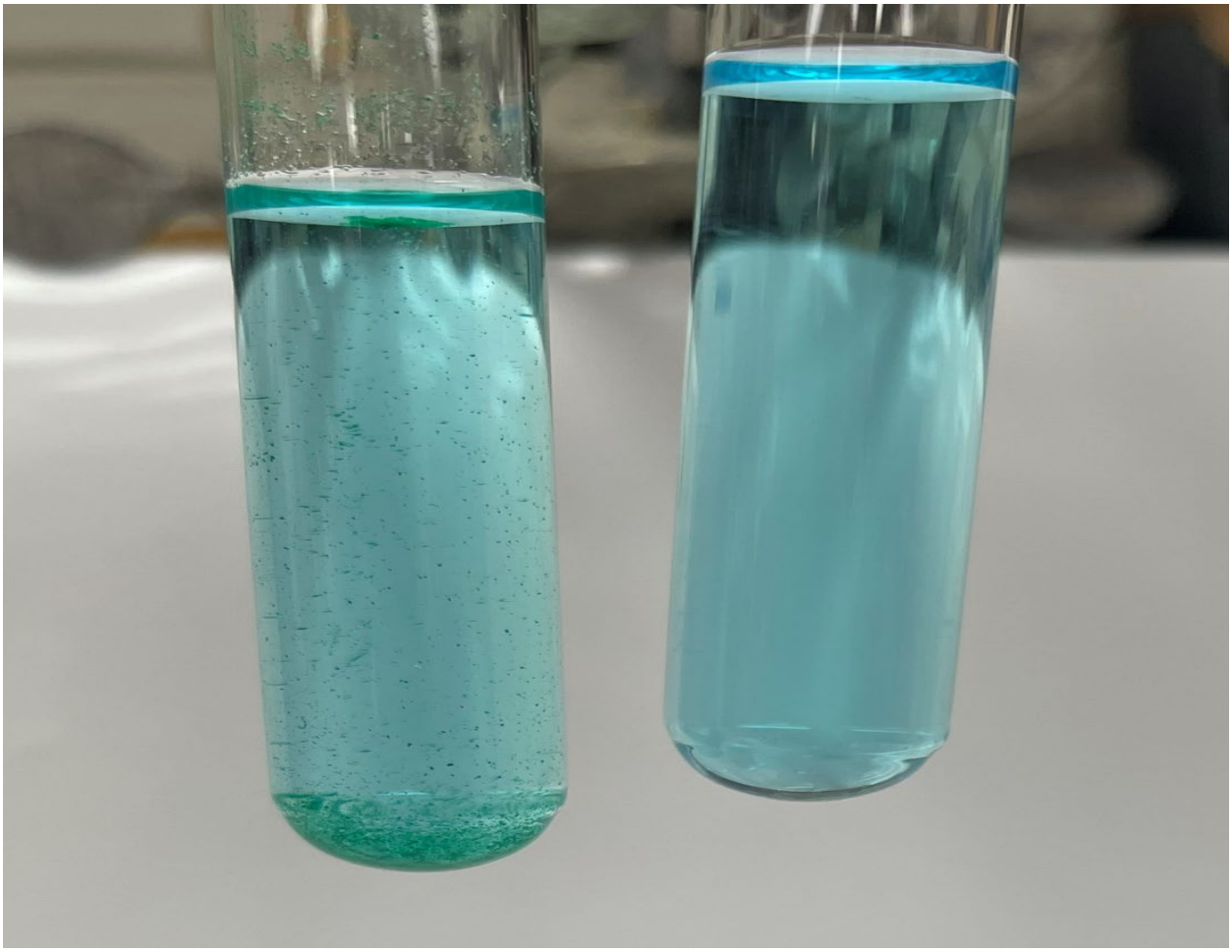

*Picture 1 Filtrate from Filter Paper Experiment of TTDPA $CuCl_2$ 1:5 (left) and $CuCl_2$ 0.0015M (right), showing formation of large amounts of crystal growth with the vast majority of crystals being green in color. There are clear crystals present, just few and difficult to spot. Note there is not crystal formation in the $CuCl_2$ control solution (right).*

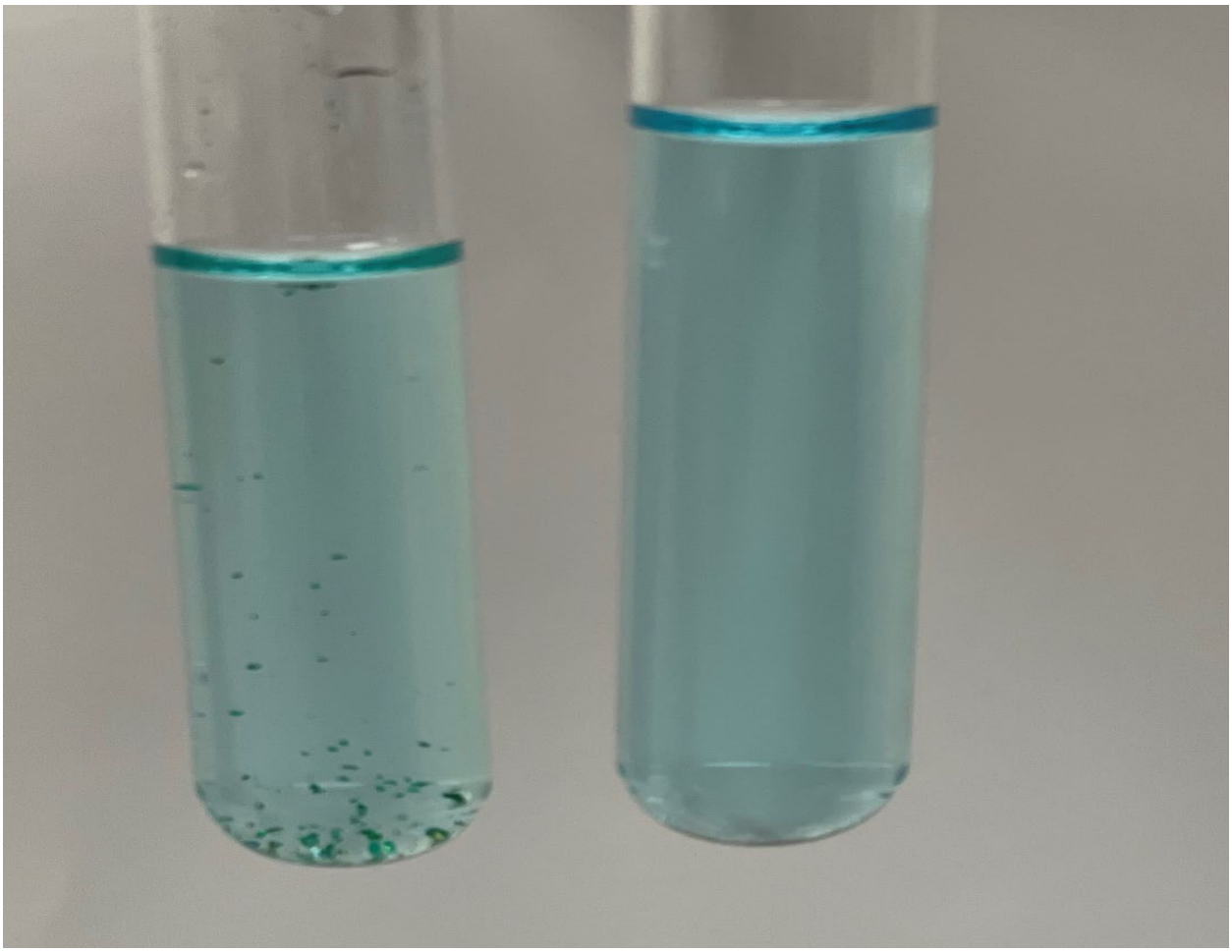

*Picture 2 Filtrate from Filter Paper Experiment of TTDPA: $CuCl_2$ 1:3 (left) and $CuCl_2$ 0.0009M (right), showing formation of crystal growth with the vast majority of crystals being green in color. There are clear crystals present, just few and difficult to spot. Note there is not crystal formation in the $CuCl_2$ control solution (right).*

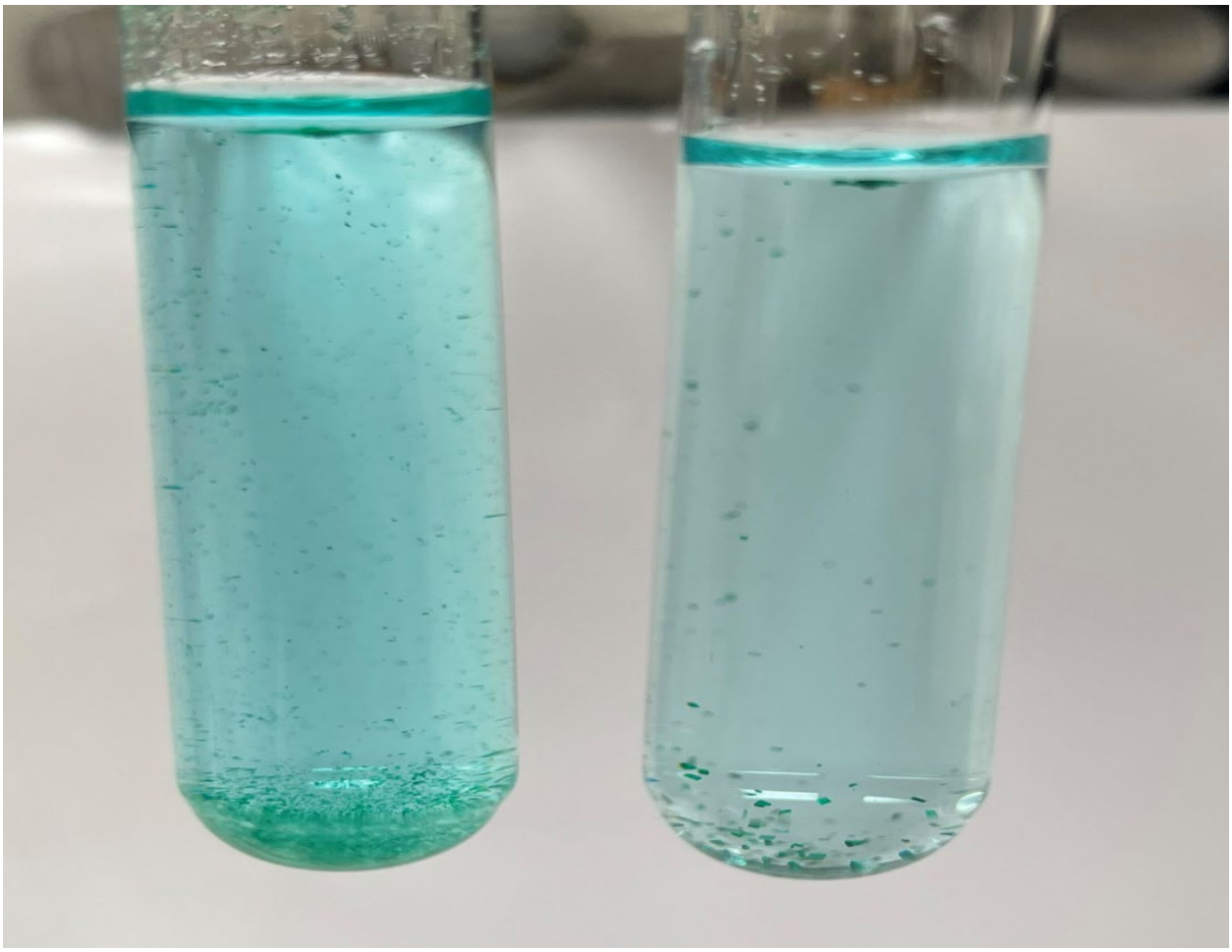

*Picture 3 Filtrate from Filter Paper Experiment of TTDPA: $CuCl_2$ 1:5 (left) and 1:3 (right), showing the various amount of crystal growth. More crystals grow when copper is in a larger excess (1:5, left), whereas the crystals grow larger in the 1:3 (right) mixture*

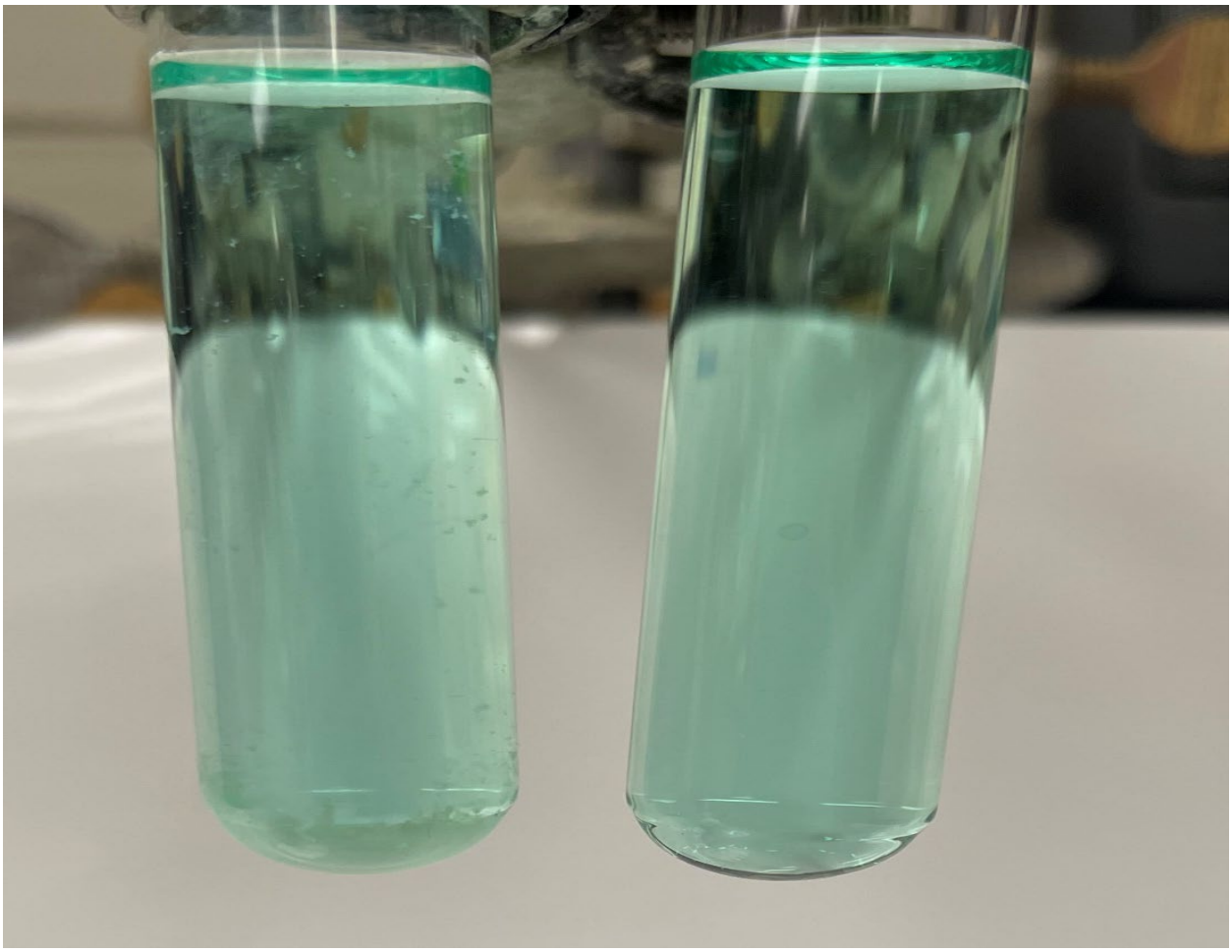

*Picture 4 Filtrate from Filter Paper Experiment of TTDPA $NiCl_2$ 1:5 (left) and $NiCl_2$ 0.0015M (right), showing precipitate formation (pooled at bottom of tube) even after the solution had been filtered. There is no crystallization or precipitate formation in the $NiCl_2$ control tube.*

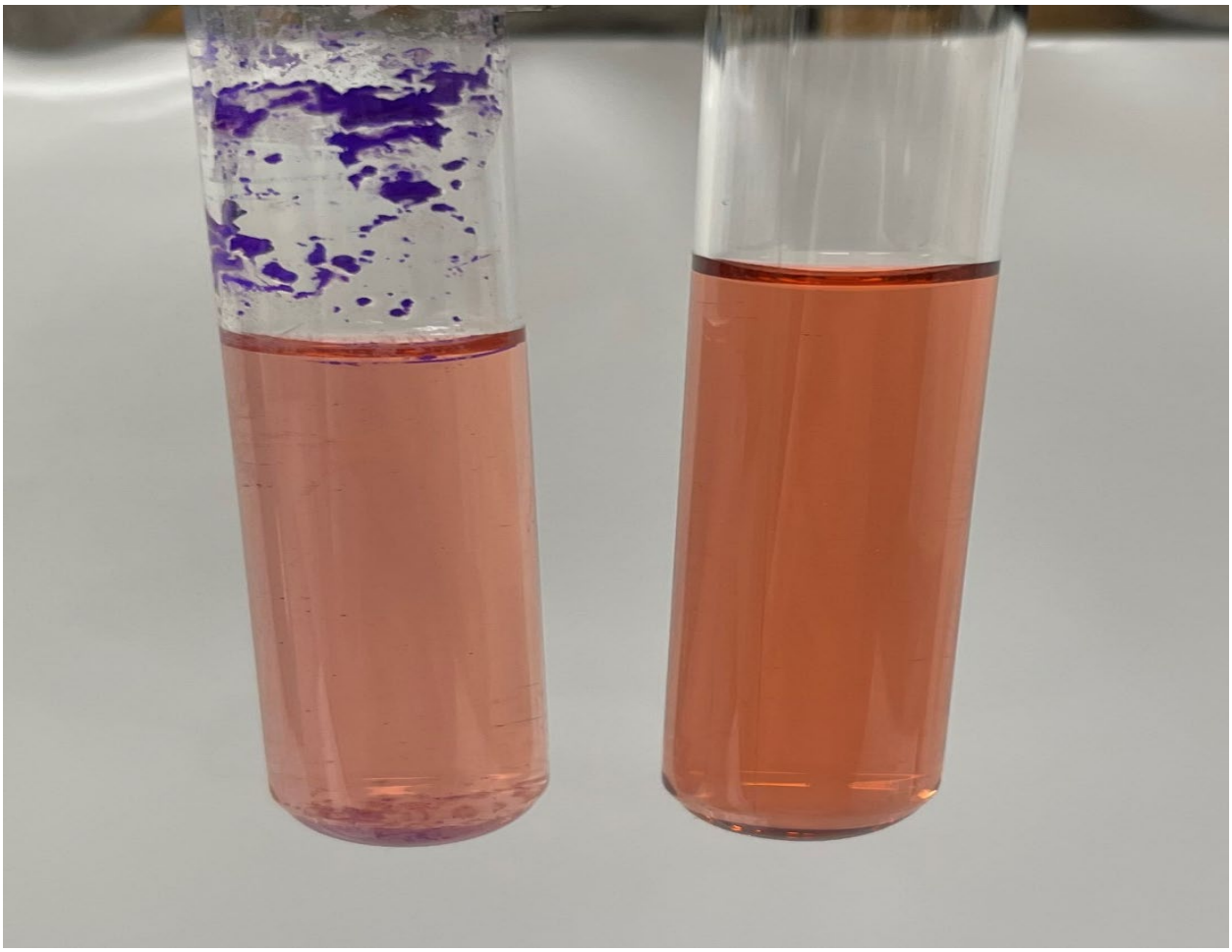

*Picture 5 Filtrate from Filter Paper Experiment of TTDPA $CoCl_2$ 1:5 (left) and $CoCl_2$ 0.0015M (right), although there was no crystal formation there is a large amount of purple precipitate that is not found in the $CoCl_2$ control tube (right). This precipitate is most likely complexes of TTDPA with $Co^{2+}$.*

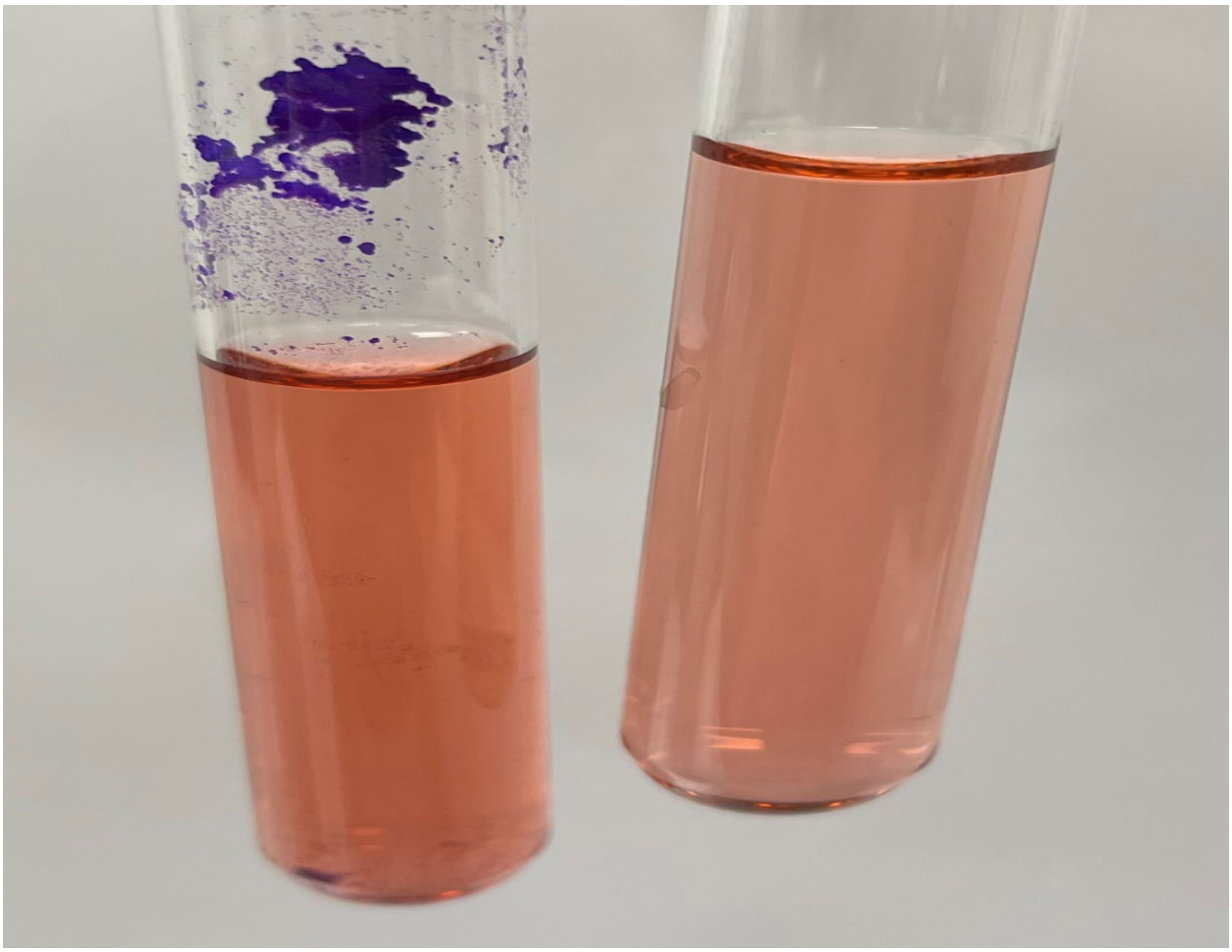

*Picture Filtrate from Filter Paper Experiment of TTDPA $CoCl_2$ 1:3 (left) and $CoCl_2$ 0.0009M (right), although there was no crystal formation there is a large amount of purple precipitate that is not found in the $CoCl_2$ control tube (right). This precipitate is most likely complexes of TTDPA with $Co^{2+}$.*

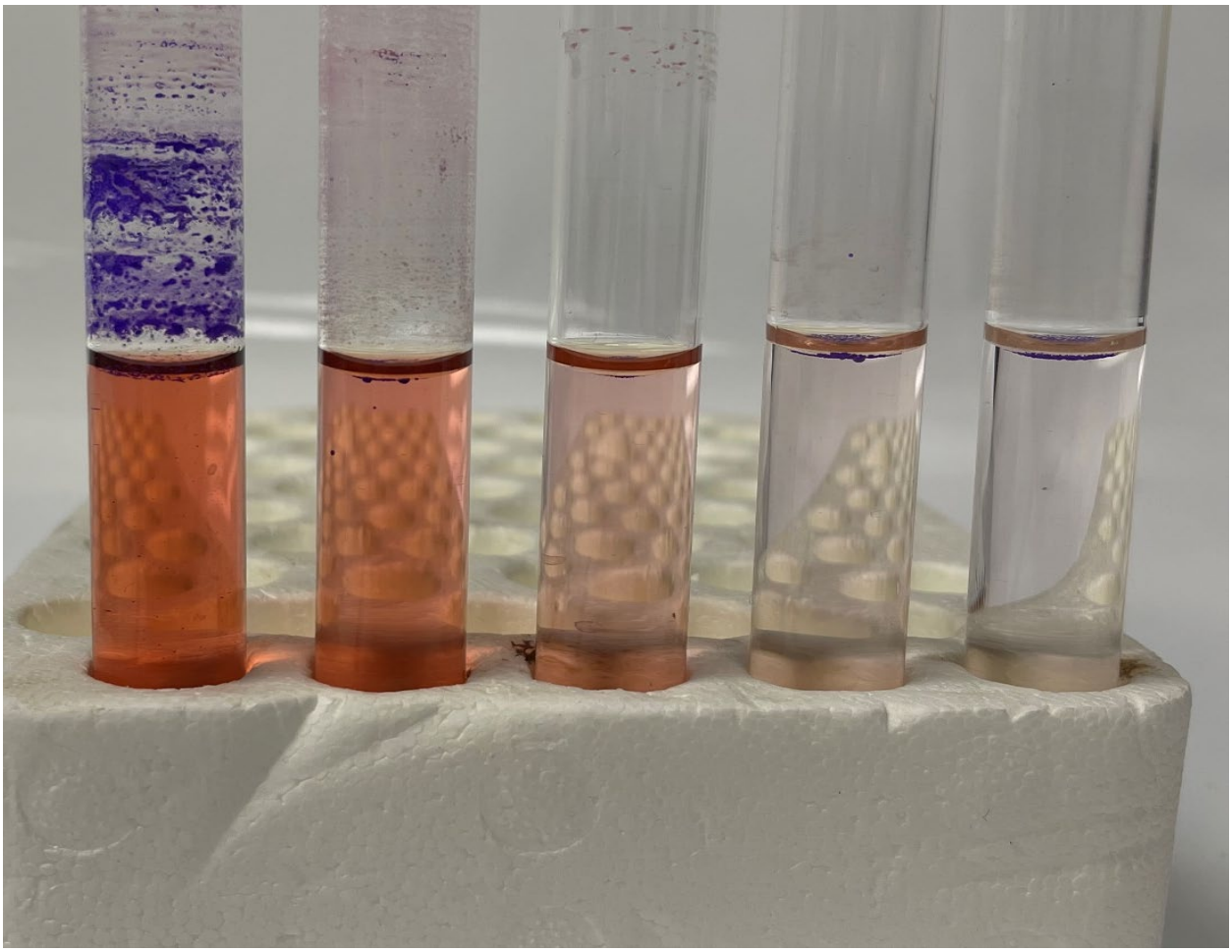

*Picture 7 Full ratio mixtures of TTDPA: $CoCl_2$ (1:5, 1:3, 1:1, 3:1, 5:1, left to right). Showing the decrease in purple precipitate formation as the initial $Co^{2+}$ concentration decreases. Although there is still precipitate formation at the 5:1 ratio (far right), which has the lowest amount of $CoCl_2$, it is nominal compared to the amount of precipitate formation in solutions with larger relative amounts of $CoCl_2$ (1:5, far left).*

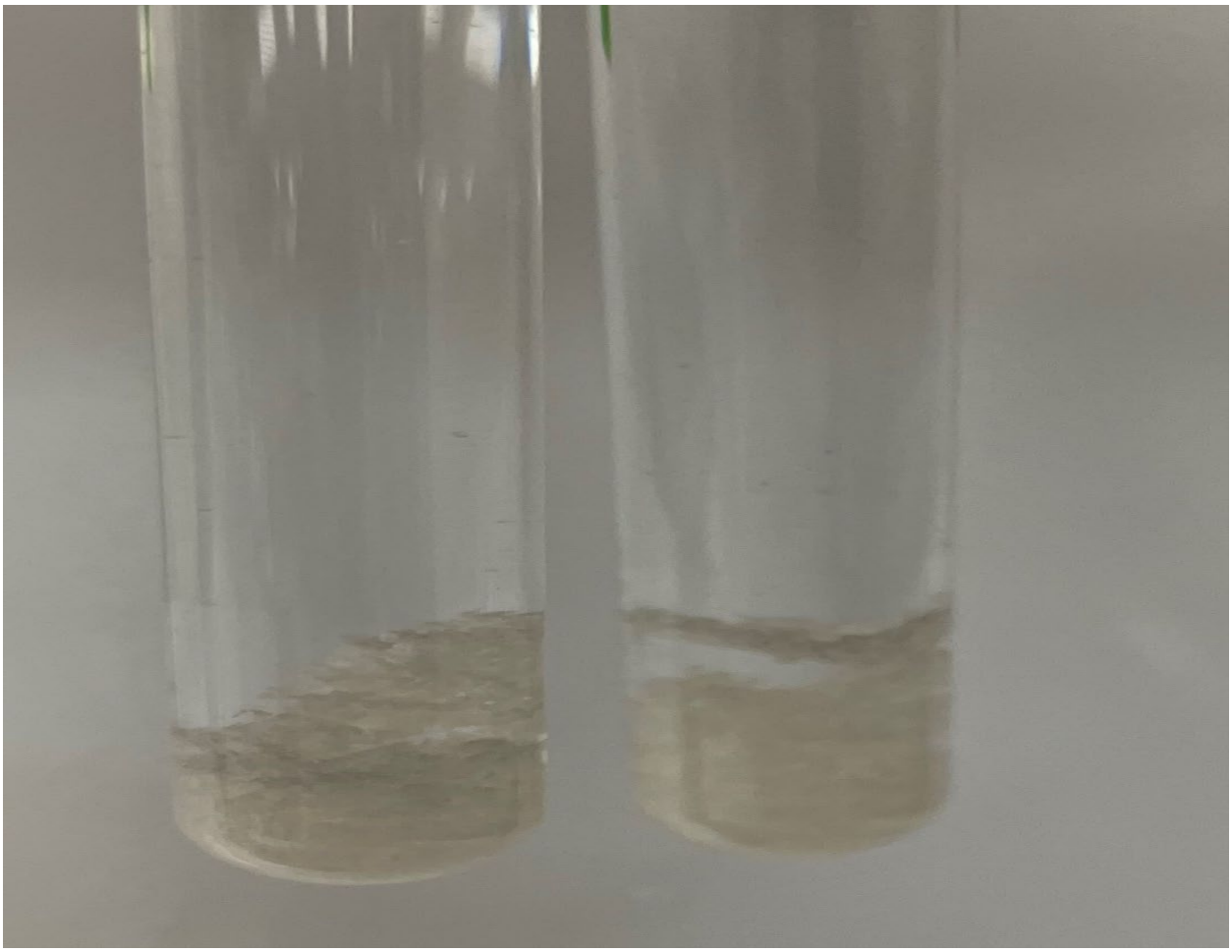

*Picture 8 Duplicate trials of TTDPA: $MnCl_2$ in equimolar quantities. The white precipitate shown only forms after the solutions had been sitting undisturbed for about 5 days. Mostly likely this precipitate is the same as that captured in the 1:5 ratio mixture, but took longer to form due to decreased amount of $Mn^{2+}$.*

**Appendix II: Full Data Reports of Crystal Structure Refinements.**

**Section 1. 2,5,8-Trithianone-1,9-dicarboxylic Acid (TTDAA) - Data and structure provided by Doug Powell at the University of Oklahoma.**

Table 1. Crystal data and structure refinement for TTDAA.

| | | |
|---|---|---|
| Empirical formula | $C_8 H_{14} O_4 S_3$ | |
| Formula weight | 270.37 | |
| Crystal system | triclinic | |
| Space group | $P\bar{1}$ | |
| Unit cell dimensions | $a$ = 5.0818(2) Å | a= 100.7017(12)° |
| | $b$ = 9.9284(3) Å | b= 95.1509(12)° |
| | $c$ = 11.8728(4) Å | g= 95.8971(11)° |
| Volume | 581.86(4) $Å^3$ | |
| Z, Z' | 2, 1 | |
| Density (calculated) | 1.543 $Mg/m^3$ | |
| Wavelength | 0.71073 Å | |
| Temperature | 100(2) K | |
| $F$(000) | 284 | |
| Absorption coefficient | 0.628 $mm^{-1}$ | |
| Absorption correction | semi-empirical from equivalents | |
| Max. and min. transmission | 0.7469 and 0.6424 | |
| Theta range for data collection | 2.103 to 35.041° | |
| Reflections collected | 55247 | |
| Independent reflections | 5125 [R(int) = 0.0476] | |
| Data / restraints / parameters | 5125 / 0 / 142 | |
| $wR(F^2$ all data) | $wR2$ = 0.0810 | |
| $R$($F$ obsd data) | $R1$ = 0.0288 | |
| Goodness-of-fit on $F^2$ | 1.008 | |
| Observed data [I > 2s(I)] | 4301 | |
| Largest and mean shift / s.u. | 0.001 and 0.000 | |
| Largest diff. peak and hole | 0.498 and -0.305 e/$Å^3$ | |

---

$wR2 = \{ S [w(F_o^2 - F_c^2)^2] / S [w(F_o^2)^2] \}^{1/2}$

$R1 = S ||F_o| - |F_c|| / S |F_o|$

Table 2. Atomic coordinates and equivalent isotropic displacement parameters for TTDAA. U(eq) is defined as one third of the trace of the orthogonalized $U_{ij}$ tensor.

| | x | y | z | U(eq) |
|---|---|---|---|---|
| S(1) | 0.51748(5) | 0.98191(2) | 0.31674(2) | 0.01979(6) |
| S(2) | 0.87620(5) | 0.63930(2) | 0.44251(2) | 0.01928(6) |
| S(3) | 0.73438(5) | 0.74625(2) | 0.81083(2) | 0.01967(6) |
| O(1) | 0.62511(14) | 0.71385(7) | 0.09260(6) | 0.02163(14) |
| O(2) | 0.31606(15) | 0.84325(8) | 0.04317(7) | 0.02185(14) |
| O(3) | 1.14227(13) | 0.58612(7) | 0.92047(6) | 0.01951(13) |
| O(4) | 0.94559(14) | 0.38148(7) | 0.82182(6) | 0.01840(12) |
| C(1) | 0.53851(18) | 0.82536(9) | 0.10213(8) | 0.01632(15) |
| C(2) | 0.67307(19) | 0.95324(9) | 0.18352(8) | 0.01835(16) |
| C(3) | 0.55576(18) | 0.82336(10) | 0.36862(8) | 0.01816(15) |
| C(4) | 0.84193(18) | 0.80846(9) | 0.41012(8) | 0.01756(15) |
| C(5) | 0.71972(19) | 0.64929(10) | 0.57478(8) | 0.01795(15) |
| C(6) | 0.89805(19) | 0.73090(10) | 0.68001(8) | 0.01837(15) |
| C(7) | 0.69530(17) | 0.56884(9) | 0.82640(8) | 0.01666(15) |
| C(8) | 0.95147(17) | 0.51596(9) | 0.86071(7) | 0.01427(14) |

Table 3. Bond lengths [Å] and angles [°] for TTDAA.

| | | | |
|---|---|---|---|
| S(1)-C(3) | 1.8157(9) | C(2)-H(2AB) | 0.9900 |
| S(1)-C(2) | 1.8197(10) | C(3)-C(4) | 1.5239(13) |
| S(2)-C(4) | 1.8129(9) | C(3)-H(3A) | 0.9900 |
| S(2)-C(5) | 1.8141(9) | C(3)-H(3AB) | 0.9900 |
| S(3)-C(7) | 1.7977(9) | C(4)-H(4A) | 0.9900 |
| S(3)-C(6) | 1.8159(10) | C(4)-H(4AB) | 0.9900 |
| O(1)-C(1) | 1.2226(11) | C(5)-C(6) | 1.5195(14) |
| O(2)-C(1) | 1.3209(11) | C(5)-H(5A) | 0.9900 |
| O(2)-H(2) | 0.832(15) | C(5)-H(5AB) | 0.9900 |
| O(3)-C(8) | 1.2178(11) | C(6)-H(6A) | 0.9900 |
| O(4)-C(8) | 1.3256(11) | C(6)-H(6AB) | 0.9900 |
| O(4)-H(4) | 0.839(15) | C(7)-C(8) | 1.5037(12) |
| C(1)-C(2) | 1.5035(13) | C(7)-H(7A) | 0.9900 |
| C(2)-H(2A) | 0.9900 | C(7)-H(7AB) | 0.9900 |

| | | | |
|---|---|---|---|
| C(3)-S(1)-C(2) | 101.96(4) | S(2)-C(5)-H(5A) | 109.0 |
| C(4)-S(2)-C(5) | 101.32(4) | C(6)-C(5)-H(5AB) | 109.0 |
| C(7)-S(3)-C(6) | 100.25(4) | S(2)-C(5)-H(5AB) | 109.0 |
| C(1)-O(2)-H(2) | 109.7(10) | H(5A)-C(5)-H(5AB) | 107.8 |
| C(8)-O(4)-H(4) | 108.0(10) | C(5)-C(6)-S(3) | 112.67(7) |
| O(1)-C(1)-O(2) | 122.83(8) | C(5)-C(6)-H(6A) | 109.1 |
| O(1)-C(1)-C(2) | 122.94(8) | S(3)-C(6)-H(6A) | 109.1 |
| O(2)-C(1)-C(2) | 114.22(8) | C(5)-C(6)-H(6AB) | 109.1 |
| C(1)-C(2)-S(1) | 110.98(6) | S(3)-C(6)-H(6AB) | 109.1 |
| C(1)-C(2)-H(2A) | 109.4 | H(6A)-C(6)-H(6AB) | 107.8 |
| S(1)-C(2)-H(2A) | 109.4 | C(8)-C(7)-S(3) | 114.09(6) |
| C(1)-C(2)-H(2AB) | 109.4 | C(8)-C(7)-H(7A) | 108.7 |
| S(1)-C(2)-H(2AB) | 109.4 | S(3)-C(7)-H(7A) | 108.7 |
| H(2A)-C(2)-H(2AB) | 108.0 | C(8)-C(7)-H(7AB) | 108.7 |
| C(4)-C(3)-S(1) | 114.09(6) | S(3)-C(7)-H(7AB) | 108.7 |
| C(4)-C(3)-H(3A) | 108.7 | H(7A)-C(7)-H(7AB) | 107.6 |
| S(1)-C(3)-H(3A) | 108.7 | O(3)-C(8)-O(4) | 122.77(8) |
| C(4)-C(3)-H(3AB) | 108.7 | O(3)-C(8)-C(7) | 124.71(8) |
| S(1)-C(3)-H(3AB) | 108.7 | O(4)-C(8)-C(7) | 112.48(7) |
| H(3A)-C(3)-H(3AB) | 107.6 | | |
| C(3)-C(4)-S(2) | 112.36(6) | | |
| C(3)-C(4)-H(4A) | 109.1 | | |
| S(2)-C(4)-H(4A) | 109.1 | | |
| C(3)-C(4)-H(4AB) | 109.1 | | |
| S(2)-C(4)-H(4AB) | 109.1 | | |
| H(4A)-C(4)-H(4AB) | 107.9 | | |
| C(6)-C(5)-S(2) | 113.09(7) | | |
| C(6)-C(5)-H(5A) | 109.0 | | |

Table 4. Anisotropic displacement parameters ($Å^2 x\ 10^3$) for TTDAA. The anisotropic displacement factor exponent takes the form:
$-2\ p^2[\ h^2\ a^{*2}\ U_{11} + ... + 2\ h\ k\ a^*\ b^*\ U_{12}]$

| | $U_{11}$ | $U_{22}$ | $U_{33}$ | $U_{23}$ | $U_{13}$ | $U_{12}$ |
|---|---|---|---|---|---|---|
| S(1) | 25(1) | 17(1) | 18(1) | 3(1) | 2(1) | 7(1) |
| S(2) | 25(1) | 17(1) | 17(1) | 5(1) | 5(1) | 6(1) |
| S(3) | 26(1) | 16(1) | 17(1) | 2(1) | 3(1) | 6(1) |
| O(1) | 22(1) | 18(1) | 23(1) | 1(1) | -1(1) | 7(1) |
| O(2) | 22(1) | 17(1) | 24(1) | 2(1) | -6(1) | 3(1) |
| O(3) | 16(1) | 19(1) | 22(1) | 1(1) | -1(1) | 0(1) |
| O(4) | 19(1) | 16(1) | 18(1) | 0(1) | -1(1) | 4(1) |
| C(1) | 18(1) | 16(1) | 15(1) | 4(1) | 2(1) | 2(1) |
| C(2) | 21(1) | 17(1) | 17(1) | 3(1) | 0(1) | 0(1) |
| C(3) | 18(1) | 18(1) | 19(1) | 6(1) | 1(1) | 1(1) |
| C(4) | 18(1) | 16(1) | 19(1) | 5(1) | 1(1) | 1(1) |
| C(5) | 20(1) | 18(1) | 15(1) | 4(1) | 2(1) | 0(1) |
| C(6) | 19(1) | 18(1) | 17(1) | 4(1) | 1(1) | 0(1) |
| C(7) | 16(1) | 18(1) | 17(1) | 4(1) | 2(1) | 2(1) |
| C(8) | 15(1) | 16(1) | 12(1) | 3(1) | 3(1) | 2(1) |

Table 5. Hydrogen coordinates and isotropic displacement parameters for TTDAA.

| | x | y | z | U(eq) |
|---|---|---|---|---|
| H(2) | 0.248(3) | 0.7685(16) | 0.0022(13) | 0.026 |
| H(4) | 1.087(3) | 0.3569(15) | 0.8486(12) | 0.022 |
| H(2A) | 0.662312 | 1.034020 | 0.146136 | 0.022 |
| H(2AB) | 0.863500 | 0.943606 | 0.201323 | 0.022 |
| H(3A) | 0.445731 | 0.819502 | 0.432922 | 0.022 |
| H(3AB) | 0.486677 | 0.743898 | 0.305749 | 0.022 |
| H(4A) | 0.903425 | 0.879765 | 0.480198 | 0.021 |
| H(4AB) | 0.957307 | 0.824646 | 0.349864 | 0.021 |
| H(5A) | 0.554422 | 0.693014 | 0.566308 | 0.022 |
| H(5AB) | 0.669472 | 0.554543 | 0.587115 | 0.022 |
| H(6A) | 0.954507 | 0.824476 | 0.666487 | 0.022 |
| H(6AB) | 1.059864 | 0.684945 | 0.690615 | 0.022 |
| H(7A) | 0.572447 | 0.558638 | 0.885267 | 0.020 |
| H(7AB) | 0.611747 | 0.510812 | 0.752334 | 0.020 |

Table 6. Torsion angles [°] for TTDAA.

| | |
|---|---|
| O(1)-C(1)-C(2)-S(1) | -98.28(10) |
| O(2)-C(1)-C(2)-S(1) | 80.62(9) |
| C(3)-S(1)-C(2)-C(1) | 58.44(7) |
| C(2)-S(1)-C(3)-C(4) | 69.79(8) |
| S(1)-C(3)-C(4)-S(2) | -172.18(5) |
| C(5)-S(2)-C(4)-C(3) | -72.20(7) |
| C(4)-S(2)-C(5)-C(6) | -78.12(8) |
| S(2)-C(5)-C(6)-S(3) | 177.60(5) |
| C(7)-S(3)-C(6)-C(5) | 66.35(8) |
| C(6)-S(3)-C(7)-C(8) | 70.84(7) |
| S(3)-C(7)-C(8)-O(3) | 31.36(11) |
| S(3)-C(7)-C(8)-O(4) | -150.81(6) |

Table 7. Hydrogen bonds for TTDAA [Å and °].

| D-H...A | d(D-H) | d(H...A) | d(D...A) | <(DHA) |
|---|---|---|---|---|
| O(2)-H(2)...O(3)#1 | 0.832(15) | 1.887(16) | 2.7100(10) | 170.2(14) |
| O(4)-H(4)...O(1)#2 | 0.839(15) | 1.823(15) | 2.6592(10) | 173.9(14) |
| C(3)-H(3AB)...O(1) | 0.99 | 2.66 | 3.3180(12) | 124.2 |
| C(3)-H(3AB)...O(4)#3 | 0.99 | 2.61 | 3.4543(11) | 143.3 |
| C(7)-H(7A)...O(1)#4 | 0.99 | 2.63 | 3.2873(12) | 124.3 |
| C(7)-H(7A)...O(3)#5 | 0.99 | 2.30 | 3.1251(11) | 140.6 |

Symmetry transformations used to generate equivalent atoms:
#1 x-1, y, z-1 #2 -x+2, -y+1, -z+1 #3 -x+1, -y+1, -z+1
#4 x, y, z+1 #5 x-1, y, z

**Acknowledgment**

The authors thank the National Science Foundation (grant CHE-1726630) and the University of Oklahoma for funds to purchase of the X-ray instrument and computers. This structure was determined by Douglas R. Powell.

**References**

(1) (a) Data Collection: APEX3 (2018) Bruker Inc., Madison, Wisconsin, USA. (b) Data Reduction: SAINT (2016) Bruker Inc., Madison, Wisconsin, USA.

(2) L. Krause, R. Herbst-Irmer, G. M. Sheldrick, and D. Stalke (2015). *J. Appl. Cryst., 48*, 3-10.

(3) (a) G. M. Sheldrick (2015). *Acta Cryst., A71*, 3-8. (b) G. M. Sheldrick (2015). *Acta Cryst., C71*, 3-8.

**Section 2. 2,5,8-Trithianonane-1,9-diamide (TTDAce).**

| **Table 1 Crystal data and structure refinement for 20220421_COD_Ace_auto.** | |
|---|---|
| Identification code | 20220421_COD_Ace_auto |
| Empirical formula | $C_{16}H_{32}N_4O_4S_6$ |
| Formula weight | 536.81 |
| Temperature/K | 293(2) |
| Crystal system | triclinic |
| Space group | P-1 |
| a/Å | 5.10520(10) |
| b/Å | 9.0197(2) |
| c/Å | 26.6367(8) |
| α/° | 92.959(2) |
| β/° | 95.215(2) |
| γ/° | 91.944(2) |
| Volume/Å$^3$ | 1218.92(5) |
| Z | 2 |
| $\rho_{calc}$g/cm$^3$ | 1.463 |
| μ/mm$^{-1}$ | 5.445 |
| F(000) | 568.0 |
| Crystal size/mm$^3$ | 0.55 × 0.23 × 0.17 |
| Radiation | Cu Kα (λ = 1.54184) |
| 2Θ range for data collection/° | 3.336 to 142.91 |
| Index ranges | $-6 \leq h \leq 6$, $-11 \leq k \leq 10$, $-31 \leq l \leq 32$ |
| Reflections collected | 21322 |
| Independent reflections | 4594 [$R_{int}$ = 0.0759, $R_{sigma}$ = 0.0439] |
| Data/restraints/parameters | 4594/0/271 |
| Goodness-of-fit on F$^2$ | 1.146 |
| Final R indexes [I>=2σ (I)] | $R_1$ = 0.0847, $wR_2$ = 0.2614 |
| Final R indexes [all data] | $R_1$ = 0.0991, $wR_2$ = 0.2799 |
| Largest diff. peak/hole / e Å$^{-3}$ | 1.51/-0.58 |

| Table 2 Fractional Atomic Coordinates (×10$^4$) and Equivalent Isotropic Displacement Parameters (Å$^2$×10$^3$) for 20220421_COD_Ace_auto. $U_{eq}$ is defined as 1/3 of the trace of the orthogonalised $U_{IJ}$ tensor. | | | | |
|---|---|---|---|---|
| **Atom** | ***x*** | ***y*** | ***z*** | **U(eq)** |
| S2 | 10144.3(18) | 4876.4(10) | 2505.5(4) | 30.6(3) |
| S5 | 5141.0(19) | -166.8(10) | 2493.4(4) | 31.2(3) |
| S6 | 2336(2) | 2949.8(11) | 3652.1(4) | 34.5(3) |
| S3 | 6912(2) | 7876.1(11) | 3653.9(4) | 36.8(4) |
| S1 | 7064(2) | 7893.2(12) | 1347.5(4) | 40.7(4) |
| S4 | 2072(2) | 2895.5(12) | 1346.9(4) | 41.5(4) |
| O2 | 7615(5) | 6043(3) | 4608.9(11) | 35.5(7) |
| O04 | 7286(5) | 1012(3) | 4606.1(11) | 38.5(7) |
| N3 | 4543(6) | 1661(3) | 399.9(11) | 25.9(7) |
| N1 | 9544(6) | 6661(3) | 402.6(11) | 25.6(7) |
| N4 | 2854(6) | 1060(3) | 4588.2(11) | 25.8(7) |
| O1 | 7417(6) | 4410(3) | 407.1(12) | 42.5(8) |
| O3 | 2422(6) | -587(3) | 409.0(12) | 42.8(8) |
| N2 | 12019(6) | 5987(3) | 4575.0(12) | 30.7(7) |
| C16 | 5121(7) | 1533(4) | 4450.7(14) | 28.3(8) |
| C5 | 9982(7) | 6323(4) | 3003.9(15) | 29.2(8) |
| C13 | 5135(7) | 1285(4) | 2991.8(14) | 29.5(8) |
| C8 | 9708(8) | 6538(4) | 4451.6(14) | 30.0(9) |
| C14 | 2570(7) | 1314(4) | 3232.0(15) | 30.6(9) |
| C4 | 8016(8) | 5630(4) | 2005.3(15) | 30.6(9) |
| C12 | 3022(7) | 621(4) | 1999.9(14) | 30.2(8) |
| C3 | 9328(8) | 6896(4) | 1762.5(15) | 31.1(9) |
| C9 | 2750(8) | 812(5) | 545.2(14) | 33.9(9) |
| C1 | 7746(7) | 5809(5) | 547.7(14) | 33.2(9) |
| C6 | 7395(8) | 6251(4) | 3241.1(15) | 31.4(9) |
| C11 | 4330(8) | 1889(4) | 1757.2(15) | 31.7(9) |
| C15 | 5160(8) | 2802(4) | 4097.1(15) | 33.3(9) |
| C7 | 9696(8) | 7839(4) | 4114.1(15) | 35.5(9) |
| C10 | 787(8) | 1445(6) | 888.4(16) | 42.7(11) |
| C2 | 5799(8) | 6443(6) | 889.9(16) | 42.0(11) |

| Table 3 Anisotropic Displacement Parameters ($Å^2×10^3$) for 20220421_COD_Ace_auto. The Anisotropic displacement factor exponent takes the form: $-2\pi^2[h^2a^{*2}U_{11}+2hka^*b^*U_{12}+\ldots]$. | | | | | | |
|---|---|---|---|---|---|---|
| **Atom** | **$U_{11}$** | **$U_{22}$** | **$U_{33}$** | **$U_{23}$** | **$U_{13}$** | **$U_{12}$** |
| S2 | 31.9(6) | 25.8(5) | 35.1(6) | 2.2(4) | 6.1(4) | 6.3(4) |
| S5 | 34.0(6) | 25.2(5) | 35.5(6) | 2.0(4) | 6.0(4) | 7.2(4) |
| S6 | 37.9(6) | 30.5(6) | 36.6(6) | 4.5(4) | 6.0(4) | 13.6(4) |
| S3 | 41.7(7) | 33.8(6) | 36.8(6) | 4.6(4) | 6.1(4) | 16.5(4) |
| S1 | 55.4(8) | 35.4(6) | 32.9(6) | 0.6(4) | 6.8(5) | 21.5(5) |
| S4 | 58.0(8) | 34.8(6) | 33.3(6) | 0.8(4) | 6.8(5) | 22.2(5) |
| O2 | 23.1(14) | 34.7(15) | 49.7(17) | 6.8(12) | 5.6(11) | 1.0(11) |
| O04 | 24.8(15) | 35.3(16) | 57.6(19) | 6.9(13) | 11.3(12) | 7.8(11) |
| N3 | 24.2(16) | 19.6(15) | 34.7(17) | -2.2(12) | 9.8(12) | 1.6(12) |
| N1 | 26.3(17) | 18.2(14) | 33.1(17) | -2.6(12) | 8.3(12) | 2.4(12) |
| N4 | 18.2(15) | 25.5(15) | 34.6(17) | 10.1(13) | 1.8(12) | 4.7(12) |
| O1 | 47.3(19) | 27.2(15) | 55.7(19) | 8.1(13) | 15.5(14) | 3.8(13) |
| O3 | 46.5(19) | 27.9(15) | 57(2) | 7.6(13) | 16.4(14) | 3.4(13) |
| N2 | 26.0(17) | 27.5(17) | 41.4(19) | 8.6(14) | 12.7(13) | 6.0(13) |
| C16 | 30(2) | 21.8(18) | 32(2) | -2.4(15) | 4.3(14) | 0.9(14) |
| C5 | 24(2) | 27.9(19) | 35(2) | 0.2(15) | 3.1(14) | -0.2(15) |
| C13 | 26(2) | 28.8(19) | 34(2) | 0.5(15) | 2.7(15) | 3.1(15) |
| C8 | 38(2) | 21.7(18) | 30(2) | -2.2(15) | 2.2(15) | 1.5(15) |
| C14 | 28(2) | 30(2) | 34(2) | -3.4(16) | 4.2(15) | 5.0(15) |
| C4 | 29(2) | 28(2) | 34(2) | -1.6(15) | 2.9(15) | -0.4(15) |
| C12 | 29(2) | 30(2) | 32(2) | -1.4(15) | 3.5(15) | 0.8(15) |
| C3 | 32(2) | 28(2) | 33(2) | 1.3(16) | 5.1(16) | 0.7(16) |
| C9 | 31(2) | 43(2) | 28(2) | 0.4(17) | 0.2(16) | 18.1(18) |
| C1 | 29(2) | 42(2) | 29(2) | 0.7(17) | 0.7(15) | 18.2(17) |
| C6 | 30(2) | 30(2) | 34(2) | -2.4(16) | 4.8(15) | 0.6(16) |
| C11 | 33(2) | 30(2) | 32(2) | 2.6(16) | 1.9(16) | -0.9(16) |
| C15 | 40(2) | 21.6(18) | 38(2) | 3.9(15) | 2.8(16) | -3.1(15) |
| C7 | 44(2) | 23.2(19) | 39(2) | 1.3(16) | 0.6(17) | 0.0(16) |
| C10 | 33(2) | 62(3) | 34(2) | -4(2) | 3.4(17) | 20(2) |
| C2 | 29(2) | 64(3) | 34(2) | -7(2) | 3.4(16) | 19(2) |

| Table 4 Bond Lengths for 20220421_COD_Ace_auto. | | | | | | |
|---|---|---|---|---|---|---|
| **Atom** | **Atom** | **Length/Å** | | **Atom** | **Atom** | **Length/Å** |
| S2 | C5 | 1.822(4) | | N3 | C9 | 1.273(5) |
| S2 | C4 | 1.816(4) | | N1 | C1 | 1.276(5) |
| S5 | C13 | 1.816(4) | | N4 | C16 | 1.310(5) |
| S5 | C12 | 1.815(4) | | O1 | C1 | 1.298(5) |
| S6 | C14 | 1.819(4) | | O3 | C9 | 1.296(5) |
| S6 | C15 | 1.794(4) | | N2 | C8 | 1.317(5) |
| S3 | C6 | 1.824(4) | | C16 | C15 | 1.520(5) |
| S3 | C7 | 1.793(4) | | C5 | C6 | 1.516(5) |
| S1 | C3 | 1.819(4) | | C13 | C14 | 1.509(5) |
| S1 | C2 | 1.803(5) | | C8 | C7 | 1.515(5) |
| S4 | C11 | 1.814(4) | | C4 | C3 | 1.508(5) |
| S4 | C10 | 1.807(5) | | C12 | C11 | 1.508(5) |
| O2 | C8 | 1.259(4) | | C9 | C10 | 1.522(5) |
| O04 | C16 | 1.260(5) | | C1 | C2 | 1.515(5) |

| Table 5 Bond Angles for 20220421_COD_Ace_auto. | | | | | | | | |
|---|---|---|---|---|---|---|---|---|
| **Atom** | **Atom** | **Atom** | **Angle/°** | | **Atom** | **Atom** | **Atom** | **Angle/°** |
| C4 | S2 | C5 | 100.06(18) | | C3 | C4 | S2 | 112.6(3) |
| C12 | S5 | C13 | 100.36(18) | | C11 | C12 | S5 | 113.3(3) |
| C15 | S6 | C14 | 101.81(18) | | C4 | C3 | S1 | 113.3(3) |
| C7 | S3 | C6 | 101.86(19) | | N3 | C9 | O3 | 124.0(3) |
| C2 | S1 | C3 | 101.9(2) | | N3 | C9 | C10 | 119.7(4) |
| C10 | S4 | C11 | 101.7(2) | | O3 | C9 | C10 | 116.3(4) |
| O04 | C16 | N4 | 123.3(3) | | N1 | C1 | O1 | 123.7(3) |
| O04 | C16 | C15 | 118.1(3) | | N1 | C1 | C2 | 119.5(4) |
| N4 | C16 | C15 | 118.6(3) | | O1 | C1 | C2 | 116.7(4) |
| C6 | C5 | S2 | 112.3(3) | | C5 | C6 | S3 | 113.3(3) |
| C14 | C13 | S5 | 112.7(3) | | C12 | C11 | S4 | 113.5(3) |
| O2 | C8 | N2 | 122.7(3) | | C16 | C15 | S6 | 117.3(3) |
| O2 | C8 | C7 | 121.1(3) | | C8 | C7 | S3 | 115.4(3) |
| N2 | C8 | C7 | 116.2(3) | | C9 | C10 | S4 | 115.8(3) |
| C13 | C14 | S6 | 112.9(3) | | C1 | C2 | S1 | 116.2(3) |

| Table 6 Torsion Angles for 20220421_COD_Ace_auto. | | | | | | | | | | |
|---|---|---|---|---|---|---|---|---|---|---|
| **A** | **B** | **C** | **D** | **Angle/°** | | **A** | **B** | **C** | **D** | **Angle/°** |
| S2 | C5 | C6 | S3 | -169.08(19) | | C5 | S2 | C4 | C3 | 75.8(3) |
| S2 | C4 | C3 | S1 | -169.00(19) | | C13 | S5 | C12 | C11 | 73.9(3) |
| S5 | C13 | C14 | S6 | -170.01(19) | | C14 | S6 | C15 | C16 | -68.3(3) |
| S5 | C12 | C11 | S4 | -169.5(2) | | C4 | S2 | C5 | C6 | 75.3(3) |
| O2 | C8 | C7 | S3 | -38.0(5) | | C12 | S5 | C13 | C14 | 73.6(3) |
| O04 | C16 | C15 | S6 | 150.7(3) | | C3 | S1 | C2 | C1 | -67.0(4) |
| N3 | C9 | C10 | S4 | -35.3(5) | | C6 | S3 | C7 | C8 | -66.6(3) |
| N1 | C1 | C2 | S1 | -35.1(5) | | C11 | S4 | C10 | C9 | -66.9(4) |
| N4 | C16 | C15 | S6 | -30.9(5) | | C15 | S6 | C14 | C13 | -57.9(3) |
| O1 | C1 | C2 | S1 | 146.9(3) | | C7 | S3 | C6 | C5 | -59.3(3) |
| O3 | C9 | C10 | S4 | 146.3(3) | | C10 | S4 | C11 | C12 | -59.4(3) |
| N2 | C8 | C7 | S3 | 143.3(3) | | C2 | S1 | C3 | C4 | -59.4(3) |

| Table 7 Hydrogen Atom Coordinates (Å×10$^4$) and Isotropic Displacement Parameters (Å$^2$×10$^3$) for 20220421_COD_Ace_auto. | | | | |
|---|---|---|---|---|
| **Atom** | ***x*** | ***y*** | ***z*** | **U(eq)** |
| H00Q | 5627.92 | 1313.32 | 199.21 | 31 |
| H00R | 4668.35 | 2582.95 | 502.56 | 31 |
| H00A | 10622.62 | 6314.94 | 200.2 | 31 |
| H00B | 9676.26 | 7580.7 | 507.29 | 31 |
| H00S | 2794.88 | 359.23 | 4794.57 | 31 |
| H00T | 1423.62 | 1449.33 | 4472.19 | 31 |
| H00C | 12142.74 | 5258.48 | 4770.86 | 37 |
| H00D | 13405.8 | 6355.02 | 4459.83 | 37 |
| H00E | 11417.41 | 6221.32 | 3262.99 | 35 |
| H00F | 10205.03 | 7287.3 | 2864.74 | 35 |
| H00U | 6555.45 | 1134.48 | 3249.43 | 35 |
| H00V | 5464.89 | 2239.58 | 2853.11 | 35 |
| H00W | 2391.56 | 431.97 | 3421.44 | 37 |
| H00X | 1124.96 | 1286.82 | 2968.41 | 37 |
| H00G | 7489.6 | 4845.82 | 1749.29 | 37 |
| H00H | 6437.17 | 5975.79 | 2143.24 | 37 |
| H00Y | 2467.39 | -152.75 | 1742.04 | 36 |
| H | 1457.93 | 972.02 | 2142.27 | 36 |
| H00I | 10701.46 | 6508.42 | 1569.73 | 37 |
| H00J | 10157.03 | 7587.36 | 2025.36 | 37 |
| H00K | 7329.26 | 5370.54 | 3434.4 | 38 |
| H00L | 5960.66 | 6155.89 | 2974.97 | 38 |
| H00Z | 5694.24 | 1501.3 | 1562.32 | 38 |
| HA | 5169.5 | 2575.8 | 2020.3 | 38 |
| H00 | 6693.4 | 2710.27 | 3909.3 | 40 |
| HB | 5396.39 | 3726.15 | 4301.82 | 40 |
| H00M | 11280.46 | 7827.54 | 3938.95 | 43 |
| H00N | 9770.6 | 8750.15 | 4325.59 | 43 |
| H1 | 69.47 | 638.27 | 1067.53 | 51 |
| HC | -656.4 | 1833.7 | 678.72 | 51 |
| H00O | 5082.81 | 5636.13 | 1069.44 | 50 |
| H00P | 4353.35 | 6828.56 | 680.03 | 50 |

**Experimental**

Single crystals of $C_{16}H_{32}N_4O_4S_6$ **[20220421_COD_Ace_auto]** were **[]**. A suitable crystal was selected and **[]** on a **XtaLAB Synergy, Single source at home/near, HyPix** diffractometer. The crystal was kept at 293(2) K during data collection. Using Olex2 [1], the structure was solved with the SHELXT [2] structure solution program using Intrinsic Phasing and refined with the SHELXL [3] refinement package using Least Squares minimisation.


1. Dolomanov, O.V., Bourhis, L.J., Gildea, R.J, Howard, J.A.K. & Puschmann, H. (2009), J. Appl. Cryst. 42, 339-341.
2. Sheldrick, G.M. (2015). Acta Cryst. A71, 3-8.
3. Sheldrick, G.M. (2015). Acta Cryst. C71, 3-8.


**Crystal structure determination of [20220421_COD_Ace_auto]**

**Crystal Data** for $C_{16}H_{32}N_4O_4S_6$ ($M$ =536.81 g/mol): triclinic, space group P-1 (no. 2), $a$ = 5.10520(10) Å, $b$ = 9.0197(2) Å, $c$ = 26.6367(8) Å, $\alpha$ = 92.959(2)°, $\beta$ = 95.215(2)°, $\gamma$ = 91.944(2)°, $V$ = 1218.92(5) Å$^3$, $Z$ = 2, $T$ = 293(2) K, μ(Cu Kα) = 5.445 mm$^{-1}$, *Dcalc* = 1.463 g/cm$^3$, 21322 reflections measured (3.336° ≤ 2Θ ≤ 142.91°), 4594 unique ($R_{int}$ = 0.0759, $R_{sigma}$ = 0.0439) which were used in all calculations. The final $R_1$ was 0.0847 (I > 2σ(I)) and $wR_2$ was 0.2799 (all data).

**Refinement model description**

Number of restraints - 0, number of constraints - unknown.

Details:

1. Fixed Uiso
 At 1.2 times of:
  All C(H,H) groups, All N(H,H) groups
2.a Secondary CH2 refined with riding coordinates:
 C5(H00E,H00F), C13(H00U,H00V), C14(H00W,H00X), C4(H00G,H00H), C12(H00Y,H),
 C3(H00I,H00J), C6(H00K,H00L), C11(H00Z,HA), C15(H00,HB), C7(H00M,H00N), C10(H1,
 HC), C2(H00O,H00P)
2.b X=CH2 refined with riding coordinates:
 N3(H00Q,H00R), N1(H00A,H00B), N4(H00S,H00T), N2(H00C,H00D)

This report has been created with Olex2, compiled on 2022.04.12 svn.rca3783a0 for Rigaku Oxford Diffraction.

**Section 3. Clear Crystal - μCl-bis-(Cu-L)**

| **Table 1 Crystal data and structure refinement for 20220709_COD_C7_auto.** | |
|---|---|
| Identification code | 20220709_COD_C7_auto (2) |
| Empirical formula | $C_{20}H_{33}ClCu_2O_8S_6$ |
| Formula weight | 756.421 |
| Temperature/K | 773.15 |
| Crystal system | orthorhombic |
| Space group | $Pca2_1$ |
| a/Å | 12.1018(2) |
| b/Å | 9.9499(2) |
| c/Å | 24.4174(4) |
| α/° | 90 |
| β/° | 90 |
| γ/° | 90 |
| Volume/Å$^3$ | 2940.14(9) |
| Z | 4 |
| $\rho_{calc}$g/cm$^3$ | 1.709 |
| μ/mm$^{-1}$ | 6.974 |
| F(000) | 1549.3 |
| Crystal size/mm$^3$ | 0.13 × 0.08 × 0.06 |
| Radiation | Cu Kα (λ = 1.54184) |
| 2Θ range for data collection/° | 7.24 to 160.14 |
| Index ranges | $-15 \leq h \leq 15$, $-12 \leq k \leq 12$, $-31 \leq l \leq 30$ |
| Reflections collected | 29441 |
| Independent reflections | 5657 [$R_{int}$ = 0.0538, $R_{sigma}$ = 0.0371] |
| Data/restraints/parameters | 5657/1/335 |
| Goodness-of-fit on $F^2$ | 1.073 |
| Final R indexes [I>=2σ (I)] | $R_1$ = 0.0421, $wR_2$ = 0.1350 |
| Final R indexes [all data] | $R_1$ = 0.0478, $wR_2$ = 0.1432 |
| Largest diff. peak/hole / e Å$^{-3}$ | 0.48/-0.63 |
| Flack parameter | 0.05(4) |

**Table 2 Fractional Atomic Coordinates ($\times 10^4$) and Equivalent Isotropic Displacement Parameters ($Å^2 \times 10^3$) for 20220709_COD_C7_auto (2). $U_{eq}$ is defined as 1/3 of the trace of the orthogonalised $U_{IJ}$ tensor.**

| Atom | *x* | *y* | *z* | U(eq) |
|---|---|---|---|---|
| Cu2 | 3420.6(3) | 8866.7(4) | 5021.0(4) | 38.91(15) |
| Cu1 | 6511.2(3) | 6331.0(4) | 5022.5(4) | 39.38(15) |
| S6 | 3109.4(14) | 10019.1(17) | 4226.9(7) | 38.6(3) |
| S3 | 6763.0(13) | 5091.2(17) | 4237.4(7) | 37.6(3) |
| S2 | 8336.7(4) | 7130.5(6) | 5024.5(8) | 35.05(16) |
| S5 | 1649.6(4) | 7870.3(6) | 5024.5(9) | 37.61(17) |
| S1 | 6766.1(13) | 5091.4(17) | 5811.0(7) | 38.7(3) |
| S4 | 3116.8(13) | 10018.7(17) | 5820.8(7) | 40.2(3) |
| Cl1 | 4943.3(4) | 7557.4(6) | 5030.3(15) | 72.3(3) |
| C18 | 3454(7) | 8907(9) | 3680(4) | 54.2(19) |
| C8 | 6562(6) | 6142(10) | 3629(4) | 55(2) |
| C14 | 1597(6) | 9945(9) | 5807(3) | 58.1(18) |
| O07 | 3434(6) | 11588(7) | 2677(3) | 96(2) |
| C12 | 3266(7) | 9455(9) | 6910(3) | 62(2) |
| O3 | 6087(6) | 3018(6) | 2985(3) | 91.4(19) |
| C5 | 8854(6) | 6249(7) | 5622(3) | 40.0(14) |
| O4 | 4772(5) | 4467(8) | 3239(2) | 75.0(18) |
| C2 | 6567(7) | 5345(10) | 6928(3) | 58(2) |
| O2 | 4748(5) | 4430(8) | 6821(2) | 80.5(17) |
| O6 | 4845(6) | 10894(6) | 6866(2) | 77.7(16) |
| O8 | 4827(6) | 10899(8) | 3191(3) | 79(2) |
| C4 | 8243(5) | 4959(8) | 5784(3) | 42.9(14) |
| C7 | 8261(5) | 4934(7) | 4279(3) | 43.8(14) |
| C15 | 1101(6) | 8694(7) | 5625(3) | 45.2(14) |
| O1 | 6051(4) | 3029(6) | 7041(2) | 78.8(16) |
| O5 | 3509(5) | 11562(7) | 7409(3) | 80(2) |
| C1 | 5677(5) | 4221(8) | 6929(3) | 52.3(15) |
| C20 | 3896(6) | 10710(8) | 2985(3) | 54.3(18) |
| C16 | 1065(5) | 8731(8) | 4436(3) | 58.0(19) |
| C11 | 3935(9) | 10762(7) | 7058(3) | 65(2) |
| C6 | 8862(5) | 6200(7) | 4442(3) | 46.0(15) |
| C10 | 5750(8) | 4226(9) | 3109(3) | 65(2) |
| C9 | 6622(6) | 5291(10) | 3110(2) | 54(2) |
| C19 | 3235(6) | 9521(9) | 3100(3) | 49.5(16) |
| C17 | 1641(5) | 10042(6) | 4248(3) | 43.7(13) |
| C3 | 6517(6) | 6140(9) | 6407(2) | 49.6(19) |
| C13 | 3509(7) | 8874(9) | 6375(3) | 45.9(18) |

| Table 3 Anisotropic Displacement Parameters ($Å^2×10^3$) for 20220709_COD_C7_auto (2). The Anisotropic displacement factor exponent takes the form: $-2\pi^2[h^2a^{*2}U_{11}+2hka^*b^*U_{12}+\ldots]$. | | | | | | |
|---|---|---|---|---|---|---|
| **Atom** | **$U_{11}$** | **$U_{22}$** | **$U_{33}$** | **$U_{12}$** | **$U_{13}$** | **$U_{23}$** |
| Cu2 | 31.2(2) | 51.0(2) | 34.5(2) | 3.69(13) | 2.0(5) | 0.1(7) |
| Cu1 | 29.3(2) | 52.5(3) | 36.3(2) | 5.77(14) | -0.6(5) | 0.9(7) |
| S6 | 43.9(7) | 39.9(7) | 31.8(6) | -5.3(7) | 0.1(7) | 1.5(6) |
| S3 | 41.4(7) | 40.3(7) | 31.0(6) | -7.0(6) | -1.0(7) | -1.2(6) |
| S2 | 31.7(3) | 32.8(3) | 40.7(3) | -1.70(18) | 1.6(8) | -1.4(9) |
| S5 | 34.0(3) | 35.3(3) | 43.5(3) | -2.17(19) | 3.0(8) | 1.4(9) |
| S1 | 37.2(6) | 44.4(8) | 34.5(7) | -6.6(6) | -2.2(7) | 1.0(7) |
| S4 | 42.9(7) | 42.0(7) | 35.6(7) | -2.6(7) | 0.8(7) | -1.2(6) |
| Cl1 | 24.3(3) | 44.4(4) | 148.3(10) | 6.3(3) | 5.8(11) | 0.7(15) |
| C18 | 60(5) | 47(3) | 56(4) | 3(3) | 4(3) | 3(3) |
| C8 | 58(5) | 44(4) | 62(5) | -2(3) | -16(3) | 5(4) |
| C14 | 40(3) | 87(5) | 47(3) | 7(3) | 7(3) | -11(3) |
| O07 | 121(5) | 65(4) | 101(5) | -25(3) | -28(4) | 19(3) |
| C12 | 95(6) | 53(4) | 37(3) | -18(4) | 6(3) | 5(3) |
| O3 | 106(4) | 70(4) | 99(4) | 16(3) | 20(4) | -24(3) |
| C5 | 36(3) | 43(3) | 42(3) | -5(2) | -6(2) | 6(2) |
| O4 | 53(3) | 87(4) | 85(4) | -7(3) | 19(3) | -15(3) |
| C2 | 57(4) | 70(6) | 46(4) | -12(4) | -4(3) | -7(4) |
| O2 | 64(4) | 120(4) | 58(3) | -13(3) | 1(3) | 18(3) |
| O6 | 94(4) | 90(4) | 50(3) | -12(3) | -3(3) | -1(3) |
| O8 | 71(4) | 86(4) | 81(4) | -37(3) | -25(3) | 17(4) |
| C4 | 40(3) | 52(3) | 36(3) | 7(3) | -2(3) | 8(3) |
| C7 | 43(3) | 31(3) | 57(3) | 1(2) | 11(3) | -4(3) |
| C15 | 45(3) | 43(3) | 48(3) | -7(2) | 5(3) | 5(2) |
| O1 | 47(2) | 98(4) | 91(4) | -21(3) | -3(3) | 2(3) |
| O5 | 96(4) | 70(5) | 75(3) | -19(3) | 20(3) | -28(3) |
| C1 | 37(3) | 81(4) | 39(3) | 4(2) | -5(2) | 10(3) |
| C20 | 57(3) | 67(5) | 38(3) | -8(3) | -4(3) | 5(3) |
| C16 | 23(3) | 78(4) | 73(5) | 0(2) | -18(3) | 26(3) |
| C11 | 93(6) | 54(4) | 47(4) | -20(4) | -6(4) | 2(3) |
| C6 | 23(3) | 54(3) | 61(4) | 4(2) | 14(2) | 0(3) |
| C10 | 103(5) | 60(5) | 31(3) | -8(4) | -16(3) | -2(3) |
| C9 | 59(4) | 77(6) | 25(3) | 0(3) | 6(3) | 2(3) |
| C19 | 59(4) | 60(4) | 30(3) | -4(3) | -4(3) | 4(3) |
| C17 | 48(3) | 27(2) | 56(3) | 9(2) | -7(3) | 5(2) |
| C3 | 71(5) | 52(4) | 27(3) | -6(3) | -3(2) | -6(3) |
| C13 | 72(5) | 42(3) | 23(3) | 3(3) | -2(2) | 6(2) |

| Table 4 Bond Lengths for 20220709_COD_C7_auto (2). | | | | | |
|---|---|---|---|---|---|
| **Atom** | **Atom** | **Length/Å** | **Atom** | **Atom** | **Length/Å** |
| Cu2 | S6 | 2.284(2) | C18 | C19 | 1.565(12) |
| Cu2 | S5 | 2.3614(7) | C8 | C9 | 1.527(13) |
| Cu2 | S4 | 2.2943(19) | C14 | C15 | 1.452(12) |
| Cu2 | Cl1 | 2.2569(6) | O07 | C20 | 1.282(10) |
| Cu1 | S3 | 2.2998(18) | C12 | C11 | 1.574(11) |
| Cu1 | S2 | 2.3480(6) | C12 | C13 | 1.459(11) |
| Cu1 | S1 | 2.3072(19) | O3 | C10 | 1.305(10) |
| Cu1 | Cl1 | 2.2561(6) | C5 | C4 | 1.534(10) |
| S6 | C18 | 1.784(9) | O4 | C10 | 1.249(11) |
| S6 | C17 | 1.778(6) | C2 | C1 | 1.553(11) |
| S3 | C8 | 1.832(9) | C2 | C3 | 1.500(12) |
| S3 | C7 | 1.822(6) | O2 | C1 | 1.174(9) |
| S2 | C5 | 1.813(7) | O6 | C11 | 1.204(11) |
| S2 | C6 | 1.811(7) | O8 | C20 | 1.248(9) |
| S5 | C15 | 1.806(7) | C7 | C6 | 1.508(10) |
| S5 | C16 | 1.816(7) | O1 | C1 | 1.298(9) |
| S1 | C4 | 1.793(6) | O5 | C11 | 1.279(10) |
| S1 | C3 | 1.816(7) | C20 | C19 | 1.455(11) |
| S4 | C14 | 1.841(7) | C16 | C17 | 1.548(10) |
| S4 | C13 | 1.831(8) | C10 | C9 | 1.495(13) |

| Table 5 Bond Angles for 20220709_COD_C7_auto (2). | | | | | | | |
|---|---|---|---|---|---|---|---|
| **Atom** | **Atom** | **Atom** | **Angle/°** | **Atom** | **Atom** | **Atom** | **Angle/°** |
| S5 | Cu2 | S6 | 93.68(7) | Cu1 | Cl1 | Cu2 | 177.27(8) |
| S4 | Cu2 | S6 | 116.45(3) | C19 | C18 | S6 | 113.3(6) |
| S4 | Cu2 | S5 | 93.51(7) | C9 | C8 | S3 | 110.5(7) |
| Cl1 | Cu2 | S6 | 115.66(11) | C15 | C14 | S4 | 116.9(6) |
| Cl1 | Cu2 | S5 | 119.92(3) | C13 | C12 | C11 | 115.4(6) |
| Cl1 | Cu2 | S4 | 114.24(11) | C4 | C5 | S2 | 116.5(5) |
| S2 | Cu1 | S3 | 93.37(6) | C3 | C2 | C1 | 110.7(6) |
| S1 | Cu1 | S3 | 113.03(3) | C5 | C4 | S1 | 115.4(5) |
| S1 | Cu1 | S2 | 93.08(6) | C6 | C7 | S3 | 115.0(4) |
| Cl1 | Cu1 | S3 | 114.12(11) | C14 | C15 | S5 | 119.1(5) |
| Cl1 | Cu1 | S2 | 127.45(3) | O2 | C1 | C2 | 122.4(8) |
| Cl1 | Cu1 | S1 | 113.23(10) | O1 | C1 | C2 | 114.6(6) |
| C18 | S6 | Cu2 | 106.6(3) | O1 | C1 | O2 | 122.9(8) |
| C17 | S6 | Cu2 | 98.4(3) | O8 | C20 | O07 | 121.9(8) |
| C17 | S6 | C18 | 105.3(4) | C19 | C20 | O07 | 115.3(6) |
| C8 | S3 | Cu1 | 110.6(3) | C19 | C20 | O8 | 122.8(7) |
| C7 | S3 | Cu1 | 97.5(3) | C17 | C16 | S5 | 117.1(5) |
| C7 | S3 | C8 | 103.1(4) | O6 | C11 | C12 | 118.1(7) |
| C5 | S2 | Cu1 | 99.4(2) | O5 | C11 | C12 | 117.4(8) |
| C6 | S2 | Cu1 | 98.9(2) | O5 | C11 | O6 | 124.2(8) |
| C6 | S2 | C5 | 105.22(15) | C7 | C6 | S2 | 117.7(5) |
| C15 | S5 | Cu2 | 98.4(2) | O4 | C10 | O3 | 122.1(9) |
| C16 | S5 | Cu2 | 98.8(2) | C9 | C10 | O3 | 115.7(8) |
| C16 | S5 | C15 | 106.59(18) | C9 | C10 | O4 | 122.1(8) |
| C4 | S1 | Cu1 | 98.2(2) | C10 | C9 | C8 | 111.2(6) |
| C3 | S1 | Cu1 | 109.8(3) | C20 | C19 | C18 | 113.4(6) |
| C3 | S1 | C4 | 103.7(4) | C16 | C17 | S6 | 116.6(4) |
| C14 | S4 | Cu2 | 97.2(3) | C2 | C3 | S1 | 111.7(6) |
| C13 | S4 | Cu2 | 106.1(3) | C12 | C13 | S4 | 111.3(6) |
| C13 | S4 | C14 | 104.4(4) | | | | |

| Table 6 Torsion Angles for 20220709_COD_C7_auto (2). | | | | | | | | | |
|---|---|---|---|---|---|---|---|---|---|
| **A** | **B** | **C** | **D** | **Angle/°** | **A** | **B** | **C** | **D** | **Angle/°** |
| S6 | C18 | C19 | C20 | 62.5(7) | S1 | C3 | C2 | C1 | -60.4(6) |
| S6 | C17 | C16 | S5 | 43.6(6) | S4 | C13 | C12 | C11 | -64.2(6) |
| S3 | C8 | C9 | C10 | 60.1(6) | C18 | C19 | C20 | O07 | -147.8(7) |
| S3 | C7 | C6 | S2 | 47.2(6) | C18 | C19 | C20 | O8 | 29.1(8) |
| S2 | C5 | C4 | S1 | -48.0(5) | C8 | C9 | C10 | O3 | -131.9(7) |
| S5 | C15 | C14 | S4 | -44.6(5) | C8 | C9 | C10 | O4 | 45.3(8) |

| Table 7 Hydrogen Atom Coordinates (Å×10$^4$) and Isotropic Displacement Parameters (Å$^2$×10$^3$) for 20220709_COD_C7_auto (2). | | | | |
|---|---|---|---|---|
| **Atom** | ***x*** | ***y*** | ***z*** | **U(eq)** |
| H18a | 4229(7) | 8669(9) | 3708(4) | 65(2) |
| H18b | 3026(7) | 8088(9) | 3718(4) | 65(2) |
| H8a | 5847(6) | 6582(10) | 3650(4) | 66(3) |
| H8b | 7127(6) | 6833(10) | 3618(4) | 66(3) |
| H14a | 1328(6) | 10133(9) | 6174(3) | 70(2) |
| H14b | 1333(6) | 10660(9) | 5571(3) | 70(2) |
| H12a | 3413(7) | 8781(9) | 7188(3) | 74(3) |
| H12b | 2484(7) | 9664(9) | 6925(3) | 74(3) |
| H3 | 6747(6) | 3038(6) | 2910(3) | 137(3) |
| H5a | 9623(6) | 6024(7) | 5557(3) | 48.0(16) |
| H5b | 8832(6) | 6861(7) | 5931(3) | 48.0(16) |
| H2a | 6447(7) | 5938(10) | 7238(3) | 69(3) |
| H2b | 7294(7) | 4946(10) | 6966(3) | 69(3) |
| H6 | 4966(6) | 10281(6) | 6649(2) | 117(2) |
| H8 | 5000(6) | 10244(8) | 3376(3) | 119(3) |
| H4a | 8506(5) | 4676(8) | 6141(3) | 51.4(17) |
| H4b | 8435(5) | 4259(8) | 5524(3) | 51.4(17) |
| H7a | 8437(5) | 4235(7) | 4542(3) | 52.5(16) |
| H7b | 8536(5) | 4644(7) | 3925(3) | 52.5(16) |
| H15a | 323(6) | 8865(7) | 5559(3) | 54.3(17) |
| H15b | 1145(6) | 8061(7) | 5926(3) | 54.3(17) |
| H1 | 6714(4) | 3072(6) | 7106(2) | 118(2) |
| H16a | 1065(5) | 8109(8) | 4130(3) | 70(2) |
| H16b | 300(5) | 8941(8) | 4518(3) | 70(2) |
| H6a | 8865(5) | 6799(7) | 4129(3) | 55.2(18) |
| H6b | 9624(5) | 5964(7) | 4519(3) | 55.2(18) |
| H9a | 6527(6) | 5865(10) | 2792(2) | 65(2) |
| H9b | 7344(6) | 4874(10) | 3085(2) | 65(2) |
| H19a | 3391(6) | 8844(9) | 2824(3) | 59(2) |
| H19b | 2459(6) | 9754(9) | 3071(3) | 59(2) |
| H17a | 1414(5) | 10760(6) | 4492(3) | 52.4(16) |
| H17b | 1372(5) | 10264(6) | 3885(3) | 52.4(16) |
| H3a | 7066(6) | 6850(9) | 6419(2) | 60(2) |
| H3b | 5795(6) | 6556(9) | 6375(2) | 60(2) |
| H13a | 3111(7) | 8034(9) | 6334(3) | 55(2) |
| H13b | 4293(7) | 8681(9) | 6350(3) | 55(2) |

| Table 8 Atomic Occupancy for 20220709_COD_C7_auto (2). | | | | | |
|---|---|---|---|---|---|
| **Atom** | ***Occupancy*** | **Atom** | ***Occupancy*** | **Atom** | ***Occupancy*** |
| H3 | 0.250000 | H6 | 0.250000 | H8 | 0.250000 |
| H1 | 0.250000 | | | | |

**Experimental**

Single crystals of $C_{20}H_{33}ClCu_2O_8S_6$ **[20220709_COD_C7_auto (2)]** were **[]**. A suitable crystal was selected and **[]** on a diffractometer. The crystal was kept at 773.15 K during data collection. Using Olex2 [1], the structure was solved with the olex2.solve [2] structure solution program using Charge Flipping and refined with the olex2.refine [3] refinement package using Gauss-Newton minimisation.


1. Dolomanov, O.V., Bourhis, L.J., Gildea, R.J, Howard, J.A.K. & Puschmann, H. (2009), J. Appl. Cryst. 42, 339-341.
2. Bourhis, L.J., Dolomanov, O.V., Gildea, R.J., Howard, J.A.K., Puschmann, H. (2015). Acta Cryst. A71, 59-75.
3. Bourhis, L.J., Dolomanov, O.V., Gildea, R.J., Howard, J.A.K., Puschmann, H. (2015). Acta Cryst. A71, 59-75.


**Crystal structure determination of [20220709_COD_C7_auto (2)]**

**Crystal Data** for $C_{20}H_{33}ClCu_2O_8S_6$ ($M$ =756.421 g/mol): orthorhombic, space group $Pca2_1$ (no. 29), $a$ = 12.1018(2) Å, $b$ = 9.9499(2) Å, $c$ = 24.4174(4) Å, $V$ = 2940.14(9) Å$^3$, $Z$ = 4, $T$ = 773.15 K, μ(Cu Kα) = 6.974 mm$^{-1}$, *Dcalc* = 1.709 g/cm$^3$, 29441 reflections measured (7.24° ≤ 2Θ ≤ 160.14°), 5657 unique ($R_{int}$ = 0.0538, $R_{sigma}$ = 0.0371) which were used in all calculations. The final $R_1$ was 0.0421 (I>=2u(I)) and $wR_2$ was 0.1432 (all data).

**Refinement model description**

Number of restraints - 1, number of constraints - 56.

Details:

1. Twinned data refinement
 Scales: 0.55(5)
 0.45(5)
2. Fixed Uiso
 At 1.2 times of:
  All C(H,H) groups
 At 1.5 times of:
  All O(H) groups
3. Others
 Fixed Sof: H3(0.25) H6(0.25) H8(0.25) H1(0.25)
4.a Secondary CH2 refined with riding coordinates:
 C18(H18a,H18b), C8(H8a,H8b), C14(H14a,H14b), C12(H12a,H12b), C5(H5a,H5b),
 C2(H2a,H2b), C4(H4a,H4b), C7(H7a,H7b), C15(H15a,H15b), C16(H16a,H16b), C6(H6a,
 H6b), C9(H9a,H9b), C19(H19a,H19b), C17(H17a,H17b), C3(H3a,H3b), C13(H13a,H13b)
4.b Tetrahedral OH refined as rotating group:
 O3(H3), O6(H6), O8(H8), O1(H1)

**Section 4. Green Crystal: L-CuCl**

| **Table 1 Crystal data and structure refinement for 20220622_COD_Gb_auto.** | |
|---|---|
| Identification code | 20220622_COD_Gb_auto |
| Empirical formula | $C_{40}H_{92}Cl_4Cu_8O_{32}S_{12}$ |
| Formula weight | 2124.00 |
| Temperature/K | 293(2) |
| Crystal system | monoclinic |
| Space group | $P2_1/c$ |
| a/Å | 25.5617(3) |
| b/Å | 10.72810(10) |
| c/Å | 14.7307(2) |
| α/° | 90 |
| β/° | 100.8080(10) |
| γ/° | 90 |
| Volume/Å$^3$ | 3967.92(8) |
| Z | 2 |
| $\rho_{calc}$g/cm$^3$ | 1.778 |
| μ/mm$^{-1}$ | 7.145 |
| F(000) | 2168.0 |
| Crystal size/mm$^3$ | 0.19 × 0.16 × 0.05 |
| Radiation | Cu Kα (λ = 1.54184) |
| 2Θ range for data collection/° | 7.042 to 168.81 |
| Index ranges | $-32 \leq h \leq 32$, $-13 \leq k \leq 13$, $-17 \leq l \leq 18$ |
| Reflections collected | 58507 |
| Independent reflections | 8400 [$R_{int}$ = 0.0565, $R_{sigma}$ = 0.0300] |
| Data/restraints/parameters | 8400/2/457 |
| Goodness-of-fit on $F^2$ | 1.023 |
| Final R indexes [I>=2σ (I)] | $R_1$ = 0.0619, $wR_2$ = 0.1824 |
| Final R indexes [all data] | $R_1$ = 0.0675, $wR_2$ = 0.1890 |
| Largest diff. peak/hole / e Å$^{-3}$ | 1.94/-0.86 |

| Table 2 Fractional Atomic Coordinates ($\times 10^4$) and Equivalent Isotropic Displacement Parameters ($Å^2 \times 10^3$) for 20220622_COD_Gb_auto. $U_{eq}$ is defined as 1/3 of the trace of the orthogonalised $U_{IJ}$ tensor. | | | | |
|---|---|---|---|---|
| **Atom** | ***x*** | ***y*** | ***z*** | **U(eq)** |
| Cu01 | -109.4(2) | 528.8(6) | -817.3(4) | 34.04(17) |
| Cu02 | 5125.3(2) | 5696.0(6) | 5738.7(5) | 39.65(18) |
| Cu03 | 7153.0(3) | 1701.8(7) | 7989.5(6) | 50.2(2) |
| Cu04 | 2140.1(3) | 3276.6(7) | 3398.1(6) | 51.7(2) |
| Cl05 | 6751.3(5) | 3223.0(13) | 8707.2(8) | 54.8(3) |
| Cl06 | 1715.1(5) | 1774.8(13) | 4059.6(8) | 54.5(3) |
| S007 | 7808.4(4) | 454.7(11) | 8863.7(8) | 44.2(3) |
| S008 | 2787.2(4) | 4548.9(11) | 4214.9(9) | 45.5(3) |
| S009 | 7723.6(5) | 2255.6(11) | 6948.0(9) | 46.7(3) |
| S00A | 6602.0(4) | 580.8(11) | 6838.4(9) | 47.3(3) |
| S00B | 1543.3(5) | 4309.0(11) | 2261.0(10) | 52.0(3) |
| S00C | 2688.8(5) | 2711.7(12) | 2316.0(9) | 48.9(3) |
| O00D | 9216.1(12) | 980(3) | 9574(2) | 46.3(8) |
| O00E | 9402.8(13) | 88(4) | 10959(2) | 48.3(8) |
| O00F | 4218.3(12) | 3975(4) | 4753(2) | 49.8(8) |
| O00G | 221.6(15) | 2007(3) | -188(3) | 55.4(9) |
| O00H | 433.6(15) | 1100(4) | 1197(3) | 58.4(10) |
| O00I | 4434.7(13) | 5147(4) | 6006(2) | 54.2(9) |
| O00J | 5453.0(16) | 4176(4) | 6305(3) | 59.4(10) |
| O00K | -276.2(18) | 1353(4) | -2148(2) | 59.6(10) |
| O00L | 5235.6(17) | 2964(4) | 5074(3) | 64.8(11) |
| O00M | 5359(2) | 6662(4) | 7006(3) | 68.0(11) |
| O00N | -342(2) | 3897(4) | -2104(4) | 72.9(12) |
| O00O | -787(2) | 1221(4) | -5411(4) | 80.9(14) |
| O00P | -673(2) | -58(6) | -3705(3) | 81.5(14) |
| C00Q | 9097.8(16) | 644(4) | 10325(3) | 36.2(9) |
| O00R | 5289(2) | 9164(5) | 7069(4) | 77.3(13) |
| C00S | 434.7(18) | 2001(4) | 629(4) | 46.7(11) |
| C00T | 4122.3(16) | 4456(4) | 5482(3) | 39.6(9) |
| C00U | 5448.6(18) | 3164(5) | 5903(4) | 50.0(12) |
| C00V | 8239.2(18) | 275(5) | 8026(4) | 48.2(11) |
| C00W | 3185.9(19) | 4770(5) | 3330(4) | 50.6(12) |
| C00X | 8553.3(19) | 947(6) | 10505(3) | 54.0(13) |
| O00Y | 5755(3) | 5160(7) | 8560(4) | 99.2(17) |
| C00Z | 7093(2) | 207(5) | 6143(4) | 52.2(12) |
| C010 | 3181.1(18) | 3527(5) | 5059(4) | 50.2(11) |
| C011 | 8320.5(18) | 1438(6) | 7491(4) | 51.8(12) |
| C012 | 8161.7(18) | 1532(5) | 9715(4) | 47.5(11) |
| C013 | 7453(2) | 1277(6) | 5973(4) | 55.2(13) |
| C014 | 3275.9(19) | 3620(6) | 2797(4) | 53.9(12) |
| C015 | 3600.4(19) | 4176(7) | 5765(3) | 57.8(14) |
| C016 | 6217(2) | 1748(5) | 6090(4) | 54.4(13) |
| C017 | 1995(2) | 4632(5) | 1469(4) | 57.6(13) |
| C018 | 2367(2) | 3594(6) | 1327(4) | 62.5(15) |
| O019 | 5724(3) | 6139(6) | 10288(5) | 124(3) |
| C01A | 5733(2) | 2085(6) | 6457(5) | 63.1(15) |
| C01B | 733(2) | 3174(5) | 1008(5) | 68.5(19) |
| C01C | 1154(3) | 2964(6) | 1789(6) | 81(2) |

| Table 3 Anisotropic Displacement Parameters ($Å^2×10^3$) for 20220622_COD_Gb_auto. The Anisotropic displacement factor exponent takes the form: $-2\pi^2[h^2a^{*2}U_{11}+2hka^*b^*U_{12}+\ldots]$. | | | | | | |
|---|---|---|---|---|---|---|
| **Atom** | **$U_{11}$** | **$U_{22}$** | **$U_{33}$** | **$U_{23}$** | **$U_{13}$** | **$U_{12}$** |
| Cu01 | 26.2(3) | 36.2(3) | 37.8(3) | -0.8(2) | 1.2(2) | -1.0(2) |
| Cu02 | 27.2(3) | 44.2(4) | 45.3(4) | -3.8(3) | 0.7(3) | 1.4(2) |
| Cu03 | 32.4(3) | 61.5(5) | 55.2(4) | 6.2(3) | 4.2(3) | 6.9(3) |
| Cu04 | 30.9(3) | 59.4(5) | 60.9(5) | -6.5(3) | -1.4(3) | -6.6(3) |
| Cl05 | 58.8(7) | 63.8(7) | 38.2(6) | -6.3(5) | -0.3(5) | 22.1(6) |
| Cl06 | 52.2(6) | 68.3(8) | 41.2(6) | 4.7(5) | 4.1(5) | -22.0(6) |
| S007 | 33.7(5) | 46.5(6) | 48.8(6) | 8.4(5) | -1.6(4) | 2.4(4) |
| S008 | 31.3(5) | 49.8(6) | 50.8(6) | -9.5(5) | -4.4(4) | -2.1(4) |
| S009 | 38.2(5) | 45.2(6) | 56.6(7) | 9.5(5) | 8.4(5) | -0.8(4) |
| S00A | 31.4(5) | 45.1(6) | 60.6(7) | 14.5(5) | -4.1(5) | 0.6(4) |
| S00B | 33.4(5) | 42.6(6) | 71.0(8) | -14.6(5) | -13.1(5) | 0.4(4) |
| S00C | 43.9(6) | 47.3(6) | 52.6(7) | -6.7(5) | 1.5(5) | 8.0(5) |
| O00D | 28.7(14) | 64(2) | 46.2(18) | 8.6(15) | 6.4(13) | 7.4(14) |
| O00E | 38.1(16) | 67(2) | 40.0(17) | 6.6(15) | 8.7(13) | 11.5(15) |
| O00F | 30.0(15) | 72(2) | 47.7(18) | -9.0(17) | 8.0(13) | -8.8(15) |
| O00G | 56(2) | 40.2(17) | 62(2) | -5.0(16) | -7.2(17) | -10.8(15) |
| O00H | 57(2) | 54(2) | 57(2) | -13.5(17) | -8.5(17) | -14.0(17) |
| O00I | 35.8(16) | 75(2) | 52(2) | -13.7(18) | 8.9(15) | -7.0(16) |
| O00J | 55(2) | 56(2) | 61(2) | 9.7(18) | -4.6(17) | 10.2(17) |
| O00K | 80(3) | 54(2) | 38.5(18) | 7.0(15) | -5.7(17) | -2(2) |
| O00L | 63(2) | 44.2(19) | 83(3) | 2.3(19) | 4(2) | 12.5(17) |
| O00M | 77(3) | 66(2) | 54(2) | -17.6(19) | -7(2) | 4(2) |
| O00N | 86(3) | 62(3) | 73(3) | 17(2) | 21(2) | 12(2) |
| O00O | 108(4) | 53(2) | 86(3) | -9(2) | 27(3) | -20(2) |
| O00P | 82(3) | 98(4) | 60(3) | -6(3) | 3(2) | -23(3) |
| C00Q | 27.3(18) | 39(2) | 41(2) | -5.3(17) | 3.1(16) | -1.1(15) |
| O00R | 88(3) | 70(3) | 75(3) | -5(2) | 14(3) | -3(2) |
| C00S | 33(2) | 31(2) | 73(3) | -8(2) | 1(2) | -0.5(16) |
| C00T | 24.5(18) | 52(3) | 40(2) | 2.7(19) | 0.1(16) | 1.7(17) |
| C00U | 30(2) | 54(3) | 64(3) | 11(2) | 2(2) | 5.5(19) |
| C00V | 36(2) | 53(3) | 50(3) | -9(2) | -6.5(19) | 11.7(19) |
| C00W | 38(2) | 56(3) | 53(3) | 11(2) | -5(2) | -12(2) |
| C00X | 36(2) | 86(4) | 40(2) | -6(2) | 7.6(19) | 10(2) |
| O00Y | 104(4) | 112(4) | 78(4) | 5(3) | 6(3) | 18(4) |
| C00Z | 45(3) | 52(3) | 54(3) | 1(2) | -6(2) | 4(2) |
| C010 | 33(2) | 61(3) | 55(3) | 7(2) | 6(2) | -12(2) |
| C011 | 31(2) | 75(3) | 48(3) | -3(2) | 4.0(19) | -1(2) |
| C012 | 35(2) | 57(3) | 50(3) | -8(2) | 6.9(19) | 12(2) |
| C013 | 44(3) | 72(3) | 47(3) | 12(2) | 3(2) | 3(2) |
| C014 | 35(2) | 74(3) | 50(3) | 4(3) | 2(2) | 4(2) |
| C015 | 32(2) | 102(4) | 38(2) | 2(3) | 4.2(19) | -11(2) |
| C016 | 43(3) | 59(3) | 59(3) | 18(2) | 4(2) | 9(2) |
| C017 | 56(3) | 56(3) | 52(3) | -4(2) | -13(2) | 7(2) |
| C018 | 62(3) | 76(4) | 42(3) | -9(3) | -10(2) | 16(3) |
| O019 | 200(8) | 92(4) | 88(4) | 16(4) | 45(5) | 69(5) |
| C01A | 49(3) | 62(3) | 79(4) | 23(3) | 14(3) | 15(3) |
| C01B | 59(3) | 37(3) | 94(5) | -12(3) | -25(3) | -2(2) |
| C01C | 57(3) | 46(3) | 121(6) | -9(3) | -34(4) | -7(3) |

| Table 4 Bond Lengths for 20220622_COD_Gb_auto. | | | | | |
|---|---|---|---|---|---|
| **Atom** | **Atom** | **Length/Å** | **Atom** | **Atom** | **Length/Å** |
| Cu01 | Cu01[1] | 2.6254(12) | S00A | C00Z | 1.807(6) |
| Cu01 | O00D[2] | 1.978(3) | S00A | C016 | 1.830(5) |
| Cu01 | O00E[3] | 1.971(3) | S00B | C017 | 1.822(7) |
| Cu01 | O00G | 1.948(3) | S00B | C01C | 1.815(5) |
| Cu01 | O00H[1] | 1.969(4) | S00C | C014 | 1.818(5) |
| Cu01 | O00K | 2.120(4) | S00C | C018 | 1.802(6) |
| Cu02 | Cu02[4] | 2.6179(13) | O00D | C00Q | 1.253(6) |
| Cu02 | O00F[4] | 1.980(3) | O00E | C00Q | 1.250(5) |
| Cu02 | O00I | 1.970(3) | O00F | C00T | 1.258(6) |
| Cu02 | O00J | 1.948(4) | O00G | C00S | 1.225(7) |
| Cu02 | O00L[4] | 1.984(4) | O00H | C00S | 1.279(7) |
| Cu02 | O00M | 2.121(4) | O00I | C00T | 1.246(6) |
| Cu03 | Cl05 | 2.2896(14) | O00J | C00U | 1.236(7) |
| Cu03 | S007 | 2.3336(12) | O00L | C00U | 1.259(7) |
| Cu03 | S009 | 2.3820(14) | C00Q | C00X | 1.501(6) |
| Cu03 | S00A | 2.3258(15) | C00S | C01B | 1.522(6) |
| Cu04 | Cl06 | 2.2632(14) | C00T | C015 | 1.500(6) |
| Cu04 | S008 | 2.3023(12) | C00U | C01A | 1.521(7) |
| Cu04 | S00B | 2.3241(14) | C00V | C011 | 1.511(8) |
| Cu04 | S00C | 2.3903(15) | C00W | C014 | 1.504(8) |
| S007 | C00V | 1.811(5) | C00X | C012 | 1.521(7) |
| S007 | C012 | 1.816(5) | C00Z | C013 | 1.521(8) |
| S008 | C00W | 1.814(6) | C010 | C015 | 1.515(7) |
| S008 | C010 | 1.815(5) | C016 | C01A | 1.483(8) |
| S009 | C011 | 1.811(5) | C017 | C018 | 1.504(8) |
| S009 | C013 | 1.809(6) | C01B | C01C | 1.438(8) |

[1]-X,-Y,-Z; [2]-1+X,+Y,-1+Z; [3]1-X,-Y,1-Z; [4]1-X,1-Y,1-Z

| Table 5 Bond Angles for 20220622_COD_Gb_auto. | | | | | | | |
|---|---|---|---|---|---|---|---|
| **Atom** | **Atom** | **Atom** | **Angle/°** | **Atom** | **Atom** | **Atom** | **Angle/°** |
| O00D[1] | Cu01 | Cu01[2] | 83.45(10) | C011 | S009 | Cu03 | 99.29(18) |
| O00D[1] | Cu01 | O00K | 97.60(16) | C013 | S009 | Cu03 | 100.19(18) |
| O00E[3] | Cu01 | Cu01[2] | 84.85(10) | C013 | S009 | C011 | 103.6(3) |
| O00E[3] | Cu01 | O00D[1] | 168.30(14) | C00Z | S00A | Cu03 | 97.95(17) |
| O00E[3] | Cu01 | O00K | 94.10(16) | C00Z | S00A | C016 | 99.4(3) |
| O00G | Cu01 | Cu01[2] | 85.23(12) | C016 | S00A | Cu03 | 105.6(2) |
| O00G | Cu01 | O00D[1] | 89.23(17) | C017 | S00B | Cu04 | 98.22(17) |
| O00G | Cu01 | O00E[3] | 89.94(17) | C01C | S00B | Cu04 | 97.8(2) |
| O00G | Cu01 | O00H[2] | 168.35(17) | C01C | S00B | C017 | 105.9(4) |
| O00G | Cu01 | O00K | 95.41(16) | C014 | S00C | Cu04 | 98.58(19) |
| O00H[2] | Cu01 | Cu01[2] | 83.29(12) | C018 | S00C | Cu04 | 99.8(2) |
| O00H[2] | Cu01 | O00D[1] | 87.52(17) | C018 | S00C | C014 | 104.6(3) |
| O00H[2] | Cu01 | O00E[3] | 90.98(17) | C00Q | O00D | Cu01[5] | 123.7(3) |
| O00H[2] | Cu01 | O00K | 96.11(16) | C00Q | O00E | Cu01[3] | 122.4(3) |
| O00K | Cu01 | Cu01[2] | 178.78(13) | C00T | O00F | Cu02[4] | 123.6(3) |
| O00F[4] | Cu02 | Cu02[4] | 83.68(11) | C00S | O00G | Cu01 | 122.4(3) |
| O00F[4] | Cu02 | O00L[4] | 88.87(18) | C00S | O00H | Cu01[2] | 122.5(3) |
| O00F[4] | Cu02 | O00M | 96.71(18) | C00T | O00I | Cu02 | 123.2(3) |
| O00I | Cu02 | Cu02[4] | 84.68(11) | C00U | O00J | Cu02 | 124.5(4) |
| O00I | Cu02 | O00F[4] | 168.35(15) | C00U | O00L | Cu02[4] | 122.0(4) |
| O00I | Cu02 | O00L[4] | 90.26(18) | O00D | C00Q | C00X | 118.6(4) |
| O00I | Cu02 | O00M | 94.84(18) | O00E | C00Q | O00D | 125.2(4) |
| O00J | Cu02 | Cu02[4] | 84.07(13) | O00E | C00Q | C00X | 116.1(4) |
| O00J | Cu02 | O00F[4] | 88.85(17) | O00G | C00S | O00H | 126.3(4) |
| O00J | Cu02 | O00I | 89.64(18) | O00G | C00S | C01B | 117.1(5) |
| O00J | Cu02 | O00L[4] | 168.19(18) | O00H | C00S | C01B | 116.6(5) |
| O00J | Cu02 | O00M | 90.29(17) | O00F | C00T | C015 | 118.7(4) |
| O00L[4] | Cu02 | Cu02[4] | 84.16(13) | O00I | C00T | O00F | 124.7(4) |
| O00L[4] | Cu02 | O00M | 101.48(18) | O00I | C00T | C015 | 116.6(4) |
| O00M | Cu02 | Cu02[4] | 174.35(13) | O00J | C00U | O00L | 125.3(5) |
| Cl05 | Cu03 | S007 | 119.44(5) | O00J | C00U | C01A | 116.8(5) |
| Cl05 | Cu03 | S009 | 120.10(6) | O00L | C00U | C01A | 117.9(5) |
| Cl05 | Cu03 | S00A | 116.26(5) | C011 | C00V | S007 | 115.3(3) |
| S007 | Cu03 | S009 | 92.04(5) | C014 | C00W | S008 | 115.4(4) |
| S00A | Cu03 | S007 | 112.32(5) | C00Q | C00X | C012 | 116.9(4) |
| S00A | Cu03 | S009 | 91.12(5) | C013 | C00Z | S00A | 115.5(4) |
| Cl06 | Cu04 | S008 | 123.56(6) | C015 | C010 | S008 | 115.0(4) |
| Cl06 | Cu04 | S00B | 110.27(5) | C00V | C011 | S009 | 116.3(3) |
| Cl06 | Cu04 | S00C | 119.71(6) | C00X | C012 | S007 | 115.9(4) |
| S008 | Cu04 | S00B | 113.84(5) | C00Z | C013 | S009 | 117.5(4) |
| S008 | Cu04 | S00C | 92.58(5) | C00W | C014 | S00C | 116.6(4) |
| S00B | Cu04 | S00C | 91.61(6) | C00T | C015 | C010 | 117.0(4) |
| C00V | S007 | Cu03 | 98.65(16) | C01A | C016 | S00A | 109.8(4) |
| C00V | S007 | C012 | 104.5(2) | C018 | C017 | S00B | 116.2(4) |
| C012 | S007 | Cu03 | 103.21(16) | C017 | C018 | S00C | 118.7(4) |
| C00W | S008 | Cu04 | 98.47(16) | C016 | C01A | C00U | 109.7(5) |
| C00W | S008 | C010 | 104.9(2) | C01C | C01B | C00S | 114.4(5) |
| C010 | S008 | Cu04 | 104.59(17) | C01B | C01C | S00B | 117.2(5) |

[1]-1+X,+Y,-1+Z; [2]-X,-Y,-Z; [3]1-X,-Y,1-Z; [4]1-X,1-Y,1-Z; [5]1+X,+Y,1+Z

| Table 6 Torsion Angles for 20220622_COD_Gb_auto. | | | | | | | | | |
|---|---|---|---|---|---|---|---|---|---|
| **A** | **B** | **C** | **D** | **Angle/°** | **A** | **B** | **C** | **D** | **Angle/°** |
| Cu01[1] | O00D | C00Q | O00E | 7.1(7) | S007 | C00V | C011 | S009 | -51.0(5) |
| Cu01[1] | O00D | C00Q | C00X | -174.5(4) | S008 | C00W | C014 | S00C | 50.3(5) |
| Cu01[2] | O00E | C00Q | O00D | -7.2(7) | S008 | C010 | C015 | C00T | -83.3(6) |
| Cu01[2] | O00E | C00Q | C00X | 174.3(4) | S00A | C00Z | C013 | S009 | 44.2(5) |
| Cu01 | O00G | C00S | O00H | -6.4(8) | S00A | C016 | C01A | C00U | 173.2(4) |
| Cu01 | O00G | C00S | C01B | 173.2(4) | S00B | C017 | C018 | S00C | -42.3(6) |
| Cu01[3] | O00H | C00S | O00G | 3.7(8) | O00D | C00Q | C00X | C012 | 6.0(7) |
| Cu01[3] | O00H | C00S | C01B | -175.9(4) | O00E | C00Q | C00X | C012 | -175.4(5) |
| Cu02[4] | O00F | C00T | O00I | -3.5(7) | O00F | C00T | C015 | C010 | -11.2(8) |
| Cu02[4] | O00F | C00T | C015 | 177.5(4) | O00G | C00S | C01B | C01C | -153.7(7) |
| Cu02 | O00I | C00T | O00F | 3.9(7) | O00H | C00S | C01B | C01C | 25.9(9) |
| Cu02 | O00I | C00T | C015 | -177.1(4) | O00I | C00T | C015 | C010 | 169.7(5) |
| Cu02 | O00J | C00U | O00L | 0.3(8) | O00J | C00U | C01A | C016 | -111.1(6) |
| Cu02 | O00J | C00U | C01A | 179.1(4) | O00L | C00U | C01A | C016 | 67.8(7) |
| Cu02[4] | O00L | C00U | O00J | 1.1(8) | C00Q | C00X | C012 | S007 | 82.8(6) |
| Cu02[4] | O00L | C00U | C01A | -177.7(4) | C00S | C01B | C01C | S00B | 178.2(5) |
| Cu03 | S007 | C00V | C011 | 41.3(4) | C00V | S007 | C012 | C00X | -88.1(4) |
| Cu03 | S007 | C012 | C00X | 169.2(3) | C00W | S008 | C010 | C015 | 83.7(4) |
| Cu03 | S009 | C011 | C00V | 28.9(4) | C00Z | S00A | C016 | C01A | 172.1(5) |
| Cu03 | S009 | C013 | C00Z | -16.3(4) | C010 | S008 | C00W | C014 | 65.1(4) |
| Cu03 | S00A | C00Z | C013 | -45.0(4) | C011 | S009 | C013 | C00Z | 85.9(4) |
| Cu03 | S00A | C016 | C01A | -86.8(4) | C012 | S007 | C00V | C011 | -64.8(4) |
| Cu04 | S008 | C00W | C014 | -42.6(4) | C013 | S009 | C011 | C00V | -74.0(4) |
| Cu04 | S008 | C010 | C015 | -173.2(3) | C014 | S00C | C018 | C017 | -84.9(5) |
| Cu04 | S00B | C017 | C018 | 41.8(4) | C016 | S00A | C00Z | C013 | 62.4(4) |
| Cu04 | S00B | C01C | C01B | -177.6(6) | C017 | S00B | C01C | C01B | -76.7(7) |
| Cu04 | S00C | C014 | C00W | -26.8(4) | C018 | S00C | C014 | C00W | 75.8(5) |
| Cu04 | S00C | C018 | C017 | 16.7(5) | C01C | S00B | C017 | C018 | -58.8(5) |

[1]1+X,+Y,1+Z; [2]1-X,-Y,1-Z; [3]-X,-Y,-Z; [4]1-X,1-Y,1-Z

| Table 7 Hydrogen Atom Coordinates (Å×10$^4$) and Isotropic Displacement Parameters (Å$^2$×10$^3$) for 20220622_COD_Gb_auto. | | | | |
|---|---|---|---|---|
| **Atom** | ***x*** | ***y*** | ***z*** | **U(eq)** |
| H00A | -291.8 | 2125.66 | -2279.16 | 89 |
| H00B | -380.08 | 989.26 | -2662.46 | 89 |
| H00C | 5354.27 | 7445.08 | 7092.21 | 102 |
| H00D | 5455.1 | 6357.08 | 7543.8 | 102 |
| H00M | -41.48 | 3608.6 | -1846.82 | 109 |
| H00N | -277.95 | 4641.91 | -2246.95 | 109 |
| H00O | -595.2 | 679.61 | -5615.16 | 121 |
| H00P | -570.94 | 1802.78 | -5205.71 | 121 |
| H00Q | -773.69 | 474.9 | -4128.91 | 122 |
| H00R | -925.05 | -586.29 | -3766.36 | 122 |
| H00S | 4989.88 | 8812.19 | 6881.88 | 116 |
| H00T | 5214.77 | 9935.2 | 7084.62 | 116 |
| H00E | 8584.26 | -14.26 | 8346.68 | 58 |
| H00F | 8091.47 | -368.22 | 7589.9 | 58 |
| H00G | 3013.79 | 5392.12 | 2896.88 | 61 |
| H00H | 3529.88 | 5100.95 | 3620.42 | 61 |
| H00I | 8594.46 | 1509.5 | 11029.48 | 65 |
| H00J | 8396.3 | 183.89 | 10684.52 | 65 |
| H00U | 5893.83 | 4489.22 | 8799.83 | 149 |
| H00V | 5889.24 | 5727.13 | 8934.88 | 149 |
| H00K | 7314.31 | -464.83 | 6442.76 | 63 |
| H00L | 6908.47 | -102.07 | 5549.77 | 63 |
| H01A | 2942.57 | 3079.9 | 5384.18 | 60 |
| H01B | 3356.1 | 2915.62 | 4733.15 | 60 |
| H01C | 8518.77 | 1212.1 | 7015.22 | 62 |
| H01D | 8539.95 | 2010.87 | 7908.78 | 62 |
| H01E | 8354.25 | 2119.65 | 9399.66 | 57 |
| H01F | 7901.05 | 2002.32 | 9975.16 | 57 |
| H01G | 7253.03 | 1804.66 | 5495.67 | 66 |
| H01H | 7748.17 | 929.4 | 5729.41 | 66 |
| H01I | 3520.99 | 3081.69 | 3201.5 | 65 |
| H01J | 3449.5 | 3867.2 | 2293.18 | 65 |
| H01K | 3451.33 | 4955.13 | 5932.6 | 69 |
| H01L | 3671.17 | 3661.76 | 6315.73 | 69 |
| H01M | 6432.94 | 2485.64 | 6061.8 | 65 |
| H01N | 6114.77 | 1418.16 | 5468.83 | 65 |
| H01O | 1783.67 | 4851.44 | 872.68 | 69 |
| H01P | 2207.7 | 5355.72 | 1695.44 | 69 |
| H01Q | 2643.5 | 3948.13 | 1036.05 | 75 |
| H01R | 2168.01 | 3012.15 | 888.84 | 75 |
| H01Y | 5493.77 | 5565.09 | 10271.08 | 186 |
| H | 5567.79 | 6833.69 | 10158.93 | 186 |
| H01S | 5832.71 | 2320.89 | 7101.52 | 76 |
| H01T | 5497 | 1371.29 | 6415.72 | 76 |
| H01U | 883.21 | 3558.62 | 518.83 | 82 |
| H01V | 480.97 | 3757.47 | 1186.96 | 82 |
| H01W | 1396.22 | 2353.6 | 1611.02 | 97 |
| H01X | 999.14 | 2596.74 | 2278.65 | 97 |

**Experimental**

Single crystals of $C_{40}H_{96}Cl_4Cu_8O_{32}S_{12}$ **[20220622_COD_Gb_auto]** were **[]**. A suitable crystal was selected and **[]** on a diffractometer. The crystal was kept at 293(2) K during data collection. Using Olex2 [1], the structure was solved with the olex2.solve [2] structure solution program using Charge Flipping and refined with the olex2.refine [3] refinement package using Gauss-Newton minimisation.


1. Dolomanov, O.V., Bourhis, L.J., Gildea, R.J, Howard, J.A.K. & Puschmann, H. (2009), J. Appl. Cryst. 42, 339-341.
2. Bourhis, L.J., Dolomanov, O.V., Gildea, R.J., Howard, J.A.K., Puschmann, H. (2015). Acta Cryst. A71, 59-75.
3. Bourhis, L.J., Dolomanov, O.V., Gildea, R.J., Howard, J.A.K., Puschmann, H. (2015). Acta Cryst. A71, 59-75.


**Crystal structure determination of [20220622_COD_Gb_auto]**

**Crystal Data** for $C_{40}H_{96}Cl_4Cu_8O_{32}S_{12}$ ($M$ =2124.00 g/mol): monoclinic, space group $P2_1/c$ (no. 14), $a$ = 25.5617(3) Å, $b$ = 10.72810(10) Å, $c$ = 14.7307(2) Å, $\beta$ = 100.8080(10)°, $V$ = 3967.92(8) Å$^3$, $Z$ = 2, $T$ = 293(2) K, μ(Cu Kα) = 7.145 mm$^{-1}$, *Dcalc* = 1.778 g/cm$^3$, 58507 reflections measured (7.042° ≤ 2Θ ≤ 168.81°), 8400 unique ($R_{int}$ = 0.0565, $R_{sigma}$ = 0.0300) which were used in all calculations. The final $R_1$ was 0.0619 (I > 2σ(I)) and $wR_2$ was 0.1890 (all data).

**Refinement model description**

Number of restraints - 2, number of constraints - unknown.
Details:
1. Fixed Uiso
 At 1.2 times of:
  All C(H,H) groups
 At 1.5 times of:
  All O(H,H) groups
2. Restrained distances
 Cu01-H00a ≈ Cu01-H00b
 with sigma of 0.02
 Cu02-H00c ≈ Cu02-H00d
 with sigma of 0.02
3.a Free rotating group:
 O00K(H00a,H00b), O00M(H00c,H00d), O00N(H00m,H00n), O00O(H00o,H00p), O00P(H00q, H00r), O00R(H00s,H00t), O00Y(H00u,H00v), O019(H01y,H)
3.b Secondary CH2 refined with riding coordinates:
 C00V(H00e,H00f), C00W(H00g,H00h), C00X(H00i,H00j), C00Z(H00k,H00l), C010(H01a, H01b), C011(H01c,H01d), C012(H01e,H01f), C013(H01g,H01h), C014(H01i,H01j), C015(H01k,H01l), C016(H01m,H01n), C017(H01o,H01p), C018(H01q,H01r), C01A(H01s, H01t), C01B(H01u,H01v), C01C(H01w,H01x)